



UNIL | Université de Lausanne

Unicentre

CH-1015 Lausanne

<http://serval.unil.ch>

Year : 2022

The Role of Interferon-Inducible Guanylate-Binding Proteins (GBPs) in Non-Canonical Inflammasome Activation

Dilucca Marisa

Dilucca Marisa, 2022, The Role of Interferon-Inducible Guanylate-Binding Proteins (GBPs) in Non-Canonical Inflammasome Activation

Originally published at : Thesis, University of Lausanne

Posted at the University of Lausanne Open Archive <http://serval.unil.ch>

Document URN : urn:nbn:ch:serval-BIB_AFDFF71AC2106

Droits d'auteur

L'Université de Lausanne attire expressément l'attention des utilisateurs sur le fait que tous les documents publiés dans l'Archive SERVAL sont protégés par le droit d'auteur, conformément à la loi fédérale sur le droit d'auteur et les droits voisins (LDA). A ce titre, il est indispensable d'obtenir le consentement préalable de l'auteur et/ou de l'éditeur avant toute utilisation d'une oeuvre ou d'une partie d'une oeuvre ne relevant pas d'une utilisation à des fins personnelles au sens de la LDA (art. 19, al. 1 lettre a). A défaut, tout contrevenant s'expose aux sanctions prévues par cette loi. Nous déclinons toute responsabilité en la matière.

Copyright

The University of Lausanne expressly draws the attention of users to the fact that all documents published in the SERVAL Archive are protected by copyright in accordance with federal law on copyright and similar rights (LDA). Accordingly it is indispensable to obtain prior consent from the author and/or publisher before any use of a work or part of a work for purposes other than personal use within the meaning of LDA (art. 19, para. 1 letter a). Failure to do so will expose offenders to the sanctions laid down by this law. We accept no liability in this respect.



UNIL | Université de Lausanne

Faculté de biologie
et de médecine

Département de Immunobiologie

The Role of Interferon-Inducible Guanylate-Binding Proteins (GBPs) in Non-Canonical Inflammasome Activation

Thèse de doctorat ès sciences de la vie (PhD)

présentée à la

Faculté de biologie et de médecine
de l'Université de Lausanne

par

Marisa DILUCCA

Biologiste diplômé ou Master de l'Université de Siena

Jury

Prof. Monika Hegi, Présidente
Prof. Petr Broz, Directeur de thèse
Prof. Thierry Roger, Expert
Prof. Thomas Henry, Expert

Lausanne
(2022)



UNIL | Université de Lausanne

Faculté de biologie
et de médecine

Département de Immunobiologie

The Role of Interferon-Inducible Guanylate-Binding Proteins (GBPs) in Non-Canonical Inflammasome Activation

Thèse de doctorat ès sciences de la vie (PhD)

présentée à la

Faculté de biologie et de médecine
de l'Université de Lausanne

par

Marisa DILUCCA

Biologiste diplômé ou Master de l'Université de Siena

Jury

Prof. Monika Hegi, Présidente
Prof. Petr Broz, Directeur de thèse
Prof. Thierry Roger, Expert
Prof. Thomas Henry, Expert

Lausanne
(2022)



UNIL | Université de Lausanne

Faculté de biologie
et de médecine

Ecole Doctorale

Doctorat ès sciences de la vie

Imprimatur

Vu le rapport présenté par le jury d'examen, composé de

| | | | | |
|---------------------------------|----------|-------|---------|--------------|
| Président-e | Madame | Prof. | Monika | Hegi |
| Directeur-trice de thèse | Monsieur | Prof. | Petr | Broz |
| Expert-e-s | Monsieur | Prof. | Thierry | Roger |
| | Monsieur | Dr | Thomas | Henry |

le Conseil de Faculté autorise l'impression de la thèse de

Marisa Dilucca

Master degree in Molecular and cellular biology, Università degli Studi di Siena, Italie

intitulée

**The role of interferon-inducible Guanylate-Binding Proteins
(GBPs) in non-canonical inflammasome activation**

Lausanne, le 27 février 2023

pour le Doyen
de la Faculté de biologie et de médecine

Prof. Monika Hegi

Acknowledgments

I would like to thank my supervisor, Prof. Petr Broz, for his guidance and valuable comments and suggestions that helped develop my research agenda.

I would like to sincerely thank all the members of the laboratory, whose support and brilliant suggestions have improved the quality of my work. The most sincere thanks go to Dr. Jose Santos, who has guided me with his knowledge and expertise over the years.

I would like to express my sincere gratitude to my family, especially my mother and sister, and my partner, who gave me the encouragement and strength I needed throughout this process. I hope I have made you all proud of me.

Abstract

Inflammasomes are cytosolic multiprotein signaling complexes that are activated upon pattern-recognition receptors (PRRs)-mediated recognition of pathogen-associated molecular patterns (PAMPs) and damage-associated molecular patterns (DAMPs). Their assembly activates downstream inflammatory caspases that induce cytokine release and pyroptotic cell death through the cleavage of the pore-forming effector Gasdermin D. The so-called non-canonical inflammasome activates human caspase-4/-5 or mouse caspase-11 and serves as a cytosolic detection mechanism for lipopolysaccharide (LPS), the major component of Gram-negative bacteria cell wall. In mouse macrophages activation of caspase-11 in response to cytosolic LPS and intracellular Gram-negative bacteria requires the expression of the interferon (IFN)-inducible GTPases Guanylate-Binding Proteins (GBPs). During my PhD, I investigated the role of IFNs and GBPs in activating the human non-canonical inflammasome. I showed that human GBP1 is a bona-fide PRR for cytosolic LPS, that binds LPS on the membrane of Gram-negative bacteria and drives the recruitment of additional hGBPs, which form a signaling hub that mediates the recruitment and activation of human caspase-4. In addition, I reported that IFN γ protects human epithelial cells against *Burkholderia*-induced multi-nucleated giant cell (MNGC) formation, specifically through the action hGBP1. Mechanistically, GBP1 acts by inducing caspase-4-dependent cell death through pyroptosis, allowing the infected cells to be quickly eliminated before bacterial spread and MNGCs formation. Eventually, I aimed to define which individual murine Gbps were necessary for LPS-induced non-canonical inflammasome activation in mouse macrophages. Murine Gbps are distributed in two clusters on chromosomes 3 and 5. I found that among the Gbps encoded by chromosome 3, mGbp2 and mGbp3 are key activators of the caspase-11 inflammasome. Moreover, I showed that Gbps on chromosome 5 controls LPS-driven caspase-11 activation in a priming-dependent manner: their participation is only detectable under IFN γ priming conditions. Overall, these findings provide new insights into the noncanonical inflammasome activation pathway and potentially open new perspectives for therapeutic approaches against sepsis and melioidosis.

Resumé

Les inflammasomes sont des complexes de signalisation multiprotéiques cytosoliques qui sont activés lors de la reconnaissance, par des récepteurs de reconnaissance de motifs (PRR), de motifs moléculaires associés à des agents pathogènes (PAMP) et de motifs moléculaires associés à des dommages (DAMP). Leur assemblage active les caspases inflammatoires en aval qui induisent la libération de cytokines et la mort cellulaire pyroptotique par le clivage de l'effecteur de formation de pores Gasdermin D. L'inflammasome dit non canonique active la caspase-4/-5 humaine ou la caspase-11 de la souris et sert de mécanisme de détection cytosolique du lipopolysaccharide (LPS), le principal composant de la paroi cellulaire des bactéries Gram-négatives. Dans les macrophages de souris, l'activation de la caspase-11 en réponse au LPS cytosolique et aux bactéries Gram-négatives intracellulaires nécessite l'expression des GTPases Guanylate-Binding Proteins (GBP) inductibles par l'interféron (IFN). Au cours de mon doctorat, j'ai étudié le rôle des IFN et des GBP dans l'activation de l'inflammasome non canonique humain. J'ai montré que la GBP1 humaine est un véritable PRR pour les LPS cytosoliques, qui se lie aux LPS sur la membrane des bactéries Gram-négatives et entraîne le recrutement d'autres hGBP, qui forment un nœud de signalisation médiant le recrutement et l'activation de la caspase-4 humaine. De plus, j'ai rapporté que IFN γ protège les cellules épithéliales humaines contre la formation de cellules géantes multi-nucléées (MNGC) induite par *Burkholderia*, spécifiquement par l'action de hGBP1. Mécaniquement, GBP1 agit en induisant une mort cellulaire dépendante de la caspase-4 par pyroptose, permettant aux cellules infectées d'être rapidement éliminées avant la propagation bactérienne et la formation de MNGC. Finalement, j'ai cherché à définir quels Gbps murins individuels étaient nécessaires pour l'activation de l'inflammasome non canonique induite par le LPS dans les macrophages de souris. Les Gbps murins sont répartis en deux groupes sur les chromosomes 3 et 5. J'ai découvert que parmi les Gbps codés par le chromosome 3, mGbp2 et mGbp3 sont des activateurs clés de l'inflammasome caspase-11. De plus, j'ai montré que les Gbps du chromosome 5 contrôlent l'activation de la caspase-11 par le LPS d'une manière dépendante de l'amorçage : leur participation n'est détectable que dans des conditions d'amorçage IFN γ . Dans

l'ensemble, ces résultats fournissent de nouvelles informations sur la voie d'activation non canonique de l'inflammasome et ouvrent potentiellement de nouvelles perspectives pour les approches thérapeutiques contre la septicémie et la mélioïdose.

Table of contents

| | |
|--|------------|
| List of Abbreviations | 1 |
| List of Figures | 5 |
| 1. Introduction | 7 |
| 1.1 Immune system | 9 |
| 1.1.1 Innate immune system | 9 |
| 1.1.2 Adaptive immune system | 10 |
| 1.2. Interferons | 12 |
| 1.2.1 The discovery of Interferons | 12 |
| 1.2.1.1 Type I interferons | 12 |
| 1.2.1.2 Type II interferon..... | 13 |
| 1.2.1.3 Type III interferons | 14 |
| 1.2.2 Interferon signaling pathways..... | 14 |
| 1.2.3 Interferon-stimulated genes (ISGs)..... | 16 |
| 1.2.3.1 Role of ISGs in the antiviral response..... | 16 |
| 1.2.3.2 Effects of ISGs on innate and adaptive immunity..... | 18 |
| 1.2.3.3 Role of ISGs in the antibacterial response..... | 18 |
| 1.2.3.4 Role of ISGs against parasites..... | 21 |
| 1.3 Inflammasomes | 23 |
| 1.3.1 Pyroptosis and inflammasome: the discovery | 23 |
| 1.3.2 The canonical inflammasomes | 24 |
| 1.3.2.1 NLRP1 inflammasome..... | 25 |
| 1.3.2.2 NLRP3 inflammasome..... | 27 |
| 1.3.2.3 NLRC4 inflammasome..... | 30 |
| 1.3.2.4 AIM2 inflammasome..... | 32 |
| 1.3.2.5 Pyrin inflammasome..... | 33 |
| 1.3.2.6 Other inflammasomes..... | 34 |
| 1.3.3 Non-canonical inflammasome..... | 35 |
| 1.3.4 The pyroptotic executor GasderminD (GSDMD)..... | 37 |
| 1.3.4.1 Sub-lytic cell death..... | 40 |
| 1.4. Guanylate-binding proteins | 41 |
| 1.4.1 Interferon-inducible GTPases..... | 41 |
| 1.4.1.1 Biochemical and structural analysis of GBPs..... | 42 |
| 1.4.2 GBP evolution and expression profile..... | 44 |
| 1.4.3 When GBPs meet intracellular pathogens..... | 46 |
| 1.4.3.1 Antiviral GBPs..... | 46 |
| 1.4.3.2 GBPs and parasite infections..... | 47 |
| 1.4.3.3 GBPs and antibacterial defense..... | 49 |
| 1.4.4 Guanylate-binding proteins and inflammasome..... | 50 |
| 1.4.4.1 GBPs and canonical inflammasome..... | 51 |
| 1.4.4.2 GBPs and non-canonical inflammasome..... | 52 |
| 2. Aim of the thesis | 58 |
| 3. Results | 60 |
| 3.1 Research Project I: Human GBP1 binds LPS to initiate assembly of a caspase-4 activating platform on cytosolic bacteria | 62 |
| Summary of the results | 63 |
| 3.2. Research Project II: Guanylate-Binding Protein-Dependent Noncanonical Inflammasome Activation Prevents <i>Burkholderia thailandensis</i>-Induced Multinucleated Giant Cell Formation | 115 |

| | |
|---|------------|
| Summary of the results | 117 |
| 3.3 Research Project III: Interferon gamma-induced murine guanylate-binding protein 4 (Gbp4) orchestrates caspase-11-mediated pyroptosis..... | 141 |
| Summary of the results | 142 |
| 4. Discussion | 163 |
| 4.1 Research project I: Human GBP1 binds LPS to initiate assembly of a caspase-4 activating platform on cytosolic bacteria | 165 |
| 4.1.1) How do GBPs promote Caspase-4 recruitment and activation? | 165 |
| 4.1.2) What is the role of GBPs in response to parasitic infections? | 166 |
| 4.1.3) Does lipid A acylation have a role in GBP recruitment? | 167 |
| 4.1.4) Is there a unifying model that explains the GBP-dependent caspase-4 activation?..... | 167 |
| 4.2 Research Project II: Guanylate-Binding Protein-Dependent Noncanonical Inflammasome Activation Prevents <i>Burkholderia thailandensis</i>-Induced Multinucleated Giant Cell Formation | 170 |
| 4.2.1) Why does the GBPs coat not block the polymerization of <i>Burkholderia</i> actin tails? | 170 |
| 4.2.2) Would <i>B. pseudomallei</i> be able to activate caspase-4-mediated pyroptosis? | 171 |
| 4.2.3) Can GSDMD directly kill bacteria? | 172 |
| 4.3 Research Project III: Interferon gamma-induced murine guanylate-binding protein 4 (GBP4) orchestrates caspase-11-mediated pyroptosis. | 174 |
| 4.3.1) Are the non-canonical mouse and human inflammasomes regulated differently by GBPs? | 174 |
| 4.3.2) What are the murine Gbps involved in LPS-driven caspase-11 activation? | 175 |
| 4.3.3) What is the role of the Gbp cluster on chromosome 5 in non-canonical inflammasome activation? | 176 |
| 4.4 Discussion and future research | 177 |
| 5. Appendix..... | 180 |
| Related article: Caspase-1 cleaves Bid to release mitochondrial SMAC and drive secondary necrosis in the absence of GSDMD..... | 182 |
| 6. References..... | 204 |

List of Abbreviations

| | |
|-------------------------------|--|
| AIM2 | Absent in melanoma 2 |
| APOBEC3 | Apolipoprotein B mRNA-editing enzyme catalytic polypeptide 3 |
| ASC | Apoptosis-associated speck-like protein containing a CARD |
| ATF2 | Activating transcription factor 2 |
| ATG16L1 | Autophagy Related 16 Like 1 |
| BCR | B-cell antigen specific receptor |
| BMDM | Bone marrow-derived mouse macrophages |
| CAPS | Cryopyrin-associated periodic syndromes |
| CFU | Colony-forming unit |
| cGAMP | 2'3' cyclic GMP-AMP |
| cGAS | Cyclic GMP-AMP synthase |
| CLR | C-type lectin receptors |
| CT | C-terminal |
| CXCL | C-X-C Motif Chemokine Ligand |
| DAMP | Damage-associated molecular patterns |
| DMEM | Dulbecco's modified Eagle's medium |
| DUOX | Dual oxidase |
| EMCV | Encephalomyocarditis virus |
| ER | Endoplasmic reticulum |
| ES | Embryonic stem cell |
| ESCRT | Endosomal sorting complexes required for transport |
| ET | Edema toxin |
| FADD | Fas-associated protein with death domain |
| FCS | Fetal calf serum |
| FIIND | Function-to-find domain |
| FMF | Familial Mediterranean fever |
| FRET | Förster resonance energy transfer |
| GAP | GTPase-activating protein |
| GBP | Guanylate-binding protein |
| GDI | Guanine nucleotide dissociation inhibitor |
| GED | GTPase effector domain |
| GEF | Guanine nucleotide exchange factor |
| GRA | Granule antigen |
| GSDM | Gasdermin |
| H ₂ O ₂ | Hydrogen peroxide |
| HCV | Hepatitis C virus |
| hMDM | Human monocyte-derived macrophage |
| HSC | Hematopoietic stem cell |
| ICAM1 | Intracellular adhesion molecule 1 |
| ICE | Interleukin-1 β converting enzyme |

| | |
|------------------|--|
| iE-DAP | Isoglutamate diaminopimelic acid |
| IFI | IFN γ -inducible protein |
| IFITM | IFN-induced transmembrane proteins |
| IFN | Interferon |
| IFNAR | IFN α receptor |
| IFNGR | IFN γ receptor |
| IFNLR | IFN λ receptor |
| IL | Interleukin |
| iNOS | Inducible nitric oxide synthase |
| IRF | IFN regulating factor |
| IRG | Immunity-related GTPase |
| ISG | IFN-stimulated genes |
| ISGF3 | IFN-stimulated gene factor 3 |
| ISRE | IFN-stimulated response element |
| JAK | Janus kinase |
| KSHV | Kaposi's sarcoma-associated herpesvirus |
| LBP | LPS-binding protein |
| LDH | Lactate dehydrogenase |
| LG | Large GTPase domain |
| LPS | Lipopolysaccharide |
| LRR | Leucine-rich repeat |
| LRRK | Leucine-rich repeat-containing kinase |
| LT | Lethal toxin |
| LTA | Lipoteichoic acid |
| MAPK | Mitogen-activated protein kinase |
| MAVS | Mitochondrial antiviral-signaling protein |
| MDA5 | Melanoma differentiation-associated protein |
| MDP | Muramyl dipeptide |
| MFIS | Multiparameter fluorescence image spectroscopy |
| MHC | Major histocompatibility complex |
| MNGC | Multi-nucleated giant cell |
| MOI | Multiplicity of infection |
| MYR | Myc regulatory protein |
| N ₂ O | Dinitrogen oxide |
| NADPH | Nicotinamide adenine dinucleotide phosphate |
| NAIP | NLR family apoptosis inhibitory protein |
| NBS | Nucleotide-binding site |
| NEK7 | NIMA-related kinase 7 |
| NET | Neutrophil extracellular trap |
| NF-kB | Nuclear factor-kB |

| | |
|-------------------|---|
| NINJ1 | Ninjurin 1 |
| NK | Natural killer |
| NLR | NOD-like receptor |
| NLRP | NOD-like receptor family pyrin domain containing |
| NO | Nitric oxide |
| NOD | Nucleotide-binding oligomerization domain |
| NOS | Nitric oxide synthase |
| NOX | NADPH oxidases |
| NRAMP1 | Natural resistance-associated macrophage protein 1 |
| NT | N-terminal |
| OAS | 2'-5'-oligoadenylate synthetase |
| OD | Optical density |
| OH | Hydroxyl radical |
| OMV | Outer membrane vesicle |
| ONOO ⁻ | Peroxynitrite |
| oxPAPC | Oxidized 1-palmitoyl-2-arachidonoyl-sn-glycero-3-phosphorylcholine |
| PA | Protective agent |
| PAMP | Pathogen-associated molecular pattern |
| PCV | Pathogen-containing vacuole |
| PI | Propidium-iodide |
| PKC | Protein kinase C |
| PKN1/2 | Protein kinase N1 and N2 |
| PKR | RNA-dependent protein kinase |
| PMR | Plasma membrane rupture |
| PRR | Pattern-recognition receptor |
| PVM | Parasitophorous vacuole membrane |
| PYD | Pyrin domain |
| PYHIN | Pyrin and HIN domain-containing protein |
| RIG1 | Retinoic acid-inducible gene 1 |
| RLR | RIG1-like receptor |
| RNS | Reactive nitrogen species |
| ROP | Rhoptry |
| ROS | Reactive oxygen species |
| RSNO | Nitrosothiol adduct |
| RTA | Replication and transcription activator |
| SNARE | Soluble N-ethylmaleimide-sensitive factor attachment protein receptor protein |
| SPR | Surface plasmon resonance |
| SQSTM1 | Sequestosome 1 |
| STAT | Transducer and activator of transcription |
| STING | Stimulator of interferon genes |
| T3SS | Type 3 secretion systems |
| T4SS | Type 4 secretion systems |
| TASL | TLR adaptor interacting with SLC15A4 on the lysosome |

| | |
|------|---|
| TBK1 | TANK binding kinase 1 |
| TCR | T-cell antigen-specific receptor |
| TLR | Toll-like receptor |
| TNF | Tumor necrosis factor |
| TRAF | TNF receptor-associated factor 3 |
| TRIF | TLR adaptor protein 1 |
| TRIM | Tripartite motif-containing |
| TYK | Tyrosine kinase |
| ULK | Unc-51 Like Autophagy Activating Kinase |
| VLIG | Very large IFN-inducible GTPase |
| VLS | Vesicle-like structure |
| VSV | Vesicular stomatitis viruses |

List of Figures

| | |
|--|-----|
| Figure 1.1 Interferon signaling pathways..... | 16 |
| Figure 1.2 NLRP1 inflammasome. | 27 |
| Figure 1.3 NLRP3 inflammasome. | 30 |
| Figure 1.4 NLRC4 inflammasome. | 32 |
| Figure 1.5 AIM2 inflammasome. | 33 |
| Figure 1.6 Biochemical and structural analysis of GBPs..... | 43 |
| Figure 1.7 GBPs and non-canonical inflammasome. | 56 |
| | |
| Figure 3.1 Generation of <i>Gbp^{Chr3-}</i> and <i>Gbp^{Chr5-}</i> -deficient mice. | 146 |
| Figure 3.2 The cluster of Gbps on chromosome 5 do not promote canonical inflammasome activation..... | 148 |
| Figure 3.3 Gbp cluster on chromosome 5 does not impair <i>Burkholderia</i> actin-based motility..... | 149 |
| Figure 3.4 Gbps on chromosome 5 orchestrate the non-canonical inflammasome activation in IFN γ -primed conditions..... | 151 |
| Figure 3.5 INF γ -stimulated macrophages require murine Gbp4 for optimal caspase-11 inflammasome activation..... | 153 |
| Figure 3.6 Schematic representation of caspase-4/-11-driven pyroptosis..... | 157 |

1. Introduction

1.1 Immune system

1.1.1 Innate immune system

All living organisms are constantly threatened by invading pathogens and therefore have evolved strategies to discriminate between self and non-self. The immune system enables organisms to fight infections by triggering the immune response. In vertebrates, the immune system comprises two branches: the innate and adaptive immune systems. The innate immune system is the first line of host defense, detecting the presence of infection within hours of encountering an antigen. However, it lacks the potential to generate long-lasting immunological memory^{1,2}. The innate immune system includes chemical and physical barriers, such as saliva, skin, stomach acids, and urine flow, as well as humoral innate immune components, which include soluble proteins that are constitutively found in biological fluids (e.g., complement proteins, defensin, etc.)³. Lastly, the innate immune response relies on germline-encoded membrane-bound or cytosolic receptors, namely pattern-recognition receptors (PRRs)⁴. There are four major families of PRRs: Toll-like receptors (TLRs), NOD-like receptors (NLRs), retinoic acid-inducible gene 1 (RIG-1)-like receptors (RLRs), and the C-type lectin receptors (CLRs)⁵. PRRs recognize microbial products, known collectively as pathogen-associated molecular patterns (PAMPs), like lipopolysaccharide (LPS). As PAMPs are produced exclusively by microbes, their recognition by the innate immune system allows a distinction between self and non-self antigens. In addition, PAMPs are ideal targets for host innate immune recognition because, being essential for microbial survival, they do not mutate and are conserved among microorganisms of a given class, allowing the limited number of germline-encoded PRRs to detect the presence of a wide variety of pathogens^{5,6}. PRRs also detect host-derived danger signals (DAMPs), which are endogenous molecules released from damaged or dying cells, and perturbations of cytoplasmic homeostasis^{7,8}. PRRs are expressed by epithelial cells and specialized innate immune cells, which include monocytes, macrophages, dendritic cells, natural killer cells, neutrophils, and other granulocytes. These cells originate from bone marrow hematopoietic stem cells (HSCs), which undergo several stages of differentiation to mature into innate immune cells, blood cells, and lymphocytes⁹. Innate immune cells perform several functions that help fight invading pathogens and initiate the adaptive immune response. Downstream activities of PRR signaling

include the production of cytokines, e.g., interferons (IFNs) (that will be the focus of this thesis), interleukin-1 β (IL-1 β), and tumor necrosis factors (TNFs), which activate antimicrobial and proinflammatory activities and the maturation of adaptive immune cells⁹.

1.1.2 Adaptive immune system

Although the innate immune system can differentiate the self from the non-self, its response is considered non-specific, since PRRs are limited to conserved patterns of foreign antigens^{5,6}. Unlike the innate immune system, adaptive immunity is considered specific because it relies on B- and T-cell antigen-specific receptors (BCRs and TCRs). These receptors are generated by somatic rearrangement of antigen-receptor genes via a mechanism known as rearrangement¹. This mechanism ensures the formation of a huge repertoire of antigen-specific receptors, each with specificity for different antigens. Antigen recognition is followed by clonal expansion of receptors with relative specificity. Notably, in contrast to innate immune mechanisms, specific clone expansion and differentiation into effector cells require 4-7 days¹. B and T lymphocytes differentially contribute to the adaptive immune response. T cells originate from bone marrow HSCs but migrate to the thymus to complete their differentiation, while B cells complete their differentiation in the bone marrow⁹. The differentiation process within the thymus gives rise to different subpopulations of T cells, discriminated on the basis of surface molecules, which migrate to secondary lymphoid organs (e.g., lymph nodes, spleen, etc.) where they can be activated by foreign antigens. TCRs cannot recognize PAMPs or DAMPs directly, but they recognize antigen peptides loaded on the major histocompatibility complex (MHC I or MHC II) of antigen-presenting cells (mainly dendritic cells)¹⁰. Following antigen recognition, subpopulations of T cells undergo clonal expansion and exert effector functions: cytotoxic T cells (CD8⁺) kill infected cells by inducing their apoptosis; T-helper cells (CD4⁺) produce cytokines (e.g., IFN γ , IL-4, IL-17, etc.) that regulate the antimicrobial activity of innate immune cells and B cells^{11,12}. A subset of CD4⁺ T cells, known as regulatory T cells (Treg), limits and suppresses the immune response¹³. After infection resolution, most CD8⁺ T lymphocytes die, but some are retained as memory cells that can rapidly differentiate into effector cells when they encounter the same antigen¹¹. B cells are responsible for the humoral

adaptive immune response. Unlike TCRs, BCRs can recognize antigens in their native form without the need for antigen-presenting cells. When activated by the antigens, they proliferate and differentiate into antibodies-secreting plasma cells and memory B cells¹⁴. Secreted antibodies bind antigens exposed on the microbial surface by signaling them for killing through complement activation, opsonization, and elimination by immune cells¹⁵. Plasma cells are considered short-lived cells because they die after performing their effector functions. Memory B cells, on the other hand, are long-lived cells that persist after antigen elimination and can rapidly produce antibodies after re-exposure to the same antigen¹⁴. In summary, the synergy between innate and adaptive immune responses is essential to fight invading pathogens. Specifically, the rapid innate immune response is necessary to prevent the uncontrolled growth of pathogens within the host, but it lacks the ability to lead to a long-lasting memory of specific pathogens, a hallmark of adaptive immunity.

1.2. Interferons

1.2.1 The discovery of Interferons

The discovery of IFNs dates back to 1957 when Alick Isaac and Jean Lindenmann were studying viral homotypic and heterotypic interference, the phenomenon whereby a virus inhibits the replication of a second virus antigenically related or unrelated to the first. They incubated chick chorioallantoic membranes (highly vascularized extraembryonic membranes) with heat-inactivated influenza virus, a procedure that retains the virus's ability to be internalized while losing its replication activity. Such membranes infected a second time with live influenza virus showed low virus yields. A series of studies identified that de novo production of a soluble host-derived antiviral factor modulates interference with the infectious influenza virus^{16–18}. This soluble product was called “interferon”^{16–18}. Thenceforth, many studies have been conducted to elucidate the pathways that regulate IFN production and IFN-induced signaling cascades, leading to insights into its role in the innate immune defense in response to both viruses and bacteria pathogens. Several IFN types have been characterized based on the cell type where their antiviral activity was exhibited and their stability at different pH, grouped into three distinct IFN families: Type I; Type II, and Type III IFN.

1.2.1.1 Type I interferons. The type I IFNs family is a multi-gene cytokine family that encodes for IFN α , IFN β , and several poorly described single gene products^{19,20}. Of IFN α , first described as produced in leukocytes, there are 13 subtypes in humans (14 in mice), whereas there is a single IFN β , first identified in fibroblasts²¹. Type I IFN production is stimulated by the activation of PRRs, in particular by cell-surface and intracellular receptors that respond to foreign nucleic acids and other PAMPs²². dsRNA in the endosomal lumen is recognized by the TLR3²³. Following dsRNA recognition, TLR3 is phosphorylated and dimerized, triggering the activation of the TLR adaptor protein 1 (TRIF)²⁴. There are two main pathways downstream of TRIF activation that led to the production of type I IFNs. On one hand, the TNF receptor-associated factor 3 (TRAF3) and the TANK binding kinase (TBK1) trigger the phosphorylation of the IFN regulating factors 3 and 7 (IRF3; IRF7) – albeit other IRFs can induce IFN α/β production (e.g., IRF1, -5, and -8) – transcription factors that prompt the cells to produce type I IFN once in the nucleus^{25–27}. On the other hand,

TRIF-induced TRAF6 activation leads to the translocation of the transcription factors nuclear factor- κ B (NF- κ B), Jun, and activating transcription factor 2 (ATF2) from the cytosol to the nucleus where they promote type I IFNs transcription²⁸. Nucleic acids such as single-stranded RNA (ssRNA), through the TLR7 and TLR8, and oligodeoxyribonucleotides, through the TLR9, are also potent activators of type I IFNs production. However, TLR7, -8, and -9 preferentially signal through the myeloid differentiation primary response protein 88 (MyD88) and TRAF6 axis, rather than TRIF²⁹. Recently, it has been discovered that in plasmacytoid dendritic cells TLR7, -8 and -9 signaling requires the endolysosomal transporter SLC15A4, which, in module with TLR adaptor interacting with SLC15A4 on the lysosome (TASL), triggers type I IFN production in an IRF5-dependent manner. Therefore, like IRF3 adaptor proteins (e.g., TRIF), TASL can be considered an adaptor of innate immunity required for endolysosomal TLR signaling through IRF5³⁰. Furthermore, TRIF-mediated type I IFNs production can be induced by the cell surface receptor TLR4 which binds the LPS, the major component of the Gram-negative bacteria outer membrane²⁹.

Whereas cytosolic double-stranded RNA (dsRNA) is detected by two RNA-helicase receptors, RIG1, and the melanoma differentiation-associated protein 5 (MDA5)³¹. The mitochondrial antiviral-signaling protein MAVS (also known as VISA and IPS1) mediates the activation of IRF3 and IRF7 in response to the cytosolic receptors RIG-1 and MDA-5 stimulation by dsRNA³²⁻³⁴. In addition, type I IFNs transcription can be activated by the cytosolic cyclic GMP-AMP synthase (cGAS) in response to cytosolic double-stranded DNA (dsDNA) which can occur upon pathogen infection or cellular stress. On binding dsDNA, assembly of cGAS results in the activation of its enzymatic activity and the subsequent synthesis of 2'3' cyclic GMP-AMP (cGAMP). cGAMP binds to the stimulator of IFN genes (STING) which in turn triggers the autophosphorylation of TBK1 resulting in IRF3 and -7 activation³⁵. NF- κ B-mediated type I IFN production is also stimulated by peptidoglycan in the Gram-negative and positive bacteria cell wall, through the cytosolic sensor NOD-containing protein 1 (NOD1) and NOD2³⁶⁻³⁸.

1.2.1.2 Type II interferon. The type II IFN family is designated by a single-gene product, IFN γ , distant from the type I IFNs for its divergent amino-acid sequence and its production, which is linked primarily to natural killer cells (NK cells) and activated T lymphocytes³⁹. When macrophages and dendritic cells encounter pathogens, they

produce and release pro-inflammatory cytokines, such as IL-12 and IL-18, which drive NK cells-dependent production of IFN γ ^{40,41}. As a result of IL-12 binding, the IL-12 receptor (IL-12R) serves as a docking site for the tyrosine kinase 2 (Tyk2) and the Janus kinase 2 (JAK2) leading to phosphorylation and activation of Signal transducer and activator of transcription 4 (STAT4), which induces the transcription of IFN γ ^{42,43}. IFN γ production can also be enhanced by post-transcriptional regulation, for example IL-18 contributes to the stabilization of IFN γ mRNA by activating the Mitogen-activated protein kinase (MAPK) pathway⁴⁴.

1.2.1.3 Type III interferons. More recently, the type III IFNs family, consisting of IFN λ 1, IFN λ 2, IFN λ 3 (also known as IL-29, IL-28A, and IL-28B respectively), and IFN λ 4, has been described⁴⁵⁻⁴⁸. They share similar antiviral activity to cytokines of the type I IFN family, but to a lesser extent because their receptor expression is restricted to epithelial cell surfaces^{49,50}. Like the type I IFNs, their expression is induced by IRF- and NF- κ B-dependent activation^{51,52}, however, IFN λ transcription appears to depend primarily on a cluster of distal NF- κ B sites, and activation of IRFs is required for robust induction of IFN λ ⁵³. In addition, IFN λ production can be activated via MAVS localized at the peroxisomes in response to RIG1 activation⁵⁴. Interestingly, RIG1-mediated peroxisomal MAVS activation does not result in type I IFN production⁵⁵.

1.2.2 Interferon signaling pathways

All the IFN α subtypes and IFN β signals through IFN α receptor (IFNAR), a cell surface receptor composed of two transmembrane subunits, IFNAR1 and IFNAR2⁵⁶, associated with cytoplasmic tyrosine kinases, Janus kinase 1 (JAK1) and tyrosine kinase 2 (TYK2)^{57,58}. Following IFNAR binding, the tyrosine kinases are activated and can phosphorylate the transducer and activator of transcription 1 (STAT1) and STAT2 molecules, which dimerize, translocate to the nucleus, and bind IRF9 to form the IFN-stimulated gene (ISG) factor 3 (ISGF3) complex^{59,60}. The complex binds to its cognate DNA sequences, the IFN-stimulated response elements (ISREs), triggering the transcription of several IFN-stimulated genes (ISGs), many of which encode proteins involved in restraining viral infection^{61,62}. Along with the STAT1-STAT2 signaling, IFN α/β can signal through other STATs, such as STAT1 homodimers, STAT3, STAT4, and STAT5, stimulating the transcription of a wide

range ISGs that orchestrate the activation of pathogen restriction mechanisms⁶³ (Fig.1.1 a).

IFN γ , on the other hand, interacts with the transmembrane receptors IFN γ receptor 1 (IFNGR1) and IFNGR2^{64,65}. Following cognate receptor binding, IFN γ triggers a downstream signaling pathway through JAK kinases and STAT. Specifically, ligand binding induces JAK2 autophosphorylation that, in turn, enables JAK1 transphosphorylation by JAK2⁶⁶⁻⁶⁸. Once activated, JAK1 phosphorylates the two STAT1 docking sites on the IFNGR1 receptor, allowing STAT1 homodimer dissociation from the receptor and its translocation into the nucleus⁶⁹, where it binds IFN γ activation sites (GAS) DNA sequences thereby triggering the transcription of ISGs involved in the host defense against intracellular pathogens⁷⁰ (Fig.1.1 c).

Type III IFNs signal through a heterodimeric receptor that consists of the IFN λ receptor 1 (IFNLR1, also known as IL-28R1) chain and IL-10 receptor 2 (IL-10R2) chain^{71,72}. Despite using a different receptor, both IFN λ and IFN α/β trigger activation of the ISGF3 complex and transcription of ISRE-related ISGs⁷³. However, in contrast to IFNAR receptors that are more ubiquitously expressed, IFNLR1 expression appears to be limited mainly to lung and intestinal epithelial cells, where its tropism has been better characterized⁷⁴⁻⁷⁶ (Fig.1.1 b).

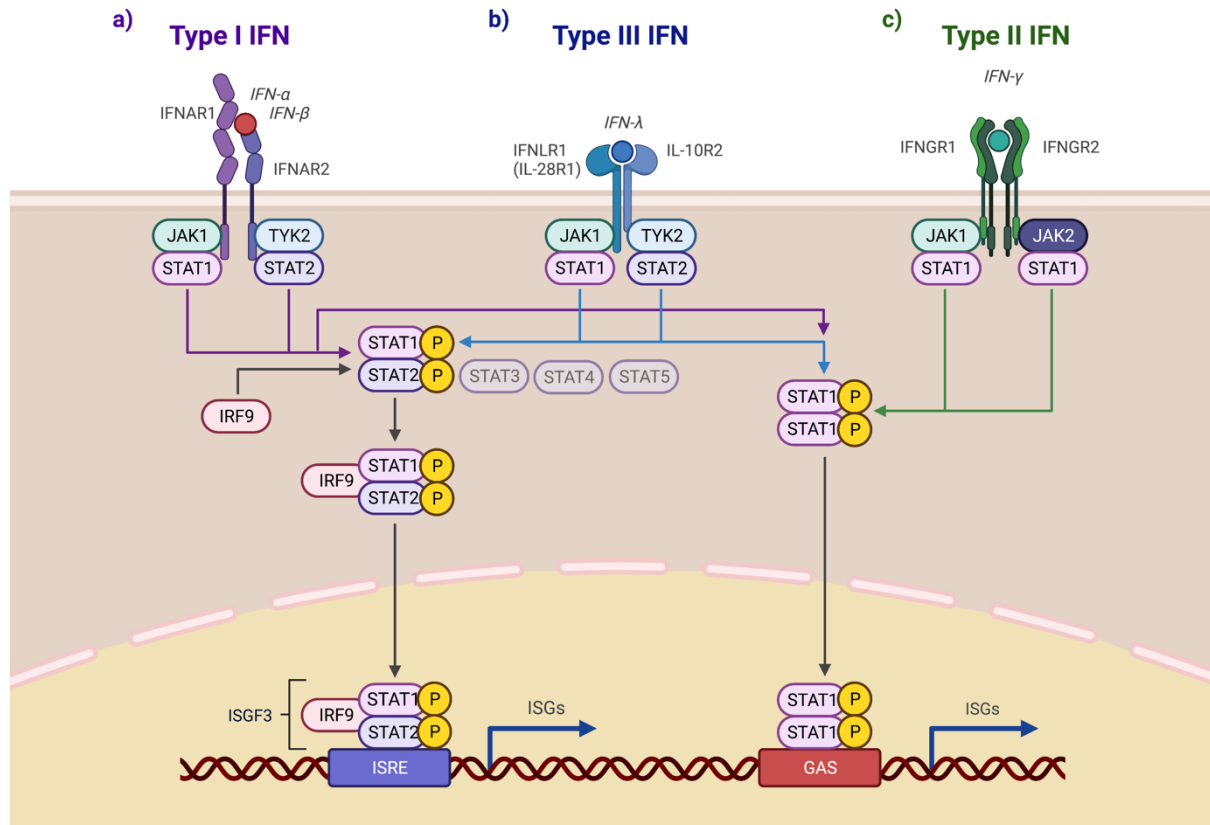


Figure 1.1 Interferon signaling pathways. **a)** After type I IFN binding to its cognate receptor (IFNAR), the tyrosine kinases JAK1 and TYK2 phosphorylate STAT1 and STAT2. The STAT1-STAT2 dimer together with IRF9 forms the ISGF3 complex, which translocates to the nucleus and triggers transcription of ISGs by binding the ISRE promoter. **b)** The ISGF3 complex is also formed when IFN λ binding to IFNLR1/IL-10R2 receptor triggering transcription of several ISGs. **c)** IFN γ binding to the IFNGR1/2 receptor drives STAT1 phosphorylation by JAK1. The STAT1 homodimer translocates into the nucleus where it triggers transcription of GAS elements. GAS-related ISGs can also be transcribed in response to IFN α/β and IFN λ when they signal through STAT1 homodimers. STAT1 can also form heterodimers with STAT3, 4, and 5.

1.2.3 Interferon-stimulated genes (ISGs)

ISGs are a group of more than 300 genes that encode proteins, which mediate the biological effect of IFN production in response to several pathogens, such as viruses, bacteria, and parasites.

1.2.3.1 Role of ISGs in the antiviral response. Many of the ISGs have been first characterized for their antiviral activity^{77,78}. Some of the best-known ISGs are 2'-5'-oligoadenylate synthetase (OAS), IFN-inducible double-stranded RNA-dependent protein kinase (PKR), IFN-induced transmembrane proteins (IFITMs), myxovirus

resistance 1 (Mx1), the tripartite motif-containing (TRIM), and apolipoprotein B mRNA-editing enzyme catalytic polypeptide 3 (APOBEC3) family of molecules.

It has been shown that OAS acts against a wide range of RNA viruses⁷⁹ by detecting foreign RNA and synthesizing 2'-5'-oligoadenylates, an intracellular second messenger that activates RNaseL, which unspecifically cleaves both host and viral RNA^{80,81}. The mechanism of action of RNaseL not only hinders the replication of several RNA viruses, but it can lead to the apoptosis of the infected cell, implying an important antitumor action along with the antiviral action⁸²⁻⁸⁴. Furthermore, it can generate a positive feedback loop in the production of type I IFN by activating cytosolic receptors, such as RIG1 and MDA5⁸⁵.

Among the ISGs that sense dsRNA, PKR plays an important role in antiviral defense. PKR is a serine/threonine kinase that triggers a global inhibition of the host protein synthesis blocking further viral replication^{86,87}. Importantly, many viruses have developed strategies to impair PKR activation, such as producing molecules that sequester dsRNA molecules, depriving PKR of its activator⁸⁸.

Other ISGs have primarily inhibit virus entry, such as the IFITMs proteins, were identified in a genome-wide screening as encoding a host factor that inhibits influenza A virus^{89,90}. They are enriched in late endosomes and lysosomes, consistent with primarily inhibiting viruses that use those compartments for optimal entry. However, the IFITMs mechanism of action is still poorly characterized⁸⁹. Likewise, IFN-induce Mx proteins inhibit virus replication acting in the early post-entry stage of viral infection⁹¹. Mx proteins are large guanosine triphosphatases (GTPases) that oligomerize in ring-like structures on the viral nucleocapsid, thereby inhibiting viral replication, and possibly directing them for degradation^{91,92}.

TRIMs proteins also block viral replication in the early stage of the virus life cycle. They belong to a large family of proteins that exhibit a wide range of antiviral activities⁹³. For example, TRIM5a is an E3 ubiquitin ligase originally identified as an inhibitor of HIV-1 infection⁹⁴. TRIM5a binds to the viral capsid accelerating uncoating and it also impairs retrovirus replication before reverse transcription by a mechanism that needs to be further investigated⁹⁵. However, it appears that it may also exert its function in a proteasome-independent manner^{96,97}.

APOBEC3 belongs to the APOBECs proteins, a family of cytidine deaminase that edits cytosine to uracil. Its antiviral activity has been better examined in response to HIV infection⁹⁸: during reverse transcription, the change operated by APOBEC3

results in a guanosine-to-adenine mutation that often encodes for a stop codon⁹⁹. Therefore, APOBEC3 reduces viral replication.

1.2.3.2 Effects of ISGs on innate and adaptive immunity. A second layer of defense operated by ISGs is the augmentation of the innate and adaptive immune response. Indeed, pathogen presence is sensed by tissue-associated and circulating dendritic cells which present pathogen-derived peptides in association with MHC class II molecules to CD4⁺ T cells¹⁰⁰. MHC class II molecule expression is upregulated in response to IFN γ , whereas type I IFNs fail to do so¹⁰¹. However, both type I and type II IFNs can enhance the expression of MHC class I molecule expressed on the infected cells in association with pathogen-derived peptide fragments, thereby inducing virus clearance by CD8⁺ T¹⁰².

In addition, IFNs are essential to promote leukocyte recruitment to the infection site. Specifically, certain ISGs can act as chemokines, such as C-X-C Motif Chemokine Ligand 9(CXCL9), CXCL10, and CXCL11, and vascular adhesion molecules, such as the intracellular adhesion molecule 1 (ICAM1), which promote the accumulation of leukocytes in the site of the infection¹⁰³.

ISGs can promote additional effects on the immune system. For example, ISGs can modulate NK cells' response by inducing expression and activation of cytosolic effectors¹⁰⁴, and B cells' antibody responses, including class switching^{105,106}.

1.2.3.3 Role of ISGs in the antibacterial response. ISGs also exert their antimicrobial activity in response to bacterial infection. The cell-autonomous defense against bacteria can be achieved through different IFN-dependent mechanisms, which include the production of oxidative and nitrosative species, restriction of cations availability in the phagosomal lumen and in the cytosol cations, and they promote phagosome-lysosome fusion¹⁰⁷. Reactive oxygen species (ROS) and reactive nitrogen species (RNS) are highly toxic molecules that target i) bacterial DNA, damaged by guanine base oxidation, ii) lipids, damaged via peroxidation, and iii) enzymes within their heme groups and iron-sulfur clusters¹⁰⁸. ROS include O₂⁻ derivatives, such as the hydroxyl radical (OH) and hydrogen peroxide (H₂O₂). Whereas RNS include nitric oxide (NO) derivatives, such as dinitrogen oxides (N₂O₃ and N₂O₄), peroxyxynitrite (ONOO⁻), and nitrosothiol adducts (RSNO)¹⁰⁹. In mammals, ROS and RNS production is controlled by three classes of IFN-inducible oxidoreductases: nicotinamide adenine dinucleotide phosphate (NADPH) oxidases

(NOXs), which catalyze O_2^- production, dual oxidases (DUOXs), which produce H_2O_2 , and nitric oxide synthases (NOSs) which synthesize NO and include the inducible nitric oxide synthase (iNOS) isoform, which produces a large amount of NO during bacterial infection¹⁰⁸. NOXs enzymes are mainly expressed in phagocytic cells and are responsible for the respiratory burst in neutrophils, macrophages, monocytes, and eosinophils. Mutation in the NOX2 gene gives rise to the chronic granulomatous syndrome, which makes individuals suffer from recurrent bacterial infections from *Staphylococcus aureus* (*S. aureus*), *Serratia marcescens* (*S. marcescens*), *Burkholderia cepacia* (*B. cepacia*), non-typhoidal *Salmonella* spp., and *Mycobacterium tuberculosis* (*M. tuberculosis*), highlighting the NOX family's importance in host defense^{110,111}. It has been shown that NOXs and DUOXs provide oxidative defense against *Listeria* and *Salmonella* spp. also in non-phagocytic cells, such as epithelial cells in the airways, oral tract, and gastrointestinal tract^{112–114}. Moreover, NOS2 expressed in response to both type I and type II IFNs in immune and non-immune cells, mediates the NO-dependent killing of *M. tuberculosis*, which is resistant to ROS killing¹¹⁵. *Listeria monocytogenes* (*L. monocytogenes*) is also sensitive to the NO-mediated killing but only when trapped in phagosomes¹¹⁶. Intracellular bacteria use host cations, mainly Mn^{2+} , Fe^{2+} , and Zn^{2+} , to sustain their growth. IFN-inducible mechanisms have evolved to reduce the phagosomal and cytosolic availability of those elements¹¹⁷. For example, $IFN\gamma$ upregulates the expression of natural resistance-associated macrophage protein 1 (NRAMP1; encoded by *Slc11a1*), a proton-dependent Mn^{2+} and Fe^{2+} efflux pump which restricts intraphagosomal cations sequestration and competes with bacterial ion transporters for these metals¹¹⁸. Indeed, in $IFN\gamma$ -stimulated macrophages *M. tuberculosis* and *S. Typhimurium* strains that lack NRAMP1 homologs show a growth defect^{119,120}. The attenuated *S. Typhimurium* growth in macrophages is also dependent on the $IFN\gamma$ -inducible expression of ferroportin 1, a Fe^{2+} exporter, on the cell surface and concomitant downregulation of transferrin receptors, which mediate Fe^{2+} uptake¹¹⁷. Furthermore, IFN stimulation drives the expression and the relocation of Cu^+ pumps on the phagosome, where Cu^+ is then used to produce ROS¹²¹. An anti-bacterial effector function of IFNs is represented by the control of lysosomal trafficking. In lysosomes, the low pH and the presence of enzymes (e.g., proteases, lipases) favor the clearance of bacteria in their vacuolar compartment^{122,123}. In order

to avoid the fusion of the pathogen-containing vacuoles (PCVs) with the lysosomes, bacteria attempt to escape into the host cell cytosol for optimal replication. However, the presence of innate immune receptors makes the cytoplasm a challenging environment to sustain bacterial growth, and indeed only few bacteria can successfully replicate within the host cell cytosol. Amongst these that are *L. monocytogenes*, *Francisella novicida* (*F. novicida*), *Shigella flexneri* (*S. flexneri*), *Burkholderia* spp., and *Rickettsia* spp.^{124–126}. PCVs also represent compartments where bacteria can establish their intracellular niche. PCV replication is facilitated by expression of bacterial virulence factors and secretory machineries, such as type 3 and type 4 secretion systems (T3SSs and T4SSs), that subvert the host cell signaling and prevent lysosome fusion¹²⁷. Nonetheless, host cells rely on IFN-inducible genes to counteract intracellular bacteria. Among the most potent inducers of antimicrobial effector factors against intracellular bacteria are the 47kDa immunity-related GTPases (IRGs), which are induced by type II IFN and, to a lesser extent, by type -I and -III IFNs^{128–130}, and are expressed in most vertebrate species. Mice encode for 23 IRGs, subdivided according to the G1 motif sequence in the GTP-binding domain into those comprising the so-called “canonical sequence”, glycine-lysine-serine (GKS) IRGs (e.g., *Irga*, *Irgb*), and those with the “non-canonical sequence” glycine-methionine-serine (GMS) IRGs (e.g., *Irgm1*, *Irgm2*, *Irgm3*)¹³¹. Humans have retained only one form of the GMS class, IRGM, which is constitutively expressed^{128,132,133}. GKS IRGs orchestrate pathogen delivery to lysosomes in conjunction with other receptors that detect both ubiquitinated structures on the bacterial surface, such as sequestosome 1 (SQSTM1)¹³⁴, NDP52¹³⁵, and optineurin¹³⁶, and glycans (e.g., galectins) exposed during the bacterial escape from the vacuole¹³⁷. Following activation, these receptors trigger the xenophagy pathway: intracellular bacteria are engulfed into autophagosomes and ultimately degraded into (auto)lysosomes¹³⁸. GKS IRGs were first identified to target *M. tuberculosis* for lysosomal degradation in IFN γ -primed macrophages¹³⁹, but they can promote cell-autonomous immunity against a wide variety of intracellular bacteria, such as *M. bovis*¹³², *S. Typhimurium*¹⁴⁰, *Legionella pneumophila* (*L. pneumophila*)¹⁴¹, *Chlamydia trachomatis* (*C. trachomatis*)¹⁴², *Chlamydia psittaci* (*C. psittaci*)¹⁴³, and Crohn's disease-associated adherent invasive *Escherichia coli* (*E. coli*)¹⁴⁴.

The GMS IRGs subclass functions mainly as regulators of other IRGs and effectors. For example, *Irgm1* targets phosphoinositide lipids on the nascent phagosome of *M. tuberculosis*^{139,145}, *S. Typhimurium*¹⁴⁰, and *L. monocytogenes*¹⁴⁵, where they regulate the recruitment of proteins required for membrane fusion events during vesicles trafficking, such as the soluble N-ethylmaleimide-sensitive factor attachment protein receptor proteins (SNARE proteins), which traffic phagosomes towards lysosomes¹⁴⁶. Furthermore, *Irgm3* in the endoplasmic reticulum (ER) keeps GKS IRGs, such as *Irga6* and *Irgb10*, in an inactive state. Once released, *Irga6* and *Irgb10* target *Chlamydia*-containing vacuoles, resulting in the engulfment of the pathogen into autophagosomes^{147,148}. GMS IRGs were also proposed to directly drive autophagy. For instance, human IRGM directly controls the autophagy machinery by promoting phosphorylation and assembly of the autophagy regulators Unc-51 Like Autophagy Activating Kinase 1 (ULK1) and Beclin 1¹⁴⁹. In addition, IRGM promotes the interaction between Autophagy Related 16 Like 1 (ATG16L1), a distinct autophagy regulator, with the PRR NOD2¹⁴⁹.

1.2.3.4 Role of ISGs against parasites. Similar to bacterial infections, the host defense against protozoan parasites relies on gases, restriction of nutrients, and vacuolar targeting¹⁰⁷. The NO-mediate killing of *Leishmania major* (*L. major*) amastigotes, the causative agent of leishmaniasis, and *Trypanosoma cruzi* (*T. cruzi*) trypomastigotes, responsible for Chagas disease, were first characterized in IFN γ -primed macrophages. Indeed, *Nos2*^{-/-} mice show high susceptibility to both those pathogens^{150,151}. Along with *Leishmania* and *T. cruzi*, NO also has a parasitocidal activity also against the apicomplexan parasite *Toxoplasma gondii* (*T. gondii*), the causative agent of toxoplasmosis. Thus, NO seems to be essential in response to type I *T. gondii* strains, which have evolved strategies to evade the targeting of IRGs¹⁵², while acting as a second layer of defense against type II *T. gondii* strains, which are successfully restricted by IFN-inducible GTPases^{153,154}. The mechanism by which NO mediates the parasites' killing remains poorly understood, most likely by inhibiting the functions of some of the parasite's enzymes¹⁰⁸.

Nutrient acquisition is restricted by the expression of the IFN-inducible NRAMP1 and indoleamine 2,3-dioxygenases (IDOs), which limit iron and amino acid availability, respectively. *Leishmania spp.* and *T. gondii* intracellular replication are affected by the expression of IDO1 and -2 in several immune and non-immune cells since they

degrade L-tryptophan, essential for parasite growth^{118,155}. In addition, derivatives of the L-tryptophan degradation are toxic for *T. cruzi*¹⁵⁶.

IFNs-inducible GTPases play an important role in restricting parasite infections. The role of IRGs has been extensively studied in the context of *Toxoplasma* infection, where GKS IRGs, especially *Irga6*, *Irgb6*, *Irgb10*, and *Irgd*, confer resistance to type II *T. gondii* by targeting its parasitophorous vacuole^{157,158}. Conversely, GSK IRGs fail to restrict type I parasites since they produce effectors that prevent targeting¹⁵². It appears that IRGs are recruited sequentially on the parasite vacuole: *Irgb6* and *Irgb10* are recruited first, followed by *Irga6* and *Irgd*^{157,158}. The recruitment culminates in the rupture of the parasite-containing vacuoles and the release of the parasite in the cytosol of the host cell. It is unclear the mechanism by which the cytosolic parasite gets killed, however, it has been observed that the cells undergo necroptosis, which could eventually lead to the death of the parasite as well¹⁵⁹.

Guanylate-binding proteins (GBPs) are another class of IFN-inducible GTPases with a prominent role in cell-autonomous immunity, particularly in inflammasome activation (see below). Their role in the restriction of viruses, intracellular bacteria, and parasites will be extensively described in the following paragraphs.

1.3 Inflammasomes

1.3.1 Pyroptosis and inflammasome: the discovery

In 1986 Arthur M. Friedlander first reported a rapid form of cell death along with the release of intracellular contents in primary mouse macrophages treated with anthrax lethal toxin (LT)¹⁶⁰. In 1992, Zychlinsky et al. described that murine macrophages undergo peculiar cell death after infection with *S. flexneri*¹⁶¹. A similar kind of cell death was observed in macrophages infected with *S. Typhimurium*, which exhibited chromatin condensation and aggregation, membrane blebbing, and cytoplasmic vacuolization, commonly considered as hallmarks of apoptotic death^{162,163}. Hence, this *Salmonella*-induced cell death, as well as that observed following *Shigella* infection, was initially mistaken as a specialized form of bacterial-induced apoptosis. However, evidence rapidly emerged differentiating this form of death from apoptosis. Thereafter, IL-1 β converting enzyme (ICE) was described as an inflammatory caspase capable of processing IL-1 β precursor into mature IL-1 β , known as caspase-1^{164,165}. Remarkably, *Shigella*- and *Salmonella*-induced cell death was associated with a massive release of mature IL-1 β , correlating this cell death with the nonapoptotic enzyme caspase-1 for the first time and underscoring the presence of a bacterial-induced inflammatory response^{166–169}. Moreover, unlike caspase-1, proapoptotic caspase-3 is dispensable for *Salmonella*-induced death^{170,171}. Morphologically, a sudden and rapid loss of membrane integrity characterizes bacterial-induced cytotoxicity, whereas following apoptotic stimuli cell integrity is lost in the late phases¹⁷¹. In addition, *Salmonella*-infected macrophages release lactate dehydrogenase (LDH), blocked by glycine treatment, which is indicative of bacterial-induced membrane leakage¹⁷⁰. In 2001, Brad T. Cookson and Molly A. Brennan coined the term pyroptosis from the Greek roots “pyro” (fire or fever), and “ptosis” (falling), to describe this pro-inflammatory and caspase-1-dependent programmed cell death¹⁷². However, very little was known about the mechanism that triggers caspase-1 activation until 2002, when a groundbreaking study published by Martinon and coworkers identified a cytoplasmic multiprotein complex, termed the inflammasome, as responsible for caspase-1 activation¹⁷³. They reported that essential components of the inflammasome complex are the NOD-like receptor family pyrin domain containing 1 (NLRP1, also known as NALP1), apoptosis-associated speck-like protein containing a CARD (ASC), and caspase-1. Self-

assembly of NLRP1 triggers the recruitment and activation of caspase-1 and, consequently, the maturation of pro-IL-1 β into its biologically active form. For this activation pathway, ASC has been described as essential for proinflammatory caspase maturation¹⁷³. NLRP1 was identified as a novel member of the nucleotide-binding site (NBS) family, which also include the apoptotic protease activating factor 1 (Apaf1) and nucleotide-binding oligomerization domain (NODs) proteins. Like the other NBS proteins, it comprises a leucine-rich repeat (LRRs) domain next to the NBS (also known as NACHT) motif, but, unlike the aforementioned proteins, the N-terminus contains a CARD-like pyrin domain (PYD) instead of the CARD domain, that is present at the C-terminus^{174–176}. It has been hypothesized that the LRR domain may recognize endogenous PAMPs and/or "alarm signals"¹⁷³, analogous to those found in TLRs¹⁷⁷. ASC consists of a PYD domain and a CARD domain, suggesting it can work as an adaptor protein between PYD- and CARD-containing proteins^{173,178}. Indeed, follow-up studies showed that ASC functions as a caspase-1 activating adaptor through CARD-CARD domain interactions^{179,180}. Rapidly, the bipartite adaptor protein ASC was involved in the assembly of the inflammasome with other PYD-containing proteins, such as the pyrin domain-containing protein 3 (NLRP3)¹⁸¹. Interestingly, patients with Muckle-Wells syndrome, characterized by intermittent fever due to high production of proinflammatory cytokines, carry a mutation in the NACHT domain of NLRP3^{182,183}. This suggested that NLRP family proteins may be involved in IL-1 β production and that mutations in this gene could dysregulate proinflammatory caspases causing the fever episodes. It soon also became clear that a second proinflammatory cytokine, IL-18, relies on caspase-1 activation for its conversion to the mature form¹⁸⁴. For a long time, pyroptosis was considered to be a cell death driven exclusively by caspase-1, but this paradigm was changed when it was demonstrated that a noncanonical inflammasome reliant on mouse caspase-11 (known as caspase-4 in humans) is required in response to LPS-induced lethality and is essential for regulating macrophage lethality during *S. Typhimurium* infection^{185,186}.

1.3.2 The canonical inflammasomes

Canonical pyroptotic death is mediated by inflammasome assembly, which triggers caspase-1-dependent Gasdermin D (GSDMD) cleavage and IL-1 β and IL-18

release. Canonical inflammasome assembly is mediated by pyrin, members of NLRs (e.g., NLRP3, NLRC4, NLRP1 etc.), and pyrin and HIN domain-containing proteins (PYHIN) (e.g., AIM2). But less well-characterized pathways have also been reported to activate caspase-1, such as NLRP6, NLRP7, NLRP12, RIG-I (also known as DDX58), and IFN γ -inducible protein 16 (IFI16)^{187–190}.

1.3.2.1 NLRP1 inflammasome. As mentioned above, NLRP1 was the first protein identified to assemble an inflammasome complex¹⁷³. Humans carry a unique NLRP1 protein, which comprises a PYD, a NOD, LRRs, a function-to-find domain (FIIND), and a carboxy-terminal CARD. In contrast, mice encode multiple paralogs, like Nlrp1a, Nlrp1b, and Nlrp1c, which share a common domain architecture although they lack the PYD portion¹⁹¹ (Fig.1.2). Two of the five alleles of mouse *Nlrp1b* have been associated with susceptibility to lethal toxin of *Bacillus anthracis* (*B. anthracis*). Anthrax toxin is composed of three subunits: the metalloproteinase lethal toxin (LT), the adenylate cyclase edema toxin (ET), and the protective agent (PA). As their name suggests, the edema toxin is associated with the edema observed in patients with cutaneous anthrax infection, whereas the LT causes death in systemic anthrax infection¹⁹². Upon infection, the edema toxin forms a membrane channel that effectively translocates ET and LT into the cytosol of the host cell, where it causes rapid necrosis, probably related to the pathology of systemic infection. However, one study revealed that inbred strains of mice show different sensitivity to the lethal anthrax toxin. This difference was mapped to a highly polymorphic gene at the *Ltsx1* locus on chromosome 11, *Nlrp1b*. Furthermore, caspase-1 was found to be activated in LT-sensitive but not in resistant strains of mice, suggesting that *Nlrp1* may directly or indirectly mediate caspase-1 activity. Subsequently, it was found that Nlrp1b is activated by LT-mediated cleavage of the N-terminus, resulting in inflammasome assembly, IL-1 β release, and macrophage pyroptosis¹⁹³. Interestingly, anthrax toxin cleaves Nlrp1b in both toxin-sensitive and toxin-resistant macrophages, implying that additional events are required to fully activate the inflammasome^{194,195}. The requirement for Nlrp1b N-terminus cleavage was thought to maintain the receptor in a state of autoinhibition; this inhibition is overridden by proteolytic cleavage¹⁹⁶. However, this model contrasts with the finding that the autoinhibition state was maintained in Nlrp1b mutants in which the N-terminus was replaced with GFP,

highlighting that the N-terminus is dispensable to maintain NLRP1 in its inactive state¹⁹⁷.

Follow-up studies have proposed a “functional degradation” model, according to which the FIIND domain undergoes self-proteolysis generating two non-covalently peptides, ZU5 and UPA. The former is associated with the N-terminal portion of Nlrp1, and the latter with the C-terminal CARD domain (Fig.1.2 (1)). This self-processing is functionally important for triggering caspase-1 activation; in fact, LT-mediated N-terminal proteolysis triggers its ubiquitination and proteasomal degradation, releasing the UPA-CARD fragment and enabling caspase-1 recruitment and activation via CARD-CARD interaction¹⁹⁸ (Fig.1.2 (2)-(5)). Similarly, the *Shigella* secreted effector IpaH7.8, an E3 ubiquitin ligase, directly ubiquitinates the Nlrp1b N-terminal domain allowing its degradation and inflammasome activation¹⁹⁹ (Fig.1.2. (6)). The NLRP1 inflammasome also confers resistance against *T. gondii* and *L. monocytogenes*, probably by detecting a cellular perturbation, such as ATP depletion^{200–203}. Surprisingly, no Nlrp1b processing is detectable in response to *T. gondii*, raising the hypothesis of an activation mechanism other than the “functional degradation” model²⁰¹.

NLRP1 can also be activated by non-pathogenic triggers, such as Val-boroPro (VbP), a small molecules inhibitor of proteases like dipeptidyl peptidases (Dpp7, -8, -9 etc.). VbP-treated murine macrophages undergo Nlrp1- and caspase-1-dependent cell death, just as genetic depletion of Dpp8/9 leads to Nlrp1-dependent pyroptosis²⁰⁴. Structural analysis revealed that in resting cells the C-terminus of Nlrp1 containing CARD is sequestered into a ternary complex comprising full-length Nlrp1 and Dpp8/9. VbP weakens the Nlrp1-Dpp8/9 interaction by accelerating Nlrp1 N-terminus degradation and inflammasome assembly^{205,206} (Fig.1.2 (7)). Likewise, picornavirus proteases have been identified as activators of Nlrp1 by inducing its N-terminal degradation^{207,208}. Intriguingly, mouse and human NLRP1 are highly divergent. Mouse and human NLRP1 differ in their domain architecture: only human NLRP1 harbor an N-terminal PYD domain to interact with ASC. Interestingly, in humans but not in mice has been described another FIIND-containing protein CARD8 which activates the inflammasome. Human NLRP1 gets activated by enteroviral 3C proteases, which cleaves the N-term portion of NLRP1 promoting the C-terminal assembly into inflammasome complex, and by viral dsRNA²⁰⁹.

A recent study showed that the Kaposi's sarcoma-associated herpesvirus (KHSV) tegument protein ORF54 activates NLRP1 in a "functional degradation"-independent manner. A biochemical approach demonstrated that, along with the ternary complex, the N-terminal and C-terminal of NLRP1 can form a complex stabilized by a linker region between the N-terminal domain and the UPA portion of the C-terminal domain in which DPP8/9 is dispensable. The authors therefore hypothesized that in these complexes ORF54 competes with C-terminus to bind the linker region, thus liberating the UPA-CARD for inflammasome assembly²¹⁰.

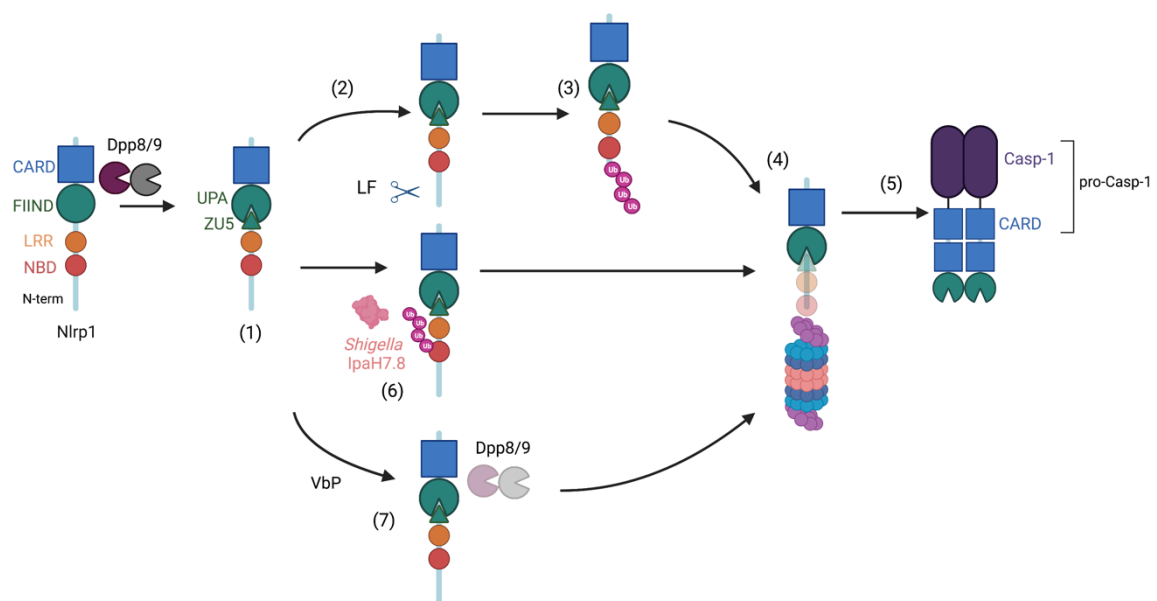


Figure 1.2 NLRP1 inflammasome. Nlrp1 self-processing within the FIIND domain generates two non-covalently associated fragments (1). LT-mediated N-terminal cleavage (2-3), or *Shigella* IpaH7.8-mediated ubiquitination (6), results in proteasomal degradation of the N-terminal fragment and release of the C-terminal portion (4). The Nlrp1 C-terminal fragment assembles the inflammasome by recruiting caspase-1 (5). Proteasome-dependent degradation of Nlrp1 N-terminal fragment can be achieved by using VbP, which weakens Dpp8/9-Nlrp1 interaction accelerating N-terminal degradation (4).

1.3.2.2 NLRP3 inflammasome. The inflammasome has been recognized as crucial for host defense against pathogens and its dysfunction is linked to the development of cancer, autoimmune diseases, and metabolic and neurodegenerative disorders. It is therefore not surprising that its expression is tightly regulated^{211,212}. Indeed, NLRP3, as well as other inflammasome receptors, requires a two-step activation

process. The first step, so-called “priming” or “signal 1”, represents an essential event to trigger the upregulation of the mRNA and protein of inflammasome components, such as NLRP3, proinflammatory cytokines, and caspase-1, as well as factors that control post-translational modification (e.g., ubiquitination, phosphorylation, sumoylation) which license receptor functions. The priming is induced by extracellular inflammatory stimuli which comprise PAMPs or DAMPs, that engage TLRs, or inflammatory cytokines, such as the TNF and IL-1 β , which trigger NF- κ B gene transcription^{213–215} (Fig.1.3).

The second step, or “signal 2”, directly promotes NLRP3 activation and assembly. NLRP3 is a tripartite protein with an amino-terminal pyrin-domain, a central NACHT domain, which has ATPase activity important for NLRP3 self-assembly, and a carboxy-terminal LRR domain thought to drive autoinhibition by folding back onto the NACHT domain. In response to certain stimuli, NLRP3 oligomerizes through homotypic interaction within the NACHT domains, an event that triggers the recruitment of the adaptor protein ASC through the PYD domain and the nucleation of ASC filaments, which converge into a macromolecule known as the ASC speck^{216,217}. In turn, the ASC speck engages caspase-1 through CARD-CARD interaction, enabling self-proteolysis and proximity-induced caspase-1 activation. Indeed, caspase-1 is composed of a CARD domain, a large central catalytic domain (p20), and a small catalytic subunit at the C-terminus (p10). Cluster formation on ASC leads to self-cleavage of the region between the p20 and p10 segments, which is the proteolytically active domain²¹⁸ (Fig.1.3).

NLRP3-mediated caspase-1 activation has been associated with a wide variety of stimuli, like crystals, pore-forming toxins, nigericin, extracellular ATP, and infection by several pathogens. Although researchers have focused on finding a common cellular event triggered by all activators, multiple activation mechanisms have been proposed. These include ion fluxes, lysosomal disruption, mitochondrial dysfunction, and trans-Golgi disassembly²¹⁹. Notably, Munoz-Parillo et al. proposed a unified model whereby all NLRP3 agonists induced cell membrane permeabilization to potassium ions (K⁺). Specifically, a decreased concentration of intracellular K⁺ was sufficient to trigger NLRP3-dependent caspase-1 activation. Yet, it remains to be determined whether NLRP3 is able to sense potassium levels directly or whether an additional event correlates its activation with intracellular potassium concentration²²⁰.

Furthermore, several reports have identified NIMA-related kinase 7 (NEK7), a serine-threonine kinase originally linked to mitotic spindle formation and centrosome separation, as a component of the NLRP3 inflammasome. Mechanistically, NEK7 acts downstream of K⁺ efflux and binds NLRP3 through its catalytic domain, although its catalytic activity is not required for activation of the NLRP3 inflammasome. NEK7 binding is essential for the optimal formation of the inflammasome complex; in fact, depletion of NEK7 in mouse macrophages abrogates caspase-1 activation and IL-1 β release downstream of potassium efflux^{221–223} (Fig.1.3). Recently, a new report proposed that NLRP11 is also a component of the NLRP3 inflammasome. Specifically, it binds NLRP3 and ASC allowing receptor oligomerization and ASC filaments polymerization. Human macrophages deficient for NLRP11 showed defective NLRP3-dependent caspase-1 activation and proinflammatory cytokines release. Interestingly, NLRP11 is also necessary for the inflammasome-driven response by cryopyrin-associated periodic syndromes (CAPS)-related NLRP3 mutants²²⁴.

Gain-of-function mutations of NLRP3 are associated with the dominantly inherited autoinflammatory disease known as CAPS. CAPS encompasses diseases with different severity levels, such as the familial cold autoinflammatory syndrome, the Muckle–Wells syndrome, and the neonatal-onset multisystem inflammatory disorder^{182,183,225}.

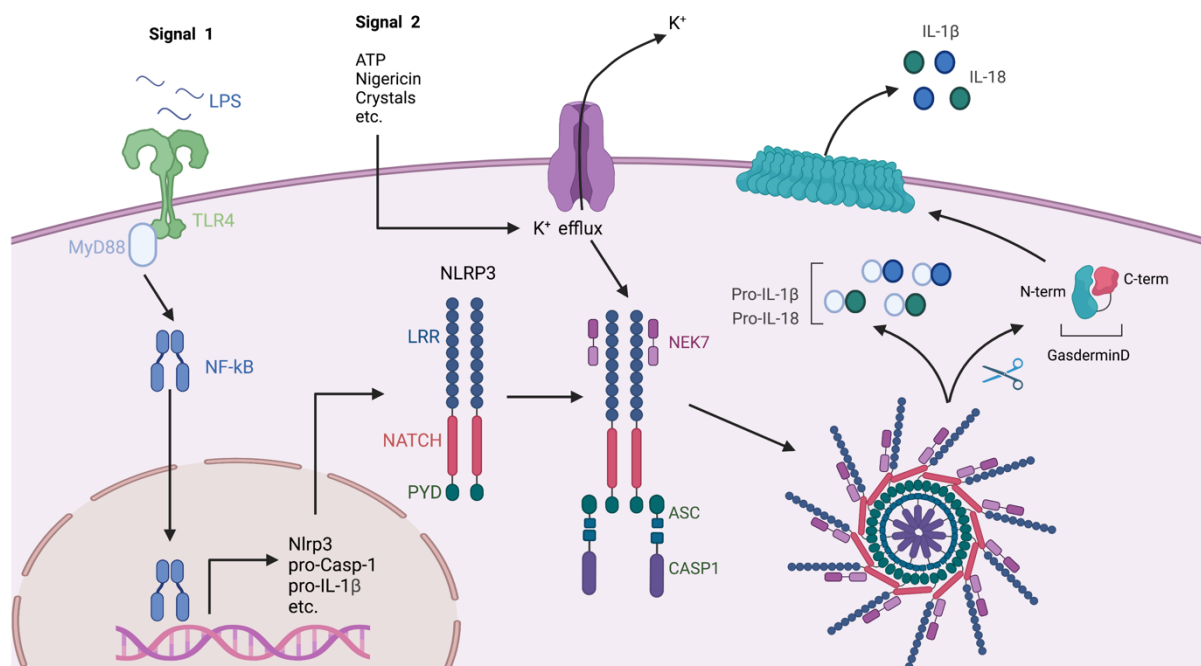


Figure 1.3 NLRP3 inflammasome. “Signal 1” triggers NF-κB-dependent transcription of several inflammasome-related genes (e.g., pro-caspase-1, pro-IL-1β, Nlrp3 etc.). Potassium efflux is associated with a variety of NLRP3 stimuli and triggers inflammasome assembly. NLRP3 triggers caspase-1 recruitment and auto-processing via ASC. NEK7 interacts with the LRR domain of NLRP3 and it is required for complex formation. Caspase-1 processes pro-IL1β and pro-IL18 to their mature forms and cleaves GSDMD, whose N-terminal assembles pores in the membrane. GSDMD pores allow the release of IL-1β and IL-18 from the cell.

1.3.2.3 NLRC4 inflammasome. NLRC4 was originally identified for its structural homology with the apoptotic protein Apaf-1, hence it was also initially called Ipaf. But the presence of an amino-terminal CARD domain, a central nucleotide-binding domain, and a carboxy-terminal LRR domain, together with its ability to activate proinflammatory caspase-1 through CARD-CARD domain interaction, soon re-classified it as an inflammasome receptor²²⁶.

NLRC4 activation was related to pathogen detection, as murine macrophages lacking NLRC4 failed to activate caspase-1 in response to *S. Typhimurium* infection²²⁷. Follow-up studies demonstrated that the *Salmonella*-derived agonist responsible for NLRC4 inflammasome activation is bacterial flagellin present in the host cell cytosol^{228,229}. Later it was shown that NLRC4 also responds to rod and needle subunits of bacterial T3SSs, a secretion system used by bacteria to deliver virulence factors into the cytosol of the host cell²³⁰.

Surprisingly, NLRC4 does not directly detect bacterial-derived products but exploits NLR family apoptosis inhibitory proteins (NAIPs) as upstream receptors^{231,232}. While mice have several NAIPs that serve as bona fide receptors for flagellin (NAIP5, NAIP6), rod proteins (NAIP2), and needle proteins (NAIP1), humans have only one NAIP that senses needle proteins. Thus, human NLRC4 does not respond to either bacterial flagellin or T3SS rod proteins (Fig.1.4)^{231,232}. Notably, purified primary human macrophages from healthy donors express a full-length NAIP isoform no longer expressed in monocytic tumor cells, rendering them sensitive to bacterial flagellin²³³.

Unlike other inflammasomes, an early study showed that NLRC4 can function independently of ASC²³⁴. The Cryo-EM structure of NLRC4 assembly further confirmed that NLRC4-CARD and ASC-CARD form filaments with an identical assembly pattern, thus validating that NLRC4 can directly recruit caspase-1 via homotypic CARD domain interaction or indirectly via ASC^{235–237}.

Because the NLRC4 inflammasome triggers a strong proinflammatory response against pathogenic Gram-negative bacteria, its expression is tightly regulated by transcriptional and post-translational modifications to prevent unregulated activation. Specifically, it is upregulated by TNF and genotoxic stress-mediated p53 activation, although the basal level of NLRC4 expression is sufficient to trigger inflammasome activation^{238,239}. In addition, phosphorylation has been reported to be important for NLRC4 activation; in particular, protein kinase C delta (PKC δ) and leucine-rich repeat-containing kinase-2 (LRRK2) have been reported to be involved in NLRC4 inflammasome phosphorylation and its subsequent activation^{240,241}. However, the involvement of PKC δ remains controversial, as other studies have found that it is not required for IL-1 β release during *Shigella* and *Salmonella* infection²⁴². Interestingly, β -arrestin, a key regulator of the G-protein-coupled receptor signaling pathway, interacts with NLRC4 and promotes its self-oligomerization. The relevance of β -arrestin in inflammasome assembly and activation was confirmed by an in vivo infection model; in fact, not only did β -arrestin deficiency rescue the weight loss observed in wild-type mice infected with *Salmonella* in the log phase but also less IL-1 β was detected²⁴³.

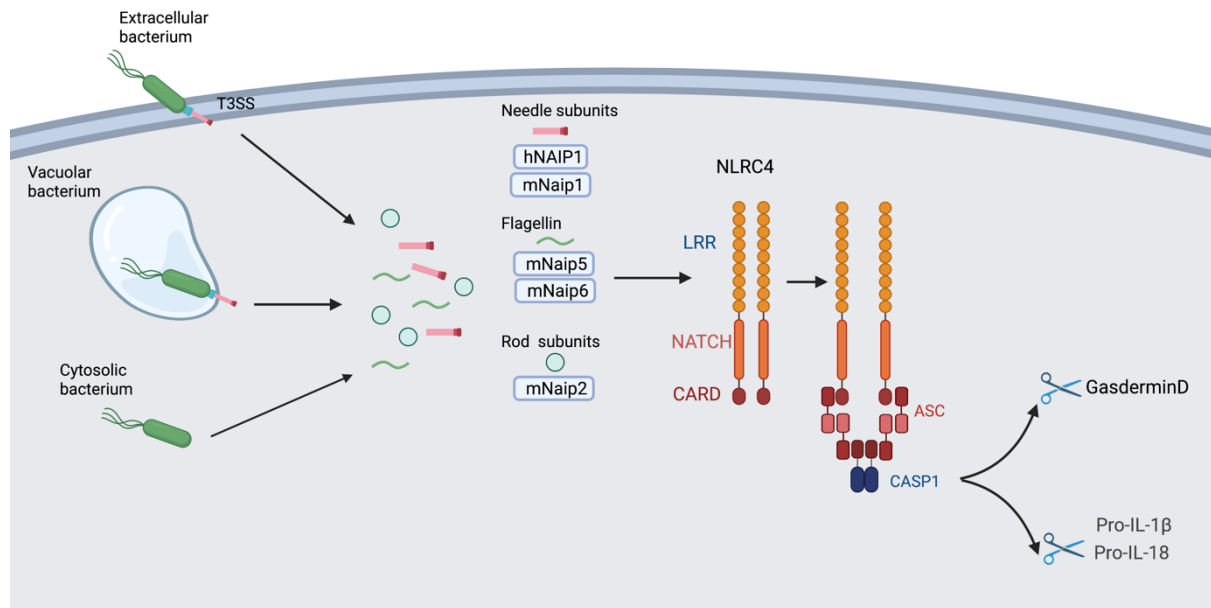


Figure 1.4 NLRP4 inflammasome. NAIP proteins directly recognize the needle and rod subunits of T3SS and flagellin. Ligand binding results in NAIP activation, allowing NLRP4 activation. NLRP4 drives caspase-1 recruitment and activation in an ASC-dependent manner, triggering GSDMD pore formation and IL-1 β /18 maturation.

1.3.2.4 AIM2 inflammasome. The discovery that viral, bacterial, and host cytoplasmic DNA activates caspase-1 in an ASC-dependent but NLRP3-independent manner led to the hypothesis of the existence of a cytosolic DNA sensor²⁴⁴. Subsequently, this cytosolic receptor was identified to be Absent in melanoma 2 (AIM2)^{245–247}. Unlike the NLR inflammasome, it features a bipartite domain structure with an N-terminal PYD and a C-terminal HIN domain²⁴⁸ (Fig.1.5). Early studies demonstrated that upon dsDNA engagement, the AIM2 PYD domain is responsible for the recruitment of the adaptor protein ASC and the subsequent inflammasome assembly^{245,246} (Fig.1.5). Mechanistically, it has been proposed that in the absence of double stranded (ds)DNA, the interaction between the PYD domain and the HIN domain maintains AIM2 in a state of autoinhibition. This autoinhibition is released by the binding of dsDNA to the HIN domain through electrostatic interactions^{249,250} (Fig. 1.5). However, Morrone et al. found that the PYD domain of AIM2 does not have an inhibitory function and that the absence of AIM2 inflammasome activation under uninfected conditions is due to its low basal expression level. Instead, its assembly depends on an increase in concentration detected following proinflammatory stimuli and dsDNA size²⁵¹.

The generation of *Aim2*-deficient mice immediately highlighted its role in host defense mechanisms against viruses such as cytomegalovirus and vaccinia virus²⁵² (Fig.1.5). Later studies extended its importance to innate immune defense against intracellular bacteria, mainly *F. novicida* or *L. monocytogenes*. Cytosolic *Francisella* is targeted by murine Gbp2 and Gbp5. However, mGbp2 and mGbp5 overexpression was not sufficient to trigger cell death, indicating that bacteria-related Aim2 inflammasome activation requires additional activation steps that trigger lysis of the intracellular pathogen²⁵³. Indeed, the bacteriolytic activity was attributed to Irgm10, which targets the bacteria in a GBP-dependent manner^{254–258} (Fig.1.5). Overactivation of the AIM2 inflammasome has been associated with several diseases (e.g., psoriasis, systemic lupus erythematosus, etc.), while its downregulation is associated with prostate and colorectal cancer^{259–262}. However, it is unknown if its role in tumor progression is related to dsDNA sensing.

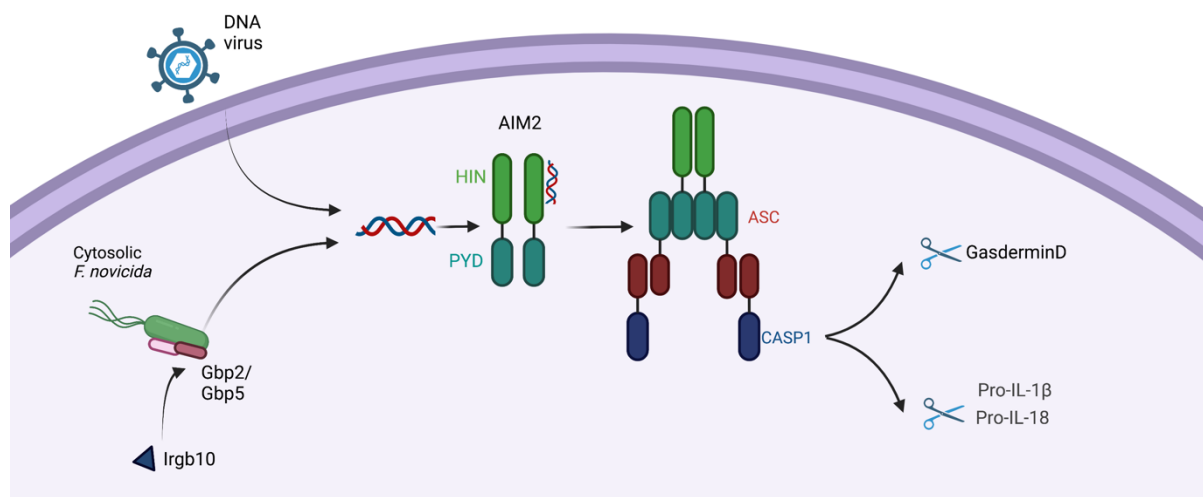


Figure 1.5 AIM2 inflammasome. AIM2 senses bacterial and viral cytosolic dsDNA. It recruits caspase-1 through ASC. Irgb10 is recruited on bacteria in a Gbp-dependent manner. Its membranolytic activity is required to liberate bacterial DNA in the host cell cytosol for Aim2 sensing. Caspase-1 proximity-induced autoproteolytic activation within the complex leads to IL-1β/18 processing and GSDMD cleavage.

1.3.2.5 Pyrin inflammasome. Pyrin is encoded by the MEFV gene and features a PYD domain, a zinc-finger domain named B-boxes, and a coiled-coiled domain. Human pyrin has an additional carboxy-terminal domain, named B30.2 domain, which mutations have been associated with familial Mediterranean fever (FMF), an

autoinflammatory disease^{263,264}. Unlike the other previously mentioned inflammasome activation mechanisms, the pyrin inflammasome senses RhoA GTPase-mediated modification and inactivation by various RhoA-inactivating toxins, such as TcdB of *Clostridium difficile*, VopS of *Vibrio parahaemolyticus*, and IbpA of *Histophilus somni*²⁶⁵. However, it was unclear how pyrin recognizes RhoA GTPase inactivation. It was shown that pyrin co-localizes with polymerizing actin and it was hypothesized that it may sense a disturbance in the actin cytoskeleton dynamics²⁶⁶. Moreover, mice homozygous for a hypomorphic allele of Wdr1 (Wdr1^{rd/rd}), a protein required for actin filaments disassembly, exhibit autoinflammatory disease and thrombocytopenia. Inflammation in these mice is indeed associated with pyrin inflammasome activation²⁶⁷. Follow-up studies have elucidated the mechanism by which the pyrin inflammasome senses RhoA inhibition. Pyrin is phosphorylated on two serine sites (S208, S242) by RhoA effector kinases, protein kinase N1 and N2 (PKN1/2), which belong to the protein kinase C (PKC) superfamily^{268,269}. At steady state, phosphorylation keeps pyrin inactive by promoting its binding to the chaperone protein 14-3-3²⁶⁸. Bacterial toxin-mediated RhoA inhibition leads to pyrin dephosphorylation and subsequent release of 14-3-3 that enables assembly and activation of pyrin inflammasome^{268,269}. Yet, pyrin dephosphorylation is not sufficient to trigger ASC speck formation and subsequent caspase-1 activation²⁷⁰. Low concentrations of steroid hormone catabolites, specifically etiocholanolone and pregnanolone, are also required for pyrin-dependent ASC oligomerization following pyrin de-phosphorylation. While high concentrations of etiocholanolone and pregnanolone rapidly trigger pyrin inflammasome activation and ASC-dependent caspase-1 activation in the absence of RhoA inhibition²⁷¹. Interestingly, pyrin activation in response to high concentrations of steroid catabolites is human-specific, as it depends on the B30.2 domain that is absent in mice²⁷¹.

1.3.2.6 Other inflammasomes. Another inflammasome is IFI16 and its murine orthologue IFI204, which have been implicated in STING-dependent production of type I IFN along with the cytosolic DNA sensor cGAS in HSV1 and Francisella infection, respectively^{272,273}. IFI16-mediated caspase-1 inflammasome activation was also detected upon KSHV and HIV infection, suggesting a potential role as a cytosolic nucleic acid sensor^{274–276}.

NLRP6 has also been investigated as forming another potential inflammasome. First, its deficiency in mouse colonic epithelial cells is associated with decreased IL-18 and altered fecal microbiota. In addition, *Nlrp6*^{-/-} mice develop spontaneous intestinal hyperplasia and are more susceptible to chemical-induced colitis²⁷⁷. The ligands that trigger NLRP6-dependent IL-18 production have been investigated in several microbiota-derived metabolites²⁷⁸. However, the exact mechanism by which proinflammatory cytokines are produced has not yet been defined. NLRP6 activation has been also observed in response to lipoteichoic acid (LTA), a component of the Gram-positive bacterial cell wall, or to *L. monocytogenes* infection. Interestingly, it has been proposed that NLRP6 activation by these stimuli triggers caspase-11 processing which, in turn, promotes caspase-1 activation²⁷⁹. Another report also suggests that NLRP6 detects RNA in the cytosol by forming signaling hubs via liquid-liquid phase separation²⁸⁰. Several reports indicate that NLRP6 dampens NF-κB activity^{281,282}. For instance, NLRP6-deficient mice are also highly resistant to infection with intracellular and extracellular bacteria (e.g., *L. monocytogenes*, *S. Typhimurium*, *E.coli*), leading to the hypothesis that, contrary to other inflammasomes, NLRP6 downregulates TLR-mediated NF-κB and MAPK signaling²⁸².

NLRP10 has also been associated with inflammatory-inhibitory functions. In particular, earlier studies suggest it blocks ASC-mediated NF-κB activation and caspase-1-dependent IL-1β maturation^{283,284}. In contrast, a recent study from Próchnicki and coworkers reveals that NLRP10 surveils mitochondria integrity. Indeed, it senses mitochondrial damage leading to ASC speck formation and caspase-1 recruitment. Remarkably, NLRP10-mediated inflammasome activation is independent of mitochondrial DNA cytosolic leakage²⁸⁵.

NLRP9b is expressed in intestinal epithelial cells and has been identified as a cytosolic inflammasome sensor for Rotavirus. Zhu S. et al. found that NLRP9b forms inflammasome complexes through ASC and caspase-1 by detecting short double-stranded RNA sequences via the RNA helicase DHX9²⁸⁶.

1.3.3 Non-canonical inflammasome.

Rather than activating caspase-1, the non-canonical pathway activates human caspase-4/-5 or mouse caspase-11 and serves as a cytosolic detection mechanism

for LPS, the major component of Gram-negative bacteria cell wall, in the host cell cytosol^{185,186,287,288}. The discovery of the non-canonical pathway dates back to 2011, when Kayagaki et al. showed that caspase-1-deficient mice used at the time also lacked a functional allele of caspase-11, and that in response to certain inflammasome activators caspase-11 but not caspase-1 mediates pyroptosis without requiring additional inflammasome components such as NLRP3 or the adaptor protein ASC¹⁸⁵. Notably, IL-1 β release under those conditions was dependent on both caspase-11 and caspase-1, NLRP3, and ASC, suggesting downstream secondary activation of NLRP3, termed noncanonical NLRP3 inflammasome activation^{289–293}.

Surprisingly, caspase-11 was designated as the effector of LPS-induced lethal septic shock, which was originally thought to be driven exclusively by TLR4^{185,287,288}. Indeed, induction of caspase-11 by poly(I:C) treatment renders *Tlr4*^{-/-} mice susceptible to LPS-induced lethality, meaning that caspase-11 directly drives LPS-induced endotoxemia whereas TLR4 only primes this response^{287,288}. This finding revealed that host cells have evolved two different mechanisms to sense extracellular and intracellular LPS. Besides LPS, oxidized 1-palmitoyl-2-arachidonoyl-sn-glycero-3-phosphorylcholine (oxPAPC), a DAMP released from dying cells, has been identified as an endogenous caspase-11 ligand in mouse dendritic cells. Interestingly, oxPAPC-induced caspase-11 activation elicits the release of IL-1 β but not cell pyroptosis²⁹⁴. In contrast to this work, Chu et al., demonstrated that oxPAPC acts as an inhibitor of the non-canonical inflammasome by competing with caspase-11 and -4 for LPS binding. Moreover, in vivo, it antagonizes sepsis in a septic shock mouse model, profiling oxPAPC as an anti-inflammatory regulator²⁹⁵.

Recently, tyrosine kinase 2 (TYK2), a cytokine receptor-associated kinase, was delineated as an upstream regulator of caspase-11, probably by amplifying the activation of caspase-11 transcriptional regulator STAT1²⁹⁶. The IFN-inducible protein Irgm2 and Gate16 have also been shown to dampen non-canonical inflammasome activation in response to LPS transfection and Gram-negative bacteria infection^{297–299}. Surprisingly, Irgm2-deficient mouse macrophages displayed aberrant activation of caspase-11 when exposed to extracellular LPS, Gram-negative bacteria, or bacterial outer membrane vesicles (OMVs)²⁹⁹.

Although caspase-5 and caspase-11 share structural similarities, caspase-4 is considered the human functional homolog of caspase-11. For instance, Casson et al. found that in primary human macrophages caspase-4 mediates pyroptosis and IL-1 β secretion upon diverse Gram-negative bacteria infection. In contrast, caspase-5 appears to have no detectable role in mediating such cell death³⁰⁰. However, it has been reported that caspase-11 as well as caspase-4 and -5, can directly bind the lipid A moiety of the LPS through their N-terminal CARD domain. Since CARD-containing receptors are dispensable for LPS-induced cytotoxicity, those caspases have been considered direct sensors of cytosolic LPS³⁰¹. How LPS activates the noncanonical inflammasome, however, has been extensively studied, and several studies have reported that rather than direct recognition of LPS through caspases, ISGs are critical for initiating the pathway^{186,302}. The role of IFN-stimulated genes, mainly GBPs, in triggering inflammasome-mediated cell death will be better described in the following paragraphs.

1.3.4 The pyroptotic executor GasderminD (GSDMD).

In humans, the GSDM superfamily is composed of GSDMA, GSDMB, GSDMC, GSDMD, GSDME (also called DFNA5), and DFNB59 (Gsdma1-3, Gsdmc1-4, Gsdmd, Dfna5, and Dfnb59 in mice). The first member of the family to be identified was GSDMA, which is expressed uniquely in the gastrointestinal tract and skin of mice³⁰³. By sequence homology, several other GSDMs have been identified and gain-of-function mutations in these proteins were linked to different diseases, such as the alopecia-like skin mutation in mice and the autosomal dominant non-syndromic hearing loss in humans^{303,304}. However, their biological functions were unknown, although early studies characterized their possible role in cytotoxicity. Indeed, cells transfected with the carboxy-terminal domain of GSDME showed an apoptotic phenotype, whereas transfection into *Saccharomyces cerevisiae* caused growth arrest^{305,306}.

Pyroptosis was later defined as GSDM-mediated cell death. GSDMD was found to be a direct substrate of noncanonical caspases, which, in contrast to caspase-1, process GSDMD independently of NLRP3 and ASC^{289,307,308}. Interestingly, caspase-1 efficiently processes the proinflammatory cytokines IL-1 β and IL-18 along with GSDMD, whereas caspase-11 processing is limited to GSDM exclusively³⁰⁹.

Structurally, with the exception of DFNB59, which has a smaller C-terminal domain, all GSDMs exhibit a two-domain structure connected by a flexible region. Caspases cleave GSDMD in the linker region generating an N-terminal fragment (GSDMD-NT) with intrinsic pore-forming properties, and a C-terminal fragment (GSDMD-CT) that acts as a repressor^{289,307,308}. Indeed, overexpression of GSDMD-NT causes pyroptosis, whereas GSDMD-CT overexpression blocks cell death³⁰⁷. Hence, the cytosolic sensors (e.g., NLRP3, NLRP1, NLRC4, AIM2 etc.) after PAMPs or DAMPs recognition recruit directly or indirectly pro-caspase-1, which, once activated, process GSDMD, IL-1 β , and IL-18. Unlike the canonical inflammasome, LPS-mediated caspase-11 (or caspase-4) oligomerization allows direct cleavage of GSDMD but not cytokine maturation. GSDMD-NT pore-driven plasma membrane permeabilization triggers pyroptosis, cell lysis and proinflammatory cytokine release. Interestingly, upon activation of the noncanonical inflammasome, GSDM pores allow potassium efflux, which, as a result, activates the NLRP3 inflammasome and, consequently, the maturation of IL-1 β and IL-18.

Although GSDMs display sequence similarities, the caspase-1 cleavage site of GSDMD (FLTD in humans and LLSD in mice) is not detected in other GSDMs, but some of them bear an apoptotic-caspase cleavage site. For example, GSDME can be cleaved by caspase-3 in its linker region³¹⁰. Cleavage and activation of GSDME by caspase-3 directly triggers pyroptosis or secondary necrosis after the initiation of apoptosis^{310,311}. On the other hand, caspase-3 negatively regulates GSDMD by cleaving within the amino-terminal domain^{310,312,313}, in contrast to pharmacological or pathogen-induced inhibition of NF- κ B (i.e. TAK1) which results in a caspase-8-mediated GSDMD pore formation^{312,314,315}.

Besides caspases, GSDMD can be cleaved by elastase, a neutrophil-specific protease, in a motif upstream of the caspase cleavage site that still results in a functional N-terminal pore-forming fragment^{316,317}. Notably, in *Gsdmd*-deficient mice, delayed neutrophil death is associated with enhanced host response against *E. coli*³¹⁷. In contrast, other reports linked GSDMD pores to the formation of neutrophil extracellular traps (NETs), a neutrophil-specific cell death that releases chromatin in the extracellular space^{316,318}. Hence, GSDMD can be considered pleiotropic, since it has been described to exert both anti- and pro-inflammatory effects.

Cleavage of GSDMD favors interaction of the N-terminal fragment with membrane lipids, where it forms ring-like structures (pores)^{319–322}. In vitro binding assays demonstrated that GSDMD-NT binds to phosphatidylinositol and phosphatidylserine phosphates, found exclusively in the inner leaflet of the cell membrane, and to cardiolipin in the inner and outer leaflets of bacterial membranes and in mitochondria inner membrane^{319,320}. Similarly, the N-terminal domain of murine GSDME, GSDMA, and GSDM3A show lipid binding affinity^{311,319}. Remarkably, the full-length GSDMB exhibited lipid-binding properties comparable to those of GSDMB-NT alone, suggesting that GSDMB-CT does not exert an inhibitory function³²³. Furthermore, high-resolution atomic force microscopy showed that GSDMD-NT inserts into a variety of lipid compositions where it assembles pores regardless of whether it has been cleaved by caspase-1, -4 or -5. Interestingly, a limiting factor in its ability to insert and form pores was identified to be the presence of cholesterol³²⁴. Apart from phospholipids, sphingomyelin strongly promotes the association of GSDMD-NT with lipid membranes; indeed, its exclusion from liposomes dampens pore formation³²¹. Pore structure and composition have been extensively studied using murine GSDMA3 as a model. At a steady state, the interaction of the N-terminal domain with the C-terminal domain maintains GSDMD3A in an autoinhibited state³¹⁹. A cryo-EM structure of GSDM pores shows that caspase-mediated disruption of autoinhibition causes drastic conformational changes in the two domains. These changes generate interfaces that guide the insertion of a GSDM-NT in the membrane. Their oligomerization results in a large pore with a 27-fold symmetry with an inner diameter of around 180 Å, an outer diameter of around 280 Å, and a height of around 70 Å³²⁵. As expected, electrostatic pore surface analysis of GSDM3A revealed that the transmembrane portion of the pores facing the lipid membrane is highly hydrophobic, while the inner leaflet contains hydrophilic residues with positive and negative charges³²⁵. At last, GSDM pores cause pyroptotic cell death.

Pyroptotic cells are characterized by membrane blebbing and subsequent ballooning, eventually leading to loss of membrane integrity. Plasma membrane rupture (PMR) has to date been defined as a passive osmotic lysis event³²⁶. Recently, a landmark study by Kayagaki et al. showed that the cell-surface protein ninjurin 1 (NINJ1) is essential in inducing PMR in response to pyroptotic, apoptotic, and necroptotic stimuli. Indeed, *Ninj1*^{-/-} macrophages exhibit defective release of intracellular proteins (e.g., LDH, HMGB1, etc.) but not impaired IL-1 β release, which

is mediated by GSDMD pores. Despite undergoing cell death – as measured by loss of ATP, mitochondrial membrane potential, and motility – cells lacking NINJ1 continue ballooning as bubbles never disintegrate. Therefore, this report separates PMR and GSDMD-mediated cytokine release as two genetically separate events. The signaling cascade that triggers NINJ1 activation and its exactly mechanism remained to be determined³²⁷. Overall, pyroptosis is considered an inflammatory cell death since the release of cytokines and intracellular molecules that acts as alarmins and “find me” signals can activate the immune response¹⁷².

1.3.4.1 Sub-lytic cell death. Several studies have reported a GSDMD-dependent release of inflammatory cytokine that occurs independently of cell lysis, defined as a sub-lytic cell death^{294,328–330}. Notably, the positive charges of IL-1 β precursors are exposed upon proteolytic cleavage by caspases, which favor mature IL-1 β release via GSDMD pores by electrostatic filtering³³¹.

Aside from IL-1 β and IL-18, lysis-independent functions of GSDM pores are thought to mediate several cytosolic proteins release, such as galectins and small GTPases³³². Moreover, GSDMD pores have an impact on ion flux²⁹³. For instance, they trigger activation of the noncanonical NLRP3 inflammasome in response to bacterial LPS causing potassium efflux. Similarly, activation of the AIM2 inflammasome in response to *L. pneumophila* causes potassium efflux, which triggers the NLRP3 inflammasome and restrains cGAS-dependent IFN- β response by disrupting ionic homeostasis^{333,334}.

Remarkably, GSDM pores formation can be reversible. Indeed, GSDMD-mediated calcium efflux serves as a signal to initiate membrane repair through the recruitment of the endosomal sorting complexes required for transport (ESCRT) machinery³³⁵.

1.4. Guanylate-binding proteins

1.4.1 Interferon-inducible GTPases.

Cells represent a nutrient source for many pathogens. Therefore, all eukaryotic cells, from protozoan to metazoan, have developed mechanisms to fight off intracellular pathogens. The capacity of a single host cell to control and possibly eliminate threats is termed cell-autonomous immunity, encompassing the detection of pathogens and the execution of effector pathways to counteract infection. Pro-inflammatory cytokines spatially and temporally regulate such effector pathways by controlling the expression of host defense proteins. The three types of IFNs have a central role in orchestrating cell-autonomous immunity by promoting the expression of ISRE- and GAS-related IFN-stimulated genes^{61,62,70}. Amongst the ISGs, four families of GTPases are prominently induced in IFNs-primed cells: the Myxovirus resistance proteins (Mx), IRGs, GBPs, and the very large IFN-inducible GTPases (VLIGs). All the IFN-inducible GTPase families share similarities with dynamin proteins: large GTPases with μM affinity for guanine nucleotides, and a high basal rate of GTP hydrolysis. GTP hydrolysis triggers self-assembly into large homotypic complexes^{336–339}. In all the GTPases, the guanine nucleotide binding site comprises of five motifs termed G1-G5, which mediate guanine nucleotide recognition, binding, and exchange³⁴⁰. The active or inactive conformation of GTPases is determined by the GTP- or GDP-bound form respectively. The transition between these forms can be mediated by additional proteins: the guanine nucleotide dissociation inhibitors (GDIs), which keep the GTPase in their inactive form by preventing GDP dissociation, the guanine nucleotide exchange factors (GEFs), that accelerate GTP binding, and the GTPase-activating proteins (GAPs), which accelerate its hydrolysis³⁴¹. Among the GTPases, GBPs are quite unique, since they require neither GDIs nor GEFs. While the role of the IFN-inducible GTPases Mx, IRGs, and GBPs in host-defense mechanisms has been extensively studied^{91,128–130}, functional studies on VLIGs have not been reported, even though they are strongly expressed in mice and zebrafish upon IFNs stimulation^{342,343}, suggesting that they might serve a function in the host defense. In humans, a single homolog of VLIGs proteins has been identified on chromosome 11³⁴³.

1.4.1.1 Biochemical and structural analysis of GBPs. GBPs are dynamin-like GTPase that are composed of an N-terminal globular large GTPase domain (LG) and an α -helical domain that consist of a middle domain (MD) and a C-terminal GTPase effector domain (GED) (Fig.1.6 a). At a steady state, the C-terminal GED domain folds over the MD and LG domains (Fig.1.6 b (1))³⁴⁴. GTP binding to monomeric GBPs is mediated by the G-motifs (Fig.1.6 b (1)). In the nucleotide-binding pocket, the G1 motif (also known as P-loop) binds the GTPase cofactor Mg^{2+} and wraps around the phosphate groups of the GTP, while the G2 and the G3 motifs coordinate the Mg^{2+} and bind the phosphate groups of the nucleotide^{345–347}. Two unique and highly flexible regions differentiate the GBPs from other GTPases: the phosphate cap, which contains the G2 motif, and the guanine cap, which shapes a hydrophobic pocket for the guanine base. Both contribute to the stabilization of the ribose moiety of the GTP³⁴⁵. Upon nucleotide binding, the guanine cap promotes GBPs dimerization via LG-LG interaction (Fig.1.6 b (2)). The conformational changes following nucleotide hydrolysis, also disrupt a network of salt bridges between the α -helix in the LG domain and aspartate residues in the GED domain, promoting the GED unfolding within the dimers (Fig.1.6 b (3))^{348–350}. Furthermore, relocation of residues in the P-loop and the phosphate cap in the dimers accelerates GBPs hydrolytic activity (Fig.1.6 b (4-6))^{345–347}.

Unlike the other IFN-inducible GTPases, GBPs can also exert GDPase activity. Indeed, they bind in equimolar affinity GTP and GDP to produce GMP. This unusual nucleotide binding can be traced to the presence of a non-canonical TLRD- or TVRD-G4 motif instead of the typical N(T/Q)KXD sequence³⁵¹. Moreover, contrary to other GTPase, GBPs have an internal GAP region that obviates the need for external GAPs and is responsible for a high two-step reaction rate of GTPase and GDPase activity^{346,352–354}. It has been shown that GMP production is favored by dimeric GBPs in their open conformation, in fact, mutants of GBPs lacking the GED domain produce more GMP than wild-type GBPs (Fig.1.6 b (5-6)). This led to the hypothesis that interaction between the GED domain and the LG domain inhibits the GMP production^{348,350}.

As dynamin-like GTPases, the GBP-mediated hydrolysis of GTP to GDP drives their self-assembly in large complexes which target pathogen-associated membranes and bacterial surfaces^{350,355,356}. Both N- and C-terminal domains contribute to the GBP

self-assembly, and it was shown that truncated forms of GBPs that lack the GED or the LG domain fail to polymerize^{350,355}. However, the engagement of GBPs on PCVs or on bacterial cell walls relies on post-translational modifications at the C-terminus. For instance, membrane binding of mouse and human GBP1, -2 and -5 is facilitated by a CaaX box at the C-terminus that can be farnesylated or geranylgeranylated, via the addition of 15-Carbon farnesyl or 20-carbon geranylgeranyl hydrophobic groups on the cysteine residue in this CaaX motif. Besides the membrane targeting, farnesylation of human GBP1 could also serve as a signal to deposit additional GBP1 on membranes³⁵⁷, similar to what has been hypothesized for mouse Gbp1 geranylgeranylation³⁵⁸. GBP membrane-bound complexes constitute sensory platforms that alert and activate host antimicrobial defense; modifications of the CaaX motif, including truncation of the C-terminus, disrupt their ability to associate into complexes^{359–361} and, in turn, the cell-autonomous immune response^{362–365}.

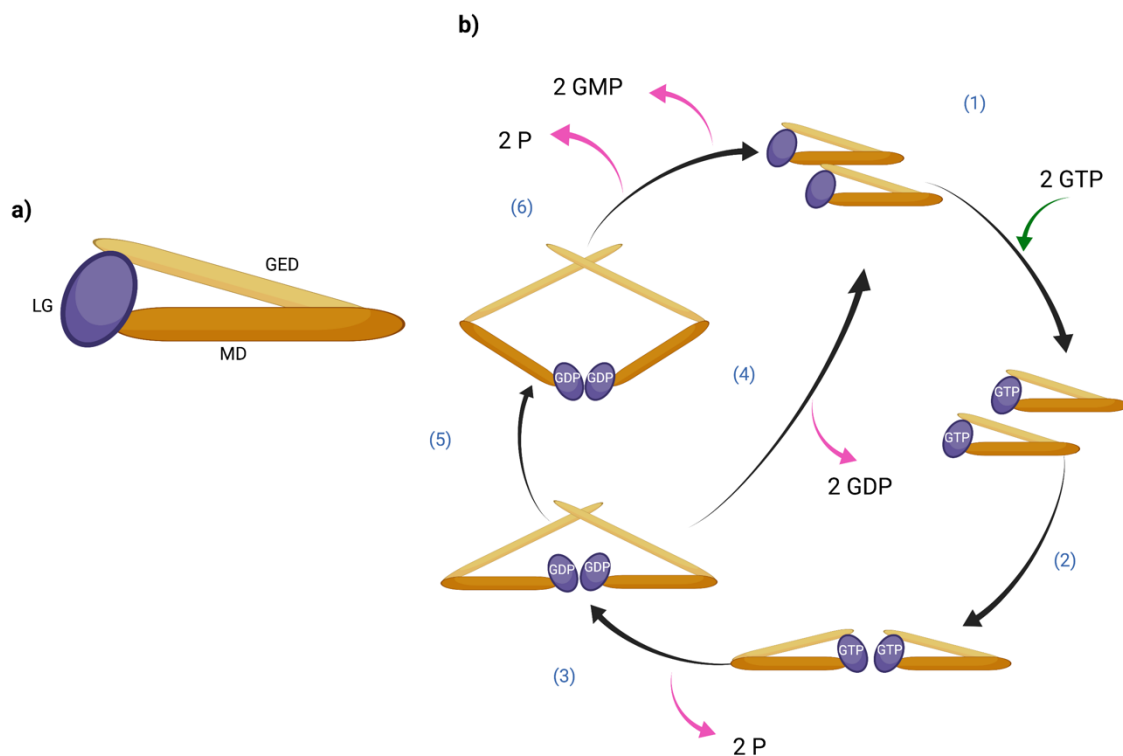


Figure 1.6 Biochemical and structural analysis of GBPs. a) LG: globular N-terminal domain with GTPase activity; MD: helical middle domain; GED: helical C-terminal effector domain. b) At steady state the GED domain folds back to the LG domain. GTP binding to monomeric GBP (1) promotes GBP dimerization via LG-LG interaction (2). GTP hydrolysis promotes GED unfolding within the dimers (3). GDP can dissociate (4) or be hydrolyzed to GMP (5). GBPs return to their close conformation once GMP dissociates from the LG domain (6). Figure adapted from Kutsch, M., & Coers, J. (2021)³⁶⁶.

1.4.2 GBP evolution and expression profile.

Phylogenetic analysis has shown that GBP-like genes are expressed in most vertebrates and bona fide orthologous have been found in protists, amoebae, and plants, suggesting a primordial defense activity that has been remodeled in jawed vertebrates to respond to IFNs³⁶⁷. Common to most species, these GBP-like genes have expanded into euchromatic clusters^{342,367}. For example, humans have seven GBPs and one pseudogene residing in a unique cluster on chromosome 1q22.2³⁶⁸. Exceptions are some rodents (e.g., *Mus musculus* and *Rattus norvegicus*), which carry two GBPs clusters on two different chromosomes³⁶⁹, and zebrafish and frogs, where GBP-genes are grouped on three small genomic islands³⁴². The evolution of GBPs has been explained by the birth-and-death process, according to which multigene families are generated by gene duplication events. Duplicated genes can be either deleted or kept in the genome. In the latter case they can acquire new functions (neofunctionalization), split functions (subfunctionalization), or lose their functions (pseudogenization)³⁷⁰. For instance, the GBP3 gene appears to have emerged in Simiiformes, a taxonomic infraorder within Primates, through duplication of GBP1 and has gained a new role in the inflammasome-mediated response³⁶¹. Duplication events of the GBP4 gene have most likely generated GBP7, which is present in primates only³⁷¹ potentially indicating that maintenance of GBP7 was positively selected for host-pathogen interactions^{372,373}. Moreover, Old-World monkeys lack GBP4 and -5, and they are more susceptible to HIV-2 infections compared to great apes where GBP5 is expressed^{374,375}. Evolutionary studies in rodents have revealed that Gbp2, -5, and -6 are orthologs of their primate counterparts³⁶⁹. The presence of Gbp2 and Gbp5 in rodents genomes further highlights their importance in host defense^{253,367}.

Genetic deletions and genomic examination of the Gbp locus in mice and zebrafish, respectively, have been powerful tools to uncover the link between GBPs and innate immune mechanisms, mainly inflammasome regulation. Mice have 11 Gbps in two clusters distributed on Chromosome 3 and 5. Engineered mice lacking the chromosome 3 cluster, which harbors Gbp1, Gbp2, Gbp3, Gbp5, and Gbp7, and single knock-out mice for these Gbps have helped investigate the role of these proteins in host immune defense and inflammasome activation^{364,376,377}. Mice lacking the entire cluster of Gbps on chromosome 5, which includes Gbp6, Gbp8, Gbp9, Gbp10, and Gbp11, have not been reported yet, although small interfering RNA

(siRNA) experiments have revealed a possible role of Gbp6 and -10 in restricting *L. monocytogenes* and *M. bovis*³⁶⁴. Recently, knock-out mice for both the Gbp clusters (*Gbp*^{Chr3/Chr5-/-}) have been described to be more susceptible to *Yersinia pestis*³⁷⁸. Interestingly, genomic analysis has shown that zebrafish GBP3 and GBP4 also have CARD domains, similar to inflammasome-related proteins like ASC, NLRP1, and caspase-4, highlighting a link between inflammasomes and GBPs^{367,379,380}. Genomic examination of the GBPs in protochordate, *Branchiostomata floridae*, predicted the involvement of its GBPs in inflammasome-independent death pathways, since they are fused with death effector domains related to human caspase-8 and Fas-associated protein with death domain (FADD), intermediaries in apoptotic signaling^{367,381}.

Unless induced, human GBPs are expressed at a low or tonic level in immune cells as well as in the lung, liver, kidney, digestive tract, brain, and skin stroma. In contrast, GBP6 is constitutively expressed only in the oropharyngeal tract, and GBP7 expression is detectable only in the liver³⁸². Notably, all GBPs are constitutively expressed at low levels in preimplantation embryos, with spikes of GBP1 expression in epiblasts, GBP2 in oocysts, and GBP5 in morula³⁸³. Constitutive expression of GBP4 is present in pluripotent embryonic stem cells but is depleted by differentiation³⁸⁴. These constitutive expression patterns may imply a cell-, stage-, tissue-specific epigenetic control. Outside of these contexts, human GBPs expression requires robust immune-receptor signaling. Similarly, murine Gbps are expressed in parenchymal and stromal cells as well as in immune lineages^{382,385}. In endothelial cells (ECs), GBP1, -2, and -3 expression can be induced by several pro-inflammatory cytokines, such as IL-1 β and TNF- α . In this context, it was suggested that GBP1 contributes to the inhibition of EC proliferation by vascular endothelial growth factor and basic fibroblast growth factor. Likewise, IL-1 β and TNF- α induce human GBPs in colonic epithelial cells, where they may mediate antitumorigenic effects, and mouse GBPs in fibroblasts^{386,387}. Beyond that, in humans and mice, the IFNs remain the most potent immune signals for GBPs induction. Following IFN γ stimulation, GBPs transcription is stimulated by the binding of STAT1 homodimers to the GAS elements³⁸⁸, however in mouse embryonic fibroblast and macrophage cell line (ANA-1), promoter sequences of mGbp1 and -2 show inactive STAT1-binding site but ISRE motifs that might act as IRF1-binding sites. It is therefore likely that

these are secondary response genes since their induction relies on de novo synthesis of IRF1 by IFN γ ^{389,390}. GBP levels are also upregulated as a result of ISGF3 binding on ISRE sequences in response to both type II and III IFNs, albeit IFN λ stimulation seems to be confined to keratinocytes and hepatocytes^{391–393}. Mouse and human GBP responsiveness is further regulated by long intergenic non-coding RNAs and microRNA respectively, which suppress expression of multiple members of the murine GBP protein family and human GBP2^{394,395}. Overall, GBPs are heavily upregulated by viruses, bacteria, and parasite infection, and their expression profile is markedly altered in cancer and auto-inflammatory diseases³⁸².

1.4.3 When GBPs meet intracellular pathogens.

Accumulating pieces of evidence have shown that GBPs take part in the host immune defense against intracellular pathogens, including viruses, bacteria, and protozoan parasites³⁶⁵.

1.4.3.1 Antiviral GBPs. More than two decades ago, Anderson et al. conducted pioneering studies showing that in HeLa cells stimulated with either IFN γ or IFN α , overexpression of GBP1 was able to restrict the RNA viruses vesicular stomatitis (VSV) and encephalomyocarditis (EMCV) viruses³⁹⁶. The role of GBPs in mediating the host antiviral defense has since been expanded to additional hosts, including mice, and different viruses. GBP1 may also exert antiviral activity by mediating actin-cytoskeleton remodeling. Indeed, it was suggested that its oligomerization and GTPase activity is required for disrupting the actin filaments used by Kaposi's sarcoma-associated herpesvirus (KSHV) to translocate into the nucleus. In support of this model, it has also been shown that the knockdown of GBP1 promotes KSHV replication. Interestingly, the virus-encoded replication and transcription activator (RTA), an E3 ligase, targets GBP1 for proteasomal degradation³⁹⁷. Further studies have shown that the GTPase activity of GBP1 is needed to restrict hepatitis C virus (HCV), as mutations in the GTP-catalyzing domain abolish its antiviral activity^{398,399}. Additionally, immunoprecipitation and mammalian two-hybrid assays have revealed that the GBP1 large domain is bound by the viral RNA-dependent RNA polymerase NS5B of HCV, which hinders its GTPase activity. The suppressive effect of NS5B on GBP1 activity could contribute to the persistence of HCV infection and replication³⁹⁹. GBP1, GBP3, and GBP3DC, a GBP3 splicing variant with a modified C-terminus

domain, display anti-influenza A viral activity mainly in lung epithelial cells. Here, the GTP binding but not its hydrolysis triggers the antiviral effector activity of the globular domain. Furthermore, GBPD3 represses the synthesis of viral RNA and proteins by inhibiting the influenza virus polymerase complex⁴⁰⁰. More recent work has extended the GBPs antiviral activity to HIV1 infection. HIV1 proteins require post-transcriptional modification and proteolytic processes prior to incorporation into viral particles. Often proteolytic cleavage of viral precursor proteins is performed by host proteases, such as furin, which cleaves the N-glycosylated envelope glycoprotein gp160 into gp120 and gp41, promoting viral particle production⁴⁰¹. GBP2 and -5 block viral particle maturation by inhibiting N-glycosylation and furin protease activity. Most likely this process takes place in the Golgi, as GBP mutants defective for isoprenylation, which is required for anchoring to the Golgi, fail to antagonize HIV1 assembly^{375,402}. Moreover, GBP2 and -5 have been described to impair the maturation of several viruses that use furin for optimal glycoprotein maturation, such as measles virus and Zika⁴⁰². So far, murine Gbp2 has been shown to inhibit the replication of VSV and EMCV⁴⁰³. More recent studies have outlined a role for murine Gbps in response to norovirus infections. In fact, membranous replication complexes of norovirus are disrupted upon Gbp2 targeting, along with other Gbps. Studies of noroviral pathogenesis in vivo have confirmed that *Ifnar1^{-/-}/Gbp^{Chr3-/-}* mice have lower survival⁴⁰⁴.

On the other hand, some GBPs have been described to have pro-viral activity. For example, murine Gbp4 negatively regulates virus-induced type I IFNs by targeting IRF7 and impairing its interaction with TRAF6⁴⁰⁵. Similarly, human GBP7 impedes NF- κ B translocation to the nucleus and attenuates phosphorylation of STAT1 and 2, favoring influenza A replication⁴⁰⁶. Whereas hGBP5 was found to be significantly upregulated in patients and cell lines infected with influenza A virus, where it inhibits virus replication by enhancing IRF3- and NF- κ B-dependent gene expression⁴⁰⁷.

1.4.3.2 GBPs and parasite infections. Several IFN-inducible effectors have been implicated in the host defense against protozoan parasite infection, such as the expression of the IFN-inducible NOS and autophagy-related pathways¹⁰⁷. The GBPs represent an additional distinct mechanism. For instance, murine Gbps belonging to both the chromosome 3 and 5 clusters have been found to target *T. gondii* parasitophorous vacuoles in embryonic fibroblast and macrophages^{356,408-410}. Further studies have demonstrated that GTP-binding and hydrolysis, as well as

membrane anchoring, allow pre-assembly of multiple GBPs in vesicle-like structures (VLSs). Förster resonance energy transfer (FRET) combined with Multiparameter fluorescence image spectroscopy (MFIS) showed intramolecular interaction of mGbp2 with itself, mGbp1, and to a lesser extent with mGbp3. These dimers are then recruited onto the PVs where they form huge multimeric complexes and lead the PVs to rupture, resulting in exposure of the underlying parasite to the host cytosol^{356,410}. Eventually, mGbp2 multimeric complexes directly target the *T. gondii* plasma membrane, thus mGbps might be involved in toxoplasma targeting and elimination, for example by activating the autophagy machinery and/or the inflammasome³⁵⁶. Whether such mechanisms depend on GBPs enzymatic activity has yet to be determined. Although other Gbps are found in the VLSs and later on the PVs, such as Gbp5 and Gbp6, FRET analysis and co-immune precipitation experiments have not revealed an interaction with Gbp2³⁵⁶. Mouse Gbp1 and -2 have been depicted as key players in the cell-autonomous immune response against *Toxoplasma*^{411,412}. However, reconstitution of Gbp2 in mouse *Gbp^{Chr3-/-}* embryonic fibroblast is not enough to control parasite's replication, and Gbp1 expression only partially restores the wild-type phenotype⁴⁰⁹. This argues in favor of a cooperative model, in which several mGbps act in concert to exploit their antiparasitic activity. In addition, Gbps successfully target PVs of avirulent strains of *Toxoplasma*, while virulent strains efficiently counteract their targeting by secreting rhoptry (ROPs) and dense granule antigen 15 (GRA15) kinases which promote Gbps lysosomal degradation^{410,413}. Other parasite effectors (e.g., TgIST) interfere with STAT1 activation thereby impacting GBPs expression^{414,415}. Recent work has revealed a pivotal role of murine Gbp7 in restricting *Toxoplasma* infection in vivo and in vitro. In fact, in response to *T. gondii* infection *Gbp7^{-/-}* mice showed high susceptibility and mortality just as *Gbp7*-deficient cells failed to restrict parasite's replication. Interestingly, Gbp7 was localized in the PVs lumen, hinting at the possibility of a direct antiparasitic function⁴¹⁶. Despite the fact that human GBPs exhibit anti-toxoplasma activity, their function seems to be narrowed to specific cell types. In primary IFN-activated mesenchymal stem cells and transformed lung epithelia, hGBP1 limits the growth of *T. gondii*, although in the latter case GBP1 does not translocate onto PVs^{417,418}. In striking contrast, in a myeloid leukemia cell line, *T. gondii* growth is restricted in a GBP-independent manner, even though the GBPs clearly target PVs⁴¹⁹. Furthermore, whereas in IFN γ -stimulated human macrophages,

GBP1 limits *T. gondii* replication by inducing apoptotic death of infected cells⁴²⁰, in human foreskin fibroblasts, the IFN γ -induced mechanism promotes resistance to *T. gondii* infection by inducing GBP-independent cell death and early parasite egress⁴²¹.

In contrast, the role of GBPs in response to other parasites remains largely uncharacterized. However, in an experimental model of *Plasmodium berghei*-induced murine cerebral malaria, a different set of mGbps is upregulated in the liver and brain of infected animals^{422,423}. In humans, a genetic study uncovered a single nucleotide polymorphism on the GBP7 promoter that correlates with elevated parasitemia, anemia, and hyperpyrexia in Cameroonian populations⁴²⁴. Upregulation of murine Gbp1 and Gbp5 mRNA has also been observed in skin, inguinal lymph nodes, spleen, and liver after infection with the kinetoplastid parasite *Leishmania major*⁴²⁵. Moreover, human and mouse GBPs have been implicated in the cell-autonomous immune response against *Leishmania donovani*. In nonphagocytic cells, GBP-mediated killing of *L. donovani* occurs by facilitating parasite delivery to autolysosomal compartments. Surprisingly, GBPs have not been detected to target the *Leishmania*-containing vacuole⁴²⁶. Furthermore, in human and murine macrophages infected with *L. donovani*, GBP1 modulates the induction of pro-inflammatory cytokines and chemokines and regulates MAP kinase activity⁴²⁷. On the contrary, GBPs fail to restrict the growth of the other kinetoplastid parasite *T. cruzi*⁴¹⁰.

1.4.3.3 GBPs and antibacterial defense. A loss-of-function screen conducted by Kim et al. on the entire 11-member of the Gbp family in mouse macrophages revealed for the first time that these GTPases are involved in IFN-mediated killing of intracellular bacteria. Specifically, Gbp knock-down by small interfering RNA (siRNA) duplexes showed that Gbp1, Gbp6, Gbp7 and Gbp10 are critical for the control of *L. monocytogenes* and *M. bovis*. In addition, increased replication of *L. monocytogenes* and *M. bovis* in *Gbp1*^{-/-} mice clearly implicated GBPs as a class of host defense proteins operating in vivo and in vitro³⁶⁴. Several antimicrobial mechanisms were proposed to explain how Gbps to reduce the intracellular replication niche of bacteria, e.g., in IFN γ -stimulated mononuclear phagocytes, such as GBP7 recruiting the components of the phagocytic oxidase complex (NADPH oxidase), gp91phox and p22phox to the phagosomes of *L. monocytogenes* and *M. bovis*, thus promoting

oxidative activity³⁶⁴. Besides oxidant defense, GBP proteins are involved in autolysosomal killing of bacteria; in fact, Gbp7 interacts with the cysteine protease Atg4 on *M. bovis* vacuoles where it potentially fosters autolysosome closure³⁶⁴. In addition, recruitment of the autophagic-related proteins SQSTM1 and galectin-3 elicits murine Gbp1 and 2 association with vacuoles harboring *Listeria*, *Legionella*, and *Yersinia pseudotuberculosis*^{428,429}.

GBP-related mechanisms also take part in protecting non-immune cells. For instance, the C-terminal RRR motif of GBP1 catalyzes hierarchical recruitment of GBP2, -3, and -4 on cytosolic *Shigella flexneri* where they inhibit *Shigella* actin-based motility and, consequently, its cell-to-cell spread. But *Shigella* escapes restriction with the bacterial E3 ubiquitin ligase, IpaH9.8, which targets GBPs for proteasomal degradation^{430,431}. A similar mechanism could be applied by *C. trachomatis*, which evades GBP targeting in IFN γ -activated human epithelial cells while being effectively detected by several murine Gbps⁴³². Furthermore, in mouse macrophages, GBPs hinder the intracellular motility of *B. thailandensis* and, thus, its spread to neighboring cells and cell-cell fusion events⁴³³. Further studies have underlined the pivotal role of GBPs in activating inflammasome components in response to several other intracellular bacteria, such as *S. Typhimurium* and *F. novicida*^{362,434}. The crosstalk between GBPs and inflammasome will be examined in the next chapter.

1.4.4 Guanylate-binding proteins and inflammasome.

IFNs are powerful signals for guiding host defense mechanisms by transcriptionally regulating many effector genes. As mentioned above, IRGs activate different mechanisms of host resistance against a variety of intracellular vacuolar bacteria¹⁰⁷, just as GBPs have been described to mediate cell-autonomous immunity to *Listeria* or *Mycobacterium* infection³⁶⁴. The inflammasome assembly tailors the innate immune host response upon pathogen infection or cellular stress. This machinery's core proteins are cytosolic sensors that, directly or indirectly through ASC, recruit caspase-1 via CARD-CARD homotypic domain interaction⁴³⁵. In silico genomic screening spanning 91 taxa identified 574 GBP-like proteins with shared homology in the GTPase domain. This set was further restricted by Hidden Markov modeling, which showed that some GBPs in lower organisms (e.g., zebrafish) harbor a CARD

domain that resembles that of ASC and NLRP1³⁶⁷. This evidence, beyond their reported role as antibacterial effectors, immediately suggested a possible function for GBPs in the cell death signaling cascades.

1.4.4.1 GBPs and canonical inflammasome. Initially, research focused mainly on the contribution of GBPs to canonical inflammasome activation. In macrophages stimulated with IFN γ and given LPS/ATP to trigger the NLRP3 inflammasome, a small interfering RNA (siRNA) against human GBP5 or its murine counterpart elicits a reduction in IL-1 β release to the same extent as silencing ASC or chemical inhibition of caspase-1. Interestingly, GBP5-dependent NLRP3 inflammasome activation is displayed in response to diverse priming conditions, such as LPS, muramyl dipeptide (MDP), isoglutamate diaminopimelic acid (iE-DAP), and *S. Typhimurium*, but not in response to the NLRP3 crystalline activator alum. Therefore, GBP5 exerts an activator function with only soluble or bacterial priming agents. Importantly, activation of AIM2 and NLRC4 inflammasomes was not affected by GBP5 deficiency³⁶⁷. Furthermore, the self-assembly of GBP5 into tetramers and their interaction with the PYD of NLRP3 favors the formation of the inflammasome complex³⁶⁷. Although GBP5 has been linked to NLRP3 activation, GBP deficiency failed to affect NLRP3 assembly in response to several sterile NLRP3 activating agents (e.g., monosodium urate, saponin, etc.), probably owing to different signaling modes^{258,436–438}. Indeed, activation of NLRP3 by sterile agents requires selective scavenger receptor-mediated endocytosis, resulting in lysosomal swelling and damage^{439,440}. Therefore, GBP5 could aid the assembly of NLRP3 in the cytosol but could be dispensable in different subcellular compartments.

The impact of GBP5 in inflammasome assembly has also been examined *in vivo*. The defective NLRP3 activation in GBP5 deficient cells upon soluble priming agents but not in response to crystalline stimuli was recapitulated *in vivo*. Indeed, *Gbp5*^{-/-} mice exhibit defects in muramyl dipeptide-induced peritonitis but not alum-induced peritonitis and a significant reduction of neutrophil recruitment³⁶⁷. After LPS challenge, *Gbp5*^{-/-} animals show a reduction in pyrogenic cytokine production, which coincide with a loss of active caspase-1 in macrophages³⁶⁷. Moreover, they show enhanced susceptibility to *Listeria* and *Francisella* infection^{258,367,437}.

The implication of GBP5 in NLRP3 inflammasome activation has raised the hypothesis that other GBPs may also be involved in this pathway. Indeed, knockout

of Gbp2 in mouse macrophages infected with numerous vacuolar Gram-negative bacteria results in reduced LDH and IL-1 β release⁴³⁶.

GBPs have also been identified as important cofactors for Aim2-dependent immunity to *F. novicida*. *Francisella* infection is detected by the cytosolic DNA sensor cGAS and its adaptor STING, activating type I IFN-dependent IRF1, which, in turn, promotes the expression of GBPs⁴³⁷. Among the Gbps, Gbp2 and Gbp5 play prominent roles in vitro and in the mouse model of tularemia; in fact, they lead to the intracellular killing of *Francisella* resulting in the release of bacterial DNA for the sensing by AIM2²⁵⁸. Mechanistically, GBP-decorated cytosolic *Francisella* are targeted by Irgb10, which directly promotes bacteriolysis and DNA release²⁵⁶. Recently, the role of Gbps in Aim2 inflammasome activation has been extended to two other members of the GBP cluster on chromosome 3, Gbp1 and Gbp3. Indeed, macrophages from *Gbp1*- and *Gbp3*-deficient mice infected with *F. novicida* showed a reduced ability to induce cleavage of caspase-1 and GSDMD, as well as the formation of ASC puncta, hallmarks of pyroptotic cell death. In vitro experiments show that an N-terminal region of Gbp1 and Gbp3 is required for pathogen membrane disruption leading to DNA release, thus attributing direct antimicrobial activity to these proteins. However, it cannot be ruled out that the defective inflammasome activation observed in *Gbp1*^{-/-} and *Gbp3*^{-/-} macrophages may be due to reduced recruitment of IRGB10⁴⁴¹. Remarkably, in human macrophages the recruitment of GBP3 to *Francisella* is detectable only in a mutant harboring penta-acylated LPS instead of the tetra-acylated LPS commonly found in these bacteria, suggesting that there might be an intrinsic difference between human and mouse GBPs⁴⁴². In addition, Gbps promote caspase-11-dependent and caspase-1-dependent inflammasome activation in *Chlamydia*-infected macrophages⁴⁴³.

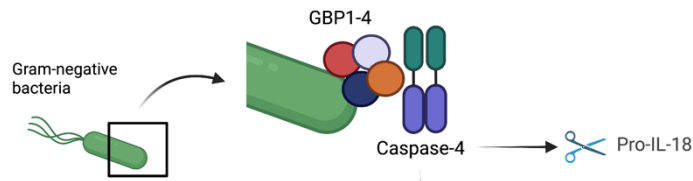
1.4.4.2 GBPs and non-canonical inflammasome. Transfection of purified LPS or its lipid A moiety into the host cell cytosol triggers non-canonical inflammasome activation bypassing TLR4 signaling^{287,288,301}. This model was proposed based on in vitro reconstitution experiments where it was observed that the lipid A portion of LPS can bind caspase-11 and caspase-4 through their CARD³⁰¹. However, TLR4- and TRIF-dependent IFN production is required for caspase-11 expression and activation by intact Gram-negative bacteria, and only partially to trigger caspase-11 expression¹⁸⁶. In addition, LPS is highly hydrophobic and normally found within the

bacterial outer membrane. Thus, the hypothesis that IFN-inducible factors are required to initiate or sustain the non-canonical inflammasome has become prominent. Indeed, several studies have shown that GBPs are essential for the recognition of Gram-negative bacteria by cytosolic immune sensors^{436,443,444}. First, they were thought to be needed to induce lysis of the PCV, allowing the release of the bacteria into the cytosol and activation of LPS-dependent activation of caspases⁴³⁶. However, pyroptosis was also found to be impaired in GBP-deficient macrophages stimulated with IFN γ after transfection with LPS derived from *E. coli*, *S. Typhimurium*, and *L. pneumophila*, suggesting that GBPs may act downstream of phagosome disruption⁴⁴⁴. A central role of GBPs in response to OMVs produced by Gram-negative bacteria, which are internalized by macrophages and serve as components for LPS delivery, has also been described. Mechanistically, *in vivo* and *in vitro*, isoprenylated GBPs associate with OMVs or cytosolic LPS, indicating that their recruitment is mediated by LPS itself⁴⁴⁵. Remarkably, most studies have linked the murine Gbp cluster on chromosome 3 to non-canonical inflammasome activation^{436,444}. In a recent pre-print, genome editing with CRISPR-Cas9 and homologous recombination made it possible to generate mice lacking individual members of the chromosome 3 cluster (Gbp1, Gbp2, Gbp3, Gbp5, and Gbp7), and mice deficient for Gbp6 and Gbp10 on chromosome 5, as they have been implicated in antibacterial defense^{364,377}. Analysis of LPS-primed macrophages transfected with LPS showed that ablation of mGbp2 and mGbp3, but not the other Gbps, results in a defective release of IL-1 β and pyroptosis, as well as defective processing of GsdmD. This study yielded a model whereby mGbp2 recruits caspase-11 for LPS recognition, while mGbp3 transports GsdmD-NT after its proteolytic cleavage by caspase-11³⁷⁷. Human caspase-4 seems to function partially differently from murine caspase-11. First, in mouse macrophages, *Francisella* is exclusively sensed by the AIM2 inflammasome despite the requirement for Gbps^{256,258,437}. Indeed, *Francisella* has an under-acylated lipid A that cannot be recognized by caspase-11 but is effectively detected by human caspase-4 through a contribution of GBP2, underscoring an intrinsic difference between caspase-11 and its human ortholog, caspase-4⁴⁴⁶. Importantly, *Francisella*-induced AIM2 inflammasome and *E. coli*-induced non-canonical inflammasome in mice relies on IRGs that are lacking in humans, suggesting that Gbp-mediated inflammasome activation may be regulated differently

in humans and mice^{128,132,133}. Indeed, Gbp-dependent Irgb10 recruitment is thought to liberate LPS in the cytosol of the host cell for caspase-11 sensing²⁵⁶. However, caspase-11 can also be recruited to the bacterial surface (Fig.1.7)⁴⁴⁷. Recently, two major studies have made important contributions to the understanding of the crosstalk between GBPs and human noncanonical inflammasome assembly. They reported that GBP stimulation is critical for *Salmonella*- and *Shigella*- or cytosolic LPS-mediated activation of caspase-4 in human epithelial cells and macrophages^{360,361}. Consistent with a previous report that identified GBP1 as crucial for caspase-4 recruitment on *Salmonella*, it was found that quickly after bacteria escape from their vacuole into the host cell cytosol, GBP1 targets the surface of cytosol-invading bacteria and drives the hierarchical recruitment of GBP2-4, converting Gram-negative bacterial surfaces into signaling platforms capable of activating activation (Fig.1.7)^{360,361}. Using IFN γ -stimulated HeLa cells overexpressing GBP1-4, both groups observed that GBPs directly decorate cytosolic bacteria rather than PCVs, as previously suggested^{360,361,436}. Both studies propose a model in which GBPs play distinct roles: GBP1 and 4 are considered essential for the recruitment of caspase-4, while GBP3 is necessary its activation^{360,361}. However, the models differ slightly, as Wandel et al. suggested that GBP2 is also pivotal for caspase-4 recruitment³⁶¹. Surface plasmon resonance (SPR) revealed that GBP1 can directly bind LPS with kinetics that fit a two-state reaction model, thus initial binding is followed by conformational changes. Interestingly, *Salmonella* mutants lacking the O-antigen or the outer core, the outermost parts of the LPS, still recruit GBP1 and caspase-4, suggesting that lipid A and the inner core are sufficient to trigger pyroptosis³⁶⁰. Thus, the research focuses on understanding the nature of the link that governs the GBP1-LPS interaction. Evidence suggests that GBP1-LPS interaction involves electrostatic forces; in this respect, neutralization of negative charge or dephosphorylation of lipid A strongly reduces LPS-mediated cell death. Finally, mutation of the triple lysine patch in the globular domain of GBP1 leads to significantly reduced targeting of cytosolic *Salmonella*, suggesting that these positive residues are necessary for binding³⁶⁰. Therefore, GBP1 can be considered a pattern recognition receptor that binds LPS and initiates a signaling hub on the bacterial surface to trigger caspase-4-mediated inflammasome activation and, thus, disrupt *Salmonella* and *Shigella*'s intracellular niche. Likewise, GBP1 acts by inducing

caspase-4-dependent pyroptosis in human epithelial cells infected with *B. thailandensis*, limiting the formation of multinucleated giant cells resulting from its spread into neighboring cells⁴⁴⁸. However, it remains to be determined how the GBP coat causes caspase-4 activation, given that lipid A is an integral component of the bacterial outer membrane and is not readily accessible. Consistent with a previous study reporting a direct contribution of LPS to caspase-4 engagement, IFN γ -primed cells infected with *S. flexneri* and expressing a caspase-4 mutant that lacks the ability to bind LPS, do not undergo pyroptosis³⁶¹. This leads to the hypothesis that GBPs support this interaction by disrupting the integrity of the bacterial membrane³⁰¹. Indeed, in vitro binding assays have demonstrated that GBP1 can act as a surfactant, disrupting the O-antigen barrier and making the lipid A portion more accessible for caspase recognition. Furthermore, incubation of *Shigella* with purified human GBP1 renders these bacteria more susceptible to polymyxin B, an antimicrobial peptide that binds lipid A phosphate groups with high affinity⁴⁴⁹. Conversely, in a cell culture system, GBP1 recruitment on the bacterial surface does not trigger direct bacteriolysis^{360,448}. Hence, further investigations are needed to understand the exact mechanism by which GBPs mediate non-canonical inflammasome activation.

1) Human non-canonical inflammasome



2) Murine non-canonical inflammasome

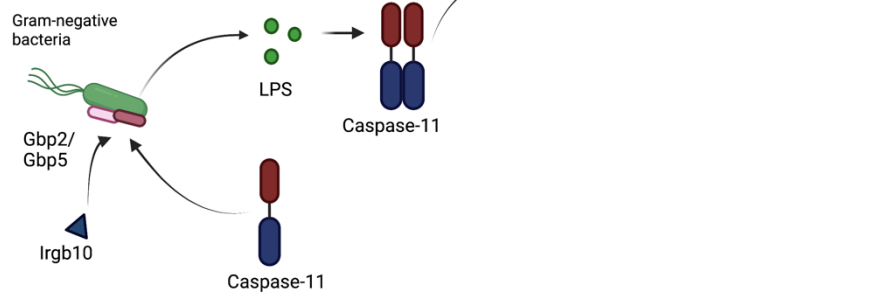


Figure 1.7 GBPs and non-canonical inflammasome. The human non-canonical inflammasome is activated by the recognition of LPS by GBP1, which drives the hierarchical recruitment of GBP2-4 on Gram-negative bacteria. GBP1-4 forms a signaling hub on the bacterial surface that enables the recruitment and activation of caspase-4. The murine non-canonical inflammasome is activated in response to cytosolic LPS, which is released into the cytosol by Gbp-dependent Irgb10 recruitment onto bacteria. Caspase-11 is also recruited on the bacterial surface. Both caspase-4 and -11 drive the cleavage of GSDMD, but only caspase-4 can process IL-18.

2. Aim of the thesis

The aim of my PhD thesis was to investigate the role of human and mouse GBPs in controlling non-canonical inflammasome activation in response to intracellular Gram-negative bacteria and cytosolic LPS. In the first part, I investigated the role of human IFN-inducible Guanylate-Binding Proteins (GBPs) in activating the caspase-4 non-canonical inflammasome in response to *S. Typhimurium* and *B. thailandensis* in human epithelial cells and macrophages. In addition, I sought to define which individual murine Gbps on chromosome 3 and chromosome 5 were necessary for LPS-induced non-canonical inflammasome activation.

3. Results

3.1 Research Project I: Human GBP1 binds LPS to initiate assembly of a caspase-4 activating platform on cytosolic bacteria

José Carlos Santos^{1*}, Dave Boucher^{1*}, Larisa Kapinos Schneider², Benjamin Demarco¹, **Marisa Dilucca**¹, Kateryna Shkarina¹, Rosalie Heilig¹, Kaiwen W. Chen¹, Roderick Y. H. Lim² & Petr Broz^{1†}

¹ Department of Biochemistry, University of Lausanne, Chemin des Boveresses 155, 1066, Epalinges, Switzerland

² Biozentrum, University of Basel, Klingelbergstrasse 50/70, 4056, Basel, Switzerland

[†] Corresponding author. Email: petr.broz@unil.ch

* These authors contributed equally to this work

Statement of contribution:

J.C.S., D.B., and P.B. designed the study, performed and analyzed experiments and wrote the manuscript. L.K.S. and R.Y.H.L. assisted with and analyzed the SPR and MST experiments., B.D., K.W.C., and **M.D.** performed experiments, K.S. and R.H. contributed expression vectors.

Specific contribution:

Generation of HeLa cell lines deficient for GBP1, GBP2, GBP3, GBP4, GSDMD, and CASP4 via CRISPR-Cas9 technology.

Generation of knock-out single clones by serial dilution.

Single clone screening by performing the T7 endonuclease I assay, verified by sequencing of the PCR fragments, and confirmed by western blotting.

Summary of the results

The bacterial endotoxin, LPS, is the most potent mediator of septic shock, a severe systemic response to Gram-negative bacteria infection often associated with a high mortality rate. LPS is sensed by TLR4 in the extracellular milieu or within endosomes, where it induces cytokine and IFN production via the MyD88 and TRIF signaling pathways⁴⁵⁰. Upon entry of bacteria into the host cell cytosol, their LPS is detected by the non-canonical inflammasome pathway, e.g., human caspase-4 and caspase-5 or mouse caspase-11^{287,288,451}. These caspases were thought to be the cytosolic receptors that directly bind LPS released from Gram-negative bacteria, such as *S. Typhimurium* and *S. flexneri* as they escape into the cytosol of host cells. Indeed, in vitro experiments have demonstrated that recombinant caspase-4 and caspase-11 can be activated by the direct binding of the lipid A moiety of LPS to their CARD domain⁴⁵¹. Once activated, human caspase-4 (and murine caspase-11) proteolytically cleaves the pore-forming protein GSDMD leading to the pyroptosis of infected cells^{452,453}.

However, the highly hydrophobic nature of lipid A and its localization within the bacterial outer membrane made the presence of additional factors that might initiate or sustain non-canonical inflammasome activation conceivable. Furthermore, non-canonical inflammasome activation in mouse macrophages transfected with LPS or infected with Gram-negative bacteria requires IFN-inducible genes, Gbps and IRGs^{256,436,445,454}. Besides targeting cytosolic bacteria, the engagement of Gbps and Irgb10 on Gram-negative bacteria correlates with bacterial lysis and caspase-11 activation, yielding a model in which Gbp-decorated bacteria are further targeted by Irgb10, which exerts membranolytic activity that releases LPS for detection caspase-11²⁵⁶. GBPs are also required for LPS-induced caspase-4 activation, although the IRG family is lacking in humans^{133,455}. Therefore, it was unclear how hGBPs can promote LPS release and caspase-4 activation.

Our group and a related work published by Wandel et al. found that human GBP1 is a bona fide cytosolic pattern recognition receptor for LPS, that binds LPS on the membranes of Gram-negative bacteria, giving rise to a signaling hub that mediates the recruitment and activation of human caspase-4 on the surface of cytosolic bacteria^{360,456}. Specifically, we found that in IFN γ -stimulated HeLa cells *S. Typhimurium* growth was restricted, and the cytosolic bacteria were targeted by

caspase-4 and that caspase-4 recruitment required GBP1. Overexpression of tagged GBPs showed that cytosolic *Salmonella* are targeted by GBP1-4: recruitment of GBP2, -3, and -4 on bacteria is reliant on GBP1, the first GBP that coats *Salmonella*. Mechanistically, GBP1 and GBP4 are required for caspase-4 recruitment, whereas GBP3 is crucial for its activation.

Also, using a biochemical approach we found that monomeric GBP1 associates in large oligomer complexes when incubated with LPS, hinting that LPS is the putative ligand of GBP1. We also proved that the association of GBP1 with LPS occurs via an electrostatic interaction between a positively charged lysine patch in the GTPase domain of GBP1 and the negative charged LPS. Indeed, mutations of lysine residues abrogates GBP1-LPS association and impede GBP1 recruitment on *Salmonella*. In order to identify the portion of LPS recognized by GBP1, we employed mutant strains of *Salmonella* lacking the O-antigen and/or outer core; surprisingly, these bacteria were still decorated by GBP1, suggesting that lipid A might be the essential mediator of this interaction. How GBP1 gains access to lipid A and how this GBP-rich signaling platform enables the interaction of CASP4 with lipid A, otherwise hidden in the bacterial membrane, needs further investigation. In summary, with our study, we provide evidence to designate GBP1 as a novel innate immune receptor; moreover, we have identified its ligand and the characteristics of their interaction.

Human GBP1 binds LPS to initiate assembly of a caspase-4 activating platform on cytosolic bacteria

José Carlos Santos^{1,3}, Dave Boucher^{1,3}, Larisa Kapinos Schneider², Benjamin Demarco¹, Marisa Dilucca¹, Kateryna Shkarina¹, Rosalie Heilig¹, Kaiwen W. Chen¹, Roderick Y. H. Lim² & Petr Broz¹✉

The human non-canonical inflammasome controls caspase-4 activation and gasdermin-D-dependent pyroptosis in response to cytosolic bacterial lipopolysaccharide (LPS). Since LPS binds and oligomerizes caspase-4, the pathway is thought to proceed without dedicated LPS sensors or an activation platform. Here we report that interferon-induced guanylate-binding proteins (GBPs) are required for non-canonical inflammasome activation by cytosolic *Salmonella* or upon cytosolic delivery of LPS. GBP1 associates with the surface of cytosolic *Salmonella* seconds after bacterial escape from their vacuole, initiating the recruitment of GBP2-4 to assemble a GBP coat. The GBP coat then promotes the recruitment of caspase-4 to the bacterial surface and caspase activation, in absence of bacteriolysis. Mechanistically, GBP1 binds LPS with high affinity through electrostatic interactions. Our findings indicate that in human epithelial cells GBP1 acts as a cytosolic LPS sensor and assembles a platform for caspase-4 recruitment and activation at LPS-containing membranes as the first step of non-canonical inflammasome signaling.

¹Department of Biochemistry, University of Lausanne, Chemin des Boveresses 155, 1066 Epalinges, Switzerland. ²Biozentrum, University of Basel, Klingelbergstrasse 50/70, 4056 Basel, Switzerland. ³These authors contributed equally: José Carlos Santos, Dave Boucher. ✉email: petr.broz@unil.ch

Detection of lipopolysaccharide (LPS) is central to host defense against Gram-negative bacterial infections and to the pathogenesis of sepsis. Extracellular LPS is sensed by Toll-like receptor 4 (TLR4), which induces the production of cytokines via the MyD88 and TRIF signaling pathways¹. Cytosolic LPS, on the other hand, is detected by the so-called non-canonical inflammasome, which controls the activation of caspase-4/–5 in humans and caspase-11 in mice^{2–6}. These caspases cleave the pore-forming cell death effector gasdermin D (GSDMD) to induce pyroptosis and cytokine release. While the activation of other caspases requires their recruitment to multi-protein platforms formed by dedicated sensor and adaptor proteins (e.g., DISC, apoptosome and canonical inflammasome), no comparable platform has yet been reported for caspase-4/–5 or –11. Instead, their activation appears to involve a new mode of pattern recognition in which caspase-4/–11 act both as sensor and executor without the need for additional adaptor proteins or co-factors⁵. This model was proposed based on the observation that caspases-4/–11 binds the highly hydrophobic lipid A moiety of LPS through their CARD (caspase recruitment domain), resulting in their oligomerization and activation⁵. However, since LPS is hydrophobic and normally present within bacterial membranes, it is conceivable that cytosolic LPS sensing could require accessory factors in analogy to LPS-binding protein (LBP) or cluster of differentiation 14 (CD14) that are required for TLR4 signaling. LBP binds to LPS-containing outer membrane of bacteria and promotes the transfer of LPS onto CD14, which then delivers LPS to the MD-2/TLR4 complex^{7,8}.

Caspase-11 activation in mouse macrophages transfected with LPS or infected with Gram-negative bacteria requires the expression of interferon (IFN)-inducible GTPases, which include the GBPs (guanylate-binding proteins) or IRGs (immunity-related GTPases)^{9–12}. These GTPases are highly upregulated after type-I or type-II IFN priming, and essential for cell-autonomous immunity against a variety of viruses, bacteria and parasites¹³. In macrophages, several GBPs as well as Irgb10 were found to target intracellular Gram-negative bacteria, such as *Salmonella enterica* serovar Typhimurium (referred to as *Salmonella*), *Francisella novicida* and *Escherichia coli*. Since this recruitment correlated with bacterial lysis and the activation of caspase-11, it gave rise to a model in which GBPs recruit Irgb10 towards bacterial membranes, thereby unleashing an Irgb10-dependent membranolytic activity that kills the pathogen and concomitantly liberates LPS for the activation of non-canonical inflammasome¹¹. However, since humans lack the IRG family (except for a truncated IRGM copy and IRGC), and GBPs are nevertheless required for LPS-induced caspase-4 activation, the current model needs to be confirmed in human cells^{14,15}.

Here we report that IFN γ priming and the induction of GBPs are necessary for caspase-4 activation in human epithelial cells and monocytes/macrophages during infection with the Gram-negative bacterium *Salmonella* or after cytosolic LPS delivery by transfection or electroporation. We show that human GBP1 targets cytosolic *Salmonella* seconds after the bacteria escape from the vacuole and enter into the cytosol, and that GBP1 initiates the hierarchical recruitment of GBP2-4 and the assembly of a GBP coat on cytosolic bacteria. This GBP coat does not induce bacteriolysis, but instead initiates the recruitment and activation of caspase-4 to the surface of cytosolic bacteria. Human GBPs play distinct functional roles in this process: GBP1 together with GBP4 recruit caspase-4, whereas GBP3 is mainly required for caspase-4 activation. Investigating the mechanism by which GBP1 recognizes cytosol-exposed bacteria, we demonstrate that LPS associates with GBP1 in pyroptotic cells and that recombinant GBP1 binds LPS with high affinity. Monomeric GBP1 associates with LPS micelles to form a high-molecular weight complex upon

incubation with LPS, and this association occurs via electrostatic interactions involving negative charges on LPS. Consistently, mutagenesis of GBP1 shows that positively charged residues are necessary for LPS binding and recruitment to bacteria. In conclusion, we show that GBP1 acts as a bona-fide cytosolic LPS sensor that detects and targets the LPS-containing membranes of Gram-negative bacteria, where it assembles a platform that promotes caspase-4 recruitment and activation.

Results

Salmonella-induced caspase-4 activation requires IFN γ priming. To study the human non-canonical inflammasome and its modulation by priming, we infected naive or IFN γ -primed HeLa cells, which lack canonical inflammasome pathways, with the facultative intracellular bacterium *Salmonella*. Since HeLa cells express TLR4 but not MD-2 and are thus not responsive to extracellular bacterial LPS¹⁶, we primed the cells with IFN γ , a cytokine that also plays a critical role in intestinal immunity against *Salmonella*¹⁷. *Salmonella* replicated rapidly in naive HeLa cells but was strongly restricted in IFN γ -primed cells (Fig. 1a), despite similar levels of bacterial invasion (Supplementary Fig. 1a). Strikingly, IFN γ -primed HeLa cells underwent lytic cell death with typical features of pyroptosis, such as plasma membrane swelling and ballooning, and nuclear condensation (Fig. 1b, Supplementary Fig. 1b–e and Supplementary Movies 1, 2), and released mature IL-18 (Supplementary Fig. 1f). Since in epithelial cells a subset of *Salmonella* escape from the *Salmonella*-containing vacuole (SCV) into the cytosol within the first hour after entry^{18,19}, we hypothesized that *Salmonella* could activate the non-canonical inflammasome as previously observed in mouse macrophages²⁰. To test this, we infected naive or IFN γ -primed wild-type, *CASP4*^{–/–} and *GSDMD*^{–/–} HeLa (Supplementary Fig. 1g). Deletion of *CASP4* or *GSDMD* did not alter bacterial invasion, but abrogated *Salmonella*-induced IFN γ -dependent cell death (Fig. 1c and Supplementary Fig. 1h–k), confirming that *Salmonella* infection of HeLa cells activates the non-canonical inflammasome in an IFN γ -dependent manner. While bacterial replication was increased, IFN γ priming still partially reduced intracellular bacterial replication in *CASP4*^{–/–} and *GSDMD*^{–/–} HeLa (Supplementary Fig. 1l), suggesting that cell death was not the only mechanism by which IFN γ restricts bacterial growth. This finding was confirmed using *Salmonella* expressing *PuHP*T-GFP, a reporter for cytosolic replication (e.g., GFP under the control of the hexose phosphate transporter promoter, which responds to exogenous glucose-6-phosphate²¹ found exclusively in the host cytosol) (Supplementary Fig. 1m–o). Furthermore, using a chloroquine (CHQ)-resistance assay, an antimicrobial agent that only reaches bactericidal levels when concentrated within endocytic compartments^{22,23}, we found that IFN γ priming mainly restricted cytosolic *Salmonella* (Supplementary Fig. 1p, q) thus reducing hyper-replication of the cytosolic population of *Salmonella* (Supplementary Fig. 1r, s)^{24,25}. Thus, IFN γ controls a major caspase-4- and GSDMD-dependent mechanism that restricts cytosolic *Salmonella* replication by inducing host cell pyroptosis, and a minor mechanism that acts independently of cell death.

We next determined whether IFN γ was necessary to promote access of *Salmonella* or their LPS to the cytosol by quantifying bacterial resistance to CHQ at 1.5 h post-infection (p.i.). When compared with naive cells, IFN γ priming did not induce *Salmonella* escape to the host cytosol (Fig. 1d), indicating that IFN γ controlled the detection of LPS after bacterial entry into the cytosol. To confirm this, we next transfected cells with ultrapure *E. coli* or *Salmonella* LPS. Similarly to *Salmonella* infection, LPS transfection only caused cell death in IFN γ -primed HeLa and was

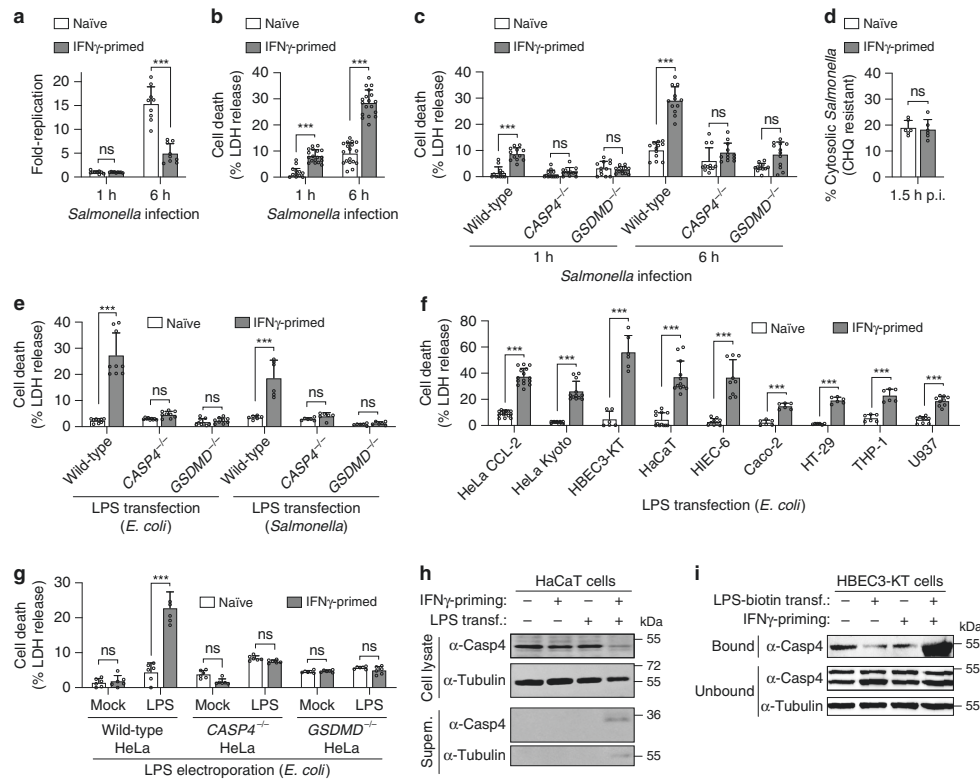


Fig. 1 IFN γ priming is required for LPS-induced caspase-4 activation in human epithelial cells. **a–c** Intracellular bacterial fold-replication (**a**) and release of LDH (**b, c**) in naive or IFN γ -primed wild-type, *CASP4*^{-/-} or *GSDMD*^{-/-} HeLa cells, at 1 or 6-h post-infection (p.i.) with *Salmonella*. Cells in 96-well plates were infected for 30 min, washed and gentamicin was added to kill extracellular bacteria. At the indicated time points supernatant was collected to determine the release of LDH, and then cells were lysed and the number of viable intracellular bacteria was determined by counting colony forming units (CFUs). The bacterial fold-replication was calculated relative to 1 h p.i. **d** Percentage of CHQ-resistant cytosolic *Salmonella* in naive or IFN γ -primed HeLa at 1.5 h p.i. Cells were infected for 30 min as in (**a**) and then treated with gentamicin \pm CHQ for an additional 1 h before cells were lysed and bacteria counted by CFUs. The percentage of cytosolic bacteria was calculated as the ratio of (CHQ + gentamicin^{resistant} / gentamicin^{resistant}). **e–g** Release of LDH from naive or IFN γ -primed cells, 5 h after transfection with LPS (2.5 μ g/50,000 cells) or 3–4 h after electroporation with LPS (300 ng/50,000 cells). **h** Western blot analysis of full length (p43) and cleaved (p32) caspase-4 in the supernatants and cell lysates from naive or IFN γ -primed HaCaT cells, upon transfection with *E. coli* LPS (2.5 μ g/50,000 cells). **i** Streptavidin pull-down assay of the binding of biotin-conjugated LPS to endogenous caspase-4 from the lysates of naive or IFN γ -primed HBEC3-KT. Cells in 6-well plates were transfected with LPS-biotin (10 μ g) or left untransfected, and biotinylated substrate was pulled down using equal amounts of streptavidin magnetic beads, which were then eluted in equal volumes of SDS-PAGE reducing sample buffer. Streptavidin-bound and -unbound fractions were analyzed by immunoblotting for caspase-4. Graphs show the mean \pm SD, and data are pooled from two to six independent experiments performed in triplicate (**a–g**) or representative of two (**h, i**) independent experiments. *** $P < 0.001$; ns, not significant; two-tailed *t*-test.

completely abrogated by deletion of *CASP4* or *GSDMD* (Fig. 1e and Supplementary Fig. 2a). IFN γ -priming was also required for pyroptosis and IL-18 release after LPS transfection (Fig. 1f and Supplementary Fig. 2b–d) and after LPS electroporation (Fig. 1g and Supplementary Fig. 2e) in a panel of human cell lines and primary cells, including human small intestinal epithelial cells (HIEC-6). To further substantiate that caspase-4 activation requires IFN γ , we transfected LPS into naive or IFN γ -primed cells and pulled down active caspase-4 using a cell-permeable pan-caspase activity probe, biotin-VAD(Ome)-fmk (bVAD-fmk)²⁶. Active caspase-4 was only pulled down when cells were first primed with IFN γ and then transfected with LPS

(Supplementary Fig. 2f). In accordance, LPS transfection only induced caspase-4 and GSDMD cleavage in IFN γ -primed cells (Fig. 1h and Supplementary Fig. 2g). Importantly, IFN γ -priming had no impact on the level of caspase-4 expression, since unlike murine caspase-11, caspase-4 was not induced by IFN γ (Fig. 1h, i and Supplementary Fig. 2c, g, h). To assess if IFN γ controlled caspase-4 activation upstream or downstream of LPS binding, we prepared lysates from HeLa or HBEC3-KT cells transfected with biotinylated LPS and pulled down LPS-interacting proteins with streptavidin-coupled beads. In both cell types caspase-4 could only be pulled-down with LPS in IFN γ -primed but not in naive cells (Fig. 1i and Supplementary Fig. 2h). Altogether, these

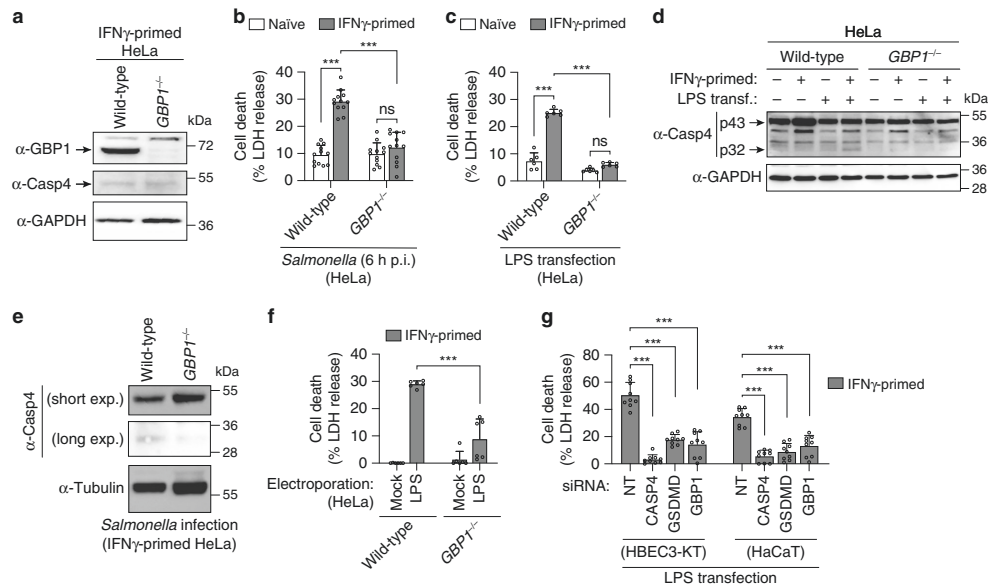


Fig. 2 GBP1 is required for *Salmonella*- and LPS-induced caspase-4 activation to induce pyroptosis in epithelial cells. **a** Immunoblots for GBP1, caspase-4 and GAPDH (loading control) in cell lysates from IFN γ -primed wild-type or *GBP1*^{-/-} HeLa. **b, c** Release of LDH from naive or IFN γ -primed wild-type or *GBP1*^{-/-} HeLa after *Salmonella* infection (**b**) or after 5 h transfection with *E. coli* LPS (2.5 μ g / 50,000 cells) (**c**). **d, e** Immunoblots for full length (p43) and cleaved (p32) caspase-4 in combined supernatants and cell lysates from naive or IFN γ -primed wild-type and *GBP1*^{-/-} HeLa, upon transfection with *E. coli* LPS for 5 h (**d**) or *Salmonella* infection (**e**). **f** Release of LDH from IFN γ -primed wild-type or *GBP1*^{-/-} HeLa, 3 h after electroporation with LPS (300 ng / 50,000 cells). **g** Release of LDH in IFN γ -primed HBEC3-KT or HaCaT cells treated with non-targeting control siRNA (NT) or with siRNAs targeting *CASP4*, *GSDMD* or *GBP1*, after *E. coli* LPS transfection. Cells were treated with siRNAs for 24 h and transfected with LPS (2.5 μ g / 50,000 cells) for 5 h. Graphs show the mean \pm SD, and data are pooled from two (**c, f**), three (**g**) or four (**b**) independent experiments performed in triplicate, or representative of three independent experiments (**d, e**). ****P* < 0.001; ns, not significant; two-tailed *t*-test.

findings suggest that in human epithelial cells one or several IFN γ -induced proteins are required for LPS-induced caspase-4 activation.

GBP1 is required for non-canonical inflammasome activation.

Since caspase-11 activation in mouse macrophages requires IFN-induced GTPases, we speculated that human GBPs were necessary for LPS-induced caspase-4 activation. In agreement with previous studies²⁷, we found that GBPs expression in HeLa cells was strongly upregulated by IFN γ priming (Supplementary Fig. 3a). RNA interference-mediated silencing of GBPs expression revealed a consistent reduction of LDH release in cells lacking GBP1 both after *Salmonella* infection as well as LPS transfection (Supplementary Fig. 3b–g). To confirm the phenotype, we generated *GBP1*^{-/-} HeLa cells by CRISPR-Cas9 genome targeting (Fig. 2a) and found that *GBP1*-deficiency completely abrogated LDH release down to the background levels that were observed in naive cells after *Salmonella* infection or LPS transfection (Fig. 2b, c and Supplementary Fig. 3h, i), without altering bacterial entry (Supplementary Fig. 3j–m). *GBP1*-deficient cells were also unable to cleave and activate caspase-4 upon LPS transfection or *Salmonella* infection (Fig. 2d, e, p32 fragment). Furthermore, GBP1 was strongly required for LDH release when LPS was delivered by electroporation (Fig. 2f). Similarly to the knockout of *CASP4* or *GSDMD*, *GBP1*-deficiency or knock-down of individual GBPs in HeLa only resulted in a partial loss of IFN γ -dependent restriction of cytosolic *Salmonella* replication (compare Supplementary

Figs. 11-s and 3n-p). Finally, GBP1 knock-down in HBEC3-KT and HaCaT cells also reduced LDH release upon LPS transfection (Fig. 2g and Supplementary Fig. 3q), demonstrating that GBP1 is important to regulate LPS-induced cell death in several human epithelial cell lines.

GBP1 targets intracellular *Salmonella* to recruit GBP2-4.

Having demonstrated a role for GBPs in caspase-4 activation, we next expressed fluorescently tagged GBPs individually in naive or primed cells to determine if they target intracellular *Salmonella*. We found that in IFN γ -primed HeLa, GBP1, -2, -3 and -4 coated around 20–30% of intracellular *Salmonella* at 1 h p.i., whereas only very few bacteria were positive for GBP5, -6 or -7 (Fig. 3a, b and Supplementary Fig. 4a). Recruitment of tagged GBP2, -3 and -4 was strongly dependent on IFN γ priming, since these GBPs only poorly associated with *Salmonella* when expressed in naive cells. By contrast, eGFP-GBP1 associated with *Salmonella* even when expressed in naive cells, albeit at lower levels than in primed cells.

GBPs are known to homo- and hetero-oligomerize, forming a coat when recruited to intracellular pathogens²⁸. We hypothesized that GBP1 had the ability to target *Salmonella* independently of other GBPs, whereas GBP2-4 required GBP1 for recruitment²⁷. Indeed, recruitment of GBP2, -3 and -4 to *Salmonella* was completely abrogated in IFN γ -primed *GBP1*^{-/-} HeLa cells (Fig. 3c). Furthermore, GBP1 co-expression in naive cells was sufficient to induce recruitment of tagged GBP2-4 to

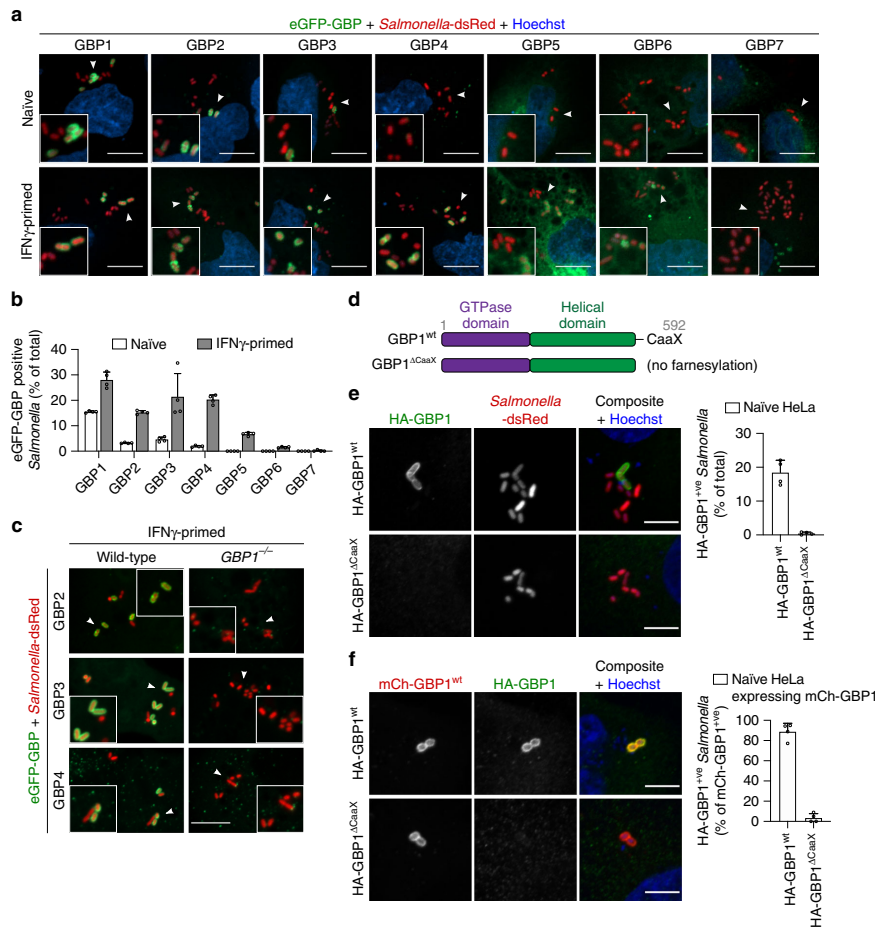


Fig. 3 GBP1 targets *Salmonella* and controls recruitment of GBP2-4. **a** Fluorescence confocal microscopy of naive or IFN γ -primed HeLa expressing N-terminal tagged eGFP-GBP1-7 (green) and infected with *Salmonella*-dsRed (red) for 1 h. DNA was stained with Hoechst (blue). Representative confocal images are shown and scale bars correspond to 10 μ m. **b** Percentage of intracellular *Salmonella* positive for eGFP-GBP1-7 in naive or IFN γ -primed HeLa, at 1 h p.i. At least 200–300 bacteria were counted per coverslip. **c** Fluorescence confocal microscopy of IFN γ -primed wild-type or *GBP1*^{-/-} HeLa expressing eGFP-GBP2-4 (green) and infected with *Salmonella*-dsRed (red) for 1 h. Representative confocal images are shown, and scale bar corresponds to 10 μ m. **d** Schematic representation of wild-type GBP1 and a Δ CaaX mutant. **e, f** Fluorescence confocal microscopy of naive *GBP1*^{-/-} HeLa expressing HA-GBP1^{wt} or HA-GBP1 Δ CaaX (**e**) or co-expressing mCherry-GBP1^{wt} and HA-GBP1^{wt} or HA-GBP1 Δ CaaX (**f**) and infected with *Salmonella* for 1 h. HA-tagged GBP1 was visualized by immunostaining with an anti-HA antibody. Representative confocal images are shown and scale bars correspond to 5 μ m. The percentage of HA-GBP1 positive bacteria was quantified by counting around 100 bacteria per coverslip. Graphs show the mean \pm SD, and data are pooled from two (**b, e, f**) independent experiments performed in duplicate or representative of two (**a, c, e, f**) independent experiments.

intracellular *Salmonella* (Supplementary Fig. 4b, c) to levels similar to those observed in IFN γ -primed cells (Fig. 3b). GBP1 targeting of intracellular *Salmonella* was also observed in primary human small intestinal epithelial cells (Supplementary Fig. 4d). Finally, time-lapse confocal microscopy of infected cells co-expressing GBP1 and either GBP2, -3 or -4, revealed that GBP1 and GBP2 were recruited simultaneously to the bacteria (Supplementary Fig. 4e and Supplementary Movie 3), whereas GBP3 and GBP4 were only recruited to bacteria minutes after GBP1 recruitment (Supplementary Fig. 4f, g and Supplementary

Movies 4, 5). These data show that GBP1 is the first to target intracellular *Salmonella* and orchestrates the hierarchical recruitment of additional human GBP family members, namely GBP2-4. To gain further mechanistic insights on how GBP1 accumulates on intracellular *Salmonella* we analyzed different GBP1 mutants (Fig. 3d and Supplementary Fig. 5a, b)²⁹. GTP hydrolysis, a triple-arginine polybasic motif (584–586) and the C-terminal CaaX box-dependent farnesylation were all required for proper GBP1 recruitment/accumulation around intracellular *Salmonella* (Fig. 3e and Supplementary Fig. 5c). Interestingly, HA-GBP1 Δ CaaX was

still not recruited to *Salmonella* even when co-expressed with mCherry-GBP1^{wt} (Fig. 3f), suggesting that GBP1 oligomers around bacteria are only formed if monomers are farnesylated and capable of properly inserting into membranes.

GBPs target cytosolic *Salmonella* seconds after SCV rupture.

Since mouse GBPs were previously associated with vacuolar rupture¹⁰, we next asked if human GBPs associate with the SCV or cytosolic *Salmonella* by using galectin-3, a protein that binds to β -galactosides found on the inner leaflet of vacuolar membranes, as a marker for ruptured vacuoles³⁰. GBP1-4 were indeed only found in the vicinity of galectin-3-positive bacteria (Fig. 4a), but closer analysis revealed that GBPs targeted the cytosol-exposed part of the bacteria and not the galectin-3-positive ruptured vacuoles (Fig. 4a, insets). Consistently, GBPs did not co-localize with LAMP1 (Supplementary Fig. 6a), a known marker of SCV membranes³¹. Furthermore, we did not observe a reduction in the percentage of cytosolic (Fig. 4b) or galectin-3-positive *Salmonella* (Supplementary Fig. 6b) in *GBP1*^{-/-} cells, indicating that human GBP1-4 did not promote the escape of *Salmonella* from the SCV in HeLa cells, but associate with bacteria upon cytosolic entry. GBP1 also associated with *Shigella flexneri* after its escape from the endocytic vacuole but not with cytosolic *Listeria monocytogenes* (Supplementary Fig. 6c)^{27,29}.

We next used time-lapse confocal microscopy to follow the kinetics of SCV membrane rupture, GBP recruitment and pyroptosis. In *Salmonella*-infected cells, SCV rupture and galectin-3 recruitment was followed by a rapid and massive recruitment of GBP1, often occurring less than 30 seconds upon detectable galectin-3 appearance (Supplementary Fig. 6d and Supplementary Movie 6). GBP1 recruitment often started at one region of the bacterium, presumably the part exposed to the cytosol, then formed a coat around bacteria. GBP1 recruitment to cytosolic *Salmonella* was followed by pyroptotic cell death (Supplementary Fig. 6e and Supplementary Movie 7), and consistently, the majority of pyroptotic cells featured GBP1-positive *Salmonella* (Supplementary Fig. 6f).

In mouse macrophages, GBP targeting of bacteria mediates recruitment of Irgb10, which correlates with the lysis of targeted bacteria and caspase-11 activation¹¹. To determine if human GBPs lysed cytosolic *Salmonella* in HeLa cells, as a mechanism for LPS release and caspase-4 activation, we monitored GBP recruitment in *GSDMD*^{-/-} cells infected with *Salmonella*-dsRed. Live-cell imaging revealed that while the bacteria were rapidly targeted by GBP1, they continued to divide in the host cell cytosol, showing no signs of lysis or viability loss (Supplementary Fig. 7a–d and Supplementary Movies 8–11). Therefore, GBP1 targets the surface of *Salmonella* within seconds upon rupture of the SCV membrane and bacterial escape to the host cytosol, and is followed by rapid induction of caspase-4-dependent pyroptosis independently of bacteriolysis.

GBPs control caspase-4 recruitment to cytosolic *Salmonella*.

Since GBP recruitment did not lyse bacteria, we presumed that GBPs control LPS-dependent caspase-4 activation by another mechanism. When probing for the intracellular localization of caspase-4 we found that caspase-4-eGFP was recruited on *Salmonella*, often covering the entire bacterium (Fig. 4c). Caspase-4 recruitment onto *Salmonella* absolutely required IFN γ priming as it was not detectable in naive cells (Fig. 4c, d and Supplementary Fig. 8a) despite high expression levels of the caspase. Time-lapse confocal microscopy of caspase-4-eGFP-expressing IFN γ -primed HeLa infected with *Salmonella*-dsRed showed that caspase-4, although initially diffused in the cytosol, was recruited to intracellular *Salmonella* within minutes, and that caspase-4

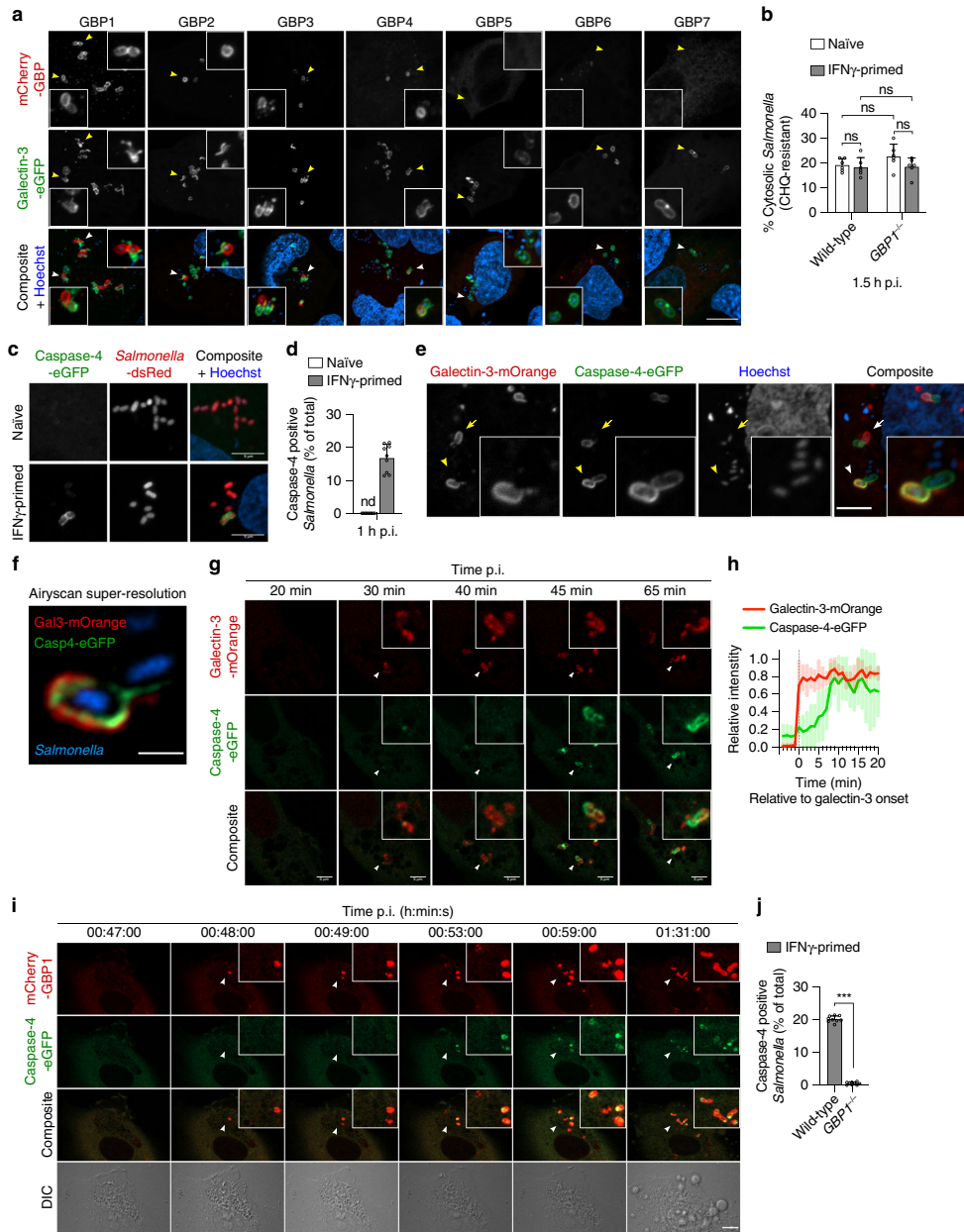
recruitment to *Salmonella* was rapidly followed by pyroptotic cell death in the majority of cells (Supplementary Fig. 8b, c and Supplementary Movie 12). Consistently, the few cells that did not recruit caspase-4 to bacteria did not initiate pyroptosis (Supplementary Fig. 8d and Supplementary Movie 13).

Recruitment of caspase-4 to *Salmonella* correlated with SCV lysis because caspase-4-positive bacteria were found in the vicinity of galectin-3-positive ruptured vacuoles (Fig. 4c and Supplementary Fig. 8e). Similarly to GBP1-4, caspase-4 did not co-localize with LAMP1-positive SCVs (Supplementary Fig. 8f), but targeted the cytosol-exposed part of the bacterium and not the lysed vacuole (Fig. 4e, arrows and arrowheads, and Supplementary Fig. 8e, inset images). Super-resolution microscopy further confirmed that caspase-4 accumulated on the bacterial surface but not on ruptured SCVs (Fig. 4f and Supplementary Fig. 8g). Finally, time-lapse confocal microscopy of infected cells showed that caspase-4 was recruited to *Salmonella* 5–10 min after the first appearance of a galectin-3 signal (Fig. 4g, h and Supplementary Movie 14), altogether demonstrating that caspase-4 targets cytosolic *Salmonella* after SCV rupture.

Since GBP1 also targeted cytosolic *Salmonella* and was required for caspase-4 activation, we hypothesized that GBPs might either control the recruitment of caspase-4 to cytosolic bacteria and/or the activation of caspase-4 at the bacterial surface. Time-lapse microscopy of HeLa cells co-expressing mCherry-GBP1 and caspase-4-eGFP showed that GBP1 recruitment preceded caspase-4 recruitment to the same bacterium by several minutes, and this was followed by pyroptosis (Fig. 4i and Supplementary Movie 15). This is consistent with the faster recruitment of GBP1 upon SCV rupture compared with the slower recruitment of caspase-4 (Supplementary Fig. 6d and Fig. 4g, h). Remarkably, we also observed a complete reduction in caspase-4 recruitment to *Salmonella* in *GBP1*^{-/-} HeLa (Fig. 4j), while GBP1 was still recruited to bacteria in *CASP4*^{-/-} cells (Supplementary Fig. 9). Together with the observation that *GBP1*-deficient cells were not able to activate caspase-4 (Fig. 2), the data suggest that GBP1, either directly or by controlling GBP2-4 recruitment, initiates the recruitment of caspase-4 to the bacterial surface.

GBP1/3/4 are sufficient for LPS-induced caspase-4 activation.

We next addressed the individual functions of GBP1-4 in caspase-4 recruitment and activation. *GBP1*^{-/-} HeLa neither recruit GBP2-4 nor caspase-4 to cytosolic bacteria (Figs. 3c and 4j), thus making it impossible to determine whether GBP1 controls caspase recruitment directly or via other GBPs. We therefore co-expressed caspase-4-eGFP and mCherry-GBP1 in naive or IFN γ -primed cells, and determined caspase targeting to cytosolic *Salmonella*. While GBP1 targeted cytosolic *Salmonella* regardless of IFN γ priming, caspase-4 was only recruited to bacteria in primed cells (Fig. 5a). Thus, other GBPs and/or an unknown IFN γ -induced factor are necessary for GBP1-dependent caspase-4 recruitment. We thus co-expressed caspase-4 and mCherry-GBP1 with either doxycycline (Dox)-inducible eGFP-tagged GBP2, GBP3 or GBP4 in naive HeLa cells and visualized caspase recruitment by confocal microscopy (Supplementary Fig. 10a and Fig. 5b). GBP1 alone, or GBP1 together with GBP2 did not restore caspase-4 recruitment to cytosolic *Salmonella* in naive cells. On the other hand, co-expression of GBP1 with GBP4 and to a lesser degree with GBP3 was sufficient to induce recruitment of caspase-4 to cytosolic bacteria (Fig. 5b, c). The same was observed when using different vectors to co-express the proteins (Supplementary Fig. 10b), which excluded vector-biased caspase-4 recruitment and indicated that GBP1



controls recruitment of caspase-4 mainly via GBP4 and partially via GBP3.

We next asked if expression of single or multiple GBPs in naive cells also restores caspase-4-dependent pyroptosis. Individual expression of GBP1-7 was not sufficient to induce LPS-induced

pyroptosis in naive cells (Supplementary Fig. 10c, d). By contrast, LPS transfection induced significantly elevated levels of LDH release in naive cells co-expressing either GBP1/3/4 or GBP1/2/3/4 (Fig. 5d and Supplementary Fig. 10e, f). Interestingly, co-expression of only GBP1/3 already restored some LPS

Fig. 4 **GBP1 targets cytosolic *Salmonella* and is required for caspase-4 recruitment to the bacterial surface.** **a** Fluorescence confocal microscopy of IFN γ -primed wild-type HeLa co-expressing galectin-3-eGFP (green) and mCherry-GBP1-7 (red) and infected with *Salmonella* for 1 h. **b** Percentage of CHQ-resistant cytosolic *Salmonella* in naive or IFN γ -primed wild-type or GBP1 $^{-/-}$ HeLa at 1.5 h p.i. Cells in triplicate wells were infected for 30 min and then treated with gentamicin \pm CHQ for an additional 1 h before lysing the cells and determining CFUs. The percentage of cytosolic bacteria was calculated as the ratio of (CHQ + gentamicin^{resistant}/gentamicin^{resistant}). **c** Fluorescence confocal microscopy of naive or IFN γ -primed HeLa expressing caspase-4-eGFP (green) and infected with *Salmonella*-dsRed for 1 h. **d** Percentage of caspase-4-eGFP positive *Salmonella* at 1 h p.i., quantified by counting 100–200 bacteria per coverslip. nd, not detected. **e, f** Fluorescence confocal microscopy of IFN γ -primed HeLa co-expressing galectin-3-mOrange (red) and caspase-4-eGFP (green) and infected with *Salmonella* for 1 h. **g** Time-lapse fluorescence confocal microscopy of IFN γ -primed HeLa expressing caspase-4-eGFP (green) and galectin-3-mOrange (red) and infected with *Salmonella*. **h** Mean normalized fluorescence intensities of galectin-3-mOrange and caspase-4-eGFP over time. Fluorescence intensities were quantified in a region of interest as exemplified in the figure, containing an event of caspase-4 and galectin-3 recruitment to an individual bacterium. The relative intensity signals were aligned using the time point of onset of galectin-3 recruitment as zero and the mean and SD of six different events were plotted. **i** Time-lapse fluorescence confocal microscopy of IFN γ -primed HeLa co-expressing caspase-4-eGFP (green) and mCherry-GBP1 (red) and infected with *Salmonella*. Images were acquired every 60 s. DIC, differential interference contrast. **j** Percentage of caspase-4-eGFP positive *Salmonella* at 1 h p.i., in IFN γ -primed wild-type and GBP1 $^{-/-}$ HeLa. 100–200 bacteria were counted per coverslip. Representative confocal images are shown and scale bars correspond to 1 μ m (**f**), 5 μ m (**c, e, g**) or 10 μ m (**a, i**). Graphs show the mean \pm SD, and data are pooled from two (**b**) or three (**d, j**) independent experiments performed in triplicate or representative from at least three independent experiments (**a, c, e–i**). *** $P < 0.001$; ns, not significant, two-tailed t -test.

transfection-induced pyroptosis, whereas co-expression of GBP1/4 had no effect even though it was sufficient to promote caspase-4 recruitment on *Salmonella* (Fig. 5b, c and Supplementary Fig. 10b). Thus, while GBP1 drives caspase-4 recruitment to cytosolic *Salmonella* mainly by GBP4, GBP3 is nevertheless necessary to yield caspase-4 activation (Fig. 5b, d). In conclusion, these experiments indicate that a complex formed by GBP1, –3 and –4 promotes caspase-4 recruitment and activation following LPS detection without the requirement for other IFN γ -induced genes.

GBP1 directly binds LPS. Since GBPs showed a recruitment to cytosolic Gram-negative bacteria, OMVs or even transfected LPS (Fig. 3, Supplementary Fig. 6c and ref. 12), we tested if GBPs can directly bind LPS. Similarly to caspase-4 (Fig. 1i and Supplementary Fig. 2g), biotin-LPS was able to pull-down eGFP-GBP1 and to a lesser degree eGFP-GBP3, but not tagged GBP2 or GBP4 (Fig. 6a) from HeLa lysates. To assess if this interaction was direct, we next purified LPS-free recombinant His-GBP1 from CleanColi[®] BL21 (DE3) bacteria that produce Lipid IV_A (which does not activate caspase-4/–11) instead of LPS followed by a lipid removal protocol³² and tested GBP1-LPS binding by surface plasmon resonance (SPR). SPR showed a direct binding of LPS to immobilized GBP1 with a K_D of ~60 nM, which is comparable to the published K_D of the LPS-caspase-4 and LPS-caspase-11 interaction (Fig. 6b–d). Kinetic analysis also showed that GBP1-LPS binding best fitted with a two-state-reaction model that describes a situation where initial binding is followed by a conformational change that stabilizes the complex. The complementary experiment with immobilized LPS also yielded similar a K_D (Supplementary Fig. 11a, b), however the response was relatively weak since only a small amount of LPS adsorbed on the chip surface. Moreover, microscale thermophoresis (MST) of GBP1 and FITC-LPS confirmed the interaction yielding a comparable K_D value (Supplementary Fig. 11c).

We next investigated the consequences of the LPS-GBP1 interaction, since LPS was suggested to induce caspase-11/–4 oligomerization⁵. LPS-free recombinant GBP1 ran as a single monomeric peak on size-exclusion chromatography (SEC), close to its predicted size of 68.5 kDa (Fig. 6e, f, Supplementary Fig. 11d and Table 1), while *E. coli* and *Salmonella* Typhimurium LPS formed micelles eluting at around 1000 kDa (void volume). When GBP1 was incubated with LPS, the elution profile changed, resulting in a shift of the majority of GBP1 to higher molecular weight peaks from the range of 400 kDa to over 1000 kDa (Fig. 6e, f, Supplementary Fig. 11d and Table 1). The most prominent

peak was found to be at 1000 kDa, indicating that GBP1 bound to LPS micelles, but smaller complexes were detected as well. Interestingly, even LPS from *Rhodobacter sphaeroides* induced a shift of GBP1 to higher molecular weight peaks (Supplementary Fig. 11d, e), despite acting as an antagonist of caspase-11 and not being able to induce oligomerization of the caspase⁵. Conversely, incubation of GBP1 with lipoteichoic acid (LTA) or peptidoglycan (Supplementary Fig. 11f, g) did not result in a similar shift. LBP and ovalbumin were used as positive and negative LPS-binding controls, respectively (Supplementary Fig. 12a)³³. We next tested what part of LPS is required for the binding of GBP1 to LPS micelles. LPS from *E. coli* Ra, Rc, Rd, Re mutant strains, which lack the O-antigen and outer core, respectively, was still bound by GBP1 as it resulted in a shift to high-molecular weight peaks (Supplementary Fig. 12b, c). Consistently, *Salmonella* Δ waal or Δ waag mutants (lacking the O-antigen or outer core, respectively) still recruited GBP1 and caspase-4 in infected cells (Supplementary Fig. 12d–f). Since the LPS-GBP1 interaction was highly sensitive to detergents, the binding to Lipid A could not be tested since this requires solubilization of Lipid A with Tween-20 or other detergents⁷. Since GBP1 displays an oligomerization-dependent activation of GTP hydrolysis³⁴, we finally assessed the impact of LPS on GBP1 GTPase activity (Fig. 6g). As reported previously, GBP1 had some intrinsic ability to hydrolyse GTP on its own, but its GTPase activity was significantly increased when incubated with LPS, supporting the fact that GBP1 interacts with LPS, and suggesting that LPS binding might promote an oligomeric state. In conclusion these findings indicated that GBP1 was able to bind directly to LPS, and that the LPS Lipid A and inner core region were sufficient for LPS-GBP1 interaction.

GBP1-LPS interaction involves electrostatic interactions. Each LPS molecule from *E. coli* has 6–8 negatively charged groups, from phosphates and acid groups in the Lipid A and inner core (Supplementary Fig. 12b)³⁵. Given that human GBP1 lacks the hydrophobic pockets that comprise the LPS binding sites in CD14 and MD-2, we hypothesized that GBP1 binds to LPS by electrostatic interactions, similarly to LBP^{36,37}. Consistently, GBP1 binding to LPS micelles was disrupted by incubation with cations (Ca²⁺), which neutralize the negative charges on LPS^{35,38}, or by incubation with polymyxin B, which interacts with the LPS Lipid A and inner core region through ionic and hydrophobic forces, resulting in more monomeric GBP1 and reduced levels of GBP1-LPS association (Fig. 7a and Supplementary Fig. 13). Furthermore, dephosphorylating LPS with alkaline phosphatase reduced GBP1-LPS binding and cell death upon LPS transfection

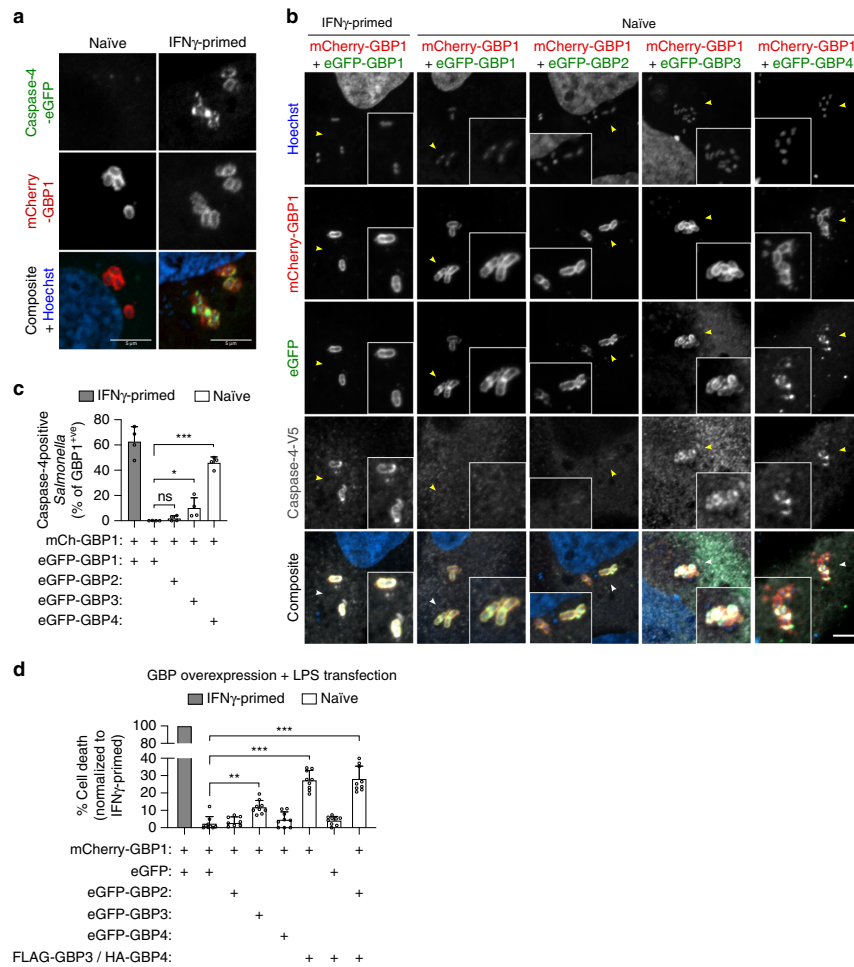


Fig. 5 GBP1/4 are sufficient to recruit caspase-4 to *Salmonella* and together with GBP3 activate the non-canonical inflammasome in naive human epithelial cells. **a** Fluorescence confocal microscopy of naive and IFN γ -primed HeLa co-expressing caspase-4-eGFP (green) and mCherry-GBP1 (red) and infected with *Salmonella* for 1 h. DNA was stained with Hoechst (blue). Representative confocal images are shown and scale bar corresponds to 5 μ m. **b** Fluorescence confocal microscopy of IFN γ -primed or naive HeLa cells co-expressing mCherry-GBP1 (red), Dox-inducible eGFP-GBP1, -2, -3 or -4 (green) and caspase-4-V5 (gray), and infected with *Salmonella* for 1 h. DNA was stained with Hoechst (blue). eGFP-GBPs were expressed by inducing cells with 1 μ g/mL Dox for 16 h. Caspase-4-V5 was visualized by immunostaining with an anti-V5 antibody. Representative confocal images are shown and scale bar corresponds to 10 μ m. **c** Percentage of caspase-4-V5 positive *Salmonella* at 1 h p.i., quantified out of the mCherry-GBP1-positive bacteria. At least 50 GBP1-positive bacteria were counted per coverslip. **d** Percentage of cell death in HeLa cells co-expressing constitutive mCherry-GBP1 and Dox-inducible eGFP or eGFP-GBP1, -2, -3 or -4. FLAG-GBP3 and HA-GBP4 were constitutively expressed together using a bicistronic plasmid. Cells were transfected with the indicated plasmids for 24 h. eGFP-GBPs were induced for 16 h with 1 μ g/mL Dox, whereas eGFP was induced for 3 h. Cells were then transfected with *E. coli*-derived LPS (2.5 μ g/50,000 cells) for 6 h and cell death values were normalized considering IFN γ -primed HeLa as 100% and naive cells co-expressing mCherry-GBP1 and eGFP as 0%. Graphs show the mean \pm SD, and data are pooled from two independent experiments performed in duplicate (**c**), pooled from three independent experiments performed in triplicate (**d**) or are representative from two (**b**) or three (**a**) independent experiments. ** P < 0.01; *** P < 0.001; one-way ANOVA.

(Fig. 7a, b and Supplementary Fig. 13), indicating that the phosphate groups found on Lipid A and inner core sugars of LPS (Supplementary Fig. 12b) play an essential role in promoting GBP1-LPS interaction and subsequent activation of the

non-canonical inflammasome pathway. Basic residues in the N-terminal domain of LBP mediate binding to LPS micelles³⁹. We thus mutated several positively charged surface patches in GBP1 and tested the impact of the mutations on GBP1-LPS interaction

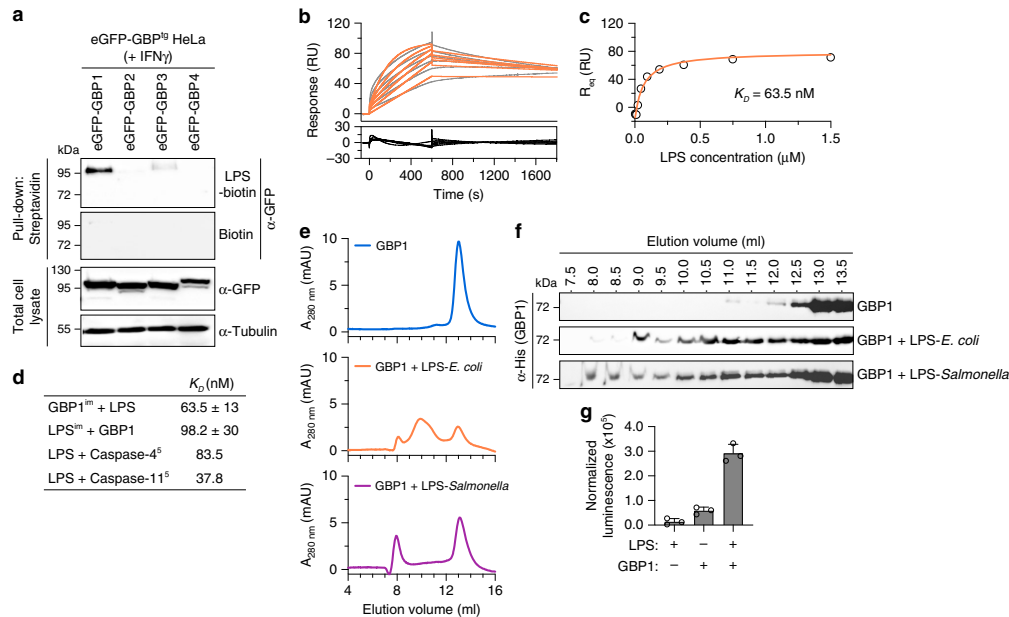


Fig. 6 LPS binds to GBP1 to induce formation of a high-molecular weight protein complex. **a** Streptavidin pull-down assay for eGFP-GBP1-4 using biotin or biotin-conjugated LPS. HeLa cells stably expressing Dox-inducible eGFP-GBP1, -2, -3, or -4 were primed with IFN γ and 1 μ g/mL Dox was added for 16 h. 1 million cells were lysed and incubated with 2 μ g LPS-biotin or biotin, and the biotinylated substrates were pulled down using equal amounts of streptavidin magnetic beads, which were then eluted in equal volumes of SDS-PAGE reducing sample buffer. Streptavidin-bound and -unbound fractions were analyzed by western blot using an antibody against GFP. **b** SPR sensorgram of *E. coli* LPS (O111:B4) binding to human GBP1 immobilized on a CM5 chip surface. Sensorgram was obtained by using different LPS concentrations (47, 94, 188, 375, 750, and 1500 nM). Gray lines correspond to SPR data and orange lines to model fits using a two-state-reaction model. **c** Saturation curve of the titration of LPS on GBP1 immobilized on a CM5 chip. **d** Calculated dissociation constants (K_D) for LPS binding to immobilized GBP1 (GBP1tm) or GBP1 binding to immobilized *E. coli* LPS (LPStm). Dissociation constants for LPS-caspase-4 and LPS-caspase-11 were previously published by Shi et al.⁵ **e, f** Size exclusion chromatograms of recombinant, LPS-free His₆-tagged GBP1 incubated with various LPS derivatives. Following purification, GBP1 (1 μ M) was incubated on ice with LPS (2 μ M) for 5 h before being subjected to size-exclusion analysis on a Superdex 200 10/30 GL column. Protein size was estimated using molecular weight standards. Curves were corrected by subtracting LPS-specific absorbance at 280 nm. Individual fractions were run on a 12% acrylamide gel and immunoblotted against His₆ to confirm the presence of GBP1 in elution peaks (**f**). **g** GTPase activity analysis of recombinant GBP1. GBP1 (500 nM) was incubated with GTP (5 μ M) with or without ultrapure LPS (5 μ M) for 30 min before the reaction was stopped. Luminescence was normalized to a buffer-only control. Graphs show the mean \pm SD, and data are representative from three (**a-d, g**) or five (**e, f**) independent experiments performed with at least three independently expressed and purified batches of recombinant His-GBP1.

| Sample | Theoretical size (kDa) | Observed size (kDa) |
|-------------------------------|------------------------|---------------------|
| GBP1 | 67.01 | 78.7 |
| GBP1 + LPS- <i>E. coli</i> | | 1028; 401.8; 78.7 |
| GBP1 + LPS- <i>Salmonella</i> | | 1140.5; 78.7 |
| GBP1 + LPS- <i>R. sph</i> | | 1318.6; 364 |

by SEC (Fig. 7c, d). While most mutations resulted in no or minor effect on the binding of GBP1 to LPS micelles, mutation of the triple-lysines 61-63 to alanines (A patch) notably reduced the formation of the higher molecular weight GBP1 peaks (~40%) and increasing the levels of monomeric GBP1, thus suggesting that these residues are required for binding (Fig. 7d and Supplementary Fig. 14a). Furthermore, expression of

GBP1^{KKK61-63AAA} (A patch) resulted in a significant reduction of targeting to cytosolic *Salmonella* compared with either GBP1^{WT} or GBP1^{KKK87-88AA} (B patch) (Fig. 7e, f and Supplementary Fig. 14b). In summary, the results demonstrate that the GBP1-LPS interaction involves electrostatic forces and that disrupting the binding by dephosphorylating LPS or mutating GBP1 results in reduced caspase-4-induced pyroptosis upon LPS transfection or impaired GBP1 targeting of the bacterial surface.

Discussion

Here we report that GBP1 functions as an LPS sensor that recognizes Gram-negative bacteria in the cytosol of human epithelial cells, and that GBP1-LPS interaction involves electrostatic forces (Supplementary Fig. 15). Given that GBP1 is necessary for LPS-induced caspase-4 activation in various human cell types and after various LPS delivery methods (electroporation, chemical transfection, Gram-negative bacteria infection), our data imply that GBP1 is the very first protein in the non-canonical

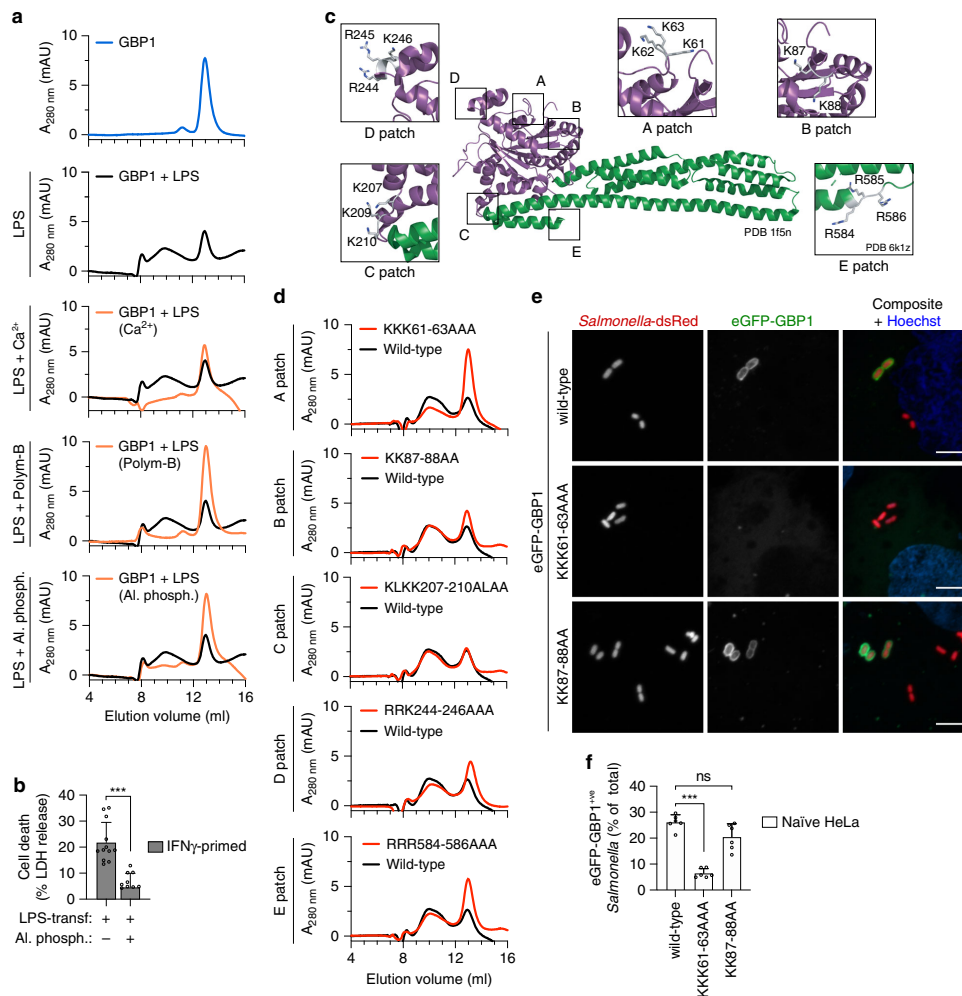


Fig. 7 GBP1 is recruited to the bacterial surface and binds LPS through electrostatic interactions. **a** Size exclusion chromatograms of recombinant His-tagged GBP1 incubated with *E. coli* LPS, or with *E. coli* LPS pre-treated with CaCl₂ (5 mM), Polymyxin B (10 μ g/mL) or with alkaline phosphatase. Curves were corrected by subtracting the respective LPS-specific absorbance at 280 nm. Black curves representing control condition were overlaid. **b** Release of LDH from IFN γ -primed HeLa 5 h after transfection with *E. coli* LPS, or after transfection with LPS previously treated with alkaline phosphatase. **c** 3D structure of human GBP1 (PDB 1f5n), highlighting five different negatively charged patches (A to E). Residues comprising patch E are only visible in PDB 6k1z. For each patch, the indicated residues were all mutated to alanines and analyzed for GBP1-LPS interaction by size exclusion chromatography. Purple indicates GTPase domain, green indicates helical domain. **d** Size exclusion chromatograms of different His-tagged GBP1 mutants incubated with *E. coli* LPS. Curves were corrected by subtracting LPS-specific absorbance at 280 nm. **e** Fluorescence confocal microscopy of naive HeLa expressing eGFP-GBP1^{wt}, eGFP-GBP1^{KKK61-63AAA} or eGFP-GBP1^{KK87-88AA} and infected with *Salmonella*-dsRed for 1 h. DNA was stained with Hoechst (blue). Representative confocal images are shown and scale bar corresponds to 5 μ m. **f** Percentage of eGFP-GBP1 positive *Salmonella* at 1 h p.i., as quantified by counting between 100–200 bacteria per coverslip. Graphs show the mean \pm SD, and data are pooled from three independent experiments performed in duplicate (**f**), four independent experiments performed in triplicate (**b**), or are representative from three (**a**, **d**, **e**) independent experiments. *** P < 0.001; ns, not significant, two-tailed t -test.

inflammasome pathway that interacts with LPS. This places GBP1 upstream of caspase-4 in cytosolic LPS sensing, raising the question if it might act similarly to LBP which acts as a co-factor for extracellular LPS detection by CD14 and MD-2/TLR4. Indeed, the finding that GBP1-LPS requires negative charges on LPS

Lipid A and the inner core sugars as well as a positively charged surface patch in GBP1 is reminiscent of the mode of LPS binding by LBP, which involves two positively charged patches at the tip of the LBP N-terminal domain. From a functional point of view LBP and GBP1 will most likely differ. LBP binds to LPS micelles

and to CD14 protein, and catalyzes multiple rounds of LPS transfer to CD14, which will then transfer a single bound LPS molecule to MD-2/TLR4. GBP1 on the other hand, does not function alone, but as part of a GBP1-4 complex that assembles on LPS-containing membranes. It is possible that this complex recruits caspase-4 and then transfers LPS onto caspase-4 thus promoting its activation. Alternatively, it is also possible that the assembly of the GBP complex and insertion of the GBPs into the bacterial membranes via lipid anchors results in a partial weakening of membrane integrity, thus allowing caspase-4 to bind the Lipid A moiety of LPS. Additional studies aimed at determining the structure and composition of the GBP complex will be necessary to understand how it promotes caspase-4 recruitment and activation.

While it is not yet clear if the GBP1-LPS interaction also requires structural determinants in LPS, the ability of GBP1 to recognize negatively charged pathogen-derived molecules might extend its function beyond the recognition of Gram-negative bacteria. Indeed, GBP1 is known to be recruited to both the surface of cytosolic parasites, such as *T. gondii*, as well as to the membrane of the *T. gondii* parasitophorous vacuole, and to assemble a GBP coat in a similar manner^{25,28}. Interestingly, in this case the GBP coat does not result in recruitment of caspase-4 (in line with the fact that parasites do not feature LPS), but in the induction of caspase-8-dependent apoptosis⁴⁰. It is thus likely that parasites or their vacuoles feature molecules with similar chemical properties as the LPS Lipid A and core polysaccharides in their cell membrane or the membrane of the parasitophorous vacuole. Identification of additional ligands that bind GBP1 or other GBP family member will enhance our understanding of host innate immunity and establish new paradigms for pattern recognition.

The human-specific mechanism reported here is in contrast to previous models that proposed that, in mice, GBPs promote non-canonical inflammasome activation by facilitating vacuolar escape and inducing bacterial membrane destruction^{10,41}. While it is unlikely that mouse GBPs function fundamentally differently from human GBPs in the mechanism by which they recognize pathogens, it is possible that the existence of IRGs in mouse enhances their downstream effector functions. The lysis of bacteria and vacuoles reported in mouse cells (but not detected in human cells), is most likely a consequence of GBP-mediated recruitment of IRGs, such as Irgb10 that is reported to have antimicrobial properties¹¹. Thus, in addition to recruiting caspase-11 directly in analogy to human GBPs, mouse GBPs might also mediate access to LPS and LPS liberation through the membranolytic activity of IRGs.

To our knowledge, our study is the first to report a ligand of GBP1 and to characterize the mode of this interaction. While our findings still need to be validated in primary human cells, it nevertheless provides the first evidence that GBP1 and possibly other GBPs function as direct innate immune receptors for pathogen-associated molecular patterns, expanding the ever-increasing repertoire of cytosolic innate immune defense pathways.

Methods

Bacterial strains and mammalian cell culture. All bacteria were grown at 37 °C in an orbital shaker. *Salmonella enterica* serovar Typhimurium strain SL1344 was grown in lysogeny broth (LB) medium supplemented with 10 g/L NaCl and streptomycin (50 µg/mL). *Salmonella* expressing dsRed (*Salmonella*-dsRed) was grown by supplementing LB medium with ampicillin (50 µg/mL). *Salmonella enterica* serovar Typhimurium strain 4/74 and their isogenic *Δ*waag or *Δ*waal mutants were a kind gift from Jay Hinton (University of Liverpool, Liverpool). *Shigella flexneri* M90T expressing the adhesin Afal was a kind gift from Jost Enninga (Institut Pasteur, Paris) and was grown in tryptic soy broth (TSB) supplemented with ampicillin (50 µg/mL). *Listeria monocytogenes* strain EGD was a

kind gift from Pascale Cossart (Institut Pasteur, Paris) and was grown in brain-heart infusion (BHI) medium. Unless stated otherwise, the HeLa clone CCL-2 from ATCC was used. Human epithelial HT-29 and HeLa (CCL-2 or Kyoto clones) cells were cultured in DMEM (Gibco) supplemented with 10% Fetal Calf Serum (FCS). Caco-2/TC-7 were cultured in DMEM supplemented with 20% FCS. HT-29 and Caco-2 cells were a kind gift from Shaynoor Dramsi (Institut Pasteur, Paris). THP-1 and U937 cells were cultured in RPMI supplemented with 10% FCS. HBEC3-KT cells were obtained from ATCC and were grown in Bronchial/Tracheal Epithelial Cell Growth Medium (Cell Applications, Inc.). HaCaT cells were obtained from CLS Cell Lines Service GmbH, and were grown in DMEM supplemented 10% FCS. HIEC-6 cells were obtained from ATCC and grown in Opti-MEM (Gibco) supplemented with 4% FCS, 10 mM Glutamine and 10 ng/mL of epidermal growth factor (EGF). Human primary monocyte-derived macrophages (hMDMs) were purified from buffy-coat obtained from the Swiss Red-Cross and purified and cultured as described previously⁴². All cells were grown at 37 °C, 5% CO₂.

Generation of CRISPR/Cas9 knockout cell lines. Knock-out HeLa cell lines were generated using the Alt-R CRISPR-Cas9 System (Integrated DNA Technologies, IDT), by using a mix of a sequence-specific CRISPR RNA (crRNA), a conserved, transactivating crRNA (tracrRNA) and recombinant Alt-R *S. pyogenes* Cas9 (IDT). crRNA and tracrRNA were mixed to 1 µM, heated 5 min at 95 °C and cooled to room temperature. 1 µM Alt-R Cas9 was mixed and incubated at room temperature for 5 min. Lipofectamine RNAiMax transfection reagent (Invitrogen) was then added and the mixture was incubated for 20 min at room temperature. 40,000 cells/well were reversely transfected with the previous mixture in 96-well plates, to achieve a concentration of 10 nM ribonucleoprotein complex. After incubation for 2 days at 37 °C, 5% CO₂, single clones were generated by serial dilutions and the desired gene knockouts were screened by performing the T7 endonuclease I assay, verified by sequencing of the PCR fragments and confirmed by western blotting. The following crRNAs were used: AGGGATCCAAACACCTTAAG (for CASP4), CCAAGTACACGTTGTCCCGC (for GSDMD) and GAACACTAATGGGCGACTGA (for GBP1).

Plasmids, siRNAs, and cell transfection. Plasmids expressing N-terminal fluorescently tagged GBPs were generated by inserting the GBPs coding sequences at the XhoI/HindIII sites of pEGFP-C1 and pmCherry-C1 (Clontech). pmIRFP703-GBP1 was generated by using the pEGFP-C1 plasmid and replacing eGFP by mIRFP703 (addgene 80001⁴³ was used as PCR amplification template) at the NheI/BglII sites, and then inserting the GBP1 coding sequence at the XhoI/HindIII sites. Caspase-4-eGFP was generated by fusing the amplified PCR products of caspase-4 and eGFP and inserting the coding sequence into the NheI/HindIII sites of pEGFP-C1. The pAIP vectors expressing HA-GBP1 or HA-GBP2 were a kind gift from T. Henry (CIRI, Lyon) and were used to generate HA-tagged GBPs, by replacing GBP1 by the GBP3 or -4 coding sequences at the EcoRI sites. The bicistronic plasmids encoding FLAG-GBP3 + HA-GBP4 were generated by inserting GBP3 or GBP4 at the NotI/PmeI sites of the pBud-EGFP vector (addgene 23027⁴⁴). Doxycycline-inducible eGFP-GBP1, -2, -3, -4 were generated by amplifying eGFP-GBPs generated above by PCR and inserting the coding sequences at the BamHI site of the pLVX-Puro vector (Clontech). All cloning was performed using In-Fusion cloning technology (Clontech) and plasmids were verified by sequencing. Plasmids encoding eGFP or mOrange tagged galectin-3 were a kind gift from Jost Enninga^{30,45}. HeLa cells were either plated onto 8-well µ-slides (Ibidi) at a density of 1.5 × 10⁴ cells/well for live imaging, onto 24-well plates containing glass coverslips at a density of 1.0 × 10⁵ cells/well, onto 96-well glass bottom plates (Greiner) or onto 96-well plates (Eppendorf) at a density of 8.0 × 10⁴ cells/well 24 h before transfection. Cells were then transfected with one, two or three expression plasmids using X-tremeGENE 9 DNA transfection reagent (Roche) for 16–48 h, according to the manufacturer's instructions. A list of the plasmids and primers used in this study is provided in Supplementary Table 1. For siRNA knock-down experiments, cells were seeded onto 96-well plates at a density of 9.0 × 10⁴ cells/well and on the following day transfected with 3 pmol (25 nM) Stealth RNAiTM siRNAs (Thermo Fisher Scientific) using Lipofectamine RNAiMax (a list of the siRNAs used in this study is shown in Supplementary Table 2). After 8 h, cells were incubated with IFN γ for an additional 16 h and experiments were then performed.

Infection assays and transfection of cells with LPS. When indicated, cells were primed with 10 ng/mL human IFN γ (Peprotech) for 16 hours. Overnight *Salmonella* cultures were sub-cultured 1/50 and grown until late exponential/early stationary phase (OD₆₀₀ = 1.5–1.8). Overnight *Shigella* or *Listeria* cultures were sub-cultured 1/100 and grown until mid-exponential phase (OD₆₀₀ = 0.5–0.7). Before infection, bacteria were collected by centrifugation, gently washed and resuspended in DMEM. *Salmonella* was added to HeLa cells in 96-well plates (approximately 50,000 cells per well) at a multiplicity of infection (MOI) of 50 and incubated for 30 min at 37 °C. For infection with *Shigella* or *Listeria*, bacteria were added to cells at a MOI of 20 and incubated for 30 min at 37 °C. Non-internalized bacteria were removed by three washes with warm DMEM and cells were incubated with DMEM containing 100 µg/mL gentamicin for 1 h to kill extracellular bacteria. Medium was then changed to DMEM containing 10 µg/mL gentamicin and 10% FCS for the remainder of the experiment. At the desired time points *p.i.*, cells were either processed for

LDH release, enumeration of intracellular bacteria or fixed for immunofluorescence assays. To enumerate intracellular bacteria, infected cells were gently washed with PBS and lysed with water containing 0.2% Triton X-100. Bacteria were then serially diluted and plated onto LB agar. To quantify the percentage of cytosolic *Salmonella* in the total population, we used a CHQ resistance assay. Briefly, infected cells were incubated with 200 µg/mL CHQ (Sigma-Aldrich) and gentamicin for 1 h (CHQ-resistant bacteria) or with gentamicin only (total bacteria). Cells were washed, lysed and bacteria were plated as described above. The percentage of cytosolic bacteria was calculated by the ratio of (CHQ + gentamicin^{resistant}/gentamicin^{resistant}). U937 and THP-1 cells were seeded and differentiated with 100 ng/mL PMA for 48 h, followed by a 24 h resting period.

Transfection of cells with smooth LPS from *E. coli* O111:B4 (Invivogen) or *Salmonella* (Sigma, L6143) was done at a concentration of 2.5 µg/50,000 cells, or 2.5 µg/80,000 cells (for THP-1 or U937), using Lipofectamine 2000 (Invitrogen). Briefly, LPS was diluted in Opti-MEM and incubated with Lipofectamine 2000 (1.0 µl/50,000 cells) for 20 min at room temperature. 75 µl of Opti-MEM was added to cells on 96-well plates and then 75 µl of LPS mixture was added on top. Plates were centrifuged for 5 min at 211 × g and then incubated at 37 °C for the indicated time points. For electroporation of HeLa or HBEC3-KT cells, the Neon Transfection System (Life Technologies) was used. Briefly, naive or IFN γ -primed cells were harvested, resuspended in resuspension buffer T and electroporated with LPS from *E. coli* O111:B4 at a concentration of 300 ng/50,000 cells, using electrolytic buffer E and 1 pulse of 1300 V for 20 ms. Cells were then added to 200 µl pre-warmed Opti-MEM in a 96-well plate, centrifuged for 5 min at 211 × g and then incubated at 37 °C. Mock electroporation and non-electroporated cells were used as controls.

Microscopy, time-lapse imaging, and image analysis. Infected cells were washed once with PBS and fixed in 4% PFA for 20 min. Cells were then washed three times, permeabilized with 0.05% saponin and blocked with 1% BSA. Coverslips were incubated with antibodies when indicated and with Hoechst (1:1000) in PBS, and then mounted in ProLong Gold Antifade (Life Technologies) for confocal microscopy. Samples were imaged with a Zeiss LSM800 confocal laser scanning microscope using a 63 \times /1.4 NA oil objective, by acquiring Z-stacks of 300 nm step size. For live imaging, infection assays were performed in EM buffer (120 mM NaCl, 7 mM KCl, 1.8 mM CaCl $_2$, 0.8 mM MgCl $_2$, 5 mM glucose, 25 mM HEPES, pH 7.3). Cells were infected for 10 min as previously described, extracellular bacteria were removed by washing with warm EM buffer, and time-lapse microscopy of living cells was performed at 37 °C using a motorized xyz stage with autofocus. Super-resolution was performed using the Zeiss LSM800 Airyscan super-resolution system using the same objective and super-resolution images were calculated using the Zeiss ZEN software. Data were further analyzed and processed using Fiji software, and all fluorescence derived images shown here correspond to maximum 3D projections.

LDH release, PI uptake, IL-18 release, and western blotting. Cell death was quantified by measuring LDH release to the supernatant, using the LDH cytotoxicity detection kit (Takara, Clontech). To normalize for spontaneous cell lysis, the percentage of cell death was calculated as follows: $(LDH_{\text{sample}} - LDH_{\text{negative control}}) / (LDH_{\text{positive control}} - LDH_{\text{negative control}}) \times 100$. PI influx measurement was performed as previously described⁴⁶. The levels of IL-18 were measured by ELISA (R&D Systems), according to the manufacturer's instructions. For western blotting analysis, cell lysates were prepared and supernatants were precipitated. Mouse anti-caspase-4 B9 (ADI-AAM-114-E, Enzo Life Sciences, 1:750), rabbit anti-GSDMD (ab210070, abcam, 1:1000), rabbit anti-GBP1 (ab121039, abcam, 1:1000), mouse anti-GAPDH (AM4300, Thermo Scientific, 1:1000), mouse anti-V5 (R960-25, Thermo Scientific, 1:2000), mouse anti-GFP (632381, Clontech, clone JL-8, 1:5000), mouse anti-HA (ENZ-ABS-118-0200, Enzo Life Sciences, 1:2000), mouse anti-tubulin (ab40742, Abcam, 1:2000) were used and detected with horseradish peroxidase-conjugated secondary antibodies (1:5000, Southern Biotech).

Active caspase pull-down. HeLa cells were seeded onto 6-well plates and primed for 16 h with 10 ng/mL human IFN γ . Approximately 3×10^6 cells were then treated with 10 µM of biotin-VAD-fmk and transfected with 20 µg of *E. coli* LPS for 3 hours. Cells were lysed and incubated overnight with 20 µl of pre-washed streptavidin magnetic beads (Thermo Scientific). The beads were washed as described elsewhere⁴⁷ and streptavidin-bound and left-over fractions (unbound) were analyzed on a 12% acrylamide gel and blotted against caspase-4.

Streptavidin pull-down assays. Approximately 2×10^6 cells were collected and lysed in pull-down buffer (50 mM Tris-HCl (pH 7.5), 150 mM NaCl, 5 mM EDTA, 1% NP40, 0.05% Na-deoxycholate and complete protease inhibitors). 700 µg of protein (as determined by BCA assay (Thermo Scientific)) from the total cell lysate was incubated with 2 µg biotinylated LPS or with biotinylated Pam $_3$ CSK $_4$ (Invivogen) at room temperature for two hours with rocking. After incubation, 20 µl of pre-washed streptavidin magnetic beads (Thermo Scientific) were added and incubated for 1 h at room temperature with constant rocking. The beads were washed three times in PBS with 0.05% Tween-20 and once with PBS and the precipitates were eluted in equal volumes of SDS-PAGE reducing sample buffer followed by western blotting analysis. 5% of the initial cell lysate (input) and equal

volumes of pull-down were analyzed. For GFP-GBP pull-down assay, cells were lysed at a concentration of 20×10^6 cells/mL of lysis buffer (50 mM Tris pH 7.4, 150 mM NaCl, 10 mM MgCl $_2$, 5 mM GTP, 300 µM AIF, 100 µg/mL digitonin (Sigma) and allowed to lyse on ice for 15 min. The cells were then spun 15 min at 6000 × g, 4 °C. The soluble extract was then incubated with 2 µg LPS/million cells equivalent and incubated at RT for 2 h with rotation. After incubation, streptavidin magnetic beads were added to the mix and incubated for an additional hour with rotation. The beads were then washed three times (30 min wash) with lysis buffer. The beads were then resuspended in reducing western blot loading buffer before being analyzed by immunoblotting.

Quantitative PCR (qPCR). Total mRNA was extracted from HeLa cells using the RNeasy Mini kit (Qiagen) and up to 400 ng were reverse transcribed into cDNA using the Verso cDNA Synthesis kit (Thermo Fisher Scientific). Gene expression levels were quantified by qPCR using a LightCycler 480 (Roche) and LightCycler 480 SYBR Green I Master (Roche), according to standard protocols, by normalizing each sample to the respective levels of the housekeeping mRNA *HPRT*. The list of primers used for qPCR is shown in Supplementary Table 3.

Purification of recombinant proteins. Full-length human GBP1 was cloned in pET-28a to generate an N-terminally His-tagged hGBP1 construct. pET-28a-hGBP1 was transformed into CleanColi BL21 (Lucigen), and the bacteria were grown in 2xYT medium until an OD $_{600}$ of 0.5–0.7. Protein expression was then induced at 30 °C for 5 h with 0.2 mM IPTG. The bacterial pellet was resuspended in resuspension buffer (50 mM Tris pH 7.4, 150 mM NaCl, 1% Tween 20) and frozen at –80 °C until purification. For most assay, protein was freshly purified on a Ni-NTA affinity column using standard protocols⁴⁸. Protein yield was quantified using Beer-Lambert law. After purification on a Ni-NTA column, GBP1 was further purified on a size exclusion chromatography column (Superdex 200 10/30 GL, GE Healthcare) in running buffer (50 mM Tris pH 7.4, 150 mM NaCl) and concentrated using Amicon Ultra4 10 kDa (Millipore).

Size exclusion chromatography of GBP1 and LPS. Freshly purified GBP1 (1 µM) was incubated on ice alone or with a two-fold molar excess of LPS or LPS-derivatives for 5 h. Ultrapure O111:B4 *E. coli* LPS (Invivogen), *Salmonella* Typhimurium Smooth LPS (Enzo Life Science), *Rhodobacter sphaeroides* ultrapur LPS (Invivogen), *E. coli* F585 diphosphoryl Lipid A (Sigma-Aldrich), *Salmonella minnesota* 595 Lipid A (Invivogen), synthetic monophosphorylated Lipid A (Invivogen), *E. coli* EH100 LPS Ra mutant (Sigma-Aldrich), *E. coli* J5 LPS Rc mutant (Sigma-Aldrich), *E. coli* F583 LPS Rd mutant (Sigma-Aldrich), *E. coli* R515 LPS Re mutant (Enzo Life Science) was used. After incubation, GBP1 alone or GBP-LPS incubations were injected into a Superdex 200 10/30 GL column and run in running buffer for 1 column volume. Individual fractions (500 µL), were collected, precipitated with methanol and chloroform⁴⁹, separated on a 12% acrylamide gel and analyzed by immunoblotting using an antibody against His $_6$ tag. Experimental molecular weights of the peaks were approximated using a gel filtration standard (1511901; Bio-Rad). Where indicated, LPS was pre-incubated with 5 mM CaCl $_2$ for 5 min on ice before being added to GBP1, as indicated above, or LPS was pre-incubated with polymyxin B (10 µg/mL) for 5 min at room temperature.

Surface plasmon resonance (SPR). SPR measurements were performed on the Biacore T200 (GE Healthcare Life Sciences). GBP1 was immobilized on a CM5 sensor chip (GE Healthcare) using the amine coupling procedure (immobilization response was 310 RU or 0.31 ng/mm 2). Then it was equilibrated in PBS buffer (pH 7.2; Gibco, Life Sciences), followed by the injection of the increasing concentrations of LPS (47, 94, 188, 375, 750, 1500 nM) into the flow channels. In the reverse experiment, when immobilizing LPS on the CM5 sensor chip, increasing concentrations of GBP1 (21.5, 43, 86, 172, 343, 688, 1375, 2750 nM) were used. Data were analyzed using BiacoreT200 Evaluation software 3.0. An equilibrium analysis was done using Langmuir isotherm fit with one equilibrium dissociation constant (K_D). The best fit for the Kinetic curves was obtained with the two-state-reaction model that assume a possible structural re-arrangement after the initial binding.

Microscale thermophoresis (MST). MST was performed on 50 nM of FITC-labeled *E. coli* LPS (Sigma-Aldrich) using freshly purified hGBP1 expressed recombinantly (as described above) or BSA as a control. Serial dilutions of GBP1 or BSA were analyzed in assay buffer (50 mM Tris pH 7.4, 150 mM NaCl). Experiment was performed on a Nanotemper Monolith NT.115 microscale electrophoresis instrument with medium MST power. Data were fitted to a 1:1 binding model with the MO.Affinity Analysis software.

GTPase activity assay. GTPase activity assay was performed using the GTPase-Glo™ kit (Promega) according to the manufacturer use. Recombinant human GBP1 (500 nM) was incubated with 5 µM LPS in GEF buffer (Promega) for 30 min at room temperature before assessing GTP hydrolysis. Luminescence values were normalized to a no-GBP1 control.

Data analysis. Data analysis was performed using the following software: Gen5, GraphPad Prism v8 and Microsoft Excel. Statistical significances are referred as *, ** or *** for *P*-values <0.05, <0.01 or <0.001, respectively. For comparison of two groups, a two-tailed *t*-test was used, whereas for comparison of three or more groups *P*-values were determined using the two-way analysis of variance for multiple comparisons.

Reporting summary. Further information on research design is available in the Nature Research Reporting Summary linked to this article.

Data availability

The source data corresponding to Figs. 1h–i, 2a, d, e, 6a, f and Supplementary Figs. 1g, 2c, f–h, 3q; 5b; 10d, f; 11e; 14b are provided as Source Data files. All other relevant data are available from the corresponding author upon reasonable request. Source data are provided with this paper.

Received: 30 March 2020; Accepted: 1 June 2020;
Published online: 24 June 2020

References

- Takeuchi, O. & Akira, S. Pattern recognition receptors and inflammation. *Cell* **140**, 805–820 (2010).
- Kayagaki, N. et al. Caspase-11 cleaves gasdermin D for non-canonical inflammasome signalling. *Nature* **526**, 666–671 (2015).
- Kayagaki, N. et al. Noncanonical inflammasome activation by intracellular LPS independent of TLR4. *Science* **341**, 1246–1249 (2013).
- Hagar, J. A., Powell, D. A., Aachoui, Y., Ernst, R. K. & Miao, E. A. Cytoplasmic LPS activates caspase-11: implications in TLR4-independent endotoxin shock. *Science* **341**, 1250–1253 (2013).
- Shi, J. et al. Inflammatory caspases are innate immune receptors for intracellular LPS. *Nature* **514**, 187–192 (2014).
- Shi, J. et al. Cleavage of GSDMD by inflammatory caspases determines pyroptotic cell death. *Nature* **526**, 660–665 (2015).
- Park, B. S. et al. The structural basis of lipopolysaccharide recognition by the TLR4-MD-2 complex. *Nature* **458**, 1191–1195 (2009).
- Gioannini, T. L. et al. Isolation of an endotoxin-MD-2 complex that produces Toll-like receptor 4-dependent cell activation at picomolar concentrations. *Proc. Natl Acad. Sci. USA* **101**, 4186–4191 (2004).
- Pilla, D. M. et al. Guanylate binding proteins promote caspase-11-dependent pyroptosis in response to cytoplasmic LPS. *Proc. Natl Acad. Sci. USA* **111**, 6046–6051 (2014).
- Meunier, E. et al. Caspase-11 activation requires lysis of pathogen-containing vacuoles by IFN-induced GTPases. *Nature* **509**, 366–370 (2014).
- Man, S. M. et al. IRGB1 liberates bacterial ligands for sensing by the AIM2 and caspase-11-NLRP3 inflammasomes. *Cell* **167**, 382–396.e17 (2016).
- Santos, J. C. et al. LPS targets host guanylate-binding proteins to the bacterial outer membrane for non-canonical inflammasome activation. *EMBO J.* **37**, e98089 (2018).
- Santos, J. C. & Broz, P. Sensing of invading pathogens by GBPs: at the crossroads between cell-autonomous and innate immunity. *J. Leukoc. Biol.* **104**, 729–735 (2018).
- Lagrange, B. et al. Human caspase-4 detects tetra-acylated LPS and cytosolic Francisella and functions differently from murine caspase-11. *Nat. Commun.* **9**, 242 (2018).
- Bekpen, C. et al. The interferon-inducible p47 (IRG) GTPases in vertebrates: loss of the cell autonomous resistance mechanism in the human lineage. *Genome Biol.* **6**, R92 (2005).
- Wyllie, D. H. et al. Evidence for an accessory protein function for Toll-like receptor 1 in anti-bacterial responses. *J. Immunol.* **165**, 7125–7132 (2000).
- Bao, S., Beagley, K. W., France, M. P., Shen, J. & Husband, A. J. Interferon-gamma plays a critical role in intestinal immunity against *Salmonella typhimurium* infection. *Immunology* **99**, 464–472 (2000).
- Santos, J. C. et al. The COPII complex and lysosomal VAMP7 determine intracellular *Salmonella* localization and growth. *Cell Microbiol.* **17**, 1699–1720 (2015).
- Fredlund, J. et al. The entry of *Salmonella* in a distinct tight compartment revealed at high temporal and ultrastructural resolution. *Cell Microbiol.* **20**, e12816 (2018).
- Broz, P. et al. Caspase-11 increases susceptibility to *Salmonella* infection in the absence of caspase-1. *Nature* **490**, 288–291 (2012).
- Finn, C. E., Chong, A., Cooper, K. G., Starr, T. & Steele-Mortimer, O. A second wave of *Salmonella* T3SS1 activity prolongs the lifespan of infected epithelial cells. *PLoS Pathog.* **13**, e1006354 (2017).
- Finlay, B. B. & Falkow, S. Comparison of the invasion strategies used by *Salmonella cholerae-suis*, *Shigella flexneri* and *Yersinia enterocolitica* to enter cultured animal cells: endosome acidification is not required for bacterial invasion or intracellular replication. *Biochimie* **70**, 1089–1099 (1988).
- Knodler, L. A., Nair, V. & Steele-Mortimer, O. Quantitative assessment of cytosolic *Salmonella* in epithelial cells. *PLoS ONE* **9**, e84681 (2014).
- Knodler, L. A. et al. Dissemination of invasive *Salmonella* via bacterial-induced extrusion of mucosal epithelia. *Proc. Natl Acad. Sci. USA* **107**, 17733–17738 (2010).
- Malik-Kale, P., Winfree, S. & Steele-Mortimer, O. The bimodal lifestyle of intracellular *Salmonella* in epithelial cells: replication in the cytosol obscures defects in vacuolar replication. *PLoS ONE* **7**, e38732 (2012).
- Boucher, D. et al. Caspase-1 self-cleavage is an intrinsic mechanism to terminate inflammasome activity. *J. Exp. Med.* **215**, 827–840 (2018).
- Wandel, M. P. et al. GBPs inhibit motility of *Shigella flexneri* but are targeted for degradation by the bacterial ubiquitin ligase IpaH9.8. *Cell Host Microbe* **22**, 507–518.e5 (2017).
- Kravets, E. et al. Guanylate binding proteins directly attack *Toxoplasma gondii* via supramolecular complexes. *Elife* **5**, e14246 (2016).
- Piro, A. et al. Detection of cytosolic *Shigella flexneri* via a C-terminal triple-arginine motif of GBP1 inhibits actin-based motility. *MBio* <https://doi.org/10.1101/212175> (2017).
- Paz, I. et al. Galectin-3, a marker for vacuole lysis by invasive pathogens. *Cell Microbiol.* **12**, 530–544 (2010).
- Steele-Mortimer, O. The *Salmonella*-containing vacuole: moving with the times. *Curr. Opin. Microbiol.* **11**, 38–45 (2008).
- An, J. et al. Caspase-4 disaggregates lipopolysaccharide micelles via LPS-CARD interaction. *Sci. Rep.* **9**, 826–829 (2019).
- Habich, C. et al. Heat shock protein 60: specific binding of lipopolysaccharide. *J. Immunol.* **174**, 1298–1305 (2005).
- Prakash, B., Praefcke, G. J., Renault, L., Wittinghofer, A. & Herrmann, C. Structure of human guanylate-binding protein 1 representing a unique class of GTP-binding proteins. *Nature* **403**, 567–571 (2000).
- Adams, P. G., Lamoureux, L., Swingle, K. L., Mukundan, H. & Montaña, G. A. Lipopolysaccharide-induced dynamic lipid membrane reorganization: tubules, perforations, and stacks. *Biophys. J.* **106**, 2395–2407 (2014).
- Lamping, N. et al. Effects of site-directed mutagenesis of basic residues (Arg 94, Lys 95, Lys 99) of lipopolysaccharide (LPS)-binding protein on binding and transfer of LPS and subsequent immune cell activation. *J. Immunol.* **157**, 4648–4656 (1996).
- Krasity, B. C. et al. Structural and functional features of a developmentally regulated lipopolysaccharide-binding protein. *MBio* **6**, e01193–15 (2015).
- Garidel, P. et al. Divalent cations affect chain mobility and aggregate structure of lipopolysaccharide from *Salmonella minnesota* reflected in a decrease of its biological activity. *Biochim Biophys. Acta* **1715**, 122–131 (2005).
- Ryu, J.-K. et al. Reconstruction of LPS transfer cascade reveals structural determinants within LBP, CD14, and TLR4-MD2 for efficient LPS recognition and transfer. *Immunity* **46**, 38–50 (2017).
- Fisch, D. et al. Human GBP1 is a microbe-specific gatekeeper of macrophage apoptosis and pyroptosis. *EMBO J.* <https://doi.org/10.15252/embj.2018100926> (2019).
- Meunier, E. et al. Guanylate-binding proteins promote activation of the AIM2 inflammasome during infection with *Francisella novicida*. *Nat. Immunol.* **16**, 476–484 (2015).
- Schroder, K. et al. Conservation and divergence in Toll-like receptor 4-regulated gene expression in primary human versus mouse macrophages. *Proc. Natl Acad. Sci. USA* **109**, E944–E953 (2012).
- Shcherbakova, D. M. et al. Bright monomeric near-infrared fluorescent proteins as tags and biosensors for multiscale imaging. *Nat. Commun.* **7**, 12405 (2016).
- Jodoin, J. et al. Loss of anti-Bax function in Gerstmann-Sträussler-Scheinker syndrome-associated prion protein mutants. *PLoS ONE* **4**, e6647 (2009).
- Ray, K. et al. Tracking the dynamic interplay between bacterial and host factors during pathogen-induced vacuole rupture in real time. *Cell Microbiol.* **12**, 545–556 (2010).
- Rühl, S. & Broz, P. Caspase-11 activates a canonical NLRP3 inflammasome by promoting K(+) efflux. *Eur. J. Immunol.* **45**, 2927–2936 (2015).
- Kim, D. I. et al. An improved smaller biotin ligase for BioID proximity labeling. *Mol. Biol. Cell* **27**, 1188–1196 (2016).
- Boucher, D. et al. General in vitro caspase assay procedures. *Methods Mol. Biol.* **1133**, 3–39 (2014).
- Gross, O. Measuring the inflammasome. *Methods Mol. Biol.* **844**, 199–222 (2012).

Acknowledgements

We thank Thomas Henry, Brice Lagrange (INSERM, Lyon) and Jost Enninga (Institut Pasteur, Paris) for plasmids and bacterial strains, Dominique Chevrier (InvivoGen) for

LPS derivatives, Tim Sharpe (Biozentrum, University of Basel) for discussion, Shaynoor Dramsi (Institut Pasteur, Paris) for cell lines, Jay Hinton (University of Liverpool) for *Salmonella* strains, the UNIL Imaging Core Facility, Saori Yoshii and Cristina Ramon-Barros for technical assistance. This work was supported by grants of the Swiss National Science Foundation (PP00P3_165893/1 to P.B.), the ERC (ERC-2017-CoG - 770988, InflammCellDeath to P.B.), the Human Frontier Science Program (CDA00032/2015-C/2 to P.B.) and a Swiss Government Excellence postdoctoral fellowship to (ESKAS 2018.0618 to K.W.C.).

Author contributions

J.C.S., D.B. and P.B. designed the study, performed and analyzed experiments and wrote the manuscript. L.K.S. and R.Y.H.L. assisted with and analyzed the SPR and MST experiments. B.D., K.W.C., and M.D. performed experiments, K.S. and R.H. contributed expression vectors.

Competing interests

The authors declare no competing interests.

Additional information

Supplementary information is available for this paper at <https://doi.org/10.1038/s41467-020-16889-z>.

Correspondence and requests for materials should be addressed to P.B.

Reprints and permission information is available at <http://www.nature.com/reprints>

Publisher's note Springer Nature remains neutral with regard to jurisdictional claims in published maps and institutional affiliations.



Open Access This article is licensed under a Creative Commons Attribution 4.0 International License, which permits use, sharing, adaptation, distribution and reproduction in any medium or format, as long as you give appropriate credit to the original author(s) and the source, provide a link to the Creative Commons license, and indicate if changes were made. The images or other third party material in this article are included in the article's Creative Commons license, unless indicated otherwise in a credit line to the material. If material is not included in the article's Creative Commons license and your intended use is not permitted by statutory regulation or exceeds the permitted use, you will need to obtain permission directly from the copyright holder. To view a copy of this license, visit <http://creativecommons.org/licenses/by/4.0/>.

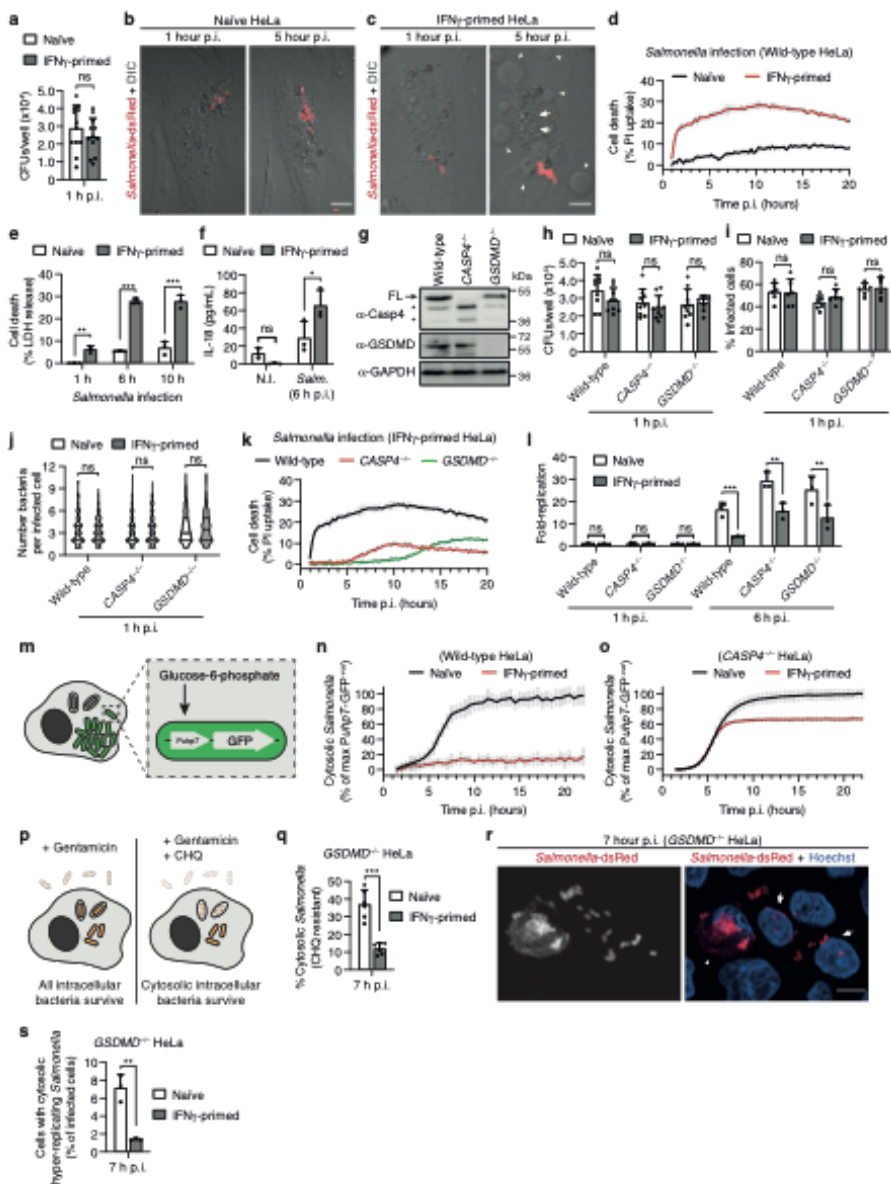
© The Author(s) 2020

Supplementary Material for

**Human GBP1 binds LPS to initiate assembly of a caspase-4 activating
platform on cytosolic bacteria**

Santos *et al.*

Supplementary Figure 1



Supplementary Fig. 1. IFN γ priming of HeLa cells induces caspase-4 activation upon *Salmonella* infection and restricts cytosolic bacterial hyper-replication.

a. Assessment of *Salmonella* invasion at 1 h post-infection (p.i.), in naïve or IFN γ -primed HeLa. Cells were infected for 30 min, washed and gentamicin was added to kill extracellular bacteria. The cells were then lysed and the number of viable intracellular bacteria was counted by CFUs.

b, c. Confocal microscopy images of naïve (b) or IFN γ -primed HeLa (c) infected with *Salmonella*-dsRed, at 1 h and 5 h p.i.. Arrows point to nuclear condensation and arrowheads to plasma membrane swelling and blebbing. Scale bars correspond to 10 μ m. DIC, differential interference contrast.

d. Propidium iodide (PI) uptake in naïve or IFN γ -primed HeLa after infection with *Salmonella*.

e, f. Release of LDH (e) or IL-18 (f) in naïve or IFN γ -primed HeLa at the indicated time points after infection with *Salmonella*. N.I., non-infected.

g. Immunoblots for caspase-4, GSDMD and GAPDH (loading control) in cell lysates from wild-type, *CASP4*^{-/-} or *GSDMD*^{-/-} HeLa. FL points to full length caspase-4 (~45 kDa), and * inactive caspase-4 isoforms lacking the CARD domain resulting from CRISPR-Cas9 genome editing.

h-j. Assessment of *Salmonella* invasion in naïve or IFN γ -primed wild-type, *CASP4*^{-/-} or *GSDMD*^{-/-} HeLa cells, at 1 h p.i.. Cells were infected as described in (a) and then were lysed and the number of viable intracellular bacteria was counted by CFUs (h). In (i, j), cells were infected with *Salmonella*-dsRed, fixed and then the percentage of infected cells or the number of bacteria per infected cell were counted by fluorescence microscopy. At least 80 cells (i) or 30 infected cells (j) were counted, in triplicate conditions.

k. PI uptake in IFN γ -primed wild-type, *CASP4*^{-/-} or *GSDMD*^{-/-} HeLa after infection with *Salmonella*.

l. Intracellular bacterial fold-replication in naïve or IFN γ -primed wild-type, *CASP4*^{-/-} or *GSDMD*^{-/-} HeLa cells, at 1 or 6 h p.i. with *Salmonella*. Cells in 96-well plates were infected for 30 min, washed and gentamicin was added to kill extracellular bacteria. At the indicated time points cells were lysed and the number of viable intracellular bacteria was determined by counting colony forming units (CFUs). The bacterial fold-replication was calculated versus 1 h p.i.

m. Schematic representation of infection of cells with a *Salmonella* reporter strain for cytosolic replication. Bacteria expressing GFP under the control of the hexose phosphate transporter promoter (*P_{uhpT}*) only turn fluorescent in response to exogenous glucose-6-phosphate found exclusively in the host cytosol.

n, o. Cytosolic replication of *Salmonella* expressing *P_{uhpT}*-GFP in naïve or IFN γ -primed wild-type (n) or *CASP4*^{-/-} (o) HeLa cells. Cells were infected and fluorescence was recorded every 30 minutes using a plate reader.

p. Schematic representation of the chloroquine (CHQ) resistance assay used to determine the percentage of cytosolic *Salmonella*. When gentamicin is added only the extracellular bacteria are

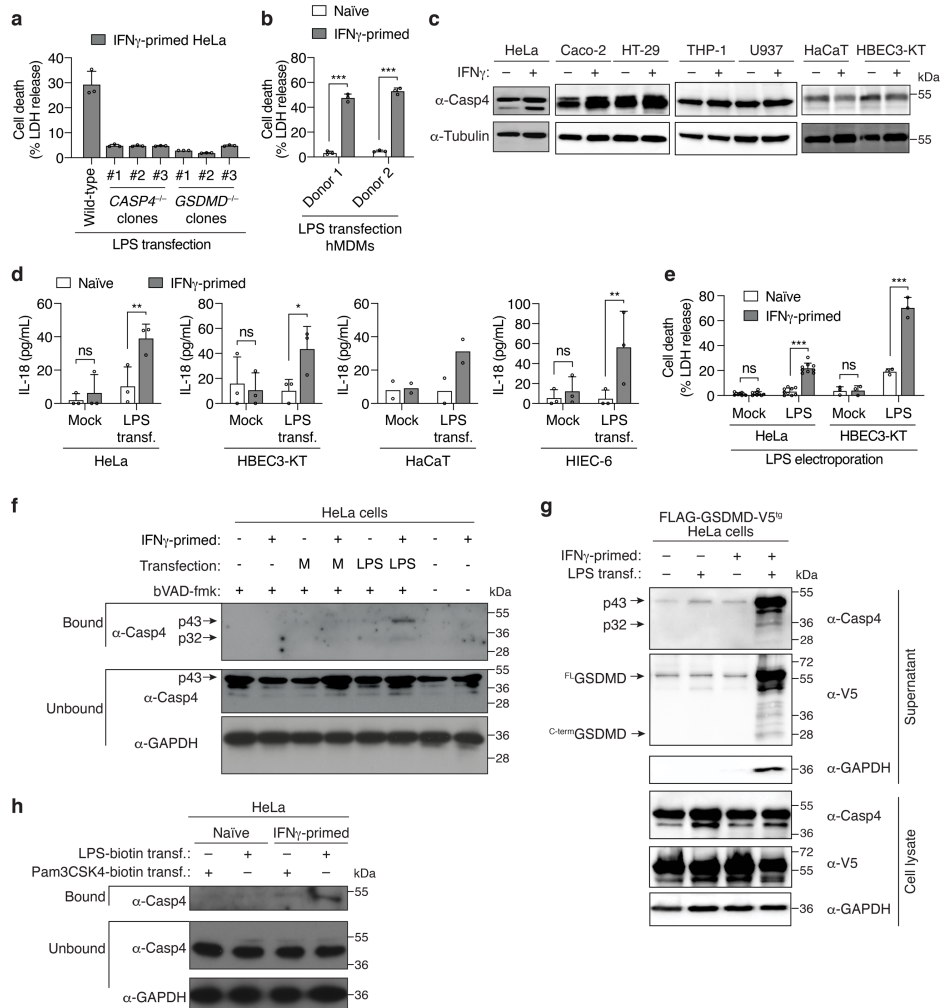
killed (left panel), whereas addition of gentamicin and CHQ kills extracellular and vacuolar bacteria (right panel).

q. Percentage of cytosolic *Salmonella* in naïve or IFN γ -primed *GSDMD*^{-/-} HeLa cells at 7 h p.i., quantified by the CHQ resistance assay. Cells in triplicate wells were infected for 30 min and then treated with gentamicin to kill extracellular bacteria. In some wells CHQ was also added for 1 h before cells were lysed and intracellular *Salmonella* enumerated. The percentage of CHQ resistant bacteria was calculated as the ratio of (CHQ+gentamicin^{resistant} / gentamicin^{resistant}).

r, s. Fluorescence confocal microscopy of *GSDMD*^{-/-} HeLa cells infected with *Salmonella*-dsRed for 7 h (r). Arrowhead points to an example of a cell containing cytosolic hyper-replicating bacteria and arrows point to cells with non-hyper-replicating *Salmonella*. Scale bar corresponds to 10 μ m. The percentage of hyper-replicating bacteria was quantified (s) by counting infected cells containing large accumulation of bacteria as shown in the image.

Graphs show the mean \pm SD, and data are representative of two (e, g, r, s) or three (b-d, f, k, l, n, o) independent experiments or pooled from two (i, j, q), three (h) or four (a) independent experiments performed in triplicate. * $P < 0.05$; ** $P < 0.01$; *** $P < 0.001$; ns, not significant; two-tailed *t*-test.

Supplementary Figure 2



Supplementary Fig. 2. IFN γ priming induces LPS-induced caspase-4 activation.

- a.** Release of LDH from IFN γ -primed wild-type HeLa cells, or from different *CASP4*^{-/-} or *GSDMD*^{-/-} clones, 5 h after transfection with *E. coli*-derived LPS.
- b.** Release of LDH from naïve or IFN γ -primed primary human monocyte-derived macrophages (hMDMs), 5 h after transfection with *E. coli*-derived LPS.
- c.** Immunoblot analysis of caspase-4 expression in cell lysates from naïve or IFN γ -primed cells.
- d.** Release of IL-18 from naïve or IFN γ -primed cells, 5 h after transfection with *E. coli*-derived LPS.

e. Release of LDH from naïve or IFN γ -primed HeLa or HBEC3-KT cells, 3-4 h after electroporation with *E. coli* LPS.

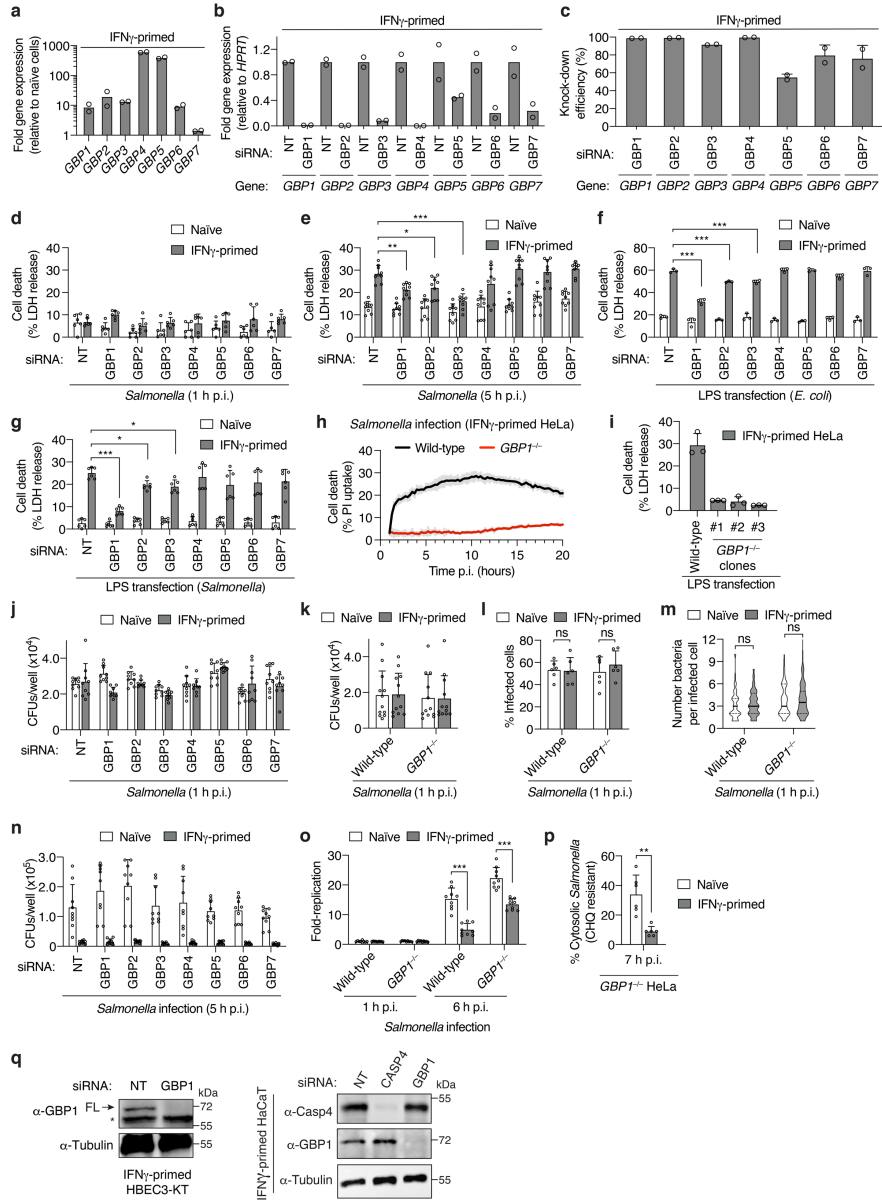
f. Pull-down of active caspase-4 from HeLa, using bVAD-fmk caspase activity probe. Approximately 3×10^6 cells were left untreated or primed with IFN γ and then transfected with *E. coli* LPS (20 μ g) for 3 h. Mock-transfected (M) cells were used as a control. Streptavidin-bound and -unbound fractions were analyzed by western blot using an antibody against caspase-4.

g. Western blot analysis of full length (FL) and cleaved (p32) caspase-4, FL and cleaved (C-term) GSDMD in the supernatants or cell lysates from naïve or IFN γ -primed HeLa stably expressing FLAG-GSDMD-V5, upon transfection with *E. coli* LPS for 6 h.

h. Streptavidin pull-down assay of the binding of biotin-conjugated LPS to endogenous caspase-4 from the lysates of naïve or IFN γ -primed HeLa. Cells in 6-well plates were transfected with LPS-biotin (10 μ g) or Pam3CSK4-biotin (2 μ g) and biotinylated substrate was pulled down using equal amounts of streptavidin magnetic beads, which were then eluted in equal volumes of SDS-PAGE reducing sample buffer. Streptavidin-bound and -unbound fractions were analyzed by western blot using an antibody against caspase-4.

Graphs show the mean \pm SD, and data are representative of two (b) or three independent experiments (a, c, e (HBEC3-KT) f-h), or pooled from three independent experiments (e, HeLa) performed in triplicate. Graphs shown in panel (d) were obtained from two (HaCaT) or three independent experiments (HeLa; HBEC3-KT; HIEC-6) where triplicate wells from the same experiment were first pooled together. * $P < 0.05$; ** $P < 0.01$; *** $P < 0.001$; ns, not significant; two-tailed *t*-test.

Supplementary Figure 3

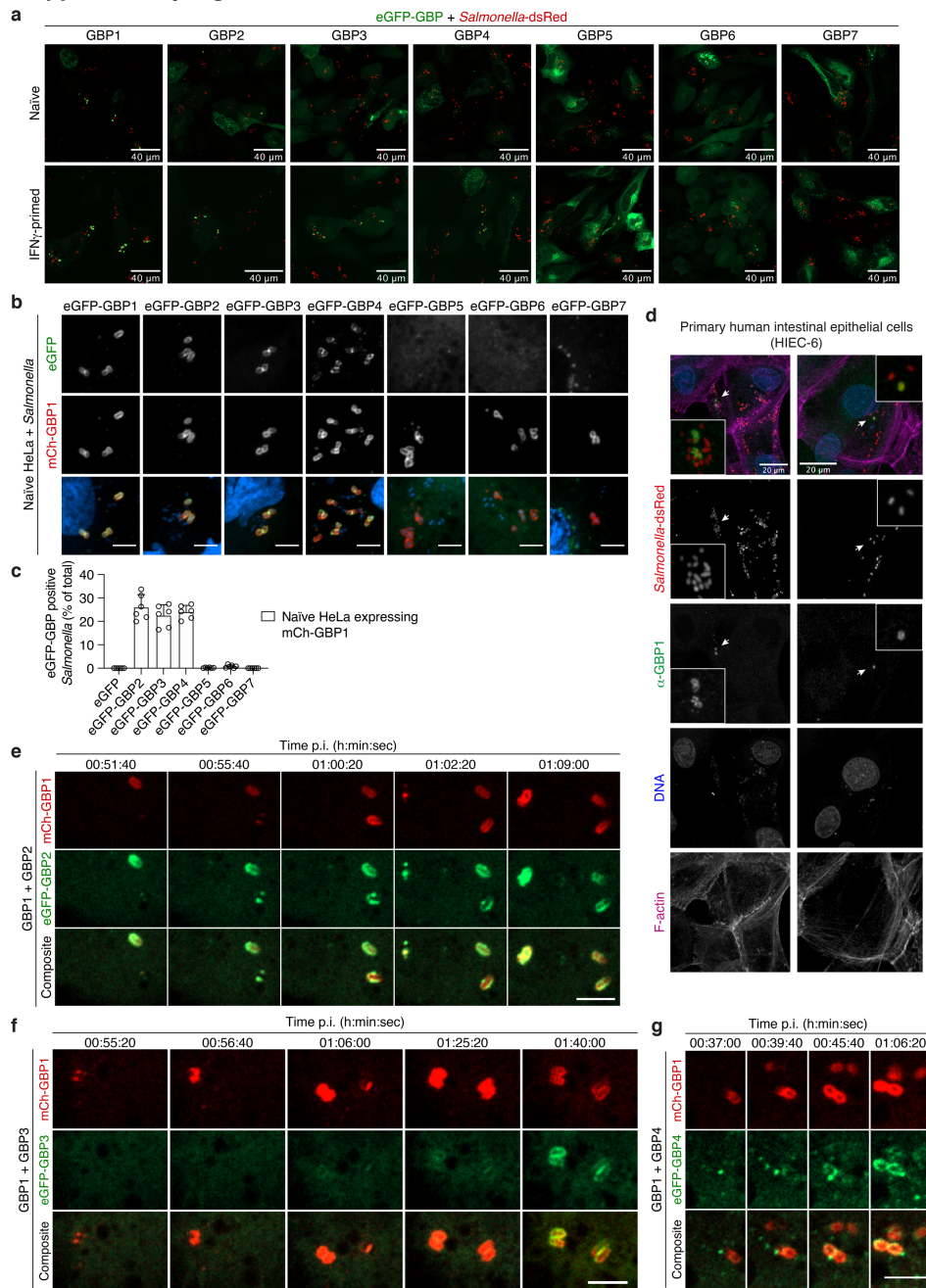


Supplementary Fig. 3. In epithelial cells, GBP1 controls non-canonical inflammasome activation in response to cytosolic LPS or *Salmonella*.

- a.** Expression levels of *GBP1-7* in IFN γ -primed HeLa, assessed by qPCR. Fold gene expression is shown relative to naïve control cells. *HPRT* was used as a housekeeping gene.
- b.** Expression levels of *GBP1-7* in IFN γ -primed HeLa upon treatment with non-targeting control siRNA (NT) or with siRNAs targeting *GBP1-7* for 24 h. Fold expression for each gene was assessed by qPCR, relative to control cells treated with NT siRNA. *HPRT* was used as a housekeeping gene.
- c.** Percentage of knock-down efficiency calculated as $(1 - 2^{\Delta\Delta Ct}) \times 100$.
- d, e.** Release of LDH from naïve or IFN γ -primed HeLa cells treated with siRNAs against GBPs, 1 h (d) or 5 h (e) after *Salmonella* infection. Cells were treated with non-targeting control siRNA (NT) or with siRNAs targeting *GBP1-7* for 24 h and infected for 30 min. Gentamicin was added to kill extracellular bacteria and cells were analyzed at the corresponding time points.
- f, g.** Release of LDH in naïve or IFN γ -primed HeLa treated with siRNAs against GBPs, 5 h after transfection with *E. coli*- (f) or *Salmonella*-derived LPS (g). Cells were treated with non-targeting control siRNA (NT) or with siRNAs targeting *GBP1-7* for 24 h and then transfected with LPS (2.5 μ g/50,000 cells).
- h.** PI uptake in IFN γ -primed wild-type, or *GBP1*^{-/-} HeLa after infection with *Salmonella*.
- i.** Release of LDH from IFN γ -primed wild-type HeLa, or from different *GBP1*^{-/-} clones, 5 h after transfection with *E. coli*-derived LPS (2.5 μ g/50,000 cells).
- j-m.** Assessment of *Salmonella* invasion at 1 h p.i., in naïve or IFN γ -primed HeLa treated with siRNAs against GBPs (i) or in wild-type and *GBP1*^{-/-} cells (k-m). In (j), cells were treated with non-targeting control siRNA (NT) or with siRNAs targeting *GBP1-7* for 24 h and infected for 30 min. Cells were then washed and gentamicin was added to kill extracellular bacteria. The cells were lysed and the number of viable intracellular bacteria was counted by CFUs (j,k). In (l, m) cells were infected with *Salmonella*-dsRed, fixed and then the percentage of infected cells or the number of bacteria per infected cell were counted by fluorescence microscopy.
- n, o.** Intracellular bacterial replication in naïve or IFN γ -primed HeLa treated with siRNAs against GBPs (n) or in wild-type and *GBP1*^{-/-} cells (o) after infection with *Salmonella*, as determined by counting CFUs. The bacterial fold-replication was calculated relative to 1 h p.i..
- p.** Percentage of cytosolic *Salmonella* in naïve or IFN γ -primed *GBP1*^{-/-} HeLa at 7 h p.i., quantified by the CHQ resistance assay. Cells in triplicate wells were infected for 30 min and then treated with gentamicin to kill extracellular bacteria. In some wells CHQ was also added for 1 h before cells were lysed and intracellular *Salmonella* enumerated.
- q.** Immunoblot for GBP1 and caspase-4 expression following treatment with non-targeting siRNA (NT) or siRNA against GBP1 or CASP4 in IFN γ -primed HBEC3-KT or HaCaT cells, as used in Fig. 2g. (*denotes a cross-reactive band).

Graphs show the mean \pm SD, and data are pooled from at least two independent experiments performed in triplicate (d-e, g, j-p), or representative of at least two independent experiments performed in duplicate (a-c) or in triplicate (f, h, i, q). * $P < 0.05$; ** $P < 0.01$; *** $P < 0.001$; ns, not significant; two-way ANOVA (e-g) or two-tailed t -test (l, m, o, p).

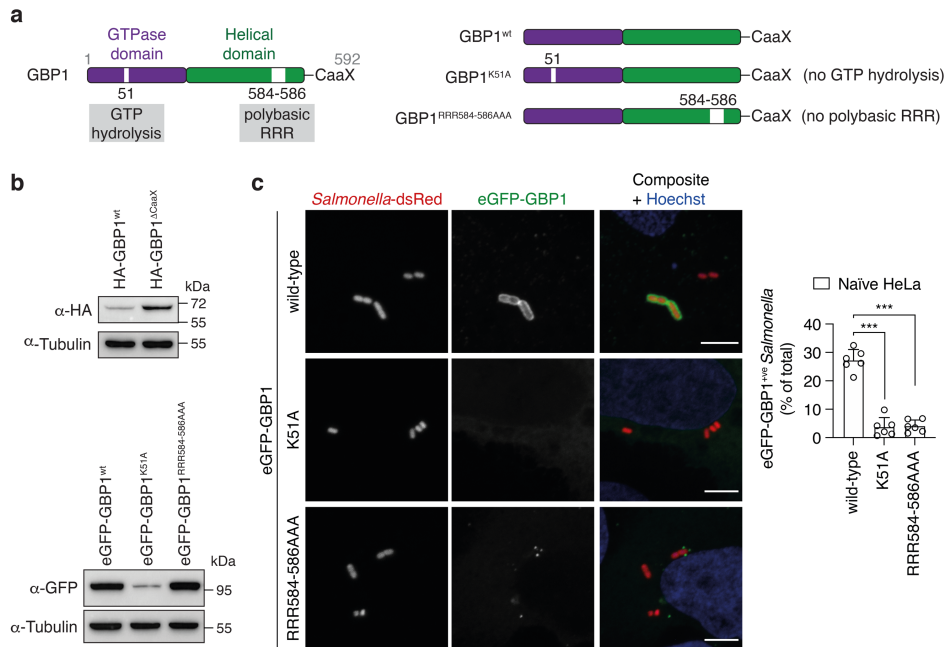
Supplementary Figure 4



Supplementary Fig. 4. GBP1 regulates hierarchical recruitment of GBP2-4 to intracellular *Salmonella*.

- a.** Fluorescence confocal microscopy of naïve or IFN γ -primed HeLa expressing N-terminal tagged eGFP-GBP1-7 (green) and infected with *Salmonella*-dsRed (red) for 1h. Representative confocal images are shown and scale bars correspond to 40 μ m.
- b.** Fluorescence confocal microscopy of naïve HeLa co-expressing mCherry-GBP1 (red) and eGFP-GBP1-7 (green) and infected with *Salmonella* for 1 h. DNA was stained with Hoechst (blue). Representative confocal images are shown and scale bars correspond to 5 μ m.
- c.** Percentage of intracellular *Salmonella* positive for eGFP-GBP2-7 in naïve HeLa co-expressing mCherry-GBP1, at 1 h p.i.. At least 100 bacteria were counted per coverslip.
- d.** Fluorescence confocal microscopy of IFN γ -primed HIEC-6 cells infected with *Salmonella*-dsRed for 1.5 h. GBP1 (green) was visualized by immunostaining with a rabbit anti-GBP1 antibody (ab121039, abcam), DNA and F-actin were stained with Hoechst (blue) or Phalloidin-647 (purple), respectively. Representative confocal images are shown. Arrows point to enlarged images.
- e-g.** Time-lapse fluorescence confocal microscopy of HeLa co-expressing mCherry-GBP1 (red) and eGFP-GBP2 (e), eGFP-GBP3 (f) or eGFP-GBP4 (g) and infected with *Salmonella*. Scale bars correspond to 5 μ m.
- Graph shown the mean \pm SD, and data are pooled from three independent experiments performed in duplicate (c) or representative of two (a, g) or three (e, f) independent experiments.

Supplementary Figure 5



Supplementary Fig. 5. GBP1 recruitment to intracellular *Salmonella* is dependent on its GTP hydrolysis and polybasic C-terminal motives.

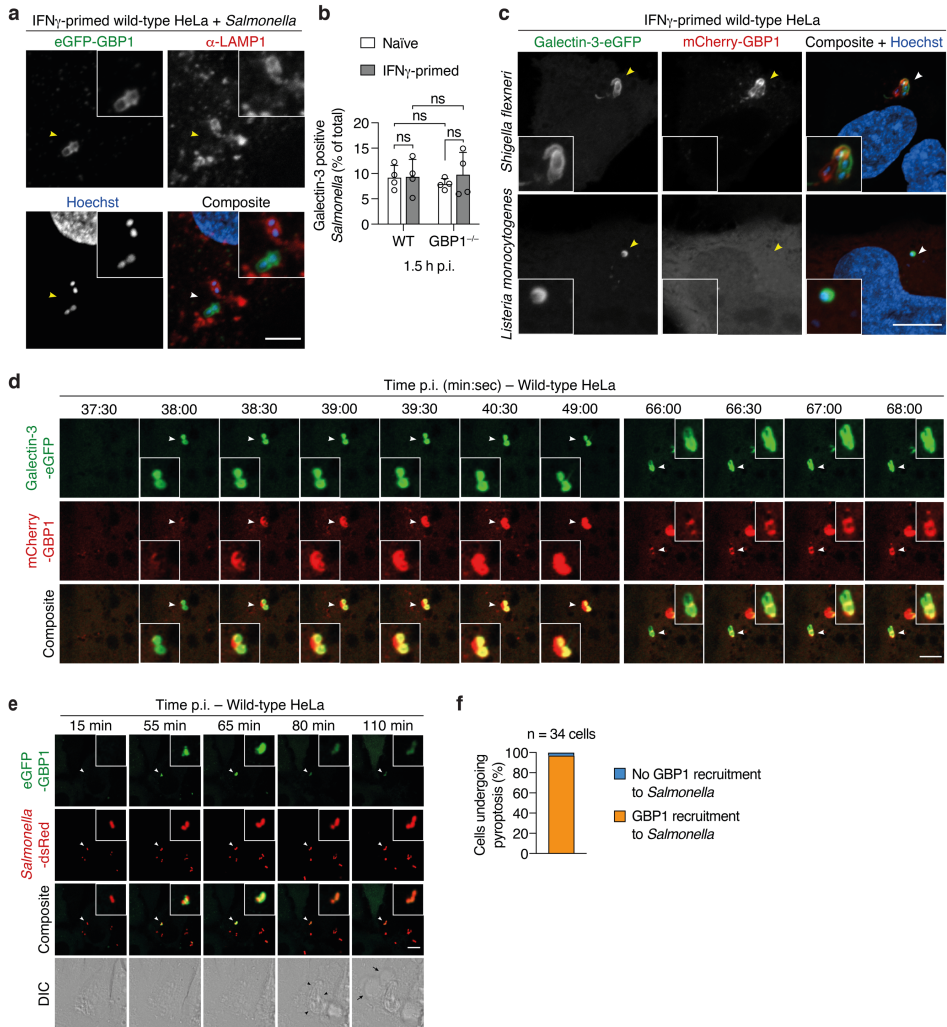
a. Schematic representation of wild-type GBP1 and two different mutants.

b. Western blot analysis for expression of HA-GBP1^{wt} and HA-GBP1^{ΔCaaX}, or eGFP-GBP1^{wt}, eGFP-GBP1^{K51A} and eGFP-GBP1^{RRR584-586AAA} in naïve HeLa cells.

c. Fluorescence confocal microscopy of naïve HeLa expressing eGFP-GBP1^{wt}, eGFP-GBP1^{K51A} or eGFP-GBP1^{RRR584-586AAA} (green) and infected with *Salmonella*-dsRed (red) for 1 h. DNA was stained with Hoechst (blue). Representative confocal images are shown and scale bars correspond to 5 μm. The percentage of eGFP-GBP1 positive *Salmonella* was quantified by counting around 100 bacteria per coverslip and the graph shows the mean ± SD from three independent experiment performed in triplicate. *** $P < 0.001$; two-tailed t -test.

Data are representative from three independent experiments (b, c).

Supplementary Figure 6

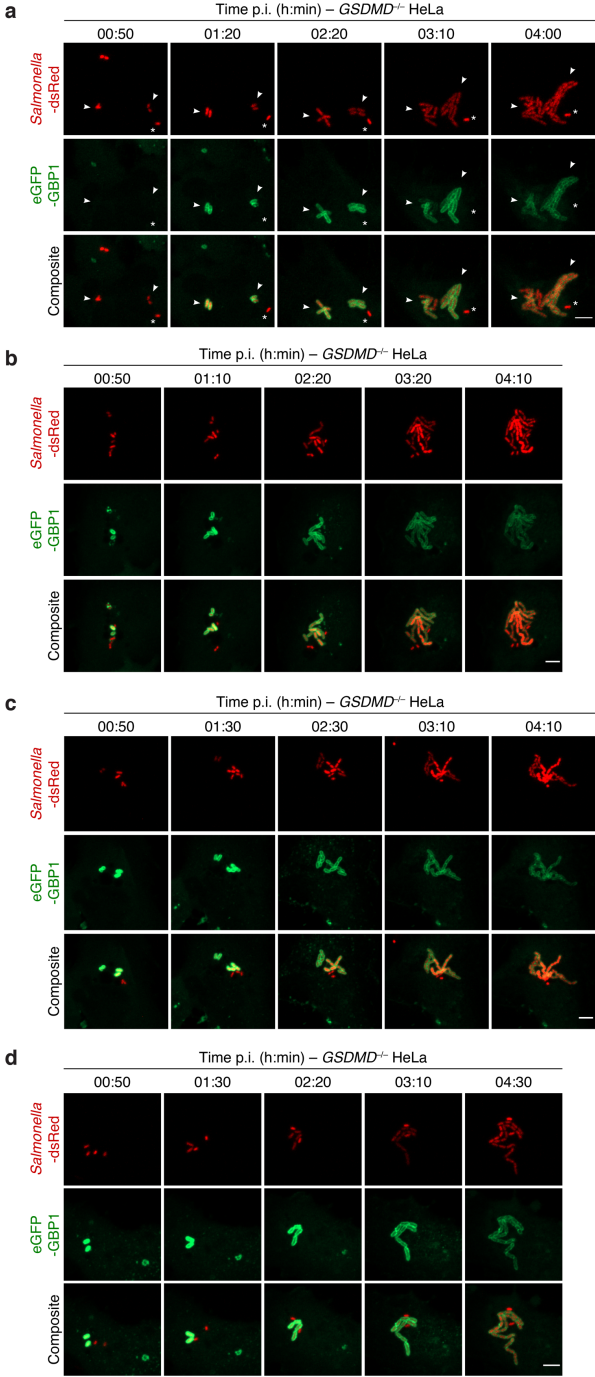


Supplementary Fig. 6. Human GBP1 does not induce SCV rupture and is recruited to cytosolic *Salmonella* immediately after SCV membrane rupture.

a. Fluorescence confocal microscopy of IFN γ -primed HeLa cells expressing eGFP-GBP1 (green) and infected with *Salmonella* for 1 hour. LAMP1 (red) was visualized by immunostaining with a rabbit anti-Lamp1 antibody (abcam 24170) and DNA was stained with Hoechst (blue). Representative confocal images are shown. Arrowheads point to enlarged images and scale bar corresponds to 5 μ m.

- b.** Percentage of galectin-3 positive *Salmonella* in naïve or IFN γ -primed wild-type or *GBP1*^{-/-} HeLa at 1.5 h p.i.. Cells expressing galectin-3-eGFP were infected with *Salmonella*-dsRed, fixed and analyzed by fluorescence confocal microscopy.
- c.** Fluorescence confocal microscopy of IFN γ -primed HeLa cells co-expressing galectin-3-eGFP (green) and mCherry-GBP1 (red) and infected with *S. flexneri* or *L. monocytogenes* for 30 min. DNA was stained with Hoechst (blue) and representative confocal images are shown. Arrowheads point to enlarged images and scale bar corresponds to 10 μ m.
- d.** Time-lapse fluorescence confocal microscopy of IFN γ -primed wild-type HeLa co-expressing galectin-3-eGFP (green) and mCherry-GBP1 (red) and infected with *Salmonella*. Images were acquired every 30 seconds and scale bar corresponds to 5 μ m.
- e.** Time-lapse fluorescence confocal microscopy of IFN γ -primed wild-type HeLa expressing eGFP-GBP1 (green) and infected with *Salmonella*-dsRed (red). Black arrowheads point to nuclear condensation and black arrows point to plasma membrane blebbing of a pyroptotic cell. Scale bar corresponds to 10 μ m. DIC, differential interference contrast.
- f.** Percentage of cells undergoing pyroptosis in which there was eGFP-GBP1 recruitment to *Salmonella* (orange, 33 out of 34 cells) or no detectable eGFP-GBP1 recruitment (blue, 1 out of 34 cells), as determined by time-lapse fluorescence microscopy. Graph shows the mean \pm SD, and data are pooled from two (b) independent experiments performed in duplicate or representative of two (a, c) or at least three independent experiments (d-f). ns, not significant, two-tailed *t*-test.

Supplementary Figure 7

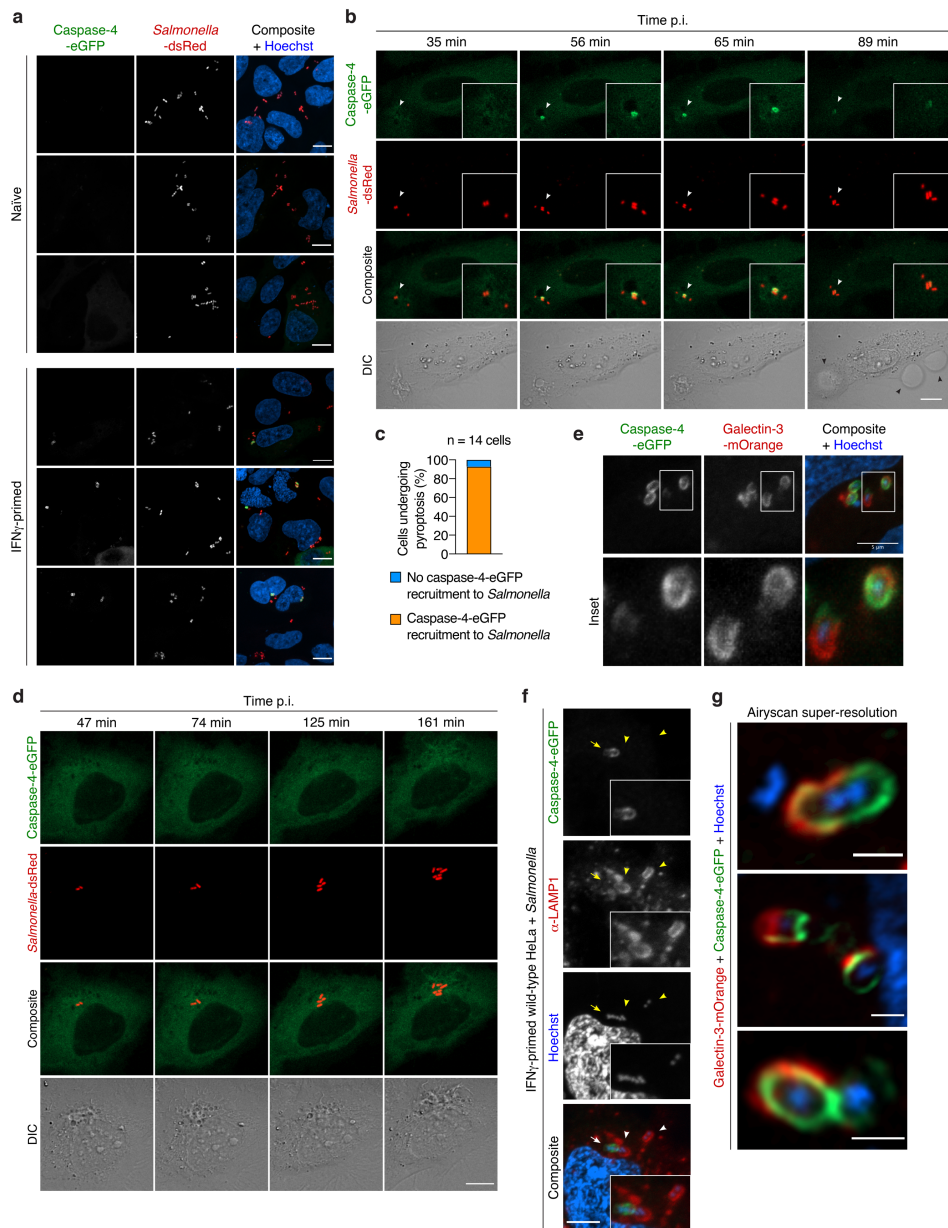


Supplementary Fig. 7. Recruitment of GBP1 to intracellular *Salmonella* does not promote bacteriolysis or restrict replication in *GSDMD*-deficient cells

a-d. Time-lapse fluorescence confocal microscopy of IFN γ -primed *GSDMD*^{-/-} HeLa expressing eGFP-GBP1 (green) and infected with *Salmonella*-dsRed (red). Cytosolic bacteria are targeted by GBP1 and undergo hyper-replication. In (a), arrowheads point to cytosolic bacteria that are targeted by GBP1 and undergo hyper-replication, whereas asterisk points to a GBP1-negative bacterium that does not replicate, and most likely remains within the SCV. Scale bars corresponds to 5 μ m.

Data are representative three independent experiments.

Supplementary Figure 8



Supplementary Fig. 8. Caspase-4 is recruited to cytosolic *Salmonella* after escape from the SCV to induce pyroptosis in epithelial cells.

a. Fluorescence confocal microscopy of naïve or IFN γ -primed HeLa expressing caspase-4-eGFP (green) and infected with *Salmonella*-dsRed for 1 h. DNA was stained with Hoechst (blue) and representative confocal images are shown. Scale bars correspond to 10 μ m.

b, d. Time-lapse fluorescence confocal microscopy of IFN γ -primed HeLa expressing caspase-4-eGFP (green) and infected with *Salmonella*-dsRed. Black arrowheads, in (b), point to plasma membrane blebbing of a pyroptotic cell. Scale bars correspond to 10 μ m. DIC, differential interference contrast.

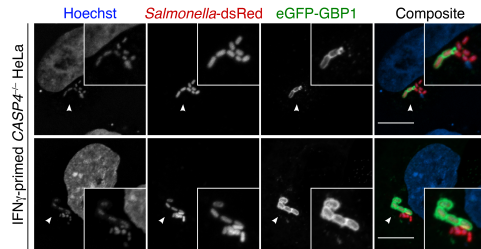
c. Percentage of cells undergoing pyroptosis in which there was caspase-4-eGFP recruitment to *Salmonella* (orange, 13 out of 14 cells) or no caspase-4-eGFP recruitment (blue, 1 out of 14 cells).

e, g. Fluorescence confocal microscopy of IFN γ -primed HeLa cells co-expressing caspase-4-eGFP (green) and galectin-3-mOrange (red) and infected with *Salmonella* for 1 h. DNA was stained with Hoechst (blue) and representative confocal images are shown. Scale bars correspond to 5 μ m (E) or 1 μ m (G).

f. Fluorescence confocal microscopy of IFN γ -primed HeLa cells expressing caspase-4-eGFP (green) and infected with *Salmonella* for 1 hour. LAMP1 (red) was visualized by immunostaining with a rabbit anti-Lamp1 antibody (abcam 24170) and DNA was stained with Hoechst (blue). Representative confocal images are shown. Arrowheads point to enlarged images and scale bar corresponds to 5 μ m.

Data are representative of three independent experiments.

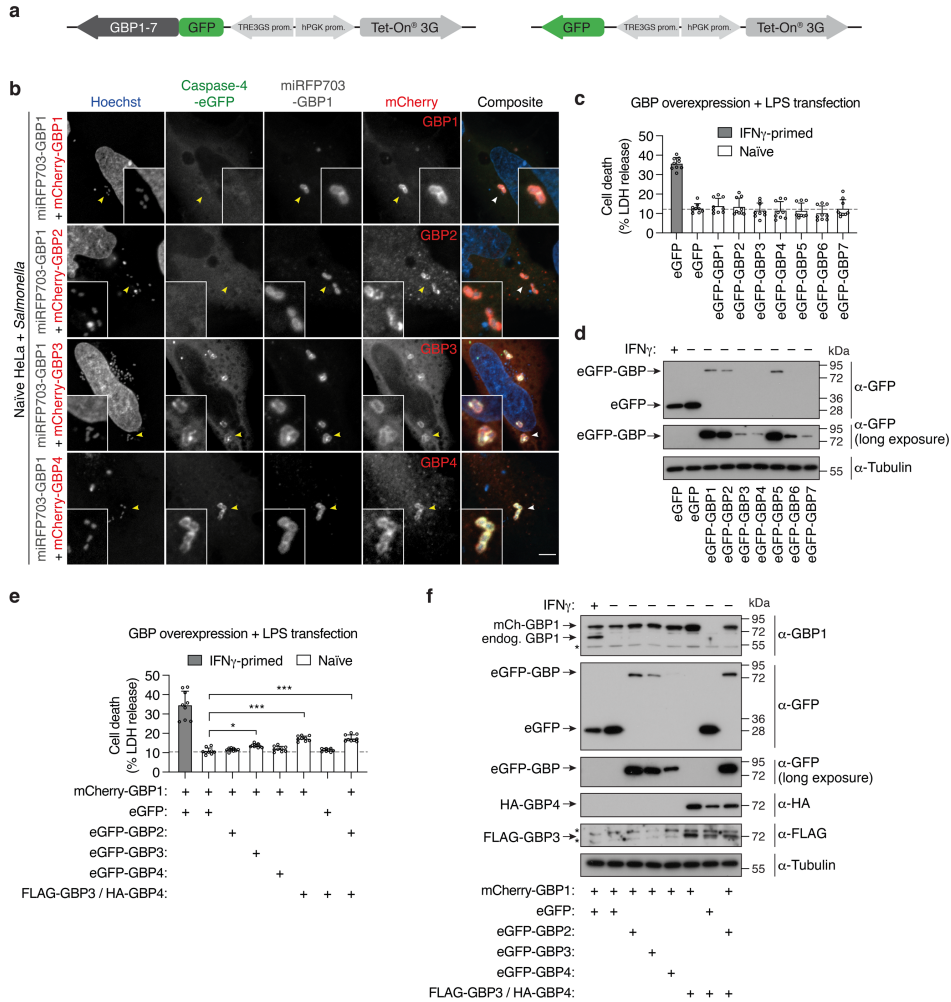
Supplementary Figure 9



Supplementary Fig. 9. GBP1 recruitment to *Salmonella* is independent of caspase-4.

Fluorescence confocal microscopy in IFN γ -primed *CASP4*^{-/-} HeLa expressing eGFP-GBP1 (green) and infected with *Salmonella*-dsRed (red) for 1 h. DNA was stained with Hoechst (blue) and two sets of representative confocal images are shown. Scale bar correspond to 10 μ m. Images are representative of two independent experiments.

Supplementary Figure 10



Supplementary Fig. 10. GBP1/3/4 overexpression is sufficient to recruit caspase-4 on *Salmonella* and induce pyroptosis in human epithelial cells.

a. Schematic representation of the pLVX-Tet-On 3G plasmids used to express doxycycline (Dox)-inducible GFP or GFP-GBP1-7.

b. Fluorescence confocal microscopy of naïve HeLa cells co-expressing caspase-4-eGFP (green), miRFP703-GBP1 (grey) and mCherry-GBP1, -2, -3 or -4 (red), and infected with *Salmonella* for 1 h. DNA was stained with Hoechst (blue). Representative confocal images are shown and scale bar corresponds to 5 μ m.

c. LDH release from naïve HeLa cells expressing Dox-inducible eGFP-GBP1-7 or eGFP. Cells were transfected with the indicated plasmids for 24 h. eGFP-GBPs were induced for 16 h with 1 $\mu\text{g/ml}$ Dox, whereas eGFP was induced for 3 h. IFN γ -primed cells expressing eGFP were used as a positive control. Cells were then transfected with *E. coli*-derived LPS (2.5 μg / 50,000 cells) for 6 h.

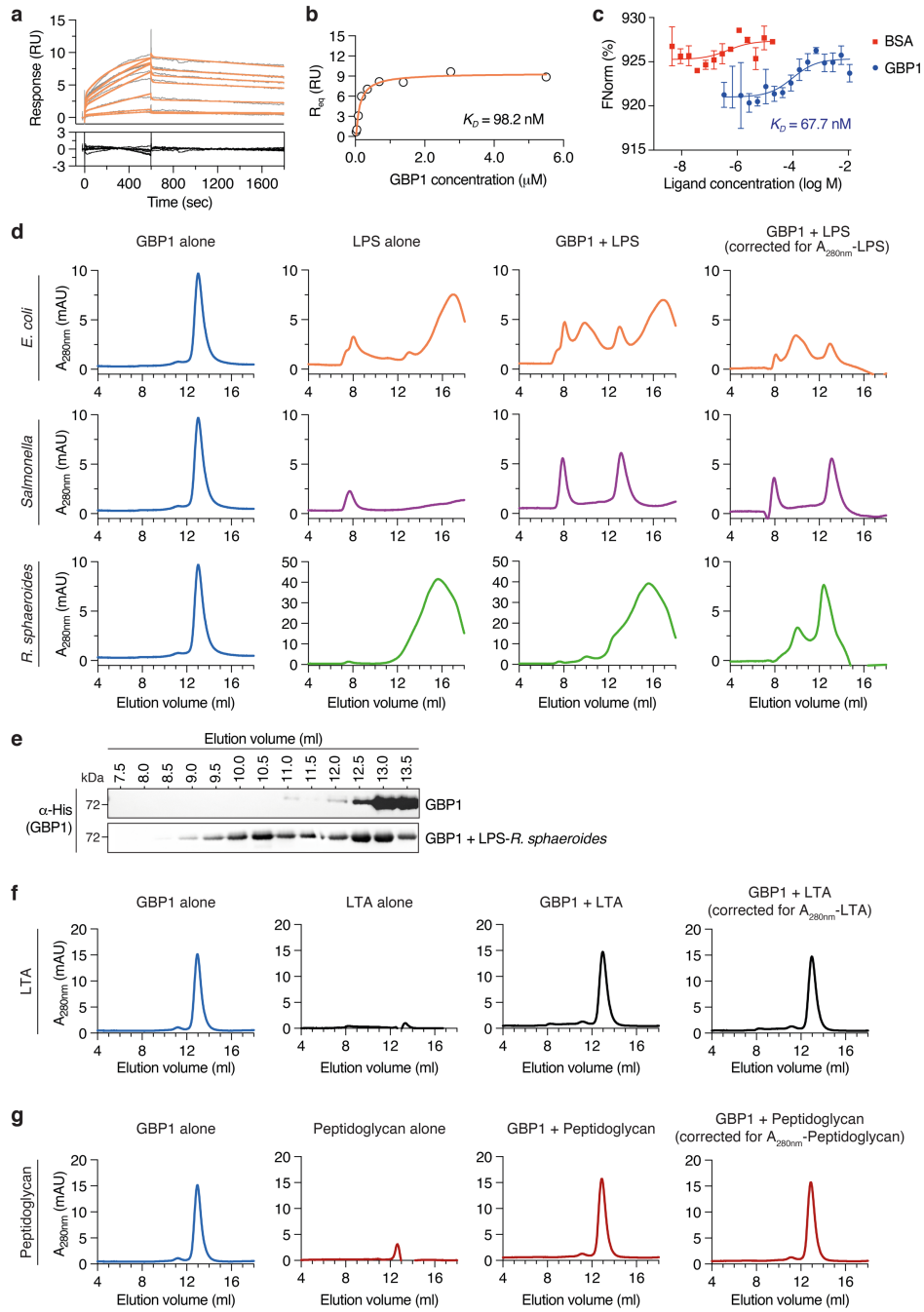
d. Western blot analysis of Dox-inducible eGFP-GBP1-7 or eGFP expression in HeLa cells.

e. LDH release from naïve HeLa cells co-expressing constitutive mCherry-GBP1 and Dox-inducible eGFP or eGFP-GBP1, -2, -3 or -4. FLAG-GBP3 and HA-GBP4 were constitutively expressed together using a bicistronic plasmid. Cells were transfected with the indicated plasmids for 24 h. eGFP-GBPs were induced for 16 h with 1 $\mu\text{g/ml}$ Dox, whereas eGFP was induced for 3 h. Cells were then transfected with *E. coli*-derived LPS (2.5 μg / 50,000 cells) for 6 h.

f. Western blot analysis of mCherry-GBP1 and endogenous (endog.) GBP1 expression (α -GBP1), Dox-inducible eGFP-GBP2-4 or eGFP expression (α -GFP), HA-GBP4 (α -HA) or FLAG-GBP3 (α -FLAG) expression, in HeLa cells. Asterisks point to non-specific bands.

Graphs show the mean \pm SD, and data are pooled from three independent experiments performed in triplicate (c, e) or are representative of two (b) or three (d, f) independent experiments. * $P < 0.05$; *** $P < 0.001$; one-way ANOVA.

Supplementary Figure 11



Supplementary Fig. 11. GBP1 interacts with LPS

a. SPR sensorgram of human GBP1 binding to *E. coli*-LPS (O111:B4) immobilized on a CM5 chip surface. Sensorgram was obtained by using different GBP1 concentrations (21.5, 43, 86, 172, 344, 688, 1375, 2750 nM). Grey lines correspond to SPR data and orange lines to model fits using a two-state-reaction model.

b. Saturation curve of the titration of GBP1 on LPS immobilized on a CM5 chip.

c. MST curves representing the interaction of GBP1 with FITC-LPS. BSA is used as a control.

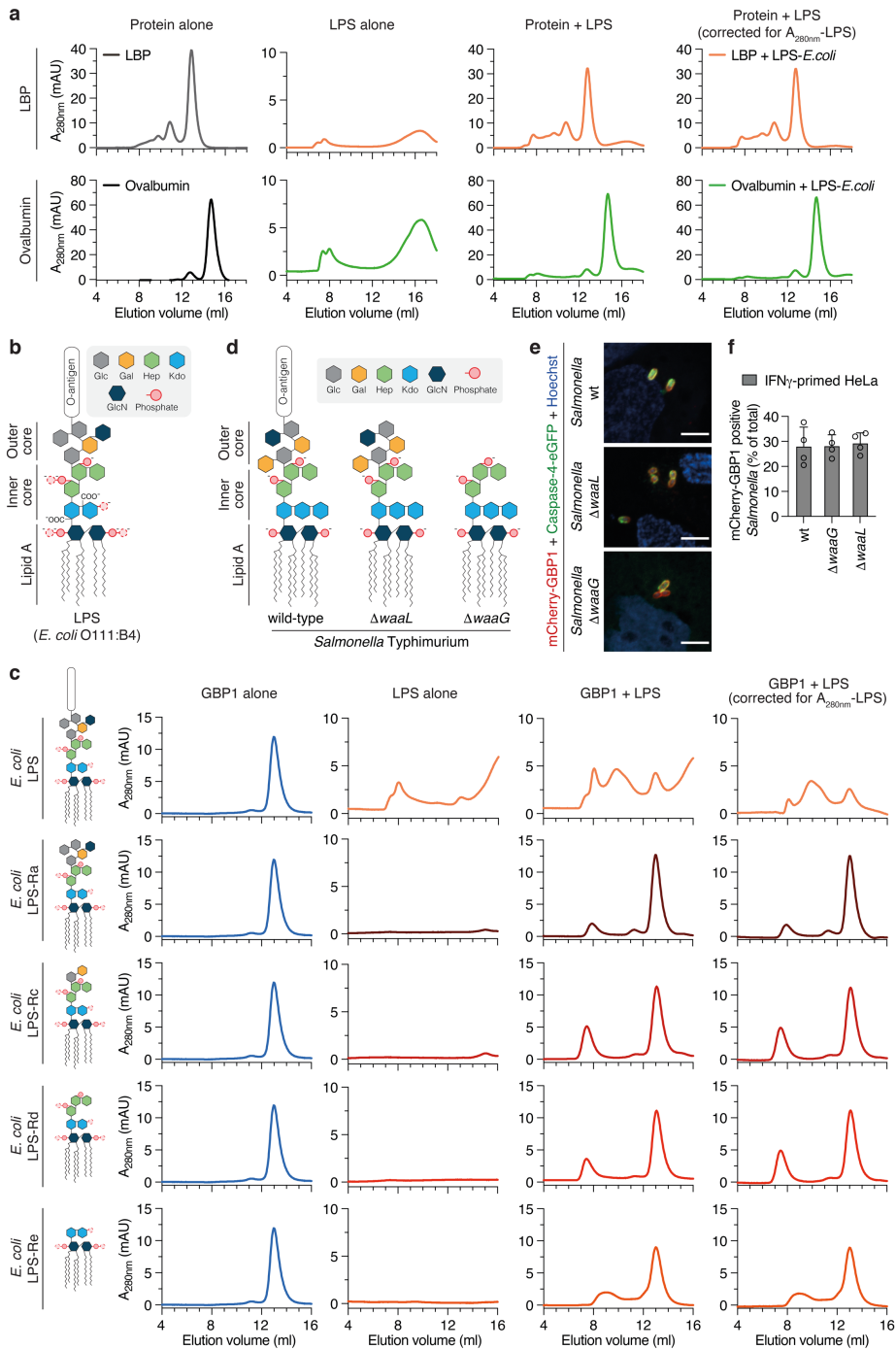
d. SEC elution profiles of GBP1 alone, LPS from *E. coli*, *Salmonella* Typhimurium or *R. sphaeroides* or GBP1 incubated with the indicated LPS. Right panels show the SEC elution profiles after correction by subtracting the LPS-specific absorbance at 280 nm. Elution profiles are representative of 5-8 independent experiments.

e. Western blot analysis of His₆ after running individual fractions on a 12% acrylamide gel to confirm the presence of GBP1 in elution peaks.

f, g. SEC elution profiles of GBP1 alone, lipoteichoic acid (LTA) or GBP1 incubated with LTA (f), or GBP1 alone, peptidoglycan or GBP1 incubated with peptidoglycan (g). Right panels show the SEC elution profiles after correction by subtracting the LTA- or peptidoglycan-specific absorbance at 280 nm.

Graphs show the mean \pm SD, and data are representative from three (a-c) or five (d-g) independent experiments performed with at least three independently expressed and purified batches of recombinant His-GBP1.

Supplementary Figure 12



24

Supplementary Fig. 12. GBP1 interacts with the inner core and Lipid A region of LPS.

a. SEC elution profiles of LBP or ovalbumin alone, LPS from *E. coli*, or LBP or ovalbumin incubated with LPS. Right panels show the SEC elution profiles after correction by subtracting the LPS-specific absorbance at 280 nm.

b. Schematic representation of the LPS structure from *E. coli* serotype O111:B4, containing 6-8 negatively charged groups. Partial modifications that may result in additional phosphate groups are shown (dotted circles) and are dependent on growth conditions and other factors.

c. SEC elution profiles of GBP1, different *E. coli* LPS variants, or GBP1 incubated with indicated LPS variants. Right panel show corrected profiles after subtracting absorbance at 280 nm for each correspondent LPS variant.

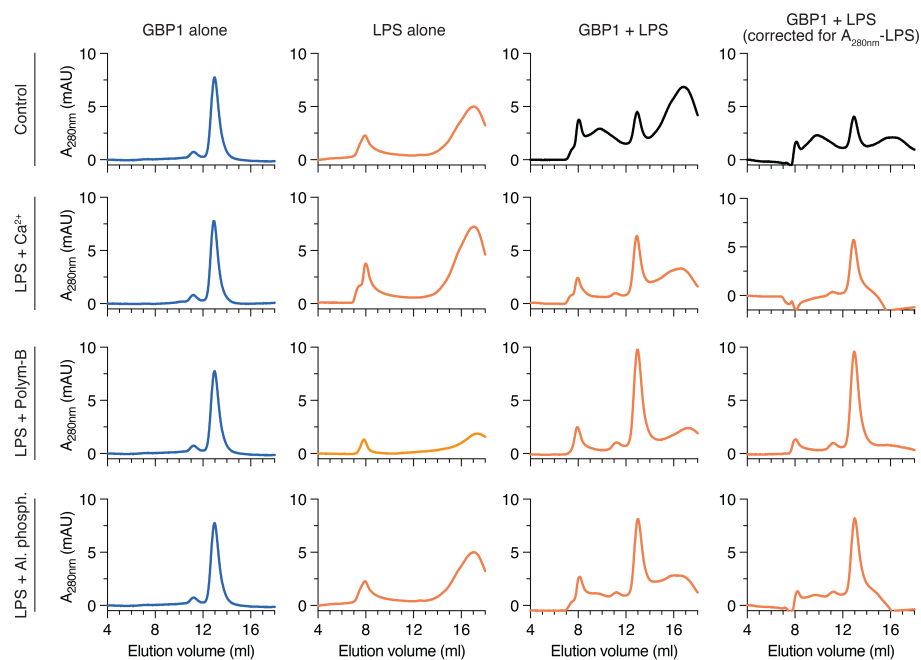
d. Schematic representation of the LPS structure from *Salmonella* Typhimurium and different mutants.

e. Fluorescence confocal microscopy of IFN γ -primed HeLa cells co-expressing mCherry-GBP1 (red) and caspase-4-eGFP (green) and infected with wild-type (wt) *Salmonella* or with its isogenic $\Delta waaL$ or $\Delta waaG$ strains for 1h. DNA was stained with Hoechst (blue). Representative confocal images are shown and scale bar corresponds to 5 μ m.

f. Percentage of mCherry-GBP1 positive *Salmonella* at 1 h p.i., as quantified by counting at least 100 bacteria per coverslip. Graph shows the mean \pm SD.

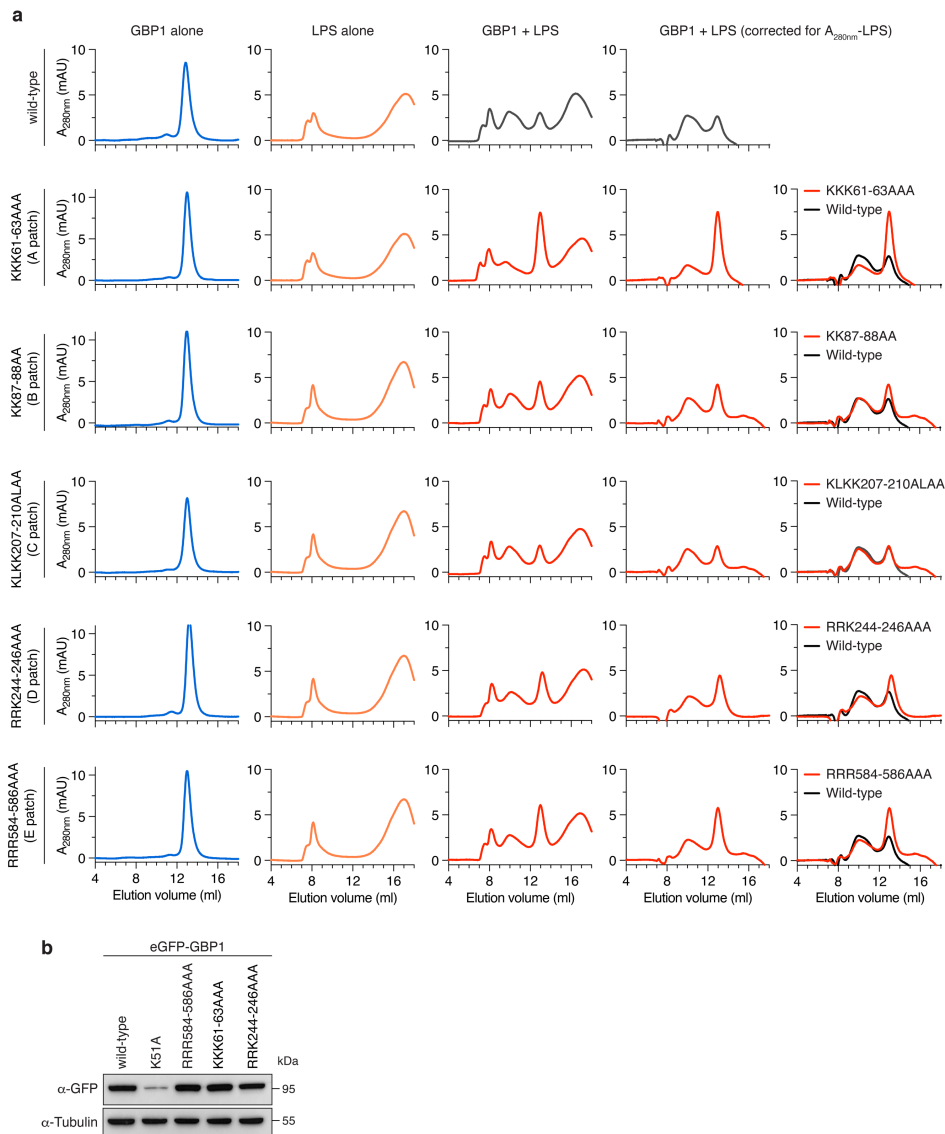
Data are representative of two (e), or at least four (a, c) independent experiments, or pooled from two independent experiments performed in duplicate (f).

Supplementary Figure 13



Supplementary Fig. 13. Negative charges on LPS are important for interaction with GBP1. SEC elution profiles of recombinant His-tagged GBP1 alone, *E. coli* LPS untreated or pre-treated with CaCl_2 (5 mM), Polymyxin B (10 $\mu\text{g}/\text{mL}$) or with alkaline phosphatase, or GBP1 incubated with the indicated LPS. Right panels show the SEC elution profiles after correction by subtracting the LPS-specific absorbance at 280 nm. Data are representative of at least three independent experiments.

Supplementary Figure 14

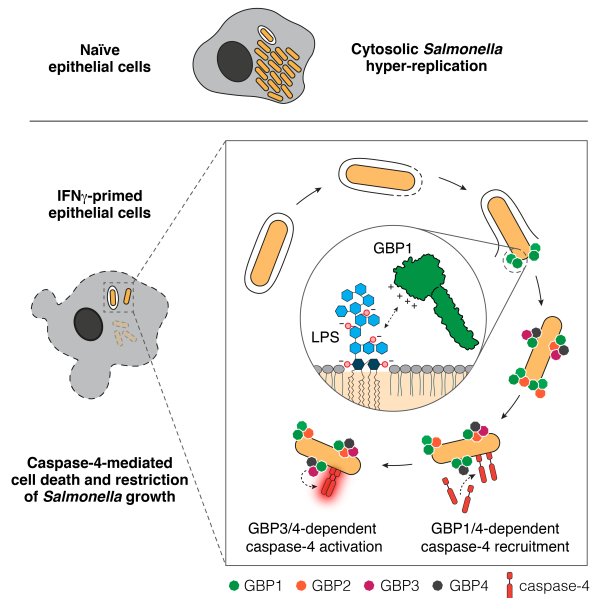


Supplementary Fig. 14. GBP1 binding to LPS involves electrostatic interactions.

a. SEC elution profiles of recombinant His-tagged GBP1 or of different GBP1 mutants, *E. coli* LPS, or the different GBP1 mutants after incubation with LPS. Right panels show the SEC elution profiles after correction by subtracting the LPS-specific absorbance at 280 nm. Data are representative of at least three independent experiments.

b. Western blot analysis for expression of different eGFP-tagged GBP1 mutants in naïve HeLa cells. Data are representative of two independent experiments.

Supplementary Figure 15



Supplementary Fig. 15. Model for GBP1 sensing of LPS and GBP-dependent recruitment of caspase-4 to cytosolic *Salmonella* for activation of non-canonical inflammasome in human epithelial cells.

In naïve epithelial cells (upper panel) *Salmonella* escape from the SCV to the cytosol, where they hyper-replicate. In IFN γ -primed epithelial cells (lower panel), GBP1 is recruited to the *Salmonella* surface immediately after SCV membrane rupture and bacterial escape to the host cytosol. GBP1 senses and binds to the LPS inner core and Lipid A, through electrostatic interactions, undergoing formation of a high-molecular weight complex and driving hierarchical recruitment of GBP2, -3 and -4 to the cytosolic bacteria. GBP1/4 additionally control recruitment of caspase-4 to the surface of cytosolic *Salmonella* and, together with GBP3, LPS-dependent activation of the caspase.

Supplementary Table 1 – Plasmids and primers used in this study.

| Plasmid | Expressed protein | Primers used | Reference |
|------------------------------|-------------------------|--|--------------------|
| pEGFP-GBP1 | eGFP-GBP1 | 5'-GGACTCAGATCTCGAGCGATGGCATCAGAGATCCACA-3' 5'-GCAGAATTCGAAGCTTTTAGCTTATGGTACATGCCT-3' | This study |
| pEGFP-GBP1 K51A | eGBP-K51A | 5'-CACAGGCGCATCCTACCTGATGAACAAGCTGGC-3' 5'-TAGGATGCGCCTGTGCGGTAGAGGCC-3' | This study |
| pEGFP-GBP2 | eGFP-GBP2 | 5'-GGACTCAGATCTCGAGCGATGGCTCCAGAGATCAACT-3' 5'-GCAGAATTCGAAGCTTTTAGAGTATGTACATATTGGC-3' | This study |
| pEGFP-GBP3 | eGFP-GBP3 | 5'-GGACTCAGATCTCGAGCGATGGCTCCAGAGATCCAC-3' 5'-GCAGAATTCGAAGCTTTAGATCTTAGCTTATGCGA-3' | This study |
| pEGFP-GBP4 | eGFP-GBP4 | 5'-GGACTCAGATCTCGAGCGATGGGTGAGAGAACTCTTC-3' 5'-GCAGAATTCGAAGCTTTAAATACGTGAGCCAAGATA-3' | This study |
| pEGFP-GBP5 | eGFP-GBP5 | 5'-GGACTCAGATCTCGAGCGATGGCTTTAGAGATCCACAT-3' 5'-GCAGAATTCGAAGCTTTAGAGTAAAACACATGGATC-3' | This study |
| pEGFP-GBP6 | eGFP-GBP6 | 5'-GGACTCAGATCTCGAGCGATGGAATCTGGACCCAAAAT-3' 5'-GCAGAATTCGAAGCTTTAAAGGGGAGCTTATGCT-3' | This study |
| pEGFP-GBP7 | eGFP-GBP7 | 5'-GGACTCAGATCTCGAGCGATGGCATCAGAGATCCACA-3' 5'-GCAGAATTCGAAGCTTTAGCTTATAATTTCTTACCA-3' | This study |
| pmCherry-GBP1 | mCherry-GBP1 | 5'-GGACTCAGATCTCGAGCGATGGCATCAGAGATCCACA-3' 5'-GCAGAATTCGAAGCTTTTAGCTTATGGTACATGCCT-3' | This study |
| pmCherry-GBP2 | mCherry-GBP2 | 5'-GGACTCAGATCTCGAGCGATGGCTCCAGAGATCAACT-3' 5'-GCAGAATTCGAAGCTTTTAGAGTATGTACATATTGGC-3' | This study |
| pmCherry-GBP3 | mCherry-GBP3 | 5'-GGACTCAGATCTCGAGCGATGGCTCCAGAGATCCAC-3' 5'-GCAGAATTCGAAGCTTTTAGATCTTAGCTTATGCGA-3' | This study |
| pmCherry-GBP4 | mCherry-GBP4 | 5'-GGACTCAGATCTCGAGCGATGGGTGAGAGAACTCTTC-3' 5'-GCAGAATTCGAAGCTTTAAATACGTGAGCCAAGATA-3' | This study |
| pmCherry-GBP5 | mCherry-GBP5 | 5'-GGACTCAGATCTCGAGCGATGGCTTTAGAGATCCACAT-3' 5'-GCAGAATTCGAAGCTTTAGAGTAAAACACATGGATC-3' | This study |
| pmCherry-GBP6 | mCherry-GBP6 | 5'-GGACTCAGATCTCGAGCGATGGAATCTGGACCCAAAAT-3' 5'-GCAGAATTCGAAGCTTTAAAGGGGAGCTTATGCT-3' | This study |
| pmCherry-GBP7 | mCherry-GBP7 | 5'-GGACTCAGATCTCGAGCGATGGCATCAGAGATCCACA-3' 5'-GCAGAATTCGAAGCTTTAGCTTATAATTTCTTACCA-3' | This study |
| piRFP703 | iRFP703 | 5'-CGTCAGATCCGCTAGCGCCACCATGGTAGCAGGT-3' 5'-CTTGAGCTCGAGATCTTCGAGATCTGAGTCCGAGCTCTCAAGCGCGGTGAT-3' | This study |
| piRFP703-GBP1 | iRFP703-GBP1 | 5'-TCTCGAAGATCTCGAGCGATGGCATCAGAGATCCACA-3' 5'-GCAGAATTCGAAGCTTTAGCTTATGGTACATGCCT-3' | This study |
| pAIP-HA-GBP1 | HA-GBP1 | ————— | Gift from T. Henry |
| pAIP-HA-GBP1 ^{CAAX} | HA-GBP1 ^{CAAX} | 5'-TGCCCTTTCGTCGTCATT-3' 5'-TAAAGACCAGAGCCTTCCTG-3' | This study |
| pAIP-HA-GBP2 | HA-GBP2 | ————— | Gift from T. Henry |
| pAIP-HA-GBP3 | HA-GBP3 | 5'-TGCCCTCTCCGAATTCGAGATATCCATCACACTGGGACATGGCTCCAGAGATCCACATG-3' 5'-GAGAGGGGCGGAATTCACGGTCGATGTAGATCTTAGCTTATGCGACATATATCTCTTGG-3' | This study |
| pAIP-HA-GBP4 | HA-GBP4 | 5'-TGCCCTCTCCGAATTCGAGATATCCATCACACTGGGACATGGGTGAGAGAACTCTTCACGC-3' 5'-GAGAGGGGCGGAATTCACGGTCGATGTAAATACGTGAGCCAAGATATTTTGTCCCT-3' | This study |
| pLVX-eGFP-GBP1 | eGFP-GBP1 | 5'-ACCGGTGCCGGCGGATGCCACCATTGGTGAGCAA-3' 5'-GAGGTGGTCTGGATCTTAGCTTATGGTACATGCCTTTCTG-3' | This study |
| pLVX-eGFP-GBP2 | eGFP-GBP2 | 5'-ACCGGTGCCGGCGGATGCCACCATTGGTGAGCAA-3' 5'-GAGGTGGTCTGGATCTTAGAGTATGTACATATTGGCTCCAATGA-3' | This study |
| pLVX-eGFP-GBP3 | eGFP-GBP3 | 5'-ACCGGTGCCGGCGGATGCCACCATTGGTGAGCAA-3' 5'-GAGGTGGTCTGGATCTTAGATCTTAGCTTATGCGACATATATCTCT-3' | This study |
| pLVX-eGFP-GBP4 | eGFP-GBP4 | 5'-ACCGGTGCCGGCGGATGCCACCATTGGTGAGCAA-3' 5'-GAGGTGGTCTGGATCTTAGATCTTAGCTTATGGTACATGCCTTTCTG-3' | This study |
| pEGFP-caspase-4 | Caspase-4-eGFP | 5'-TGGCAATGGTACCAGCTCGGCT-3' 5'-GCAGAATTCGAAGCTTTACTTGTACAGCTCGTCCATGCC-3' 5'-CGTCAGATCCGCTAGCCCCGCCACCATGGCAG-3' 5'-TCGGTACCAATTGCCAGAAAGAGGTAGAATAATCTTG-3' | This study |
| pCaspase-4-V5 | Caspase-4-V5 | 5'-TCTAGAGTCGGCCTCACGT AGA ATC GAG ACC GAG GAG AGG GTT AGG GAT AGG CTT ACCCGCCCATTTGCCAGAAAGAGGTAGAATAATC-3' | This study |

30

31

| | | | |
|--------------------|-------------------------|---|------------|
| pEGFP-Galactin3 | Galactin3-eGFP | | 1 |
| pmOrange-Galactin3 | Galactin3-mOrange | | 2 |
| pMyc-GBP1 | Myc-GBP1 | 5'-AGCAGTACTTCTAGAGGATCGCCACCATGGAGCAGAACTCATCTCTGAAGAGGATCTGGGA TCCATGGCATCAGAGATCCACATGAC-3' 5'-TATCATGTCTGAATTTCTTAGCTTATGCTTATGCTACATGCCTTTCTGT-3' | This study |
| pFLAG-GBP3 | FLAG-GBP3 | 5'-AGCAGTACTTCTAGAGGATCGCCACCATGGAGTACAAGGATGACGACGATAAGGGATCC ATGGCTCCAGAGATCCACATG-3' 5'-TATCATGTCTGAATTTCTTAGCTTATGCTTATGCTTATGCGACATATATCTCTT-3' | This study |
| pFLAG-GBP3/HA-GBP4 | FLAG-GBP3 + HA-GBP4 | 5'-TGAACACGTGGTCCGCGCGCCGCCACCATGGGTACCCITATGATGTCCAGATT ATGCCAGCGCCGCATGGGTGAGAGAACTTTCACGC-3' 5'-CTGATCAGCGGGTTTAAACTTAAATACGTGAGCCAAGATATTTGTCCCT-3' | This study |
| Pet28a-GBP1 | His-GBP1 | 5'-CGCGCGGCAGCCATACACATCATATGGCATCAGAGATCCA-3' 5'-GGTGGTGGTGCTCGATTAGCTTATGGTACATGCCCTTTCGT-3' | This study |
| Pet28a-GBP1m1 | His-GBP1 K61-63A | 5'-TGGAGCTGCTGCTGGCTTCTCTCTGGGCTCC-3' 5'-CCAGCAGCAGCTCCAGCCAGCTTGTTCATCAGG-3' | This study |
| eGFP-GBP1m1 | GFP-GBP1 K61-63A | 5'-TGGAGCTGCTGCTGGCTTCTCTCTGGGCTCC-3' 5'-CCAGCAGCAGCTCCAGCCAGCTTGTTCATCAGG-3' | This study |
| Pet28a-GBP1m2 | His-GBP1 K87-88A | 5'-ACCCCGCTGCTCCAGGCCACATCCTAGTTCTGC-3' 5'-CTGGAGCAGCGGGTGGGGCACACCCACATCC-3' | This study |
| eGFP-GBP1m2 | GFP-GBP1 K87-88A | 5'-ACCCCGCTGCTCCAGGCCACATCCTAGTTCTGC-3' 5'-CTGGAGCAGCGGGTGGGGCACACCCACATCC-3' | This study |
| Pet28a-GBP1m3 | His-GBP1 KLK207-210ALAA | 5'-TGGCTCTGGCTGCTGGTACCAGTCAAAAAGATGAAACT-3' 5'-CAGCAGCCAGAGCCAGGGAGTATGTCAGGTACTCA-3' | This study |
| Pet28a-GBP1m4 | His-GBP1 K | 5'-TCACGCCGCCGCCCTTGCCAGCTCGAGAAAC-3' 5'-AGGGCGCGGCGTGAACGGGCGGATCAAGAC-3' | This study |
| Pet28a-GBP1m5 | His-GBP1 R584-586A | 5'-AATGGCTGCTGCTAAGGCATGTACCATAAGCTAAATG-3' 5'-TTAGCAGCAGCCATTTTCGTCTGGAGATCCTG-3' | This study |

Supplementary Table 2 – siRNAs used for knock-down.

| Oligonucleotides | Source and catalogue number |
|---|--------------------------------------|
| Stealth RNAi™ siRNA negative control, Med GC | Thermo Fisher Scientific (12935300) |
| siCASP4 | Thermo Fisher Scientific (HSS141457) |
| siGSDMD | Thermo Fisher Scientific (HSS149278) |
| siGBP1 | Thermo Fisher Scientific (HSS104021) |
| siGBP2 | Thermo Fisher Scientific (HSS104025) |
| siGBP3 | Thermo Fisher Scientific (HSS104027) |
| siGBP4 | Thermo Fisher Scientific (HSS133000) |
| siGBP5 | Thermo Fisher Scientific (HSS133003) |
| siGBP6 | Thermo Fisher Scientific (HSS136383) |
| siGBP7 | Thermo Fisher Scientific (HSS139886) |

Supplementary Table 3 – Primers used for qPCR.

| Target gene | Primer pairs (5' → 3') |
|-------------|---|
| GBP1 | TCAATGAGGAAATCCCAGCCC AGGCTGTTCCCTTGCTGTTC |
| GBP2 | ATCTCTGATCTGGGAACAACAC GATAGAGGCCCAATCGCC |
| GBP3 | AGCACAGACAAGAGAACAATGCC TCTGGATTCGCCACCAGTTC |
| GBP4 | CAGTGCCACACCAGGTTATC TTCCTGTGCGGTATAGCCCT |
| GBP5 | CGGCGATTCAAAGGCAGAAC AGCCTGTTCTGCATCTGTTG |
| GBP6 | ACTGCACCATCCCATTTGTGG TGCCAACTAGAAGGCCTGC |
| GBP7 | ACTCTGGACAGAGGAACGCC TAGAGGCCACAATTGCCAC |
| HPRT | GAACCTCTCGGCTTTCCCG TACTAATCACGACGCCAGGG |

Supplementary References

1. Paz, I. *et al.* Galectin-3, a marker for vacuole lysis by invasive pathogens. *Cell Microbiol* **12**, 530–544 (2010).
2. Ray, K. *et al.* Tracking the dynamic interplay between bacterial and host factors during pathogen-induced vacuole rupture in real time. *Cell Microbiol* **12**, 545–556 (2010).

3.2. Research Project II: Guanylate-Binding Protein-Dependent Noncanonical Inflammasome Activation Prevents *Burkholderia thailandensis*-Induced Multinucleated Giant Cell Formation

Marisa Dilucca¹, Saray Ramos¹, Kateryna Shkarina¹, José Carlos Santos^{1†}, Petr Broz^{1†}

¹ Department of Biochemistry, University of Lausanne, Chemin des Boveresses 155, 1066, Epalinges, Switzerland

† Corresponding authors. Email: petr.broz@unil.ch; jose.santos@unil.ch

Statement of contribution:

M.D., J.C.S., and P.B. designed the experiments and analyzed data, conceptualized and supervised the study, and wrote the manuscript, which all authors reviewed before submission. **M.D.**, S.R., and J.C.S. performed the experiments. K.S. contributed expression vectors.

Specific contribution:

Phase-contrast imaging and quantification of *Burkholderia*-induced giant cells in wild-type, GBP1-, CASP4-, and GSDMD-deficient cell lines naïve or IFN γ -stimulated. Imaging and quantification of cell-to-cell-fusion events in wild-type and GBP1-deficient cells treated with a STAT1 inhibitor.

Generation of HeLa cells stably expressing Dox-inducible eGFP or mCherry and quantification of eGFP-positive, mCherry-positive, and eGFP/mCherry-double-positive cells in naïve and IFN γ -stimulated conditions upon *B. thailandensis* infection.

Propidium-iodide (PI) uptake in naïve and IFN γ -primed HeLa cells infected with *B. thailandensis*.

Overexpression of caspase-4-eGFP in HeLa cells and quantification of caspase-4-eGFP-positive bacteria.

Phase-contrast imaging and quantification of multi-nucleated giant cells (MNGCs) in human bronchial epithelial cells (HBEC3-KT) and keratinocytes (HaCaT).

Quantification of multinucleation events in HBEC3-KT and HaCaT cells transfected with small-interfering RNA (siRNA) to target CASP4, GBP1, and GSDMD. And immunoblot for CASP4, GBP1, GSDMD, and tubulin (loading control) 24 hours post

siRNA transfection.

Purification and differentiation of human monocyte-derived macrophages (hMDMs).
And PI-uptake assay in naïve and IFN γ -treated hMDMs after *B. thailandensis* infection.

Quantification of ASC speck in naïve and IFN γ -primed hMDMs infected with *Burkholderia* in the presence or absence of the NLRP3 inhibitor MCC950

Quantification of the colony-forming unit (CFUs) at the desired time post-infection.

Summary of the results

The genus of Gram-negative bacteria *Burkholderia* includes more than 30 species, most of which are plant pathogens. Among them, two groups can cause disease in humans: the *Burkholderia cepacia* complex, which is pathogenic to individuals with cystic fibrosis, and the *Burkholderia pseudomallei* complex, which includes *B. pseudomallei* and *B. mallei* potentially infectious to humans, and *B. thailandensis* that is rarely pathogenic. *B. mallei* is the causative agent of glanders in horses and can cause disease in humans, however, infections in any host are now only seldom reported. In contrast, *B. pseudomallei* is a soil-dwelling bacteria commonly found in tropical and subtropical regions with the ability to infect humans and animals, mainly equines. Naturally acquired infections result from exposure through skin abrasions, inhalation, and ingestion, leading to the development of a wide range of symptoms that collectively result in melioidosis. The mortality rate of melioidosis remains high despite antimicrobial therapy; in fact, *Burkholderia* is inherently resistant to many antibiotics^{126,457–459}.

Burkholderia can invade phagocytic and non-phagocytic cells via T3SS-related effector proteins^{460,461}. It readily escapes endocytic compartments to invade the cytosol of the host cell where it replicates and hijacks the host Arp2/3 actin polymerization machinery, via the bacterial protein BimA, to polymerize actin tails and invade neighboring cells^{461,462}. Interestingly, the cell-to-cell spread leads to the fusion of the host cells and the formation of the so-called MNGCs^{461,463–465}. Because of the high infectivity rate of *B. pseudomallei* and its classification as a bioterrorism weapon, *B. thailandensis* is widely used as a laboratory model to study melioidosis, as it is less virulent and shares an identical intracellular life cycle to that of the *B. pseudomallei* strain.

IFNs are key mediators in modulating the cell-autonomous immune response against a wide variety of pathogens; indeed, their protective role in response to *Burkholderia* infection has been proposed, as they induce caspase-11 expression⁴⁶⁶. However, in vivo infection models in mice revealed that mouse macrophages respond to *Burkholderia* infection by activating the NLRC4 inflammasome, which prompts the maturation of the proinflammatory cytokine IL-18. NK and T cells respond to IL-18 by producing IFN γ , which in turn promotes non-canonical inflammasome activation in mouse macrophages and neutrophils. Therefore, IFN can be considered a second

tier of defense against *Burkholderia*^{467–469}. Furthermore, GBPs, IFN-inducible GTPases, have been found to target cytosolic *Burkholderia* in bone marrow-derived mouse macrophages (BMDMs), impairing bacterial actin-based motility⁴⁷⁰.

In contrast, very little is known about the role of IFN and inflammasome in hindering *Burkholderia* infection in human cell lines. Using HeLa cells as a model of human epithelial cells, the primary host in case of *Burkholderia* infections, we found that IFN γ priming blocks MNGC formation; in fact, time-lapse confocal microscopy of a co-culture model of HeLa cells stably expressing eGFP or mCherry showed that colocalization of the two intracellular fluorescent dyes is detectable exclusively under naïve conditions. Furthermore, we found that the IFN γ -dependent restriction of MNGC formation is due to GBP1 expression; in fact, GBP1-deficient HeLa cells stimulated by IFN γ form giant cells in a manner comparable to wild-type naïve cells. Furthermore, overexpression of labeled GBP1-7 showed that intracellular bacteria are massively coated with GBP1 under both naïve and primed conditions. However, the presence of IFN γ results in the recruitment of other GBPs to the *Burkholderia* surface, more specifically GBP2, GBP3, and GBP4, corroborating our previous finding that identified GBP1 as the most upstream GBP recruited to the bacterial surface³⁶⁰. Finally, we provide evidence showing that GBP1 induces rapid cell death of the infected cell by driving the recruitment and activation of caspase-4, thereby eliminating the intracellular replication niche of *Burkholderia* and thus its spread from cell to cell. In contrast to other reports, GBP1 coating neither impairs actin-based motility nor has direct bactericidal activity^{433,449}.




We also proved that GBP1-dependent noncanonical inflammasome activation in response to *Burkholderia* prevents multinucleation events even in more physiological human cell lines, such as bronchial epithelial cells, keratinocytes, and primary human macrophages. Thus, small interfering RNA experiments revealed that targeting GBP1, CASP4 and GSDMD abrogates IFN γ -mediated restriction of MNGCs. Interestingly, in naïve primary human macrophages, we see a high rate of cell death as assessed by propidium-iodide uptake assay, suggesting that in this cell type a canonical inflammasome might be promptly upregulated upon infection. However, IFN γ stimulation hastens cell death by inducing caspase-4-dependent pyroptosis.

In summary, we found that IFN restricts MNGC formation by inducing GBP

expression and thereby fostering non-canonical inflammasome activation and subsequent pyroptotic death in the early stages of infection, thus the intracellular replication niche of *Burkholderia* is eradicated as well as its spread through actin tails is prevented.



Guanylate-Binding Protein-Dependent Noncanonical Inflammasome Activation Prevents *Burkholderia thailandensis*-Induced Multinucleated Giant Cell Formation

 Marisa Dilucca,^a
 Saray Ramos,^a
 Kateryna Shkarina,^a
 José Carlos Santos,^a
 Petr Broz^a

^aDepartment of Biochemistry, University of Lausanne, Epalinges, Switzerland

ABSTRACT Inflammasomes are cytosolic multiprotein signaling complexes that are activated upon pattern recognition receptor-mediated recognition of pathogen-derived ligands or endogenous danger signals. Their assembly activates the downstream inflammatory caspase-1 and caspase-4/5 (human) or caspase-11 (mouse), which induces cytokine release and pyroptotic cell death through the cleavage of the pore-forming effector gasdermin D. Pathogen detection by host cells also results in the production and release of interferons (IFNs), which fine-tune inflammasome-mediated responses. IFN-induced guanylate-binding proteins (GBPs) have been shown to control the activation of the noncanonical inflammasome by recruiting caspase-4 on the surface of cytosolic Gram-negative bacteria and promoting its interaction with lipopolysaccharide (LPS). The Gram-negative opportunistic bacterial pathogen *Burkholderia thailandensis* infects epithelial cells and macrophages and hijacks the host actin polymerization machinery to spread into neighboring cells. This process causes host cell fusion and the formation of so-called multinucleated giant cells (MNGCs). Caspase-1- and IFN-regulated caspase-11-mediated inflammasome pathways play an important protective role against *B. thailandensis* in mice, but little is known about the role of IFNs and inflammasomes during *B. thailandensis* infection of human cells, particularly epithelial cells. Here, we report that IFN- γ priming of human epithelial cells restricts *B. thailandensis*-induced MNGC formation in a GBP1-dependent manner. Mechanistically, GBP1 does not promote bacteriolysis or impair actin-based bacterial motility but acts by inducing caspase-4-dependent pyroptosis of the infected cell. In addition, we show that IFN- γ priming of human primary macrophages confers a more efficient antimicrobial effect through inflammasome activation, further confirming the important role that interferon signaling plays in restricting *Burkholderia* replication and spread.

IMPORTANCE The Gram-negative bacteria of the *Burkholderia* species are associated with human diseases ranging from pneumonia to life-threatening melioidosis. Upon infection through inhalation, ingestion, or the percutaneous route, these bacteria can spread and establish granuloma-like lesions resulting from the fusion of host cells to form multinucleated giant cells (MNGCs). *Burkholderia* resistance to several antibiotics highlights the importance to better understand how the innate immune system controls infections. Here, we report that interferons protect human epithelial cells against *Burkholderia*-induced MNGC formation, specifically through the action of the interferon-induced GBP1 protein. Mechanistically, GBP1 acts by inducing caspase-4-dependent cell death through pyroptosis, allowing the infected cells to be quickly eliminated before bacterial spread and the formation of MNGCs. This study provides evidence that interferon-induced innate immune activation, through GBP1 and caspase-4, confers protection against *Burkholderia* infection, potentially opening new perspectives for therapeutic approaches.

July/August 2021 Volume 12 Issue 4 e02054-21

Citation Dilucca M, Ramos S, Shkarina K, Santos JC, Broz P. 2021. Guanylate-binding protein-dependent noncanonical inflammasome activation prevents *Burkholderia thailandensis*-induced multinucleated giant cell formation. *mBio* 12: e02054-21. <https://doi.org/10.1128/mBio.02054-21>.

Editor Dominique Soldati-Favre, University of Geneva

Copyright © 2021 Dilucca et al. This is an open-access article distributed under the terms of the [Creative Commons Attribution 4.0 International license](https://creativecommons.org/licenses/by/4.0/).

Address correspondence to José Carlos Santos, jose.santos@unil.ch, or Petr Broz, petr.broz@unil.ch.

Received 15 July 2021

Accepted 16 July 2021

Published 17 August 2021

 mbio.asm.org 1

Downloaded from <https://journals.asm.org/journal/mbio> on 18 September 2022 by 2001.620.610.e02.3.

KEYWORDS antimicrobial mechanisms, guanylate-binding proteins, host-pathogen interactions, inflammasomes, innate immunity

Burkholderia is a genus of Gram-negative bacteria and includes species that are pathogenic for humans, such as *Burkholderia mallei* and the soil-dwelling species *B. pseudomallei*. The former is the causative agent of glanders, a contagious zoonotic infectious disease that primarily affects horses, whereas the latter is the etiological agent of human melioidosis (1–4). Melioidosis is an infectious disease present mostly in Asia, Africa, and South America and endemic in Thailand and northern Australia. The disease is thought to develop upon bacterial infection through inhalation, ingestion of contaminated food or water, or direct contact with the soil through skin abrasions. Depending on the infection route, patients display a wide range of clinical signs and symptoms (e.g., sepsis, pneumonia, and encephalitis, etc.) that can lead to a fatal outcome, mostly if left untreated (1–4). *B. pseudomallei* is naturally resistant to several antibiotics, and its wide environmental dissemination and ability to spread through aerosols led to its classification as a potential biowarfare/bioterrorism agent. The closely related but opportunistic pathogenic species *B. thailandensis* has been widely used as a laboratory infection model to study melioidosis, as it shares an identical intracellular life cycle with *B. mallei* and *B. pseudomallei*. The bacteria invade phagocytic and non-phagocytic cells using T3SS (type III secretion system)-injected effector proteins and quickly escape from the endocytic compartment into the host cytosol (5, 6). Once cytosolic, *B. thailandensis* replicates and uses actin-based motility by coopting the host Arp2/3 complex through the bacterial protein BimA (6, 7), which allows it to form protrusions and spread to neighboring cells in a process requiring a type VI secretion system (T6SS). A hallmark of *Burkholderia* cell-to-cell spread is host cell fusion and the formation of so-called multinucleated giant cells (MNGCs). The presence of MNGCs has been observed in the tissues of patients with melioidosis (8), and they are thought to occur through T6SS effectors, specifically the T6SS protein VgrG5 (6, 9, 10).

Interferons (IFNs) are central cytokines in modulating host cell-autonomous defense and innate immune responses against a wide variety of pathogens. IFN signaling pathways induce the expression of IFN-stimulating genes (ISGs), which encode effector proteins that participate in immunity against viruses, bacteria, and protozoan parasites (11–15). Prominent among the ISGs are the guanylate-binding proteins (GBPs), a family of dynamine-like large GTPases with the ability to target intracellular parasites and Gram-negative bacteria, thus triggering inflammasome activation and antimicrobial mechanisms in both mouse and human cells (11–13). The role of GBPs in inflammasome activation is best studied for human GBP1, which has the ability to directly interact with lipopolysaccharide (LPS), the major component of the Gram-negative bacterial outer membrane. By functioning as a bona fide LPS sensor, human GBP1 (hGBP1) assembles a platform that recruits other GBP family members (hGBP2 to -4 [hGPB2-4]) (16) and caspase-4 directly on the surface of cytosolic *Salmonella enterica* serovar Typhimurium or *Shigella flexneri* cells (17–21). This in turn allows the activation of the so-called noncanonical inflammasome via LPS-induced caspase-4 oligomerization and activation, which cleaves the pore-forming cell death effector gasdermin D (GSDMD) to induce proinflammatory pyroptosis and interleukin-18 (IL-18) release (22, 23). In mouse macrophages, however, additional IFN-inducible GTPases such as immunity-related GTPases (IRGs) (which are not present in human cells except for an IRGM truncated form and immunity-related GTPases (IRGs) [24]) seem to play an antimicrobial role (25–28). It has been shown that mouse GBPs recruit Irgb10 onto bacterial surfaces to induce bacteriolysis and the release of bacterial pathogen-associated molecular patterns (PAMPs) that induce inflammasome activation and pyroptosis (25, 27, 28).

In a mouse model of infection, IFNs have been proposed to play a protective role in restricting *Burkholderia* infection by inducing *Casp11* upregulation (29). IFN production during *Burkholderia* infection, however, seems to be only a second layer of defense and occurs as a consequence of *Burkholderia*-induced activation of the canonical NLR4 inflammasome and subsequent IL-18 secretion (30–32). Recent work has also

suggested that in mouse macrophages, GBP coating of *Burkholderia* cells restricts cell fusion by preventing bacterial actin-based motility and spread (33). Unlike the mouse infection model, where data clearly support a role for IFNs in mediating *Burkholderia* restriction, little is known about the role of this cytokine in human cells, specifically in epithelial cells, in response to *B. thailandensis*.

Here, we provide evidence that in human epithelial cells, GBP1 restricts *B. thailandensis*-induced MNGC formation and that GBP1-dependent restriction is mediated by caspase-4-induced pyroptosis of infected cells and independent of restricting bacterial motility. Moreover, we show that the IFN-mediated restriction of *B. thailandensis* expands to several physiologically more relevant human cell lines, such as keratinocytes (HaCaT) and bronchial epithelial cells (HBEC3-KT). Finally, we observe that even in primary human macrophages, IFN priming confers a much more efficient clearance of *Burkholderia* infections.

RESULTS

Interferons restrict MNGC formation in epithelial cells during *B. thailandensis* infection. In a mouse model of infection, type I and type II IFNs have been described to participate in the immune response against *B. thailandensis* (29, 33, 34). However, it has been suggested that they play differential roles in epithelial cells and macrophages (35). Moreover, how IFNs regulate defense against this bacterium in the human system remains poorly understood. To gain more insights into the role of IFN priming in protecting human epithelial cells against *B. thailandensis* infection, we infected HeLa cells with *B. thailandensis* and monitored the formation of MNGCs, a hallmark of *B. thailandensis* spread and replication. Microscopy-based analysis showed that by 20 h postinfection (p.i.), naive HeLa cells formed large cell clusters with tightly packed nuclei (Fig. 1a; see also Fig. S1a in the supplemental material), consistent with the formation of cell aggregates known as MNGCs (6, 36). Through image-based quantification, we estimated that approximately 50% of all nuclei belonged to giant cells (Fig. 1b). Strikingly, *B. thailandensis*-induced MNGC formation was almost completely restricted in IFN- γ -primed HeLa cells (Fig. 1a and b and Fig. S1a). Importantly, IFN- γ did not interfere with bacterial uptake as assayed by CFU counting (Fig. S1b).

Two main classes of IFNs have been described: type I, which includes many IFN types, such as IFN- α and IFN- β , and type II, e.g., IFN- γ . Following cognate receptor binding, both classes trigger a downstream signaling pathway through STAT1 that culminates in the transcription of interferon-stimulated genes (ISGs) (37). In order to confirm the role of IFN signaling in restricting MNGC formation, we used the STAT1 inhibitor fludarabine. IFN- γ -primed HeLa cells pretreated with fludarabine lost the ability to restrict MNGC formation upon *B. thailandensis* infection, almost to the levels found in naive cells (Fig. 1c and d). Immunoblotting confirmed the inhibition of the IFN signaling pathway, as the expression of hGBP1 (an ISG product selected as a marker to assess STAT1 inhibition) was partially reduced by fludarabine (Fig. S1c).

To better understand the cell-cell fusion dynamics and further confirm the IFN- γ -dependent restriction of MNGC formation during *B. thailandensis* infection, we used a coculture model of HeLa cells expressing doxycycline (Dox)-inducible enhanced green fluorescent protein (eGFP) (HeLa-eGFP) or Dox-inducible mCherry (HeLa-mCherry). We then performed time-lapse fluorescence confocal microscopy to track cell fusion and MNGC formation, which is characterized by the mixing and colocalization of both cytosolic fluorescent proteins (Fig. S1d). We found that infected naive cells started to fuse at about 6 to 8 h p.i. (Fig. 1e, top; Fig. S1e; and Movie S1), resulting in decreases in eGFP- or mCherry-positive cells (Fig. 1f and g) and concomitant increases in eGFP/mCherry-double-positive cells (Fig. 1h). Eventually, MNGCs were formed as a result of the fusion of several cells (Fig. 1e, top; Fig. S1e; and Movie S1). In contrast, no cell-cell fusion and MNGCs were detected in infected IFN- γ -primed cells (Fig. 1e, bottom; Fig. 1f to h; Fig. S1e; and Movie S2).

Altogether, these findings point out that in human epithelial cells, *B. thailandensis* spread and the resulting multinucleated cell formation are impaired in an IFN-dependent manner.

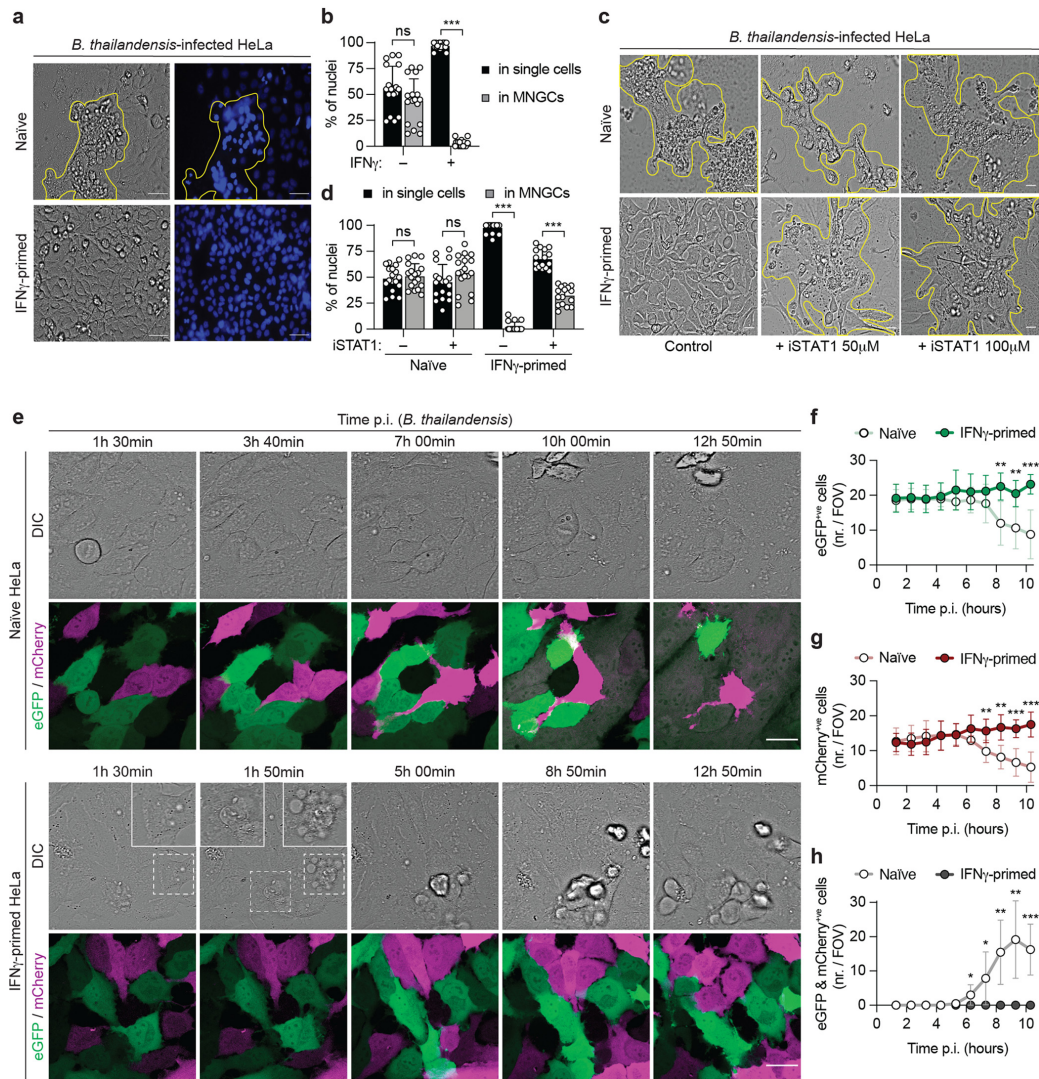


FIG 1 Interferons restrict multinucleated giant cell (MNGC) formation in epithelial cells during *B. thailandensis* infection. (a) Representative phase-contrast images (magnification, $\times 40$) of naive or IFN- γ -primed HeLa cells 20 h after infection with *B. thailandensis* (MOI of 0.3). The corresponding DNA was stained with Hoechst stain (right), and clustered nuclei, indicating MNGCs, are highlighted by yellow outlines. Bars, 100 μ m. (b) Percentage of nuclei found in MNGCs or in single cells, determined by counting nuclei of naive or IFN- γ -primed HeLa cells 20 h after infection with *B. thailandensis* (MOI of 0.3) in 6 fields of view under each experimental condition. (c) Representative phase-contrast images (magnification, $\times 40$) of naive or IFN- γ -primed HeLa cells infected with *B. thailandensis* (MOI of 100) in the presence or absence of the STAT1 inhibitor fludarabine at the indicated concentrations. Bars, 100 μ m. Yellow outlines correspond to clusters of cells forming MNGCs. (d) Percentage of nuclei in MNGCs or in single cells, determined by counting nuclei of naive or IFN- γ -primed HeLa cells 20 h after infection with *B. thailandensis* (MOI of 0.3) in the presence or absence of the STAT1 inhibitor (100 μ M) in 6 fields of view under each experimental condition. (e) Time-lapse fluorescence confocal microscopy of naive or IFN- γ -primed HeLa cells stably expressing Dox-inducible eGFP or mCherry. eGFP and mCherry expression was induced with 1 μ g/ml of Dox 4 h prior to infection. Cells were cocultured at a 1:1 ratio and infected with *B. thailandensis* (MOI of 50). Images were acquired every 10 min. Bars, 30 μ m. DIC, differential interference contrast. (f to h) Number of eGFP-positive (f), mCherry-positive (g), or eGFP/mCherry-double-positive (h) cells per field of view (FOV) in naive or IFN- γ -primed HeLa cells infected with *B. thailandensis*. Data are representative of results from at least three independent experiments performed in triplicate (a, c, and e). Graphs show the means \pm standard deviations (SD), and data are pooled from two (d) or three (b) independent experiments performed in duplicates or six independent movies (f to h). ns, not significant; *, $P < 0.05$; **, $P < 0.01$; ***, $P < 0.001$ by 2-way analysis of variance [ANOVA] (b and d) or a parametric t test [f to h]).

Human GBPs restrict MNGC formation. GBPs are well-known ISGs and have been shown to be crucial for the proper activation of innate immune defense mechanisms against Gram-negative bacteria, protozoan parasites, and viruses (12, 14, 15, 38). It was recently proposed that during *B. thailandensis* infection of mouse bone marrow-derived macrophages (BMDMs), mouse GBPs (mGBPs) contribute to restricting actin-based bacterial spread and cell-cell fusion, thus also reducing bacterium-induced pathology *in vivo* (33). Although it has been reported that *B. thailandensis* is targeted by GBP1 in human epithelial cells (16), the role of GBPs during *Burkholderia* infection of human cells, and specifically epithelial cells, is largely unknown. We first assessed if intracellular *B. thailandensis* is targeted by GBPs in HeLa cells ectopically expressing N-terminally eGFP-tagged GBPs (eGFP-GBPs). In accordance with a previous study (16), we observed that *B. thailandensis* was targeted by eGFP-GBP1 in IFN- γ -primed cells, where around 90% of the intracellular bacteria are GBP1 coated at 3 h p.i. (Fig. 2a and b). In naive cells, GBP1 was also associated with a high percentage of intracellular *B. thailandensis* bacteria, suggesting that it also senses cytosolically exposed LPS on the surface of this bacterium, similar to its role in *Salmonella* or *Shigella* infections (17–21). On the other hand, GBP2, -3, and -4 coated 40 to 20% of intracellular *Burkholderia* bacteria only in IFN- γ -primed but not in naive HeLa cells, corroborating the notion that their recruitment to cytosolic Gram-negative bacteria is driven by additional effectors that act upstream, namely, GBP1 (16–21). Similar to what has been shown upon *Shigella* infection (16), a very low percentage of bacteria positive for eGFP-GBP5, -6, and -7 was detected in both naive and IFN- γ -primed HeLa cells (Fig. 2a and b), suggesting that these three GBPs do not play a major role in recognizing this pathogen.

In order to investigate the possible role of hGBPs in restricting MNGC formation upon IFN- γ priming, we used *GBP1*^{-/-} HeLa cells previously generated by CRISPR-Cas9 genome editing (17). We found that hGBP1 is involved in restricting MNGC formation upon *B. thailandensis* infection, as IFN- γ -primed *GBP1*-deficient HeLa cells formed MNGCs in a manner comparable to that of wild-type naive cells (Fig. 2c and d and Fig. S1f and g) without affecting bacterial entry into cells (Fig. S1h). Collectively, these data suggest that hGBPs are the IFN-dependent downstream effectors responsible for restricting MNGC formation and *B. thailandensis* spread.

GBP1 promotes caspase-4-dependent pyroptosis and restricts MNGC formation and *B. thailandensis* replication. Recent studies have shown that in human epithelial cells and macrophages, GBPs are required for noncanonical inflammasome activation by targeting LPS and assembling a caspase-4-activating platform on the surface of cytosolic *Salmonella* and *Shigella* bacteria (17–21). Polymerized GBP1 on the bacterial surface was also proposed to act as an LPS surfactant that increases bacterial susceptibility to antimicrobial effectors by destabilizing the bacterial outer membrane (21). Moreover, the GBP coat assembled on *Shigella* cells appears to have an additional function of inhibiting actin-based motility and consequent bacterial cell-to-cell spread (16, 39). This same mechanism has recently been proposed to prevent *B. thailandensis* invasion of neighboring cells in murine BMDMs (33). Therefore, we speculated that one or several of these mechanisms might be responsible for the GBP1-dependent restriction of MNGC formation in human epithelial cell lines in response to *Burkholderia* infection (Fig. S2a).

Upon *B. thailandensis* infection, IFN- γ -primed HeLa cells showed signs of cell ballooning and blebbing, which are hallmarks of pyroptosis (Fig. 1e). Furthermore, a closer analysis of time-lapse confocal microscopy images of *B. thailandensis*-infected IFN- γ -primed HeLa cells showed that GBP1 targeting to cytosolic bacteria was followed by pyroptotic cell death in the majority of cases (as observed by nuclear condensation and plasma membrane swelling), with a concomitant restriction of bacterial replication (Movie S3 and Fig. S2b and c). The activation of the noncanonical inflammasome leads to caspase-4 activation and autoprocessing and the subsequent cleavage of the pyroptotic executor GSDMD (40). The cleaved GSDMD N-terminal domain forms pores that result in propidium iodide (PI) uptake, which can be used as a marker of lytic cell death. In the early stages of *B. thailandensis* infection, IFN- γ -primed wild-type HeLa cells

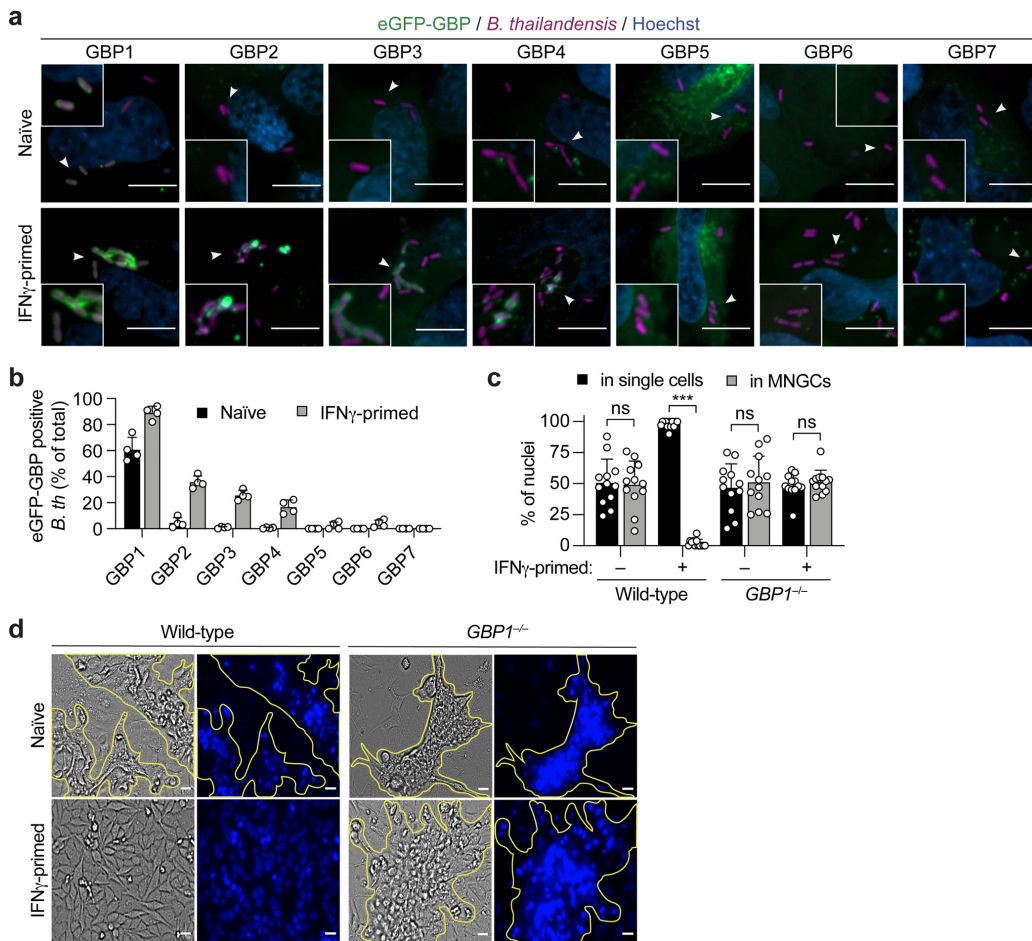


FIG 2 Human GBPs restrict MNGC formation. (a) Representative fluorescence confocal microscopy images of naive or IFN- γ -primed HeLa cells expressing N-terminally tagged eGFP-GBP1-7 and infected with *B. thailandensis*-mCherry (MOI of 30) for 3 h. DNA was stained by Hoechst stain. Bars, 10 μ m. (b) Percentage of intracellular eGFP-GBP1-7-positive *B. thailandensis* (*B. th*) bacteria in naive or IFN- γ -primed HeLa cells at 3 h p.i. At least 200 to 300 bacteria per well were counted. (c) Percentage of nuclei in MNGCs or in single cells, determined by counting the nuclei of naive or IFN- γ -primed wild-type or GBP1^{-/-} HeLa cells 20 h after infection with *B. thailandensis* (MOI of 0.3) in 6 fields of view under each experimental condition. (d) Representative phase-contrast images (magnification, $\times 40$) of naive or IFN- γ -primed wild-type or GBP1^{-/-} HeLa cells 20 h after infection with *B. thailandensis* (MOI of 0.3). The corresponding DNA was stained with Hoechst stain (right), and clustered nuclei, indicating MNGCs, are highlighted by yellow outlines. Bars, 100 μ m. Graphs show the means \pm SD, and data are pooled from two independent experiments performed in duplicate (b and c) or are representative of results from at least three independent experiments performed in triplicate (a and d). ***, $P < 0.001$; ns, not significant (by 2-way ANOVA [c]).

showed a higher percentage of PI-positive cells than did naive cells (Fig. 3a and Fig. S2d). Furthermore, we observed that *B. thailandensis* infection resulted in caspase-4 activation only in IFN- γ -primed cells (Fig. 3b, p32 fragment), which is in accordance with what has been observed during infection of epithelial cells with other cytosolic Gram-negative bacteria (17, 18). According to recent studies, coating of the surface of cytosolic Gram-negative bacteria by GBPs facilitates caspase-4 recruitment and activation, initiating the downstream pathway that culminates in the lytic death of the infected cell (17–21). Caspase-4 localization during *B. thailandensis* infection of IFN- γ -primed HeLa cells was assessed by fluorescence confocal microscopy. As expected,

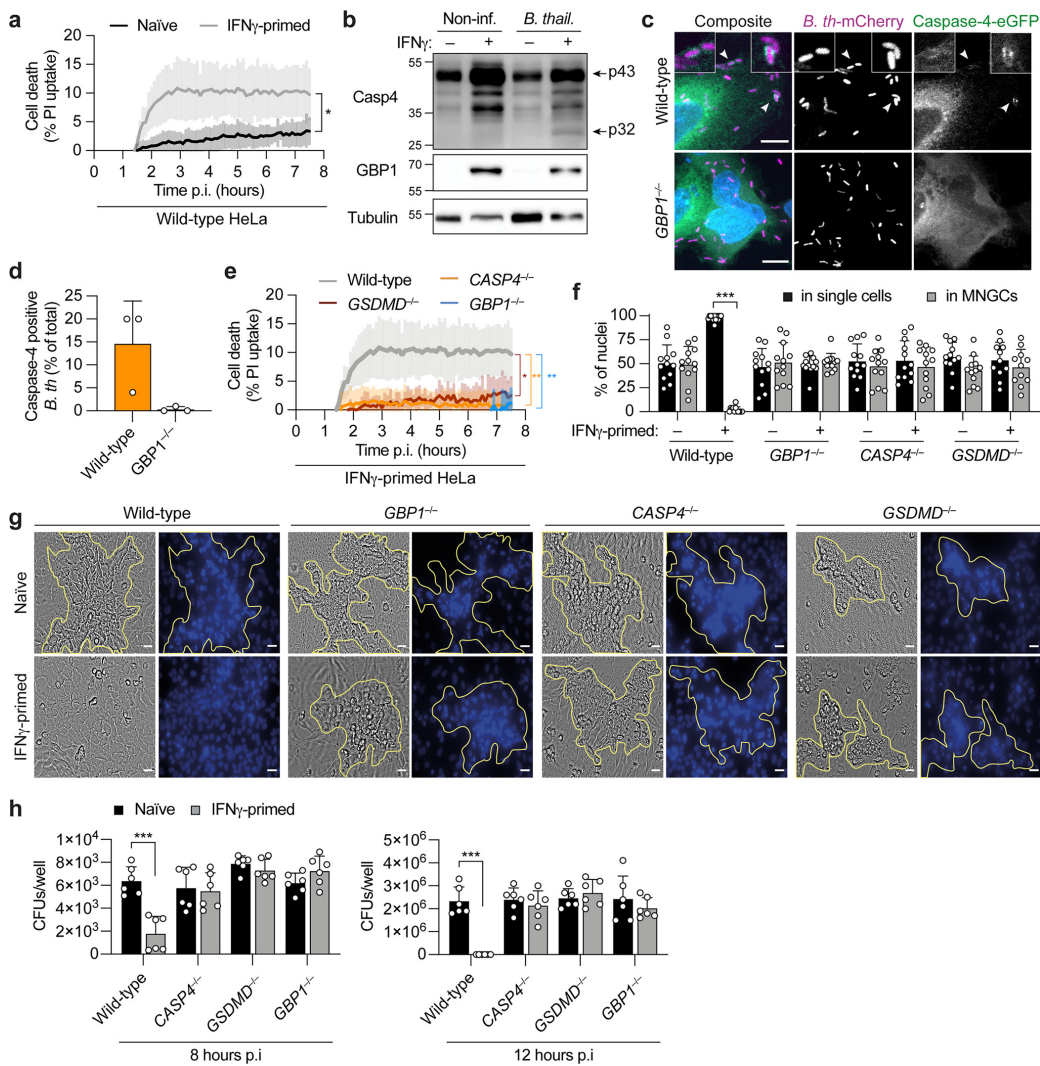


FIG 3 GBP1 promotes caspase-4-dependent pyroptosis and restricts multinucleated giant cell (MNGC) formation and *B. thailandensis* replication. (a) Percentage of PI uptake in naive or IFN- γ -primed HeLa cells infected with *B. thailandensis* (MOI of 200). (b) Immunoblotting for caspase-4 processing, GBP1, and tubulin (loading control) of combined supernatants and cell lysates of naive or IFN- γ -primed HeLa cells 6 h after infection with *B. thailandensis* (MOI of 200). (c) Representative fluorescence confocal microscopy images of IFN- γ -primed wild-type and *GBP1*^{-/-} HeLa cells treated with z-VAD-FMK (carbobenzoxy-valyl-alanyl-aspartyl-[O-methyl]-fluoromethylketone) (10 μ M). Cells expressing caspase-4-eGFP were infected with *B. thailandensis*-mCherry (MOI of 100) for 6 h. DNA was stained by Hoechst stain. Bars, 10 μ m. (d) Percentage of intracellular caspase-4-eGFP-positive *B. thailandensis*-mCherry bacteria in IFN- γ -primed HeLa cells treated with z-VAD-FMK (10 μ M) at 6 h p.i. At least 100 to 200 bacteria per well were counted. (e) Percentage of PI uptake in wild-type, *GBP1*^{-/-}, *CASP4*^{-/-}, and *GSDMD*^{-/-} IFN- γ -primed HeLa cells infected with *B. thailandensis* (MOI of 200). (f) Percentage of nuclei in MNGCs or in single cells, determined by counting the nuclei of naive or IFN- γ -primed wild-type, *GBP1*^{-/-}, *CASP4*^{-/-}, and *GSDMD*^{-/-} HeLa cells 20 h after infection with *B. thailandensis* (MOI of 0.3) in 6 fields of view under each experimental condition. (g) Representative phase-contrast images (magnification, $\times 40$) of naive or IFN- γ -primed wild-type, *GBP1*^{-/-}, *CASP4*^{-/-}, and *GSDMD*^{-/-} HeLa cells 20 h after infection with *B. thailandensis* (MOI of 0.3). The corresponding DNA was stained with Hoechst stain (right), and clustered nuclei, indicating MNGCs, are highlighted by yellow outlines. Bars, 100 μ m. (h) Assessment of bacterial invasion in naive or IFN- γ -primed wild-type, *GBP1*^{-/-}, *CASP4*^{-/-}, and *GSDMD*^{-/-} HeLa cells 8 or 12 h after infection with *B. thailandensis* (MOI of 100). Data are representative of results from at least three independent experiments (c, d, and g) or two independent experiments (b). Graphs show the means \pm SD, and data are pooled from two independent experiments performed in duplicate (f) or triplicate (h) or are representative of results from at least two independent experiments performed in triplicate (a and e). For panels a and e, the area under the curve (AUC) under each experimental condition was calculated, and data were analyzed by a parametric t test (a) or one-way ANOVA (e). *, $P < 0.05$; **, $P < 0.01$; ***, $P < 0.001$ (by 2-way ANOVA [f and h]).

caspace-4-eGFP was found to be recruited to cytosolic *B. thailandensis* in a GBP1-dependent manner (Fig. 3c and d, Fig. S3e, and Movie S4) but not to the same levels as GBP1 targeting (Fig. 2a and b). Furthermore, the recruitment of caspace-4 to bacteria correlated with pyroptosis of the infected cell, as determined by the appearance of the typical pyroptotic morphology (Fig. S2e and f and Movie S4). To test if this cell death was caused by noncanonical inflammasome activation, we used wild-type, *CASP4*^{-/-}, *GSDMD*^{-/-}, and *GBP1*^{-/-} HeLa cells, which have been previously generated and verified (17). We observed that caspace-4, GSDMD, and GBP1 were required for PI influx, indicating that the cell lysis observed upon *B. thailandensis* infection was triggered by noncanonical inflammasome activation (Fig. 3e and Fig. S2g).

Quantification of the multinucleation events confirmed that wild-type naive HeLa and IFN- γ -primed *CASP4*^{-/-}, *GSDMD*^{-/-}, and *GBP1*^{-/-} cells have similar percentages of nuclei associated with MNGCs (Fig. 3f). Furthermore, IFN- γ -primed *CASP4*^{-/-}, *GSDMD*^{-/-}, and *GBP1*^{-/-} HeLa cells infected with *B. thailandensis* formed MNGCs in a similar manner and with comparable size to those observed in wild-type naive cells (Fig. 3f and g and Fig. S3h). Notably, IFN- γ priming restricted intracellular *B. thailandensis* replication in a caspace-4-, GSDMD-, and GBP1-dependent manner at 8 and 12 h p.i. (Fig. 3h), without affecting bacterial entry (Fig. S3i).

Together with the observation that the IFN-dependent expression of GBPs is important for preventing MNGC formation (Fig. 2c and d), these data show that GBP1 induces rapid death of the infected cells by triggering caspace-4-dependent pyroptosis, thus restricting *B. thailandensis*-induced cell-to-cell fusion and bacterial spread and replication.

GBP1 does not impair actin-based motility or promote direct bacteriolysis of cytosolic *B. thailandensis*. After demonstrating that GBP1 triggers noncanonical inflammasome activation upon sensing cytosolic *B. thailandensis* in human epithelial cells, we also tested additional antimicrobial GBP-induced mechanisms that have been proposed previously (16, 33, 39, 41) (Fig. S2a). Cytosolic *Burkholderia* spp. are known to coopt the host actin polymerization machinery in order to spread from cell to cell (7). We first evaluated if IFN- γ priming and GBP1 affect actin tail polymerization on intracellular *B. thailandensis* cells by confocal microscopy. For this, we used *CASP4*-deficient HeLa cells to avoid IFN- γ -induced noncanonical activation and cell death. Surprisingly, we found that IFN- γ priming did not affect actin tail formation on intracellular *B. thailandensis* bacteria (Fig. 4a and Fig. S3a), contrary to the IFN- γ and GBP1-dependent restriction of *Shigella flexneri* actin tail formation (39) (Fig. S3b). To test if GBP1-positive *B. thailandensis* cells were able to form actin tails, we infected naive or IFN- γ -primed *CASP4*^{-/-} HeLa cells expressing iRFP703-GBP1 with *B. thailandensis*-mCherry for 5 h. Confocal microscopy analysis showed that in IFN- γ -primed cells, GBP1-positive bacteria formed actin tails to the same extent as in naive cells (Fig. 4b and c). The same was observed when we performed time-lapse fluorescence microscopy on LifeAct-GFP-expressing *GSDMD*^{-/-} infected HeLa cells; i.e., GBP1 coating of cytosolic *B. thailandensis* did not inhibit comet tail formation and actin-based bacterial motility in both naive and IFN- γ -primed cells (Fig. 4d and e and Movies S5 and S6). This suggests that GBP1, directly or in combination with other GBPs that oligomerize on the surface of cytosolic *B. thailandensis*, cannot impair *B. thailandensis* cell-to-cell spread via actin tails. To confirm this, we used *GBP1*-deficient HeLa cells and found that in infected wild-type cells, *B. thailandensis* formed actin tails to the same extent as in *GBP1*^{-/-} cells, both with and without IFN- γ priming (Fig. 4f). Interestingly, this is in contrast to what is observed in the case of *Shigella flexneri* infection, where GBP1 partially blocks actin tail formation (39) (Fig. S3b).

Furthermore, in naive HeLa cells infected with *B. thailandensis*-mCherry, the rapid oligomerization of GBP1 on the bacterial surface did not prevent bacterial replication in the host cytosol (Fig. 4g and Movie S7), and cell fusion and the formation of MNGCs were still observed (Fig. 4g, DIC [differential interference contrast]). This shows that GBP1 by itself does not appear to display antimicrobial activity when recruited to the bacteria in cells despite the previous observation that *in vitro*, the direct binding of GBP1 alone to bacteria disrupts cell envelope functions (21).

caspace-4-eGFP was found to be recruited to cytosolic *B. thailandensis* in a GBP1-dependent manner (Fig. 3c and d, Fig. S3e, and Movie S4) but not to the same levels as GBP1 targeting (Fig. 2a and b). Furthermore, the recruitment of caspace-4 to bacteria correlated with pyroptosis of the infected cell, as determined by the appearance of the typical pyroptotic morphology (Fig. S2e and f and Movie S4). To test if this cell death was caused by noncanonical inflammasome activation, we used wild-type, *CASP4*^{-/-}, *GSDMD*^{-/-}, and *GBP1*^{-/-} HeLa cells, which have been previously generated and verified (17). We observed that caspace-4, GSDMD, and GBP1 were required for PI influx, indicating that the cell lysis observed upon *B. thailandensis* infection was triggered by noncanonical inflammasome activation (Fig. 3e and Fig. S2g).

Quantification of the multinucleation events confirmed that wild-type naive HeLa and IFN- γ -primed *CASP4*^{-/-}, *GSDMD*^{-/-}, and *GBP1*^{-/-} cells have similar percentages of nuclei associated with MNGCs (Fig. 3f). Furthermore, IFN- γ -primed *CASP4*^{-/-}, *GSDMD*^{-/-}, and *GBP1*^{-/-} HeLa cells infected with *B. thailandensis* formed MNGCs in a similar manner and with comparable size to those observed in wild-type naive cells (Fig. 3f and g and Fig. S3h). Notably, IFN- γ priming restricted intracellular *B. thailandensis* replication in a caspace-4-, GSDMD-, and GBP1-dependent manner at 8 and 12 h p.i. (Fig. 3h), without affecting bacterial entry (Fig. S3i).

Together with the observation that the IFN-dependent expression of GBPs is important for preventing MNGC formation (Fig. 2c and d), these data show that GBP1 induces rapid death of the infected cells by triggering caspace-4-dependent pyroptosis, thus restricting *B. thailandensis*-induced cell-to-cell fusion and bacterial spread and replication.

GBP1 does not impair actin-based motility or promote direct bacteriolysis of cytosolic *B. thailandensis*. After demonstrating that GBP1 triggers noncanonical inflammasome activation upon sensing cytosolic *B. thailandensis* in human epithelial cells, we also tested additional antimicrobial GBP-induced mechanisms that have been proposed previously (16, 33, 39, 41) (Fig. S2a). Cytosolic *Burkholderia* spp. are known to coopt the host actin polymerization machinery in order to spread from cell to cell (7). We first evaluated if IFN- γ priming and GBP1 affect actin tail polymerization on intracellular *B. thailandensis* cells by confocal microscopy. For this, we used *CASP4*-deficient HeLa cells to avoid IFN- γ -induced noncanonical activation and cell death. Surprisingly, we found that IFN- γ priming did not affect actin tail formation on intracellular *B. thailandensis* bacteria (Fig. 4a and Fig. S3a), contrary to the IFN- γ and GBP1-dependent restriction of *Shigella flexneri* actin tail formation (39) (Fig. S3b). To test if GBP1-positive *B. thailandensis* cells were able to form actin tails, we infected naive or IFN- γ -primed *CASP4*^{-/-} HeLa cells expressing iRFP703-GBP1 with *B. thailandensis*-mCherry for 5 h. Confocal microscopy analysis showed that in IFN- γ -primed cells, GBP1-positive bacteria formed actin tails to the same extent as in naive cells (Fig. 4b and c). The same was observed when we performed time-lapse fluorescence microscopy on LifeAct-GFP-expressing *GSDMD*^{-/-} infected HeLa cells; i.e., GBP1 coating of cytosolic *B. thailandensis* did not inhibit comet tail formation and actin-based bacterial motility in both naive and IFN- γ -primed cells (Fig. 4d and e and Movies S5 and S6). This suggests that GBP1, directly or in combination with other GBPs that oligomerize on the surface of cytosolic *B. thailandensis*, cannot impair *B. thailandensis* cell-to-cell spread via actin tails. To confirm this, we used *GBP1*-deficient HeLa cells and found that in infected wild-type cells, *B. thailandensis* formed actin tails to the same extent as in *GBP1*^{-/-} cells, both with and without IFN- γ priming (Fig. 4f). Interestingly, this is in contrast to what is observed in the case of *Shigella flexneri* infection, where GBP1 partially blocks actin tail formation (39) (Fig. S3b).

Furthermore, in naive HeLa cells infected with *B. thailandensis*-mCherry, the rapid oligomerization of GBP1 on the bacterial surface did not prevent bacterial replication in the host cytosol (Fig. 4g and Movie S7), and cell fusion and the formation of MNGCs were still observed (Fig. 4g, DIC [differential interference contrast]). This shows that GBP1 by itself does not appear to display antimicrobial activity when recruited to the bacteria in cells despite the previous observation that *in vitro*, the direct binding of GBP1 alone to bacteria disrupts cell envelope functions (21).

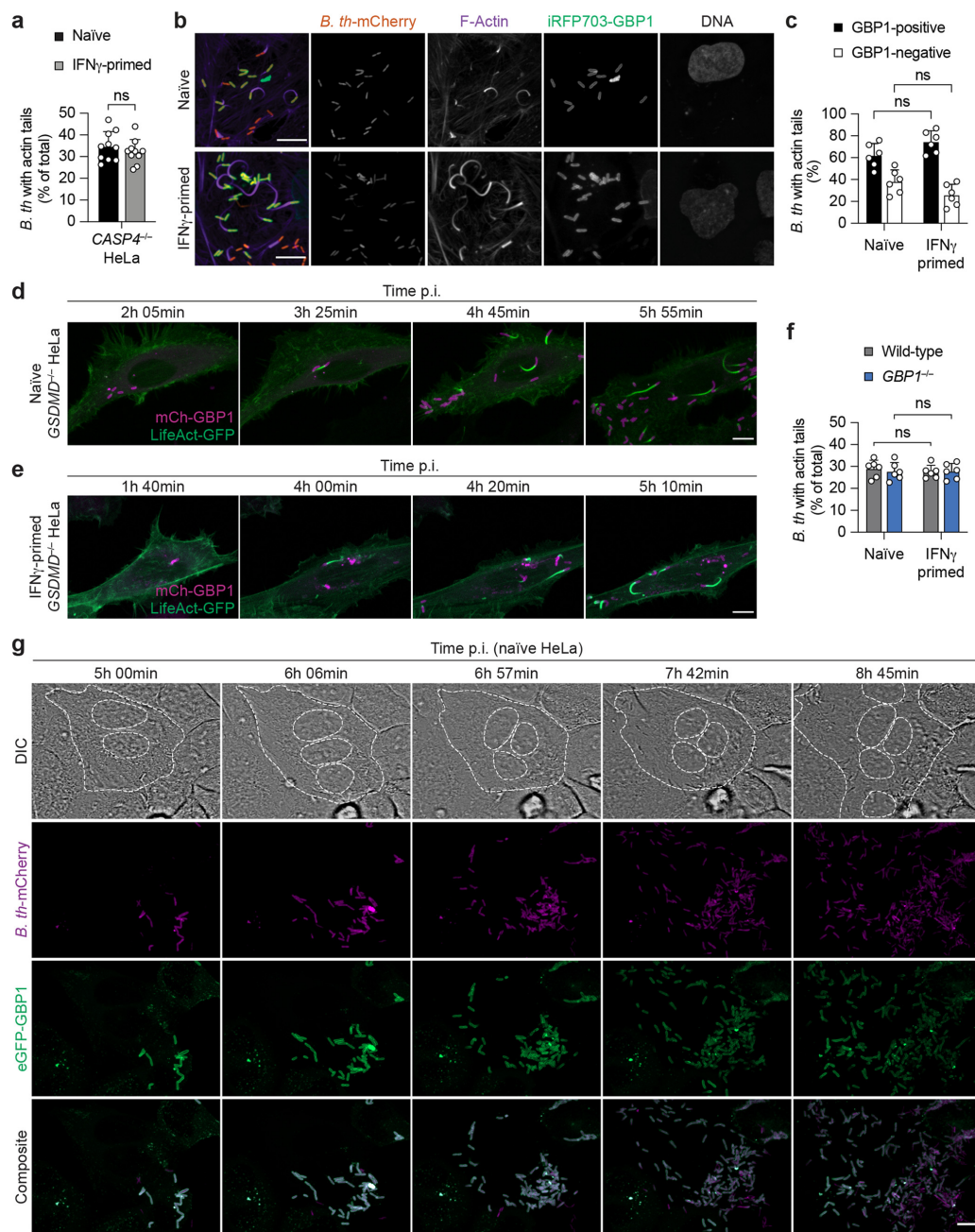


FIG 4 GBP1 does not impair actin-based motility or promote direct bacteriolysis of cytosolic *B. thailandensis*. (a) Percentage of *B. thailandensis* bacteria with actin tails at 5 h p.i. in naïve and IFN- γ -primed CASP4 $^{-/-}$ HeLa cells (MOI of 30). At least 100 to 200 bacteria per coverslip were counted. (b) (Continued on next page)

Taken together, we conclude that GBP1-dependent restriction of MNGC formation in HeLa cells is not due to bacteriolysis or impaired bacterial actin-based motility within the host cytosol.

Interferon has a protective role against *B. thailandensis* infection in human bronchial epithelial cells, keratinocytes, and primary macrophages. Since bacteria of the *Burkholderia* genus employ different routes of infection (subcutaneous infection, inhalation, ingestion of contaminated particles, and aerosol) (1), we tested if IFN- γ priming restricts MNGC formation in human cell lines that are physiologically more relevant for *Burkholderia*-induced melioidosis, such as HBEC3-KT cells (human bronchial epithelial cells), HaCaT cells (human keratinocytes), and human primary monocyte-derived macrophages (hMDMs). Similar to HeLa cells (Fig. 1a and b), naive HBEC3-KT and HaCaT cells formed MNGCs after *B. thailandensis* infection, which was almost completely blocked upon IFN- γ priming (Fig. 5a and b and Fig. S3c). IFN- γ priming did not reduce bacterial uptake in these cells (Fig. S3d and e). We next determined whether the IFN- γ -dependent restriction of giant cell formation was promoted by noncanonical inflammasome activation, as shown for HeLa cells (Fig. 3e). In accordance with what we observed in HeLa cells, small interfering RNA (siRNA)-mediated knockdown of *CASP4*, *GSDMD*, or *GBP1* in HBEC3-KT and HaCaT cells abrogated the IFN- γ -mediated restriction of MNGC formation (Fig. 5c and Fig. S3f and g).

Burkholderia can invade both phagocytic and nonphagocytic cells. Among phagocytic cells, mainly macrophages and neutrophils take part in the immune response against this pathogen. Briefly, in a murine model of infection, *Burkholderia* is initially detected by macrophages through the Naip/Nlrc4 inflammasome (32), and the consequent IL-18 release triggers the production of IFN- γ whereby in neutrophils and macrophages, caspase-11 is upregulated (32). The subsequent noncanonical inflammasome activation in both cell types represents the critical step at which the *B. thailandensis* intracellular niche is removed. Therefore, we evaluated the role of IFN- γ priming in hMDMs during *B. thailandensis* infection. Interestingly, while unprimed murine BMDMs form MNGCs upon *B. thailandensis* infection (33), we did not detect the formation of MNGCs in either naive or IFN- γ -primed hMDMs (Fig. S3h). Instead, we observed robust induction of host cell death under both conditions, although the percentage of cell death, assessed by PI influx, was significantly higher in IFN- γ -primed hMDMs than in naive hMDMs (Fig. 5d and e). These results implied that analogously to IFN- γ -primed HeLa cells, the induction of cell lysis prevents MNGC formation in hMDMs. This cell death can be driven by IFN-independent (most likely via the NLR4-caspase-1 axis) or IFN-dependent mechanisms, yet IFN signaling promotes a faster and more efficient way to activate GSDMD-induced pyroptosis and clear the bacteria. The latter most likely depends on the GBP-induced activation of the noncanonical inflammasome, as GBP1 expression in hMDMs was observed only after IFN- γ priming, whereas caspase-4 was constitutively expressed (Fig. S3i). NLRP3 can be activated downstream of caspase-4-induced GSDMD activation and cell death, further amplifying pyroptotic cell death via ASC (apoptosis-associated speck-like protein containing a CARD) speck formation and caspase-1 (Fig. S3j). To corroborate the role of *B. thailandensis*-induced noncanonical inflammasome activation in hMDMs, we treated naive or IFN- γ -primed cells with

FIG 4 Legend (Continued)

Representative fluorescence confocal microscopy images of naive and IFN- γ -primed *CASP4*^{-/-} HeLa cells expressing iRFP703-GBP1 and infected with *B. thailandensis*-mCherry (MOI of 30) for 5 h. DNA was stained by Hoechst stain, and F-actin was labeled with CellMask green actin tracking stain. Bars, 10 μ m. (c) Percentage of *B. thailandensis* bacteria with actin tails that are GBP1 positive or negative in naive and IFN- γ -primed *CASP4*^{-/-} HeLa cells expressing iRFP703-GBP1. Cells were infected with *B. thailandensis*-mCherry for 5 h (MOI of 30) and fixed, and F-actin was labeled with CellMask green actin tracking stain. Between 100 and 300 bacteria were counted per coverslip. (d and e) Time-lapse fluorescence confocal microscopy images of naive (d) and IFN- γ -primed (e) *GSDMD*^{-/-} HeLa cells expressing N-terminally mCherry-tagged GBP1 and LifeAct-eGFP infected with *B. thailandensis* (MOI of 50). Images were acquired every 5 min. Bars, 10 μ m. (f) Percentage of *B. thailandensis* bacteria with actin tails in naive and IFN- γ -primed wild-type and *GBP1*^{-/-} HeLa cells. Cells were treated with z-VAD-FMK (10 μ M) and infected for 5 h at an MOI of 30. Between 100 and 300 bacteria were counted per coverslip. (g) Time-lapse fluorescence confocal microscopy of naive HeLa cells expressing N-terminally eGFP-tagged GBP1 and infected with *B. thailandensis*-mCherry (MOI of 50). MNGCs are indicated by dashed white lines. DIC, differential interference contrast. Images were acquired every 3 min. Bars, 10 μ m. Data are representative of results from at least three independent experiments (b, d, e, and g). Graphs show the means \pm SD, and data are pooled from three (c and f) or five (a) independent experiments performed in duplicate. ns, not significant (by a parametric *t* test).

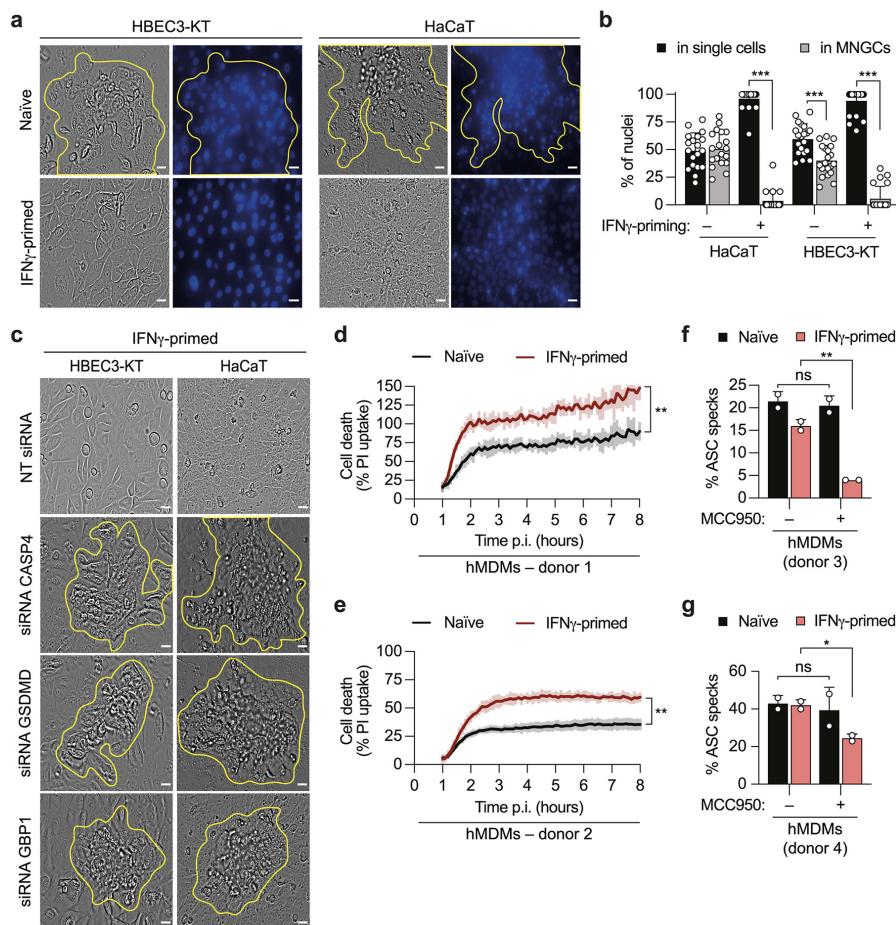


FIG 5 Interferon has a protective role against *B. thailandensis* infection in human bronchial epithelial cells, keratinocytes, and primary macrophages. (a and c) Representative phase-contrast images (magnification, $\times 40$) of naive or IFN- γ -primed HBEC3-KT and HaCaT cells 20 h after infection with *B. thailandensis* (MOI of 100). In panel c, cells were pretreated with nontargeting (NT) siRNA or siRNA targeting CASP4, GSDMD, and GBP1, 24 h prior to infection. The corresponding DNA was stained with Hoechst stain, and multinucleated giant cells (MNGCs) are indicated by yellow outlines. Bars, 100 μm . (b) Percentage of nuclei in MNGCs or in single cells determined by counting the nuclei of naive or IFN- γ -primed HBEC3-KT and HaCaT cells 20 h after infection with *B. thailandensis* (MOI of 100) in 6 fields of view under each experimental condition. (d and e) Percentage of PI uptake in naive or IFN- γ -primed hMDMs infected with *B. thailandensis* (MOI of 30) for 5 h in the presence or absence of the inhibitor MCC950. Data are representative of results from at least three independent experiments (a and c). Graphs show the means \pm SD, and data are pooled from two independent experiments performed in triplicate (b) or are representative of results from two independent experiments performed in duplicate (f and g) or triplicate (d and e). The area under the curve (AUC) under each experimental condition was calculated (d and e), and data were analyzed by a parametric *t* test. *, $P < 0.05$; **, $P < 0.01$; ***, $P < 0.001$; ns, not significant (by a parametric *t* test [f and g]).

MCC950, a known selective NLRP3 inhibitor (42, 43) (Fig. S3I), and quantified the percentage of ASC specks by fluorescence microscopy. Inhibition of NLRP3 activation reduced ASC speck formation only in IFN- γ -primed and not in unprimed hMDMs (Fig. 5f and g), indicating that the noncanonical inflammasome is activated only in IFN- γ -primed hMDMs and that unprimed cells induce inflammasome activation by canonical inflammasomes. We also hypothesize that MNGCs were not observed in hMDMs

because pyroptotic cell death occurred too quickly in response to *B. thailandensis* infection, even in naive cells. In conclusion, we demonstrate that the IFN- γ -dependent signaling axis described for HeLa cells upon *Burkholderia* infection is also found in other human epithelial cells as well as in human primary macrophages.

DISCUSSION

This study provides the first evidence that in human epithelial cells, GBP-dependent noncanonical inflammasome activation prevents *B. thailandensis*-induced MNGC formation in the early stages of infection. Our results suggest that GBP1 impairs *B. thailandensis* cell-to-cell spread by triggering caspase-4-dependent pyroptosis of infected cells.

Previous work in mouse models of infection reported that both the Naip/NLRC4 inflammasome and the caspase-11 noncanonical inflammasome participate in the immune response against *Burkholderia* (29, 32, 35). Interestingly, these reports showed that both inflammasomes are connected given that caspase-1 activation in macrophages mediates IL-18 release to drive IFN- γ -dependent caspase-11 activation in epithelial cells. In agreement with this, we show that in human epithelial cells, IFNs and caspase-4-dependent pyroptosis provide protection against *Burkholderia* infection, whereas pyroptosis in primary hMDMs is driven by IFN-dependent and -independent mechanisms. The latter observation correlates with data in murine BMDMs that suggest that both the canonical and noncanonical pathways can be activated upon *Burkholderia* infection (29–31). The importance of noncanonical inflammasome activation in response to *Burkholderia* is particularly evident in HeLa cells, which lack canonical inflammasome pathways, but even human bronchial epithelial cells and keratinocytes mainly activate the noncanonical inflammasome in response to *Burkholderia*, suggesting that also in the human system, canonical inflammasome activation is restricted to professional immune cells.

Our work provides further support for the notion that human GBP1 acts as a cytosolic pattern recognition receptor that binds LPS in order to activate caspase-4 and restrict bacterial replication (17–21). Since GBP1 recruitment alone was not sufficient to restrict *Burkholderia* replication, we propose that GBP1-dependent caspase-4 activation is linked to its ability to recruit GBP2-4 to bacteria, which might amplify its effects. Whether the GBP1-4 coat exerts a strong LPS surfactant effect in cells to disrupt bacterial membranes or whether the coat directly interacts with and activates caspase-4 will need to be addressed by additional studies. It is also conceivable that GSDMD pores amplify noncanonical inflammasome activation by disrupting bacterial envelopes, as a previous study showed that recombinant GSDMD reduces bacterial viability *in vitro* upon caspase-1 processing and that bacteria were more susceptible to microbicidal effectors when harvested from mouse wild-type macrophages rather than *Gsdmd*^{-/-} macrophages, which suggests that GSDMD can directly kill bacteria (44).

Disruption of the bacterial membrane was proposed to be the main mechanism by which mouse GBPs promote inflammasome activation, as GBPs were found to induce bacteriolysis by recruiting Irgb10 (27), a member of the IRG family of GTPases that are found in mouse but not human cells. However, a more recent study by the same authors suggested that during *B. thailandensis* infection, mouse GBPs do not lyse bacteria or activate the inflammasome but rather restrict *B. thailandensis* infection by inhibiting bacterial actin-based motility (33). Specifically, the higher number of multinucleation events observed in *Gbp2*^{-/-}, *Gbp5*^{-/-}, and *Gbp*^{Chr3} knockout (*Gbp*^{Chr3}-KO) BMDMs than in wild-type macrophages has been associated with the ability of GBPs to inhibit the host Arp2/3-dependent actin polymerization machinery and, consequently, *Burkholderia* actin tail formation (33). A similar mechanism has been reported in human cell lines infected with *Shigella flexneri*, in which the hierarchical targeting of GBPs on the bacteria, reliant on GBP1, impairs *Shigella* actin-based motility, delaying its spread (16, 39, 41). Parting ways with the literature, we did not observe any impairment in the polymerization of the *Burkholderia* actin tails upon GBP targeting in human cells, confirming that the main function of GBPs in response to *B. thailandensis* infection is to

serve as a signaling platform for caspase-4 recruitment and activation. Furthermore, *GBP1*-deficient cells show a level of MNGC formation similar to those of *CASP4*- and *GSDMD*-deficient cells, arguing that in human cells, GBPs restrict replication via pyroptosis induction and not by additional inflammasome-independent mechanisms. It is possible that this discrepancy results from species-dependent differences since additional IFN-induced factors that are not expressed in human epithelial cells might account for the restriction of *Burkholderia* actin dynamics.

In summary, our study is the first to report that interferon restricts the multinucleation events induced by *B. thailandensis* through the pyroptosis of infected cells. It is important to keep in mind, though, that *B. thailandensis* is less pathogenic than other species of the *B. pseudomallei* complex that cause severe disease in humans (1–4). Therefore, further studies are needed to understand whether interferon improves the clearance of *Burkholderia* species that are most adapted to infect humans or whether more-pathogenic species have found ways of escaping GBP/inflammasome-mediated immune surveillance.

MATERIALS AND METHODS

Bacterial and mammalian cell culture. All bacteria were grown at 37°C in an orbital shaker. *B. thailandensis* strain E264 and its isogenic strain expressing mCherry2 were kindly provided by Marek Basler (Biozentrum, Basel, Switzerland) and were grown in lysogeny broth (LB) medium supplemented with 5 g/liter NaCl. *Shigella flexneri* M90T expressing the adhesin Afal was provided by Jost Enninga (Institut Pasteur, Paris, France) and was grown in tryptic soy broth (TSB) supplemented with ampicillin (50 µg/ml). Wild-type HeLa (ATCC CCL-2) and CRISPR-Cas9 knockout HeLa cell lines, generated as previously described (17), were cultured in Dulbecco's modified Eagle's medium (DMEM; Gibco) supplemented with 10% fetal calf serum (FCS; BioConcept). HaCaT cells, obtained from CLS (Cell Lines Service) GmbH, were grown in RPMI 1640 (Gibco) supplemented with 10% FCS. HBEC3-KT cells (ATCC) were grown in bronchial/tracheal epithelial cell growth medium (Cell Applications, Inc.). Human primary monocyte-derived macrophages (hMDMs) were purified from buffy coats obtained from the Swiss Red Cross and cultured as described previously (45). Cells were grown at 37°C with 5% CO₂.

Infection assays. When indicated, cells were primed for 16 h with human IFN-γ (Peprotech) at a concentration of 10 ng/ml for HeLa cells and hMDMs or 2.5 ng/ml for HBEC3-KT and HaCaT cells. *B. thailandensis* cultures grown overnight were adjusted to an optical density at 600 nm (OD₆₀₀) of 1, subcultured 1:20, and grown until mid-exponential phase (OD₆₀₀ = 0.4 to 0.6). *S. flexneri* cultures grown overnight were subcultured 1/100 and grown until mid-exponential phase (OD₆₀₀ = 0.4 to 0.6). Before infection, bacteria were collected by centrifugation, washed, and resuspended in Opti-MEM (Gibco). Bacteria were added to confluent cells in 96-well plates (HeLa, 5 × 10⁴ cells/well; HBEC3-KT, 2.5 × 10⁴ cells/well; HaCaT, 1 × 10⁵ cells/well; hMDMs, 8 × 10⁴ cells/well) at different multiplicities of infection (MOIs), as described in the figure legends. For *B. thailandensis* infections, plates were then centrifuged at 300 × g for 5 min at 37°C and incubated for 1 h at 37°C. For *S. flexneri* infections, plates were just incubated at 37°C for 30 min. Noninternalized bacteria were then removed by washing cells three times with prewarmed medium, and cells were incubated with Opti-MEM containing 250 µg/ml kanamycin, in the case of *B. thailandensis* infections, or 100 µg/ml gentamicin, in the case of *S. flexneri* infections, in order to kill extracellular bacteria. At the desired time points postinfection (p.i.), cells were either processed for CFU analysis (CFU), multinucleated giant cell (MNGC) quantification, propidium iodide (PI) uptake, or Western blot analysis or fixed for immunofluorescence assays. To determine CFU, infected cells were gently washed with phosphate-buffered saline (PBS) and lysed with water containing 0.2% Triton X-100 at the indicated time points. Bacteria were then serially diluted and plated onto LB agar.

MNGC quantification assay. Starting at 20 h p.i., HeLa, HBEC3-KT, and HaCaT cells were stained with Hoechst stain (1:1,000) and examined by fluorescence microscopy. The extent of multinucleation was measured by counting nuclei in 6 fields of view under each experimental condition using Fiji software.

Plasmids. Plasmids expressing N-terminally fluorescently tagged GBPs were generated by inserting the GBP coding sequences at the XhoI/HindIII sites of pEGFP-C1 (Clontech) (17). Doxycycline-inducible eGFP and doxycycline-inducible mCherry plasmids were generated by amplifying eGFP and mCherry generated as described above by PCR and inserting the coding sequences at the BamHI site of the pLVX-Puro vector (Clontech). Plasmids expressing LifeAct-eGFP were generated by amplifying eGFP from pLJM1-eGFP (Addgene) and inserting the sequence into the NheI and BstBI cloning sites of a LifeAct-iRFP670 (Addgene) plasmid. All cloning was performed using In-Fusion cloning technology (Clontech), and plasmids were verified by sequencing. When required, HeLa cells were transfected with expression plasmids as previously described (17).

Lentiviral particle production and HeLa cell transduction. Lentiviral particles were produced by transfecting HEK293T cells. Cells seeded into a 6-well plate at a density of 1 × 10⁶ cells/well 24 h prior to transfection were transfected with expression plasmids (pLVX-GFP and pLVX-mCherry), packaging plasmid psPax2 (1.9 mg), and envelope plasmid pVSV-G (0.2 mg) using jetPRIME (Polyplus), according to the manufacturer's instructions. After a 24-h incubation, HEK293T medium containing lentiviral particles was transferred to HeLa cells seeded at a density of 0.8 × 10⁶ cells/well in a 6-well plate. HeLa cells were centrifuged at 2,900 rpm for 90 min and incubated for 48 h (medium was changed after incubation

overnight). Puromycin (5.0 $\mu\text{g}/\text{ml}$; InvivoGen) was added to the medium for 6 to 8 days in order to positively select transduced cells.

Microscopy, time-lapse imaging, and image analysis. Fluorescence and phase-contrast images of nonfixed samples were obtained using a Leica DFC3000G instrument (40 \times objective) for MNGC quantification. For fluorescence microscopy of fixed samples, infected HeLa cells and hMDMs were washed twice with PBS and fixed for 20 to 30 min with 4% paraformaldehyde (Electron Microscopy Sciences). Cells were washed four times with PBS and incubated with Hoechst stain (1:1,000) and, when indicated, with CellMask green actin tracking stain (catalog number A57243; Thermo Fisher Scientific) to label F-actin. For ASC speck formation assays, hMDMs were permeabilized with 0.05% saponin and blocked with 1% bovine serum albumin (BSA). Coverslips were then incubated with anti-ASC antibody (catalog number sc-22514-R; Santa Cruz Biotechnology) (1:1,000), washed four times with PBS, and incubated with Hoechst stain (1:1,000). Samples were then analyzed by confocal microscopy by imaging with a Zeiss LSM800 confocal laser scanning microscope using a 63 \times /1.4-numerical-aperture (NA) oil objective by acquiring Z-stacks with a 300-nm step size. For live imaging, HeLa cells plated onto 8-well μ -slides (ibidi) at a density of 1×10^5 cells/well were infected as described above. Extracellular *B. thailandensis* bacteria were removed by washing with warm Opti-MEM, and time-lapse microscopy of living cells was performed in Opti-MEM supplemented with kanamycin (250 $\mu\text{g}/\text{ml}$) at 37°C using a motorized xyz stage with autofocus. Samples were imaged with a Zeiss LSM800 confocal laser scanning microscope using a 63 \times /1.4-NA oil objective by acquiring Z-stacks with a 600-nm step size. Data were further analyzed and processed using Fiji software, and all fluorescence-derived images shown correspond to maximum three-dimensional (3D) projections.

siRNA-mediated knockdown. HaCaT (5×10^4 cells/well) and HBE3-KT (2.5×10^4 cells/well) cells were seeded into a 96-well plate and transfected with 25 nM or 30 nM Stealth RNAi siRNAs (Thermo Fisher Scientific) using Lipofectamine RNAiMax (Thermo Fisher Scientific). By 7 to 8 h posttransfection, cells were primed with human IFN- γ for 16 h and then infected as described above. Phase-contrast images of siRNA knockdown cells were acquired at 20 to 24 h p.i. to assess MNGC formation. The siRNA-mediated knockdown effectiveness was tested by Western blot analysis. The siRNAs used are as follows: the siRNA negative control, indicated as nontargeting (NT) siRNA (catalog number 12935300; Thermo Fisher Scientific); siRNA targeting CASP4 (siCASP4) (catalog number HSS141457; Thermo Fisher Scientific); siGSDMD (catalog number HSS149278; Thermo Fisher Scientific); and siGBP1 (catalog number HSS104021; Thermo Fisher Scientific).

PI uptake and Western blot analysis. Cell permeabilization was quantified by measuring PI uptake. PI (Thermo Fisher Scientific) was added to the medium at 12.5 $\mu\text{g}/\text{ml}$, and fluorescence was measured over time using a Cytation5 plate reader (BioTek). To account for spontaneous cell permeabilization, PI uptake was normalized to 100% lysis and the uninfected control. Western blot analysis was performed by lysing cells in 1 \times sample buffer (Thermo Fisher Scientific) with the addition of 66 mM Tris-Cl (pH 7.4), 2% SDS, and 10 mM dithiothreitol (DTT). In assays where we checked caspase-4 processing by Western blotting, cell lysates were combined with precipitated supernatants. Samples were boiled for 5 min at 95°C, and proteins were separated using 12% SDS-PAGE. Proteins were then transferred onto 0.2- μm polyvinylidene difluoride (PVDF) membranes using the Trans-Blot Turbo system (Bio-Rad). Membranes were blocked in a solution of Tris-buffered saline-Tween (TBS-T) with 5% milk and incubated with primary antibody, followed by incubation with horseradish peroxidase (HRP)-coupled secondary antibodies. Western blot membranes were analyzed by Fusion Solo S (Vilber) using the Pierce ECL Western blotting substrate (Thermo Fisher Scientific) or the Pierce ECL Plus Western blotting substrate (Thermo Fisher Scientific). The antibodies employed are as follows: mouse anti-caspase-4 clone 4B9 (catalog number ADI-AAM-114-E; Enzo Life Science) (1:750), rabbit anti-GSDMD (catalog number ab210070; Abcam) (1:1,000), rabbit anti-GSDMD (catalog number CSB-PA009956GA01HU; Cusabio) (1:1,000), rabbit anti-GBP1 (catalog number ab131255; Abcam) (1:1,000), mouse anti-alpha-tubulin-HRP conjugate (catalog number ab40742; Abcam) (1:1,000), goat anti-rabbit IgG-HRP (catalog number 4030-05; Southern Biotech) (1:5,000), and goat anti-mouse IgG-HRP (catalog number 1034-05; Southern Biotech) (1:5,000).

Data analysis. Data analysis was performed using Gen5, GraphPad Prism v9, Microsoft Excel, and Fiji software. Statistical significance is indicated as *, **, or *** for a *P* value of <0.05, <0.01, or <0.001, respectively.

SUPPLEMENTAL MATERIAL

Supplemental material is available online only.

FIG S1, TIF file, 1.7 MB.

FIG S2, TIF file, 1.4 MB.

FIG S3, TIF file, 0.9 MB.

MOVIE S1, AVI file, 9.6 MB.

MOVIE S2, AVI file, 12.1 MB.

MOVIE S3, AVI file, 1.9 MB.

MOVIE S4, AVI file, 8.6 MB.

MOVIE S5, AVI file, 2.8 MB.

MOVIE S6, AVI file, 3 MB.

MOVIE S7, AVI file, 11.3 MB.

ACKNOWLEDGMENTS

We thank Marek Basler (Biozentrum, Basel, Switzerland) and Miro Plum (Biozentrum, Basel, Switzerland) for providing essential reagents and expert advice and Jost Enninga (Institut Pasteur, Paris, France) for bacterial strains. We thank Vanessa Mack and the cellular imaging facility of the UNIL for technical and experimental support.

This work was supported by a Swiss National Science Foundation grant (310030_192523) to P.B.

M.D., J.C.S., and P.B. designed the experiments and analyzed data, conceptualized and supervised the study, and wrote the manuscript, which all authors reviewed before submission. M.D., S.R., and J.C.S. performed the experiments. K.S. contributed expression vectors.

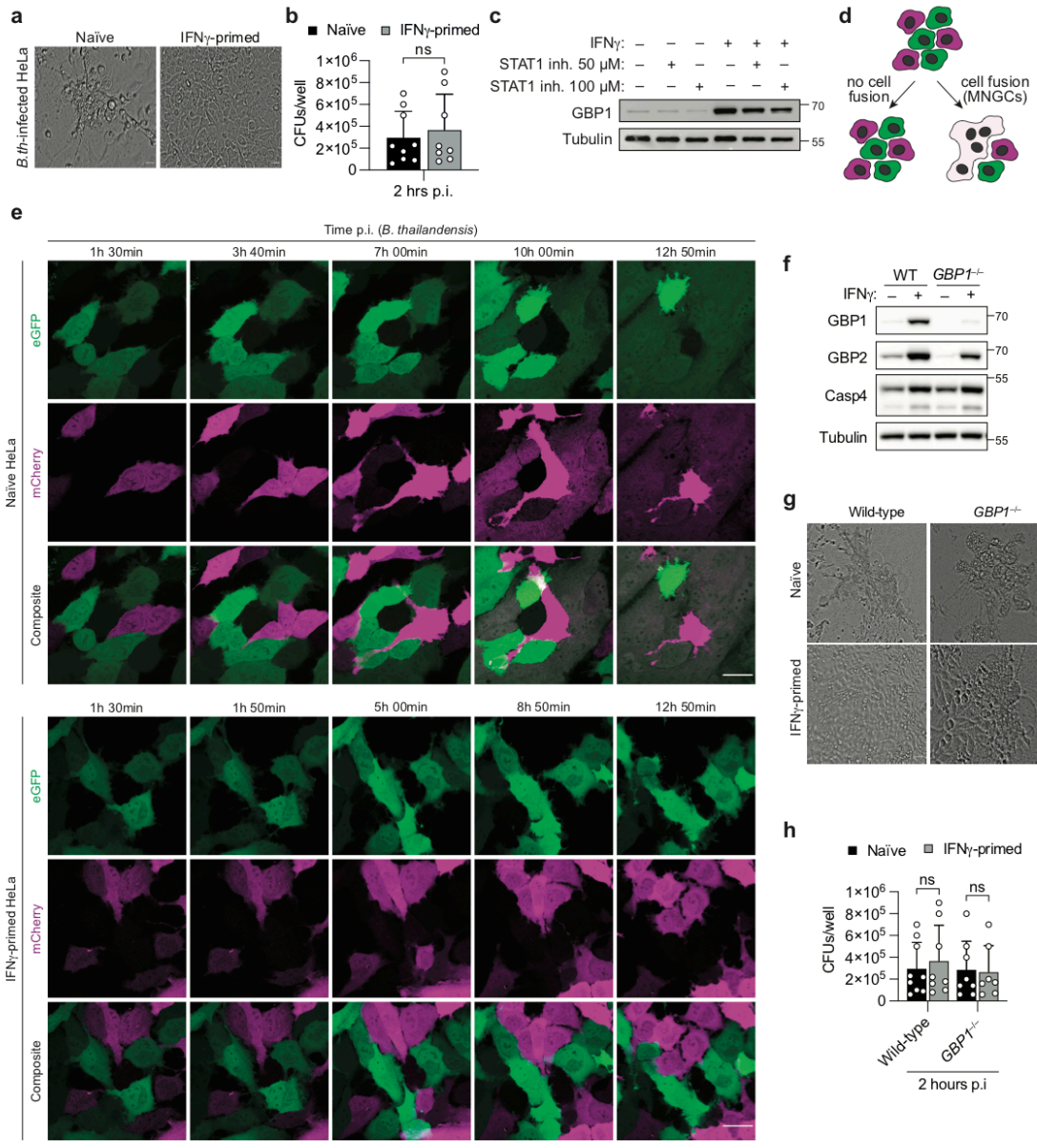
We declare that we have no competing interests.

REFERENCES

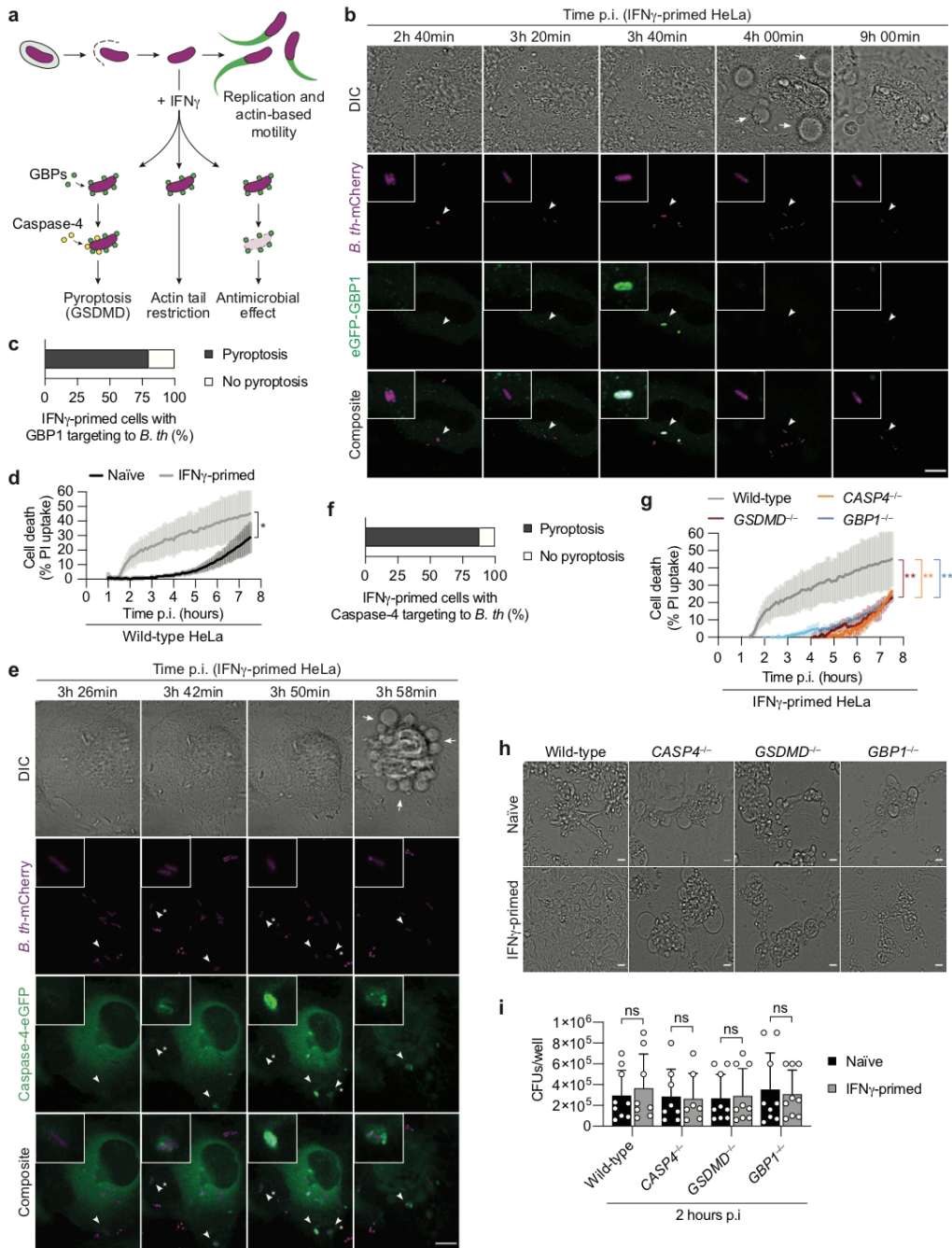
- Wiersinga WJ, van der Poll T, White NJ, Day NP, Peacock SJ. 2006. Melioidosis: insights into the pathogenicity of *Burkholderia pseudomallei*. *Nat Rev Microbiol* 4:272–282. <https://doi.org/10.1038/nrmicro1385>.
- Wiersinga WJ, Virk HS, Torres AG, Currie BJ, Peacock SJ, Dance DAB, Limmathurotsakul D. 2018. Melioidosis. *Nat Rev Dis Primers* 4:17107. <https://doi.org/10.1038/nrdp.2017.107>.
- Galyov EE, Brett PJ, Deshazer D. 2010. Molecular insights into *Burkholderia pseudomallei* and *Burkholderia mallei* pathogenesis. *Annu Rev Microbiol* 64:495–517. <https://doi.org/10.1146/annurev.micro.112408.134030>.
- Cheng AC, Currie BJ. 2005. Melioidosis: epidemiology, pathophysiology, and management. *Clin Microbiol Rev* 18:383–416. <https://doi.org/10.1128/CMR.18.2.383-416.2005>.
- Stevens MP, Wood MW, Taylor LA, Monaghan P, Hawes P, Jones PW, Wallis TS, Galyov EE. 2002. An Inv/Mxi-Spa-like type III protein secretion system in *Burkholderia pseudomallei* modulates intracellular behaviour of the pathogen. *Mol Microbiol* 46:649–659. <https://doi.org/10.1046/j.1365-2958.2002.03190.x>.
- French CT, Toesca IJ, Wu T-H, Teslaa T, Beaty SM, Wong W, Liu M, Schröder I, Chiou P-Y, Teitell MA, Miller JF. 2011. Dissection of the *Burkholderia* intracellular life cycle using a photothermal nanoblade. *Proc Natl Acad Sci U S A* 108:12095–12100. <https://doi.org/10.1073/pnas.1107183108>.
- Benanti EL, Nguyen CM, Welch MD. 2015. Virulent *Burkholderia* species mimic host actin polymerases to drive actin-based motility. *Cell* 161:348–360. <https://doi.org/10.1016/j.cell.2015.02.044>.
- Wong KT, Puthucherry SD, Vadivelu J. 1995. The histopathology of human melioidosis. *Histopathology* 26:51–55. <https://doi.org/10.1111/j.1365-2559.1995.tb00620.x>.
- Toesca IJ, French CT, Miller JF. 2014. The type VI secretion system spike protein VgrG5 mediates membrane fusion during intercellular spread by *pseudomallei* group *Burkholderia* species. *Infect Immun* 82:1436–1444. <https://doi.org/10.1128/IAI.01367-13>.
- Lennings J, West TE, Schwarz S. 2018. The *Burkholderia* type VI secretion system 5: composition, regulation and role in virulence. *Front Microbiol* 9:3339. <https://doi.org/10.3389/fmicb.2018.03339>.
- Meunier E, Broz P. 2016. Interferon-inducible GTPases in cell autonomous and innate immunity. *Cell Microbiol* 18:168–180. <https://doi.org/10.1111/cmi.12546>.
- Santos JC, Broz P. 2018. Sensing of invading pathogens by GBPs: at the crossroads between cell-autonomous and innate immunity. *J Leukoc Biol* 104:729–735. <https://doi.org/10.1002/JLB.4MR0118-038R>.
- MacMicking JD. 2012. Interferon-inducible effector mechanisms in cell-autonomous immunity. *Nat Rev Immunol* 12:367–382. <https://doi.org/10.1038/nri3210>.
- Tretina K, Park E-S, Maminska A, MacMicking JD. 2019. Interferon-induced guanylate-binding proteins: guardians of host defense in health and disease. *J Exp Med* 216:482–500. <https://doi.org/10.1084/jem.20182031>.
- Kutsch M, Coers J. 12 December 2020. Human guanylate binding proteins: nanomachines orchestrating host defense. *FEBS J* <https://doi.org/10.1111/febs.15662>.
- Piro AS, Hernandez D, Luoma S, Feeley EM, Finethy R, Yirga A, Frickel EM, Lesser CF, Coers J. 2017. Detection of cytosolic *Shigella flexneri* via a C-terminal triple-arginine motif of GBP1 inhibits actin-based motility. *mbio* 8:e01979-17. <https://doi.org/10.1128/mbio.01979-17>.
- Santos JC, Boucher D, Schneider LK, Demarco B, Dilucca M, Shkarina K, Heilig R, Chen KW, Lim RYH, Broz P. 2020. Human GBP1 binds LPS to initiate assembly of a caspase-4 activating platform on cytosolic bacteria. *Nat Commun* 11:3276. <https://doi.org/10.1038/s41467-020-16889-z>.
- Wandel MP, Kim B-H, Park E-S, Boyle KB, Nayak K, Lagrange B, Herod A, Henry T, Zilbauer M, Rohde J, MacMicking JD, Randow F. 2020. Guanylate-binding proteins convert cytosolic bacteria into caspase-4 signaling platforms. *Nat Immunol* 21:880–891. <https://doi.org/10.1038/s41590-020-0697-2>.
- Fisch D, Bando H, Clough B, Hornung V, Yamamoto M, Shenoy AR, Frickel E-M. 2019. Human GBP 1 is a microbe-specific gatekeeper of macrophage apoptosis and pyroptosis. *EMBO J* 38:e100926. <https://doi.org/10.15252/embj.2018100926>.
- Fisch D, Clough B, Domart M-C, Encheva V, Bando H, Snijders AP, Collinson LM, Yamamoto M, Shenoy AR, Frickel E-M. 2020. Human GBP1 differentially targets *Salmonella* and *Toxoplasma* to license recognition of microbial ligands and caspase-mediated death. *Cell Rep* 32:108008. <https://doi.org/10.1016/j.celrep.2020.108008>.
- Kutsch M, Sistemich L, Lesser CF, Goldberg MB, Herrmann C, Coers J. 2020. Direct binding of polymeric GBP1 to LPS disrupts bacterial cell envelope functions. *EMBO J* 39:e104926. <https://doi.org/10.15252/embj.2020104926>.
- Kayagaki N, Stowe IB, Lee BL, O'Rourke K, Anderson K, Warming S, Cuellar T, Haley B, Roose-Girma M, Phung QT, Liu PS, Lill JR, Li H, Wu J, Kummerfeld S, Zhang J, Lee WP, Snipas SJ, Salvesen GS, Morris LX, Fitzgerald L, Zhang Y, Bertram EM, Goodnow CC, Dixit VM. 2015. Caspase-11 cleaves gasdermin D for non-canonical inflammasome signalling. *Nature* 526:666–671. <https://doi.org/10.1038/nature15541>.
- Shi J, Zhao Y, Wang Y, Gao W, Ding J, Li P, Hu L, Shao F. 2014. Inflammatory caspases are innate immune receptors for intracellular LPS. *Nature* 514:187–192. <https://doi.org/10.1038/nature13683>.
- Bekpen C, Hunn JP, Rohde C, Parvanova I, Guethlein L, Dunn DM, Glowalla E, Leptin M, Howard JC. 2005. The interferon-inducible p47 (IRG) GTPases in vertebrates: loss of the cell autonomous resistance mechanism in the human lineage. *Genome Biol* 6:R92. <https://doi.org/10.1186/gb-2005-6-11-r92>.
- Pilla DM, Hagar JA, Halder AK, Mason AK, Degrandi D, Pfeffer K, Ernst RK, Yamamoto M, Miao EA, Coers J. 2014. Guanylate binding proteins promote caspase-11-dependent pyroptosis in response to cytoplasmic LPS. *Proc Natl Acad Sci U S A* 111:6046–6051. <https://doi.org/10.1073/pnas.1321700111>.
- Meunier E, Dick MS, Dreier RF, Schürmann N, Kenzelmann Broz D, Warming S, Roose-Girma M, Bumann D, Kayagaki N, Takeda K, Yamamoto M, Broz P. 2014. Caspase-11 activation requires lysis of pathogen-containing vacuoles by IFN-induced GTPases. *Nature* 509:366–370. <https://doi.org/10.1038/nature13157>.
- Man SM, Karki R, Sasai M, Place DE, Kesavardhana S, Temirov J, Frase S, Zhu Q, Malireddi RKS, Kuriakose T, Peters JL, Neale G, Brown SA, Yamamoto M, Kanneganti T-D. 2016. IRGB10 liberates bacterial ligands for sensing by the AIM2 and caspase-11-NLRP3 inflammasomes. *Cell* 167:382–396.e17. <https://doi.org/10.1016/j.cell.2016.09.012>.
- Santos JC, Dick MS, Lagrange B, Degrandi D, Pfeffer K, Yamamoto M, Meunier E, Pelczar P, Henry T, Broz P. 2018. LPS targets host guanylate-binding proteins to the bacterial outer membrane for non-canonical

- inflammasome activation. *EMBO J* 37:e98089. <https://doi.org/10.15252/embj.201798089>.
29. Aachoui Y, Leaf IA, Hagar JA, Fontana MF, Campos CG, Zak DE, Tan MH, Cotter PA, Vance RE, Aderem A, Miao EA. 2013. Caspase-11 protects against bacteria that escape the vacuole. *Science* 339:975–978. <https://doi.org/10.1126/science.1230751>.
 30. Ceballos-Olvera I, Sahoo M, Miller MA, del Barrio L, Re F. 2011. Inflammasome-dependent pyroptosis and IL-18 protect against *Burkholderia pseudomallei* lung infection while IL-1 β is deleterious. *PLoS Pathog* 7:e1002452. <https://doi.org/10.1371/journal.ppat.1002452>.
 31. Aachoui Y, Kajiwara Y, Leaf IA, Mao D, Ting JP-Y, Coers J, Aderem A, Buxbaum JD, Miao EA. 2015. Canonical inflammasomes drive IFN- γ to prime caspase-11 in defense against a cytosol-invasive bacterium. *Cell Host Microbe* 18:320–332. <https://doi.org/10.1016/j.chom.2015.07.016>.
 32. Kovacs SB, Oh C, Maltez VI, McGlaughon BD, Verma A, Miao EA, Aachoui Y. 2020. Neutrophil caspase-11 is essential to defend against a cytosol-invasive bacterium. *Cell Rep* 32:107967. <https://doi.org/10.1016/j.celrep.2020.107967>.
 33. Place DE, Briard B, Samir P, Karki R, Bhattacharya A, Guy CS, Peters JL, Frase S, Vogel P, Neale G, Yamamoto M, Kanneganti T-D. 2020. Interferon inducible GBPs restrict *Burkholderia thailandensis* motility induced cell-cell fusion. *PLoS Pathog* 16:e1008364. <https://doi.org/10.1371/journal.ppat.1008364>.
 34. Santanirand P, Harley VS, Dance DAB, Drasar BS, Bancroft GJ. 1999. Obligatory role of gamma interferon for host survival in a murine model of infection with *Burkholderia pseudomallei*. *Infect Immun* 67:3593–3600. <https://doi.org/10.1128/IAI.67.7.3593-3600.1999>.
 35. Wang J, Sahoo M, Lantier L, Warawa J, Cordero H, Deobald K, Re F. 2018. Caspase-11-dependent pyroptosis of lung epithelial cells protects from melioidosis while caspase-1 mediates macrophage pyroptosis and production of IL-18. *PLoS Pathog* 14:e1007105. <https://doi.org/10.1371/journal.ppat.1007105>.
 36. Whiteley L, Meffert T, Haug M, Weidenmaier C, Hopf V, Bitschar K, Schittek B, Kohler C, Steinmetz I, West TE, Schwarz S. 2017. Entry, intracellular survival, and multinucleated giant-cell-forming activity of *Burkholderia pseudomallei* in human primary phagocytic and nonphagocytic cells. *Infect Immun* 85:e00468-17. <https://doi.org/10.1128/IAI.00468-17>.
 37. Platanias LC. 2005. Mechanisms of type-I and type-II-interferon-mediated signalling. *Nat Rev Immunol* 5:375–386. <https://doi.org/10.1038/nri1604>.
 38. Ngo CC, Man SM. 2017. Mechanisms and functions of guanylate-binding proteins and related interferon-inducible GTPases: roles in intracellular lysis of pathogens. *Cell Microbiol* 19:e12791. <https://doi.org/10.1111/cmi.12791>.
 39. Wandel MP, Pathe C, Werner EI, Ellison CJ, Boyle KB, von der Malsburg A, Rohde J, Randow F. 2017. GBPs inhibit motility of *Shigella flexneri* but are targeted for degradation by the bacterial ubiquitin ligase IpaH9.8. *Cell Host Microbe* 22:507–518.e5. <https://doi.org/10.1016/j.chom.2017.09.007>.
 40. Shi J, Zhao Y, Wang K, Shi X, Wang Y, Huang H, Zhuang Y, Cai T, Wang F, Shao F. 2015. Cleavage of GSDMD by inflammatory caspases determines pyroptotic cell death. *Nature* 526:660–665. <https://doi.org/10.1038/nature15514>.
 41. Li P, Jiang W, Yu Q, Liu W, Zhou P, Li J, Xu J, Xu B, Wang F, Shao F. 2017. Ubiquitination and degradation of GBPs by a *Shigella* effector to suppress host defence. *Nature* 551:378–383. <https://doi.org/10.1038/nature24467>.
 42. Coll RC, Robertson AAB, Chae JJ, Higgins SC, Muñoz-Planillo R, Inerra MC, Vetter I, Dungan LS, Monks BG, Stutz A, Croker DE, Butler MS, Haneklaus M, Sutton CE, Núñez G, Latz E, Kastner DL, Mills KHG, Masters SL, Schroder K, Cooper MA, O'Neill LAJ. 2015. A small-molecule inhibitor of the NLRP3 inflammasome for the treatment of inflammatory diseases. *Nat Med* 21:248–255. <https://doi.org/10.1038/nm.3806>.
 43. Coll RC, Hill JR, Day CJ, Zamoshnikova A, Boucher D, Massey NL, Chitty JL, Fraser JA, Jennings MP, Robertson AAB, Schroder K. 2019. MCC950 directly targets the NLRP3 ATP-hydrolysis motif for inflammasome inhibition. *Nat Chem Biol* 15:556–559. <https://doi.org/10.1038/s41589-019-0277-7>.
 44. Wang J, Deobald K, Re F. 2019. Gasdermin D protects from melioidosis through pyroptosis and direct killing of bacteria. *J Immunol* 202:3468–3473. <https://doi.org/10.4049/jimmunol.1900045>.
 45. Schroder K, Irvine KM, Taylor MS, Bokil NJ, Le Cao K-A, Masterman K-A, Labzin LI, Sempke CA, Kapetanovic R, Fairbairn L, Akalin A, Faulkner GJ, Baillie JK, Gongora M, Daub CO, Kawaji H, McLachlan GJ, Goldman N, Grimmond SM, Carninci P, Suzuki H, Hayashizaki Y, Lenhard B, Hume DA, Sweet MJ. 2012. Conservation and divergence in Toll-like receptor 4-regulated gene expression in primary human versus mouse macrophages. *Proc Natl Acad Sci U S A* 109:E944–E953. <https://doi.org/10.1073/pnas.1110156109>.

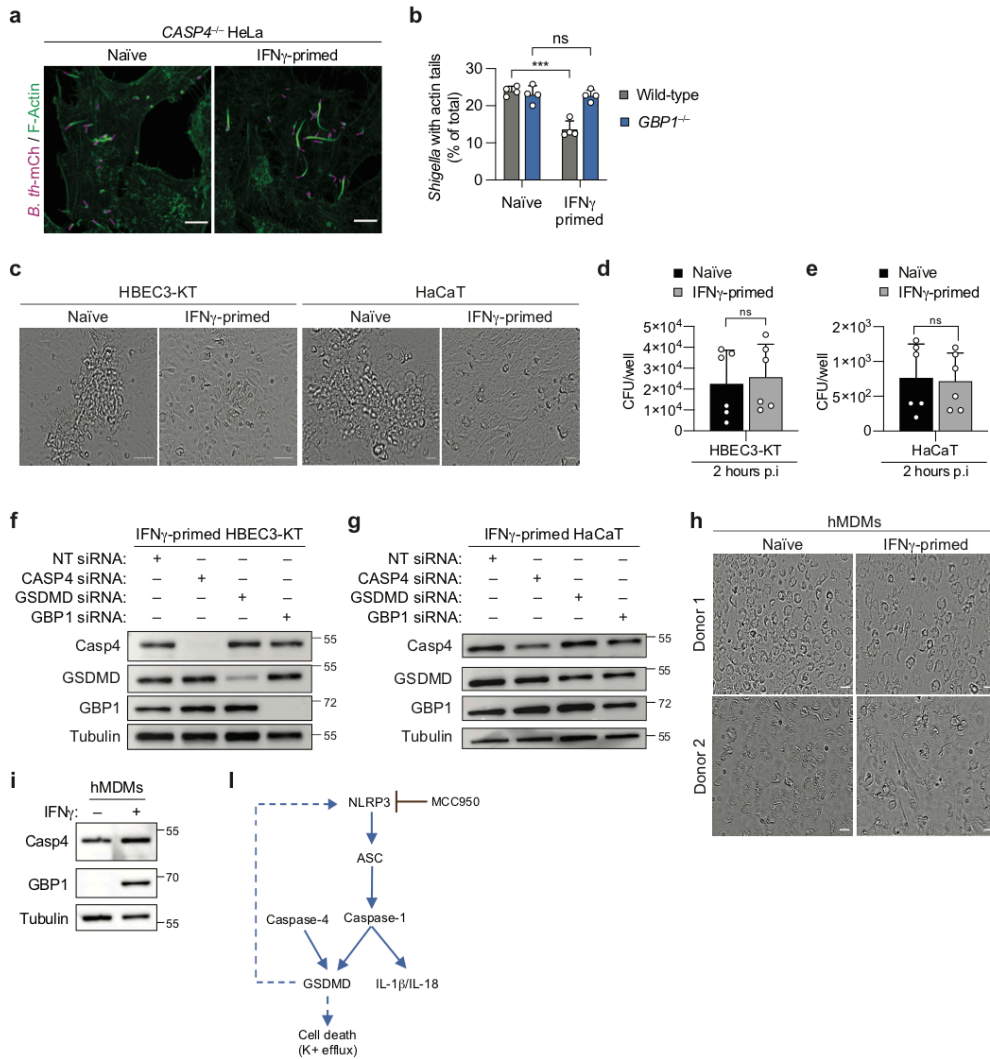
Supplementary Figure 1



Supplementary Figure 2



Supplementary Figure 3



3.3 Research Project III: Interferon gamma-induced murine guanylate-binding protein 4 (Gbp4) orchestrates caspase-11-mediated pyroptosis.

Marisa Dilucca¹, Elliott Bernard¹, Petr Broz^{1†}

¹ Department of Biochemistry, University of Lausanne, Chemin des Boveresses 155, 1066, Epalinges, Switzerland

[†] Corresponding author. Email: petr.broz@unil.ch

Specific contribution:

This unpublished research project is still in progress. I have performed all the experiments presented.

Summary of the results

Inflammasomes are cytosolic multiprotein signaling complexes that are activated upon PRRs-mediated recognition of pathogen-derived ligands or endogenous danger signals. Their assembly activates the downstream inflammatory caspase-1 and caspase-4/-5 (human) or caspase-11 (mouse) that induce cytokine release and pyroptotic cell death through the cleavage of the pore-forming effector GSDMD. TLR signaling, as well as type I and II IFNs, have been found to fine-tune inflammasome-mediated responses. Indeed, the GBPs, a family of IFN-induced GTPases, were shown to control activation of the non-canonical inflammasome in response to cytosolic Gram-negative bacteria and LPS. Moreover, in mouse macrophages, Gbps are also controlling the activation of the canonical inflammasomes, as the membranolytic effect exerted by Gbp-dependent recruitment of Irgb10 on *F. novicida* is necessary for DNA release and activation of the cytosolic DNA sensor Aim2. Finally, it has been reported that murine Gbp5 promotes the assembly of the Nlrp3 inflammasome in response to bacteria and soluble inflammasome priming agents, but not crystalline stimuli.

Mice feature 11 Gbps, which can be found on 2 clusters on chromosome 3 and chromosome 5 respectively. The study of the role of murine Gbps in host defense is restricted to Gbps on chromosome 3 due to the availability of *Gbp^{Chr3}-KO* mice. Thus far comparable tools are lacking for the Gbp cluster on chromosome 5, and not the precise function of these GBPs is still unclear, although knock-down studies suggest a role in antimicrobial defense as well³⁶⁴.

Here we have used CRISPR-Cas9 genome editing to create *Gbp^{Chr5}-/-* knock-out mice and a new line of *Gbp^{Chr3}-/-* knock-out mice in order to study the role of all murine Gbps. We found that mGbps on chromosome 5 do not contribute to canonical inflammasome activation, but that they play an important role in the activation of the non-canonical inflammasome pathway by LPS. Intriguingly, the involvement of *Gbp^{Chr5}* in LPS-driven caspase-11 activation is priming dependent and only detectable upon IFN γ priming, but not in LPS or type I IFN primed cells. Among the 6 family members on mGbpChr5, Gbp4 plays a prominent role, revealing close similarities in the hierarchical organization of murine and human GBPs.

Abstract

GBPs, a family of large IFN-inducible GTPases, have been found to participate in cell autonomous immunity against viruses, bacteria, and protozoan parasites. A consistent feature among GBP-expressing species is their organization into multigenic clustered chromosome families; for example, the 7 human GBPs are organized in a single cluster on chromosome 1, whereas the 11 murine Gbps are distributed in two clusters on chromosomes 3 and 5. Both human and murine GBPs have been shown to control the activation of inflammasomes, multiprotein cytosolic signaling complexes that are activated upon recognition of pathogen-derived ligands or endogenous danger signals by pattern recognition receptors (PRRs). Specifically, both the mouse *GbpChr3* cluster and human GBP1-4 promote the activation of caspase-11 and its human ortholog caspase-4, respectively. In addition, *GbpChr3* participates in Aim2 inflammasome activation in response to *F. novicida* infection, but not after poly (dA:dT) transfection. In contrast, very little is known about the role of *GbpChr5* in antimicrobial defense. Here we generated *GbpChr3*- and *GbpChr5*-deficient mice using CRISPR-Cas9 genomic editing. We found that *GbpChr5* controls LPS-driven caspase-11 activation in a priming-dependent manner: their participation is only detectable under IFN γ priming conditions. Furthermore, experiments with loss-of-function siRNA revealed that among *GbpChr5*, *mGbp4* is crucial for noncanonical inflammasome activation.

Introduction

Cellular self-defenses aid multicellular organisms to cope with microbial challenges. The host cell's ability to contrast threats is termed cell-autonomous immunity and it includes effector mechanisms conserved across the phyla. Beyond constitutive host defense factors, vertebrates have developed additional factors transcribed in response to cytokines, such as the IFNs, and TLRs signaling cascade⁴⁷¹. The IFNs are one of the most potent signals to drive a wide variety of effector mechanisms to fight intracellular pathogens, indeed, IFN priming upregulates the transcription of the so-called IFN-stimulated genes (ISGs), which encode proteins involved in the restriction of viruses, bacteria, and parasites¹⁰⁷. The most effective containment strategies elicited by the IFN-induced Guanylate-Binding Proteins (GBPs), a protein family whose members harbor a globular GTPase domain at the N-terminal and a

helical domain at the C-terminal, responsible for protein-protein/protein-lipid interaction^{362,363,365}. A consistent feature across species is their organization into clustered multigene families; in fact, humans have a single cluster on chromosome 1 that includes 7 GBP, whereas mice have two clusters, on chromosomes 3 and 5, comprising a total of 11 Gbp^{362,363,365}. Besides disrupting the parasite's vacuole and blocking bacterial actin-based motility, they cooperate in the activation of the inflammasome machinery^{78,356,380,430,431,433}.

The inflammasome is an intracellular signaling complex that confers host resistance against microbial pathogens. They are assembled upon pattern-recognition receptors (PRRs)-mediated recognition of inflammatory ligands, such as pathogen-associated molecular patterns (PAMPs) or damage-associated molecular patterns (DAMPs) in the cytosol of host cells⁴³⁵. Interaction between inflammasomes and ISGs gene products is best highlighted by cytosolic sensing of LPS, the major component of the Gram-negative bacterial outer membrane. It has been proposed that cytosolic LPS is detected by caspase-4/-11 (the so-called noncanonical inflammasome), causing its oligomerization and activation. Caspase-11/-4 activates GSDMD to trigger pyroptosis, but while caspase-11 is unable to mature cytokines such as IL-1 β /-18, caspase-4 is able to mature IL-18^{289,451}. It has been shown that in mouse bone marrow-derived macrophages (BMDM), caspase-11 activation in response to cytosolic LPS also requires the expression of IFN-inducible GTPases, Gbps, and IRGs, such as Irgb10^{253,256}. Contrary to the mouse model, targeting of human GBP to cytosolic bacteria does not induce bacteriolysis but instead results in the formation of a platform for caspase-4 activation. Recent work by our laboratory and a related study by Wandel et al. shown that in human epithelial cells infected with *S. Typhimurium*, GBP1 is recruited to the surface of cytosolic bacteria and directly interacts with LPS, allowing the recruitment of other GBPs (GBP2-4) and caspase-4 on the bacterial surface. Hence, GBP1 can be considered a bonafide cytosolic LPS sensor^{360,456}.

Gbps take part also in the activation of the canonical inflammasome, indeed the membranolytic effect exerted by Gbp-dependent recruitment of Irgb10 on *F. novicida* contributes to the activation of the Aim2 inflammasome, a cytosolic double-stranded DNA sensor²⁵⁶. Finally, it has been reported that murine Gbp5 promotes the assembly of the Nlrp3 inflammasome in response to bacteria and soluble

inflammasome priming agents, but not crystalline stimuli³⁶⁷. The study of the role of murine Gbps in host defense is restricted to Gbps on chromosome 3 due to the availability of *Gbp^{Chr3}*-deficient mice⁴⁰⁹. For Gbps on chromosome 5, however, no precise function or deletion has yet been reported, although experiments with small-interfering RNA (siRNA) suggest that they may play a role in antimicrobial defense³⁶⁴.

Here we first reported the generation of a *Gbp^{Chr5}*^{-/-} and a new *Gbp^{Chr3}*^{-/-} mice line via CRISPR-Cas9 genome editing, in order to study all the mGbps. We found that Gbps on chromosome 5 are dispensable for canonical inflammasome activations. Instead, mGbpChr5 contribute to the activation of the non-canonical inflammasome. Interestingly, the involvement of mGbpChr5 in LPS-driven caspase-11-activation is priming-dependent and only detectable after IFN γ stimulation. Eventually, among the 6 family members on mGbpChr5, *Gbp4* plays a prominent role, revealing close similarities in the hierarchical organization of murine and human GBPs.

1. Generation of *Gbp^{Chr3}*- and *Gbp^{Chr5}*-deficient mice

The 11 murine Gbps are distributed in two clusters on chromosome 3 and chromosome 5, respectively³⁶². Whereas chromosome 3-cluster deficient mice have been reported, no mouse models lacking the chromosome 5 cluster were available, although knock-down experiments have shown their involvement in antimicrobial defense^{364,409}. Therefore, to address whether the mGbpChr5 participate in the inflammasome activation, we used CRISPR/Cas9 genome engineering to generate chromosome 5-cluster deficient mice by removing the whole locus containing *Gbp4*, *6*, *8*, *9*, *10*, and *11*. In brief, *Gbp^{Chr5}*^{-/-} mice were generated by using two targeting gRNAs (5'-TAGCCCAGGATAGGTTGTAC-3' and 5'-GAGCGACTAGGACCAATCAGG -3') and in-vitro translated Cas9 mRNA were co-microinjected into C57BL/6 zygotes (Fig.3.1 a). Deletion of the locus was checked by PCR.

The widely used chromosome 3-cluster deficient mice (hereinafter referred to as Old *Gbp^{Chr3}*^{-/-}) were not generated by CRISPR-Cas9 genome editing, but by implanting 129 substrains embryonic stem (ES) cells harboring the chromosome 3 deletion into a C57BL/6 blastocyst³⁷⁶. Chimeric mice with the knockout allele were then backcrossed with C57BL/6 to make the mixed genetic background of the offspring

uniform to the desired genetic background⁴⁰⁹. Although microinjection of ES into the blastocyst has been a powerful tool for generating knockout mice, recent studies have revealed that improper back-crossing or passenger mutation from the 129 strain in genes neighboring the target gene account for many of the observed phenotypes in common knock-out lines^{472,473}. Hence, we determined the level of back-crossing of our old *Gbp*^{Chr3-/-} mice (that should have been back-crossed for close to 10 generations) by sending their genomic material to the Dartmouth facility for a genetic background check. The chromosome map of *Gbp*^{Chr3-/-} mice, which identifies the genetic background of each of the SNP loci throughout the genome, disclosed that these mice still harbor 15% of the genome from the 129 line (Fig.3.1 b, c). Therefore, we set out to generate a new *Gbp*^{Chr3-/-} mouse line via CRISPR-Cas9-mediated gene disruption. We targeted the GBP chromosome 3 locus, which contains *Gbp1*, *Gbp2*, *Gbp3*, *Gbp5*, and *Gbp7*, with two gRNAs (5'-GATTTGCCCTGCCCCGCCTG-3' and 5'-GCGTTCCCCAGTGATGCCTG-3') and verified the deletion by PCR (Fig.3.1 d)

Figure 1

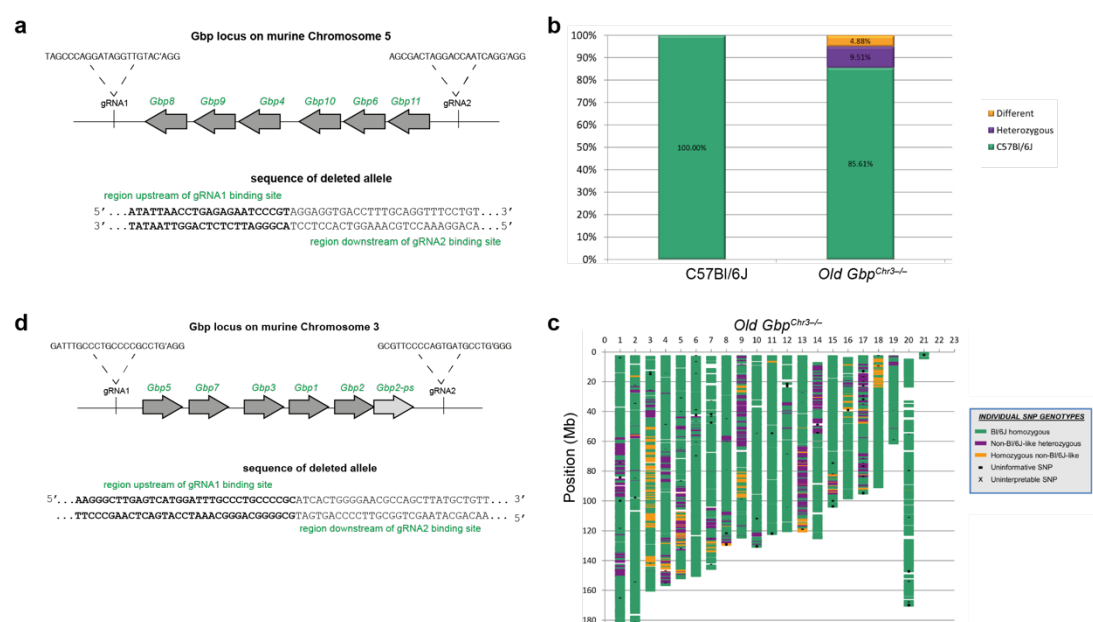


Figure 3.1 Generation of *Gbp*^{Chr3-} and *Gbp*^{Chr5-} deficient mice. a) Gene targeting strategy for *Gbp*^{Chr5} locus by CRISPR-Cas9 technology. b) and c) Tested SNPs from Dartmouth genetic background check. C57BL/6 SNPs are represented in green, 129 SNPs are in yellow, and heterozygous SNPs are represented in purple. Uninformative SNPs (-); uninterpretable SNPs (x). d)

Gene targeting strategy for Gbp^{Chr3} locus by CRISPR-Cas9 technology. **d)** Gene targeting strategy for Gbp^{Chr3} locus by CRISPR-Cas9 technology.

2. The cluster of Gbps on chromosome 5 does not promote canonical inflammasome activation.

PRRs are essential in orchestrating innate immune responses by sensing microbial products. A number of these detect nucleic acids (e.g., DNA or RNA), such as the AIM2, which recognizes cytosolic double-stranded DNA by its HIN-200 domain⁴⁷⁴. Aim2 activation initiates inflammasome assembly leading to GSDMD-dependent pyroptosis and maturation of the pyrogenic cytokines, IL-1 β /-18, through caspase-1 activation²⁴⁵. AIM2 responds to synthetic DNA, DNA virus as well as a number of Gram-positive and Gram-negative bacteria, such as *F. novicida*, *L. monocytogenes*, and *Legionella pneumophila* (*L. pneumophila*)²⁵². Interestingly, activation of the Aim2 inflammasome in BMDMs infected with *F. novicida* requires IFN production, as Gbps on chromosome 3, mainly Gbp2 and Gbp5, and Irgb10, lyse intracellular bacteria to release *Francisella*-derived nucleic acids into the cytosol^{253,256}. In contrast, transfection of synthetic double-stranded DNA such as poly(dA:dT) or viral infection does not require IFN stimulation²⁵⁶. Indeed, consistent with published studies, transfection of poly(dA:dT) into LPS-stimulated BMDMs caused massive cell death that is Aim2-dependent but Gbp^{Chr3} -independent (Fig.3.2 a). We next examined whether mGbpChr5 could participate in Aim2-driven cell death; however, LDH release was not abolished in $Gbp^{Chr5-/-}$ BMDMs, ruling out the potential involvement of mGbpChr5 in Aim2 inflammasome activation (Fig.3.2 a). Similarly, transfection of poly(dA:dT) induced robust IL-1 β release, as measured by ELISA assay, and the release of the mature cytokine was abolished in $Aim2^{-/-}$ macrophages, while it was unaffected by Gbps deficiency (Fig.3.2 b).

Figure 2

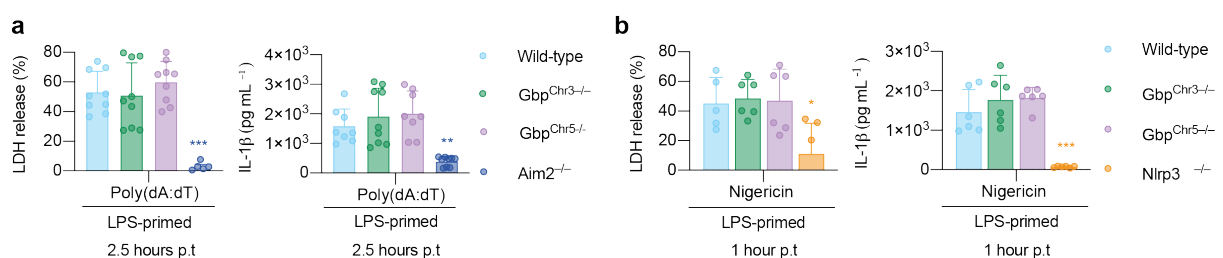


Figure 3.2 The cluster of Gbps on chromosome 5 do not promote canonical inflammasome activation. **a) to b)** BMDMs were primed with LPS (50 ng/mL) for 16 hours. **a) and b)** LDH and IL-1 β release in wild-type, $Gbp^{Chr3-/-}$, $Gbp^{Chr5-/-}$, and $Aim2^{-/-}$ BMDMs 2.5 hours post-transfection with poly (dA:dT). **c) and d)** LDH and IL-1 β release in wild-type, $Gbp^{Chr3-/-}$, $Gbp^{Chr5-/-}$, and $Nlrp3^{-/-}$ BMDMs 1 hour after nigericin (5uM) treatment. Graphs show the means \pm standard deviations (SD), and data are pooled from two (**b**) or three (**a**) independent experiments performed in triplicates. *, $P < 0.05$; **, $P < 0.01$; ***, $P < 0.001$ (by ordinary one-way analysis of variance [ANOVA]).

Canonical Nlrp3 inflammasome is induced by various soluble and/or crystalline stimuli or in response to bacterial infection⁴⁷⁵. It has been proposed that Gbp5 cooperates in Nlrp3 inflammasome assembly in response to several stimuli, including nigericin and *Listeria* and *Salmonella* infection. As a matter of fact, significant loss of IL-1 β /IL-18 release along with cleavage of caspase-1 was evident in *Gbp5*-deficient BMDMs³⁶⁷. Contradicting these findings, we observed no reduction in LDH and IL-1 β release in nigericin-treated Gbp^{Chr3} -deficient cells after stimulation with LPS (Fig.3.2 a, b). The rate of cell death and the amount of IL-1 β release also remained unchanged in *GbpChr5*-knockout macrophages, thus excluding that they may contribute to Nlrp3 inflammasome activation. (Fig.3.2 a, b).

Taken together, these results indicate that canonical inflammasomes function independently from the Gbp cluster on chromosome 5.

3. Gbp cluster on chromosome 5 does not impair *Burkholderia* actin-based motility.

Cytosolic *Shigella flexneri* (*S. flexneri*) is targeted by human GBP1-4 in a hierarchical and GBP1-dependent manner. Interestingly, GBP1-decorated bacteria retain the ability to replicate in the cytosol but fail to polymerize actin tails and thus the ability to spread throughout cells^{430,431}. Likewise, in mouse bone marrow-derived macrophages, Gbp^{Chr3} have been found to decorate *Burkholderia thailandensis* (*B. thailandensis*) that escapes endocytic compartments and impair its actin-based motility⁴³³. Therefore, we examined the possibility that Gbp^{Chr5} , as well as Gbps on chromosome 3, may participate in actin-based restriction of bacterial motility. By confocal microscopy, we quantified the amount of *Burkholderia* actin tails-positive bacteria in wild-type, $Gbp^{Chr3-/-}$ and $Gbp^{Chr5-/-}$ BMDM under naïve or IFN γ primed

conditions (to stimulate Gbp induction). In agreement with previous results, in IFN γ -stimulated wild-type BMDMs, we detected few actin tails-positive bacteria compared with those found in *Gbp^{Chr3-/-}* BMDMs (Fig.3.3 a, b). In contrast, we found that IFN γ stimulation antagonizes actin tails polymerization in *Gbp^{Chr5-/-}*-deficient macrophages in a manner comparable to IFN γ -primed wild-type cells, implying no role for those Gbps in restricting bacterial spread (Fig.3.3 a, b).

Figure 3

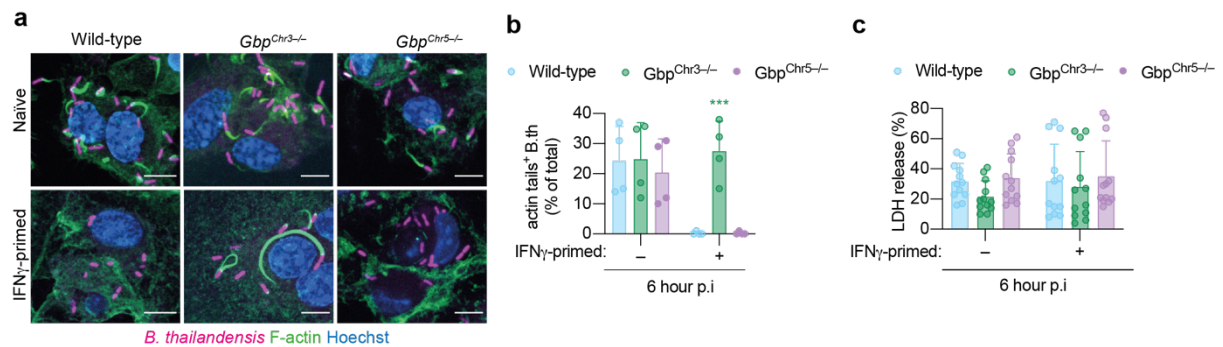


Figure 3.3 Gbp cluster on chromosome 5 does not impair *Burkholderia* actin-based motility. a) to **c**) BMDMs were primed with IFN γ (10ng/mL) for 16 hours prior infection with *B. thailandensis*-mCherry (MOI 50). **a**) Representative fluorescence confocal microscopy images of IFN γ -primed wild-type, *Gbp^{Chr3-/-}*, and *Gbp^{Chr5-/-}* cells infected with *B. thailandensis*-mCherry (purple) for 6 h. F-actin (green) was labeled with CellMask green actin tracking stain, and DNA (blue) was stained by Hoechst stain. Bars, 80 μ m. **b**) Percentage of *B. thailandensis* actin tails positive bacteria in naive and IFN γ -primed wild-type, *Gbp^{Chr3-/-}*, and *Gbp^{Chr5-/-}* 6 post-infections. At least 300 to 400 bacteria per coverslip were counted. **c**) LDH release in unprimed and IFN γ -stimulated wild-type, *Gbp^{Chr3-/-}*, and *Gbp^{Chr5-/-}* BMDMs 6 hours p.i with *B. thailandensis*-mCherry. Graphs show the means \pm standard deviations (SD), and data are pooled from two (**b**) or three (**c**) independent experiments performed in duplicates (**b**) or triplicates (**c**).

To exclude that IFN γ priming inhibits actin tail polymerization by promoting inflammasome activation, we measured cell death in wild-type and *Gbp^{Chr5-/-}* - and *Gbp^{Chr3-/-}* -knockout cells infected with *B. thailandensis*. Notably, wild-type cells showed a similar rate of LDH release as *Gbp*-deficient BMDMs (Fig.3.3 c), suggesting that IFN γ inhibits actin tail polymerization by promoting Gbp expression but not cell death.

Thus, in contrast to Gbps located on chromosome 3, Gbps on chromosome 5 do not

restrain bacterial actin-dependent motility.

4. Gbps on chromosome 5 orchestrate the non-canonical inflammasome activation in IFN γ -primed conditions.

The response to cytosolic LPS triggers pyroptosis, an inflammatory form of cell death, by binding murine caspase-11 or human caspase-4. These non-canonical inflammatory caspases regulate pyroptosis by enzymatically cleaving the pore-forming protein GSDMD, whose N-terminal domain oligomerizes to form a pore in the plasma membrane that leads to cell death^{288,289,445,456}. Interestingly, activation of the non-canonical inflammasome can also trigger the maturation of proinflammatory cytokines; in fact, the potassium efflux resulting from the caspase-4/-11-induced GSDMD pores activates NLRP3 and subsequently caspase-1²⁹³. For optimal activation, the noncanonical inflammasome requires IFN priming, which simultaneously upregulates the expression of caspase-11 and the Gbps, which are recruited directly to the bacterial membrane, where they support the release of microbial ligands^{289,436}. This can be achieved by TLR agonists, such as LPS, which induces NF κ B-dependent pro-IL-1 β /-18 upregulation and indirectly caspase-11 and Gbps expression via TRIF-dependent type I IFN production^{186,302}. In addition, these IFN-inducible genes can also be upregulated by type I IFNs (IFN α/β) or IFN γ , the sole type II IFN, signaling through STATs^{130,364}. Notably, type I and II IFN priming does not activate the NF κ B signaling cascade and, therefore, increases the expression of neither pro-inflammatory cytokines nor NLRP3. Also, previous studies have shown that Gbp expression is highly upregulated by IFN γ and to a lesser extent by type I IFNs³⁶⁴.

To determine the relative abilities of type I/II IFNs and LPS to induce caspase-11-dependent pyroptosis, we stimulated wild-type, *Gbp*^{Chr3 $^{-/-}$} , *Gbp*^{Chr5 $^{-/-}$} , and *Casp11* ^{$^{-/-}$} BMDMs for 16 hours with LPS, IFN β , or IFN γ prior to LPS transfection and monitored inflammasome activation by measuring LDH release. As expected, priming significantly increased LDH release compared with the non-priming condition, although to a lesser extent in the case of stimulation with type I IFN (Fig.3.4 a). Notably, the rate of cell death was significantly higher under IFN γ priming conditions than under other stimuli (Fig.3.4 a). Consistent with previous studies, caspase-11 inflammasome activation by cytosolic LPS was dependent on GbpChr3 in response

to all priming agents^{256,444,445}. Surprisingly, in IFN γ -stimulated BMDMs, LPS-induced cell death also depended on GbpChr5 (Fig.3.4 a). To test whether the *Gbp* chromosome 5-dependent cell death detected in response to IFN γ is also reflected in reduced inflammatory cytokine maturation, we evaluated IL-1 β release in naive, LPS- and LPS/IFN γ -primed BMDM transfected with LPS. Double priming is necessary to assess IL-1 β production since IFNs do not promote the NF- κ B signaling cascade. We found that priming agents enhance IL-1 β production, as the level of IL-1 β release detected under naïve conditions is significantly lower than under stimulated conditions (Fig.3.4 b). In addition, we detected decreased IL-1 β release in *Gbp*^{Chr3-/-} BMDMs in response to both LPS and LPS/IFN γ priming (Fig. 3.4 b), whereas dependence on GbpChr5 was only observed under double priming conditions (Fig.3.4 b), supporting the hypothesis that Gbps on chromosome 5 are required for optimal caspase-11 activation if cells are stimulated with IFN γ . To test if Gbp chromosome 5 cluster orchestrates the activation of the AIM2 and NLRP3 inflammasomes upon type II IFN stimulation, we evaluated the release of LDH and IL-1 β in response to poly (dA:dT) transfection or nigericin treatment in IFN γ -primed BMDMs. However, no detectable reduction of inflammatory cytokine and cell death was observed, confirming that those mGbps do not participate in the activation of the canonical inflammasomes even under these conditions (data not shown).

Figure 4

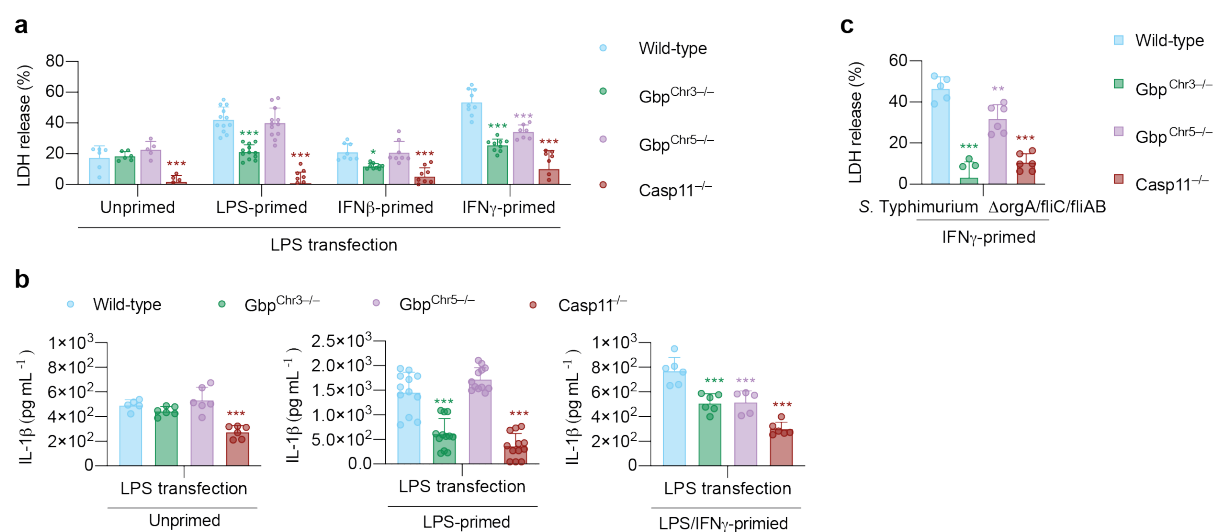


Figure 3.4 Gbps on chromosome 5 orchestrate the non-canonical inflammasome activation in IFN γ -primed conditions. a) Wild-type, *Gbp*^{Chr3-/-}, *Gbp*^{Chr5-/-}, and *Casp11*^{-/-} BMDMs were primed for

16 h overnight with the following treatments: unprimed (N/A), IFN γ (10ng/mL), IFN β (10 ng/mL), or LPS (50 ng/mL). LDH release was measured 6 hours post-transfection with LPS (5 ug/mL). **b**) BMDMs were left unprimed or primed with LPS for 16 hours or with IFN γ (16h) and LPS (4h) prior to transfection with LPS. IL-1 β release was measured 6 hours post LPS transfection. **c**) LDH release in IFN γ -primed (16h) wild-type, *Gbp^{Chr3-/-}*, *Gbp^{Chr5-/-}*, and *Casp11^{-/-}* was measured 22 hours after infection with *S. Typhimurium* Δ *orgA/fliC/fljAB* (MOI 50). Graphs show the means \pm standard deviations (SD), and data are pooled from three (**a**) or two (**b, d**) independent experiments performed in triplicates or are representative of one (**c**) independent experiments performed in triplicates. *, P < 0.05; **, P < 0.01; ***, P < 0.001 (by ordinary one-way analysis of variance [ANOVA]).

Since Gbps are required for non-canonical inflammasome activation in response to cytosolic *S. Typhimurium*^{256,362,365}, we decided to assess whether GbpChr5 are also required in response to bacterial infection. To test this, we primed mouse wild-type, *Gbp^{Chr3-/-}*, *Gbp^{Chr5-/-}*, and *Casp11^{-/-}* BMDMs with IFN γ for 16 hours and we performed the infection with stationary phase *S. Typhimurium* Δ *orgA/fliC/fljAB* strain, which lacks SPI-1, T3SS, and flagellin, to prevent Nlr4 inflammasome activation. Cell death was strongly impaired in *Gbp^{Chr3-/-}*-deficient and *Casp11^{-/-}* macrophages, suggesting that *Salmonella* infection in IFN γ -activated BMDMs activates the noncanonical inflammasome (Fig.3.4 c). In analogy with the phenotype observed in response to LPS transfection, we found that GbpChr5 are involved in *Salmonella*-induced pyroptosis since the rate of cell death was reduced in BMDMs lacking GbpChr5 expression when compared with wild-type cells (Fig.3.4 c).

Taken together these results confirmed that GbpChr5 participate in activating the non-canonical inflammasome, but this is only observed in IFN γ -stimulated cells.

5. IFN γ -stimulated macrophages require murine Gbp4 for optimal caspase-11 inflammasome activation.

Because noncanonical inflammasome activation under IFN γ -primed conditions required GbpChr5, but not upon stimulation with type I IFN, we hypothesized that different priming agents induce the expression of a different set of mGbps. Specifically, we thought that LPS and IFN β induce uniquely the expression of Gbps encoded on chromosome 3, whereas IFN γ upregulates the expression of both Gbps on chromosome 3 and 5, thus amplifying the level of non-canonical inflammasome

activation, which is consistent with higher LDH levels in LPS-transfected IFN γ -primed BMDMs (Fig.3.4 a). To test this hypothesis, we monitored by RT-qPCR the mRNA expression of all *Gbp*-encoding genes in wild-type BMDMs under different priming conditions; the results are represented as the ratio of target gene expression in treatment versus unprimed BMDMs. We found that the chromosome 3 cluster of *Gbp*-encoding genes were induced by IFN γ priming to a greater extent than LPS or IFN β stimulation (Fig.3.5. a). Remarkably, we found that GBPs on chromosome 5 were most strongly induced by IFN γ priming and much less by LPS or IFN β (Fig.3.5 b), indicating that indeed the expression levels could account for the differences observed before. Also, the expression of mGbp10 did not increase in response to any priming agent, raising the hypothesis that it may be mutated into a pseudogene.

Figure 5

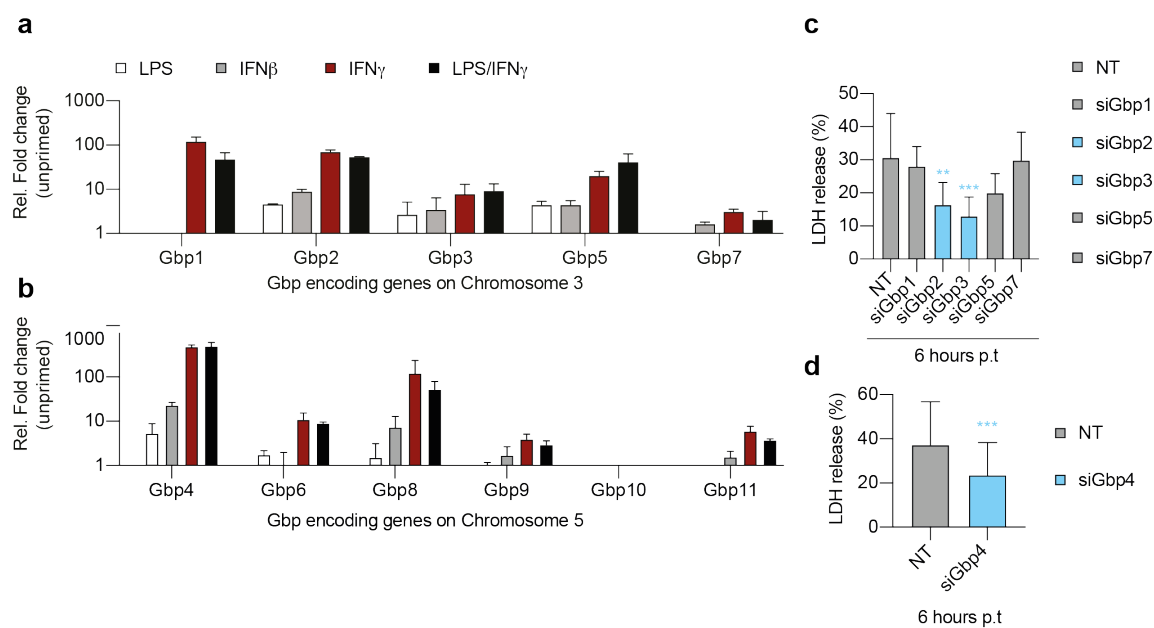


Figure 3.5 IFN γ -stimulated macrophages require murine Gbp4 for optimal caspase-11 inflammasome activation. **a)** and **b)** Fold-change mRNA expression of different murine *Gbp* genes in wild-type BMDMs primed with LPS (50 ng/mL), IFN β (10 ng/mL), or IFN γ (10ng/mL) for 16 hours, or double primed with IFN γ overnight and LPS for 4 hours. **c)** and **d)** LDH release in IFN γ -stimulated wild-type BMDMs transfected for 6 h with LPS (5 ug/mL). BMDMs were treated with the indicated siRNA for 48 h before transfection. Graphs show the means \pm standard deviations (SD), and data are representative of three (**a, b**) independent experiments performed in duplicates or are pooled (**c, d**) from three independent experiments performed in triplicates. *, P < 0.05; **, P < 0.01; ***, P < 0.001 (by ordinary one-way analysis of variance [ANOVA]).

To better define which individual Gbps on chromosome 3 or chromosome 5 were necessary for LPS-induced non-canonical inflammasome activation, we next used siRNA to knock-down the Gbps in both clusters. As proposed by a recent preprint³⁷⁷, RNA interference-mediated silencing of Gbp cluster expression on chromosome 3 in IFN γ -stimulated wild-type BMDMs revealed a consistent reduction in LDH release in cells lacking Gbp2 and Gbp3 after transfection with LPS (Fig.3.5 c), indicating their pivotal role in caspase-11 driven inflammasome³⁷⁷. Based on the fact that among Gbps on chromosome 5 Gbp4 was most strongly upregulated, we first focused on this family member and knock-down its expression. In addition, human GBP4 contributes to the assembly of the signaling hub that recruits caspase-4 after *S. Typhimurium* infection^{360,456}. Indeed, by knocking down the mouse *Gbp4* encoding gene, we measured a reduced rate of cell death in wild-type BMDMs under IFN γ stimulation conditions (Fig.3.5 d). Knocking down efficiency and specificity were tested by RT-qPCR (data not shown). However, the exact role played by mGbp4, and potentially other Gbps on chr5, in regulating caspase-11-dependent pyroptosis needs further investigation.

In conclusion, our approach identified Gbp2, 3, and 4 as the ISGs that regulate caspase-11 inflammasome in response to IFN γ priming.

Discussion

This study provides the first evidence that in IFN γ -stimulated murine BMDMs, Gbp-dependent activation of the noncanonical inflammasome in response to LPS delivery relies on the expression of the Gbp cluster on chromosome 5. Furthermore, we found that the lack of mGbp4 significantly reduces cell death, suggesting that among the Gbps present on the chromosome 5 locus, Gbp4 is certainly involved in the non-canonical inflammasome pathway.

Our work provides further support to the notion that Gbps on chromosome 3 are essential for caspase-11-mediated cell death in response to both *S. Typhimurium* infection and cytosolic LPS. Moreover, consistent with recent work, we identified the guanylate-binding proteins Gbp2 and Gbp3 as key activators of the non-canonical inflammasome³⁷⁷. However, the mechanism by which they promote caspase-11 activation is not yet understood.

While research has focused on describing the role of IFN-inducible antimicrobial mechanisms mediated by GbpChr3, little is known about GBPs on chromosome 5. Nonetheless, Kim et al. demonstrated that mGbp6 and mGbp10 are critical in controlling *L. monocytogenes* and *M. bovis* infection in loss-of-function siRNA experiments³⁶⁴. Specifically, IFN γ activation restrains bacterial replication, and this restriction is reversed by transfection of murine Gbp1, Gbp6, Gbp7, Gbp10, and, to a lesser extent, Gbp5 siRNAs³⁶⁴. In addition, the Gbp cluster on chromosome 5 has been implicated in the recognition of *Toxoplasma*-containing vacuoles. Indeed, confocal imaging studies revealed that mGbp6 and mGbp9, which belong to the GbpChr5, together with GbpChr3 (e.g. mGbp1, mGbp2, and mGbp7) accumulate on the membrane of the parasite vacuole and mediate antiparasitic resistance^{356,408}. Nonetheless, the lack of a mouse model in which chromosome 5 deletion is present has been a limiting factor in understanding the exact role of these Gbps in response to both bacterial and parasitic pathogens. Therefore, the mouse line *Gbp^{Chr5-/-}* we generated can represent a powerful tool to better investigate *in vitro* and *in vivo* their role in cell-autonomous immunity.

Our research has focused on understanding the role of all the murine Gbps in response to a variety of inflammasome stimuli. As previously shown, we found that activation of the Aim2 inflammasome by poly (dA:dT) transfection requires neither

Gbps on chromosome 3 nor Gbps on chromosome 5. Likewise, the Gbp clusters are not required for the Nlrp3 inflammasome activation in response to nigericin treatment. Our data are in contrast with a previous report assessing the involvement of mGbp5 in assembling the Nlrp3 inflammasome³⁶⁷. This discrepancy might be due to a difference in the mouse model employed since the *Gbp5*^{-/-} mice generated via ES mutagenesis and subsequently backcrossed with C57BL/6 might harbor a mixed genetic background. Further, it has been found that in mouse BMDMs, GbpChr3 restrict *Burkholderia* actin-based motility and the consequent cell-to-cell fusion by inhibiting the host actin polymerization machinery Arp2/3. Remarkably, no participation of the Gbp cluster on chromosome 5 was detected in restricting the polymerization of *Burkholderia* actin tails, suggesting that although Gbps on both clusters have a conserved domain architecture, they differ in the function they serve. It would be interesting to study whether GbpChr5 provides resistance against Aim2-activating bacteria, such as *F. novicida*, since host cells strongly rely on IFN production to eradicate *Francisella* replication niche.

Interestingly, consistent with our data, Brubaker et al. showed that IFN γ , as compared to type I IFNs, is the most potent activator of the caspase-11-dependent inflammasome. Specifically, they found that the increased activation of the caspase-11 inflammasome is independent of the *Gbps* encoded on chromosome 3, suggesting a possible role of the *Gbps* cluster on chromosome 5 in mediating non-canonical inflammasome activation⁴⁷⁶. Indeed, we found that the GbpChr5 is required for caspase-11-mediated pyroptosis and that its role is relevant in response to transfection with LPS. Also, we identified mGbp4 as an important regulator in mediating non-canonical inflammasome activation upon LPS delivery, revealing close similarities in the hierarchical organization of murine and human GBPs (Fig.3.6). Whether mGbp4 directly recognizes LPS or detects cytosolic *Salmonella* requires further investigation. Eventually, it would be interesting to elucidate if any other GbpChr5 besides mGbp4 controls LPS-driven caspase-11 activation.

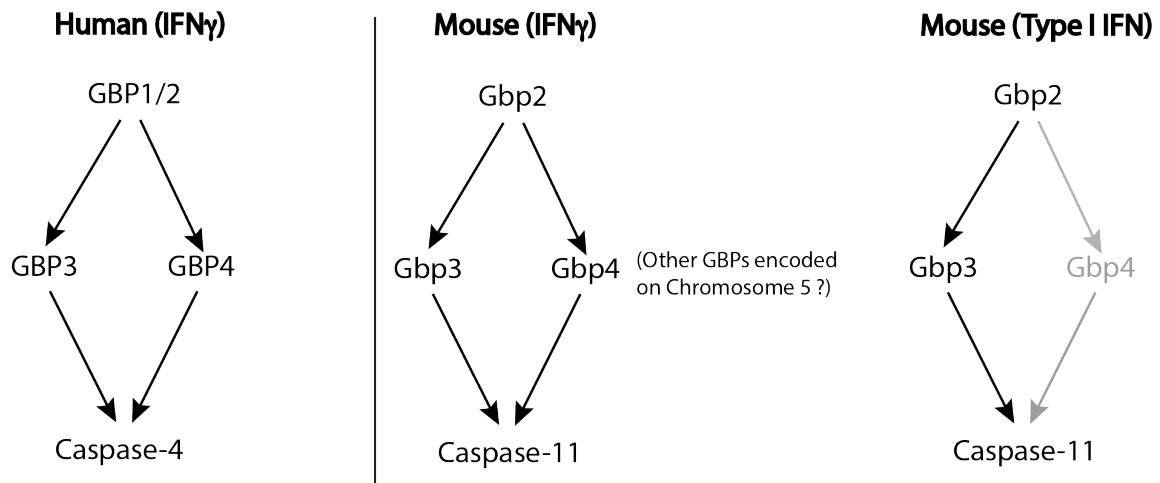


Figure 3.6 Schematic representation of caspase-4/-11-driven pyroptosis. In human epithelial cells the hierarchical recruitment of GBP1-4, reliant on GBP1, drives caspase-4 recruitment and activation. Likewise, mGBP2, mGBP3, and mGBP4 are required for caspase-11-induced cell death in response to LPS transfection. Surprisingly, requirement of mGBP4 is priming-dependent, indeed, it is detectable only in response to IFN γ stimulation.

Materials and methods

Mice

Gbp^{Chr5-/-} and *Gbp^{Chr3-/-}* mice were generated at the Center for Transgenic model of the University of Basel. Deletion of the entire *GbpChr5* locus was achieved as follows: two gRNAs targeting flanking regions of *Gbp8* and *Gbp11* using gRNA sequences (including PAM) 5'-TAGCCCAGGATAGGTTGTAC-3' and 5'-GAGCGACTAGGACCAATCAGG -3'; two gRNAs targeting flanking regions of *Gbp5* and *Gbp2-ps* using gRNA sequences (including PAM) 5'-GATTTGCCCTGCCCCGCCTG-3' and 5'-GCGTTCCCCAGTGATGCCTG-3'. Injection of the gRNAs and Cas9 protein into C57BL/6 embryos was done as described before (Hermann et al, 2014). Biopsies for genotyping were taken at an age of 10–12 days. DNA extraction was performed using the KAPA HotStart Mouse Genotyping Kit according to the manufacturer's protocol. Genotyping PCR was done using..... which were designed using Primer3 v.0.4.0 giving a fragment of 768 bp. The PCR product was sequenced using Oligo.507. All mice were bred at the pathogen-free facility of the University of Lausanne. *Casp11^{-/-}*, *Nlrp3^{-/-}*, *Aim2^{-/-}*, and *Old Gbp^{Chr3-/-}* mice have been previously described.

SNPs sequencing

DNA extraction from *Old Gbp^{Chr3-/-}* BMDMs was performed with DNeasy Blood & Tissue Kits (QIAGEN) using the manufacturer's instructions. The sample was sent to Dartmouse for a genetic background check and was interrogated for over 5300 SNPs space along the mouse genome using an Illumina Infinium Genotyping Assay

Cell culture and transfection

Bone marrow-derived macrophages were differentiated in Dulbecco's modified Eagle's medium (DMEM) high glucose (with GlutaMAX™-I, 4500 mg/L D-Glucose, Sodium Pyruvate) (Gibco) supplemented with 10% heat-inactivated calf serum (FCS) (Bioconcept), 20% L929 mouse fibroblast supernatants as a source of colony-stimulating factor (M-CSF), 5% HEPES (Sigma-Aldrich), 5% nonessential amino acids (Life Technologies), and 5% penicillin-streptomycin solution (Sigma-Aldrich). Cells were grown at 37°C with 5% CO₂. Macrophages were seeded into 96-well plates at a density of 5x10⁴ 24 hours prior to treatment. For microscopy-based

experiments cells were seeded one day before treatment into 24-well plates at a density of $2,5 \times 10^5$ on coverslips. When indicated, cells were also primed overnight with 50ng/mL LPS (LPS from *E. coli* 055:B5, Invivogen), 10ng/mL mouse IFN β (R&D system), or 10ng/mL mouse IFN γ (PeproTech). Transfection of cells with poly(dA:dT) (Invivogen, 25ng/50,000 cells) was done using Lipofectamine 2000 (Invitrogen) in Opti-MEM. Transfection of cells with LPS from *E. coli* O111:B4 (Invivogen), was done at a concentration of 5ug/mL, using FuGeneHD (Promega) transfection reagent in Opti-MEM. In Fig 5B, LPS O111:B4 was transfected with Lipofectamine 2000.

Bacterial strains and infection assays

All bacteria were grown at 37°C in an orbital shaker. When indicated, cells were primed for 16 h with human IFN γ (PeproTech) at a concentration of 10 ng/ml. *B. thailandensis* strain E264 expressing mCherry was grown overnight in a low-salt LB medium. The overnight culture was adjusted to an optical density at 600 nm (OD₆₀₀) of 1, subcultured 1:20, and grown until the mid-exponential phase (OD₆₀₀ = 0.4 to 0.6). *S. Typhimurium* Δ orgA/fliC/fliAB was grown overnight with aeration in LB media. Before infection, bacteria were collected by centrifugation, washed, and resuspended in Opti-MEM (Gibco). *B. thailandensis*-mCherry was added to cells in 24-well plates at a multiplicity of infection (MOIs) 20. *S. Typhimurium* was added to cells into 96-well plates at a MOI50. For *B. thailandensis* infections, plates were then centrifuged at 300 \times g for 5 min at 37°C and incubated for 1 h at 37°C. For *S. Typhimurium* infections, plates were centrifuged at 500 \times g for 10 min at 37°C and incubated at 37°C for 1 hour. Noninternalized bacteria were then removed by washing cells three times with prewarmed medium, and cells were incubated with Opti-MEM containing 250 μ g/ml kanamycin, in the case of *B. thailandensis* infections, or 10 μ g/ml gentamicin, in the case of *S. Typhimurium* infections, in order to kill extracellular bacteria. At the desired time point post-infection (p.i.), cells were either processed for LDH and cytokines release or fixed for immunofluorescence assays.

Measurement of LDH and cytokine release

Lactate dehydrogenase (LDH) was measured by using Cytotoxicity Detection Kit (Sigma-Aldrich) following the manufacturer's protocol. To account for spontaneous

cell permeabilization, LDH release was normalized to 100% lysis and the uninfected control. The levels of IL-1 β were measured by ELISA (TermoFischer), according to the manufacturer's instructions.

Microscopy and image analysis

For fluorescence microscopy of fixed samples, infected BMDMs were washed twice with PBS and fixed for 20 min with 4% paraformaldehyde (Electron Microscopy Sciences). Cells were washed four times with PBS and incubated with Hoechst stain (1:1000) and with CellMask green actin tracking stain (catalog number A57243; Thermo Fisher Scientific, 1:1000) to label F-actin. Samples were analyzed by confocal microscopy by imaging with a Zeiss LSM800 confocal laser scanning microscope using a 63 \times /1.4-numerical-aperture (NA) oil objective by acquiring Z-stacks with a 300-nm step size. Data were further analyzed and processed using Fiji software, and all fluorescence-derived images shown correspond to maximum three-dimensional (3D) projections.

siRNA-mediated knockdown

Wild-type BMDMs were seeded into a 96-well plate and transfected with 25 nM siRNA pools (siGENOME, Horizon Discovery) using TranIT-siQUEST (Mirus). By 24 hours post-transfection (p.t.), cells were primed overnight with mouse IFN γ and then transfected with LPS O111:B4 as described above. LDH release of siRNA knockdown cells was acquired at 6 hours p.t. The siRNA-mediated knockdown effectiveness was tested by RT-qPCR. The siRNAs used are as follows: the siRNA negative control, indicated as nontargeting (NT) siRNA (catalog number D-001206-14-05; siGENOME); siRNA targeting mGBP1 (siGBP1) (M-040198-01), siGBP2 (M-040199-00), siGBP3 (M-063076-01), siGBP4 (M-047506-01), siGBP5 (M-054703-01), and siGBP7 (M-061204-01).

RT-qPCR

For RT-qPCR experiments cells were seeded one day before treatment into 24-well plates at a density of 2.5×10^5 . Cells were either left unprimed or treated overnight with 50ng/mL LPS (LPS from *E. coli* 055:B5, Invivogen), 10ng/mL mouse IFN β (R&D system), 10ng/mL mouse IFN γ (PeproTech), or double primed with LPS (50ng/mL)

and IFN γ (10ng/mL). Total RNA isolation was performed by using RNeasy Mini Kit (QIAGEN) following manufacturer's protocol. RNA was reverse transcribed using SuperScript IV Reverse Transcriptase (Invivogen) with oligo d(T) (Thermo Fischer Scientific). Total RNA was treated with RNase-Free DNase set (QIAGEN) to digest contaminating DNA and with RNaseOUT (Thermo Fischer Scientific) in order to avoid RNA degradation. cDNA was quantified using LightCycler 480 SYBR Green I Master (Roche) and transcript-specific primers. All qPCR results are normalized to actin levels and naïve control set to 1.

4. Discussion

4.1 Research project I: Human GBP1 binds LPS to initiate assembly of a caspase-4 activating platform on cytosolic bacteria

4.1.1) How do GBPs promote Caspase-4 recruitment and activation?

Our data suggest that GBP1, through electrostatic forces, functions as an LPS sensor in the context of Gram-negative bacterial infections. Specifically, we found that the negative charges on the LPS lipid A moiety, as well as the positively charged patch in the globular domain of GBP1, are essential for mediating *Salmonella* targeting and, thus, inducing caspase-4 inflammasome activation³⁶⁰. However, the mechanisms by which GBP1-dependent hierarchical recruitment of GBPs orchestrates caspase-4 recruitment and activation remain unclear. One conceivable mechanism could be the GBPs-mediated transfer of LPS on caspase-4, in analogy to the TLR4-mediated sensing of extracellular LPS. In fact, the detection of extracellular LPS by the TLR4/MD2 complex requires two other key accessory proteins: LPS-binding protein (LBP) and CD14. Mechanistically, LBP molecules catalyze the transfer of LPS molecules from bacterial membranes to CD14, which then delivers LPS to TLR4-MD2^{477,478}. Similarly, GBP1 together with GBP3/4 might shuttle to caspase-4, or at least present LPS molecules or their lipid A moiety to caspase-4, thereby allowing caspase-4 recruitment and activation. Thus, it would be interesting to reconstitute the signaling cascade using recombinant proteins, and structurally characterize the dynamics of the interactions of these components by cryo-EM. Indeed, by comparing mixtures such as *Salmonella*/LPS-GBP1, *Salmonella*/LPS-Caspase-4, and *Salmonella*/LPS-GBP1-Caspase-4, we could gain insights into the function of GBPs in mediating caspase-4 activation, exploring questions such as: does GBP1 disrupt the LPS micelle? Does it destroy the outer membrane of Gram-negative bacteria? Does the interaction of GBP1 with LPS promote caspase-4 recruitment or activation? Further, the purification and structural analysis of GBP mutants, lacking their GTP/GDPase activity or harboring post-translational modification (e.g. farnesylation), may represent a powerful tool to elucidate the role of the GTP hydrolysis and post-translational modifications in LPS sensing. Eventually, crystal structural analysis of the GBPs-Caspase-4 complex could clarify the nature of interactions between the GBPs themselves and with Caspase-4.

4.1.2) What is the role of GBPs in response to parasitic infections?

Despite their role in antibacterial defense, GBPs have also been described to participate in the restriction of intracellular parasites, such as *Toxoplasma*. Indeed, it has been shown that in IFN γ -stimulated human macrophages, GBP1 is recruited to PCVs, triggering apoptosis of the infected cell via AIM2-dependent caspase-8 activation. Surprisingly, cells transfected with soluble *T. gondii* antigens bypass the GBP1 requirement for cell death activation, indicating that GBPs could release microbial ligands for receptor sensing⁴²⁰. This raises the question of how GBP1 binding on PCVs triggers the release of *Toxoplasma* content. Since in mouse BMDMs bacterial lysis is triggered by Gbp-dependent recruitment of Irgs (which are not expressed in humans)²⁵⁶, it is conceivable that GBPs drive the recruitment of additional IFN-stimulated proteins with bacteriolytic activity; and that besides the PCV, also the parasite itself is destroyed in a Gbp-dependent manner. If this requires PCV lysis and then recruitment of Gbps, Irgs, or other lytic host factors on the parasite itself, or if PCV lysis directly affects parasite stability remains to be investigated. Work from Kravets et al. suggests though that Gbps target the membrane of parasites after the rupture of the PCV and destroy the parasite directly⁴⁷⁹.

Moreover, it is yet undefined the ligand that drives GBP1 recruitment onto *Toxoplasma*-containing vacuoles. The parasitophorous vacuole membrane (PVM) represents a dynamic interface between the parasites and the cytoplasm of the host cells. Shortly after entry, *Toxoplasma* secretes several proteins through vesicle formation, such as ROP and GRA proteins, which are crucial for the intravacuolar survival of the parasite. ROPs, along with Myc regulatory proteins (MYRs), are also part of the PVM translocation system, which allows the translocation of GRAs and other parasite-derived proteins into the cytosol of the host cell, an essential step for host cell manipulation⁴⁸⁰. Furthermore, many parasites feature unusual lipids, such as lipophosphoglycan in their membranes, which may act as PAMPs for GBPs in analogy to bacterial LPS. Hence, along with ROPs, GRAs, and MYRs, negatively charged parasite-derived molecules could be translocated onto the PVM and detected by GBP1, which would extend the GBP1 function beyond LPS recognition.

4.1.3) Does lipid A acylation have a role in GBP recruitment?

LPS, the main component of the outer leaflet of the outer membrane of Gram-negative bacteria, is composed of the lipid A moiety, which acts as a membrane anchor in the bacterial outer membrane, attached to a core oligosaccharide that harbors a variable number of O-antigen units. The lipid A portion of LPS comprises two glucosamine residues with hydrophobic acyl chains, which may vary in number, position, and length depending on the bacterial species to which they belong⁴⁸¹. While tetra-acylated lipid A escapes recognition by caspase-11, human caspase-4 responds to a wide range of acylations (tetra-, penta-, and hexa-acylated lipid A), underlining intrinsic differences among non-canonical inflammatory caspases^{482,483}. Indeed, both *S. Typhimurium*, which has a hexa-acylated lipid A, and *F. novicida*, which harbors a tetra-acylated lipid A, drive caspase-4-mediated pyroptosis^{360,361,455}. However, unlike *S. Typhimurium*, which is coated by GBP1-4, *F. novicida* is efficiently targeted by GBP1 and 2 but escapes GBP3 and GBP4 recognition⁴⁴². Strikingly, targeting of GBP3 was partially recovered in human macrophages infected with *F. novicida* $\Delta lpxF$ mutants (with penta-acylated LPS lipid A)⁴⁴². These results provide further support for the notion that lipid A may be the essential mediator of GBPs-bacteria interaction. They may also suggest that lipid A acylation determines the requirement of different sets of GBPs to activate caspase-4. The use of bacterial mutants with different acylation rates could provide a useful tool to understand whether GBP recruitment is affected by lipid A composition. Furthermore, in *Salmonella*-infected cells, GBP3 and GBP4 are crucial to mediate caspase-4 recruitment and activation³⁶⁰. Therefore, it would be interesting to investigate how differences in GBP coating on *Salmonella* (GBP1-4) and *Francisella* (GBP1/GBP2) impact caspase-4 activation.

4.1.4) Is there a unifying model that explains the GBP-dependent caspase-4 activation?

Despite our work and the related work of Wandel and coworkers showing that GBP1-4 converts cytosolic Gram-negative bacteria into a signaling hub for caspase-4 activation, these two studies exhibit discrepancies^{360,361}. Collectively, our findings demonstrate that simultaneous recruitment of GBP1 and GBP2 on cytosolic *Salmonella* is followed by recruitment of GBP3 and GBP4, suggesting a model

whereby GBP1 and GBP4 are required for caspase-4 recruitment and GBP3 for its activation. Indeed, by inducing eGFP-GBP2, -GBP3, and -GBP4 in naïve HeLa cells co-expressing caspase-4 and mCherry-GBP1, we observed that GBP1 and GBP2 alone are not sufficient to trigger caspase-4 recruitment on *Salmonella*, whereas co-expression of GBP1-GBP4, and to a lesser extent GBP1-GBP3, is sufficient to restore caspase-4 trafficking on cytosolic *Salmonella*³⁶⁰. Further, we proved that the expression of single GBPs in naïve cells does not trigger cell death in response to LPS transfection, while co-expression of GBP1 and GBP3 partially restores LPS-induced pyroptosis³⁶⁰. Surprisingly, although GBP4 is required for caspase-4 recruitment on *Salmonella*, co-expression of GBP1-GBP4 did not affect cell death following transfection with LPS, implying that GBP4 does not participate in caspase-4 activation but instead in its recruitment³⁶⁰. In a similar way, Wandel et al. showed that GBP3 is specifically required for caspase-4 activity; however, their data correlate GBP2, along with GBP1 and GBP4, with the recruitment of caspase-4 on cytosolic invading bacteria³⁶¹. Thus, although both models describe GBP1 as the most upstream member of the family and attribute the same functions to GBP3 and GBP4, they diverge in the role assigned to GBP2, most likely due to intrinsic differences in the cell line used in the studies. More profound differences in the GBP functions in activating the human non-canonical inflammasome are highlighted in the studies of Coers et al. Indeed, they proposed that GBP1 polymer organized in ring-like structures dock the bacterial surface and act as an O-antigen surfactant. Penetration into the O-antigen barrier is followed by depolymerization of GBP1 and insertion of individual GBP1 molecules into the outer membrane, allowing the formation of GBP1 protein sheets that envelop the bacteria^{363,449}. These results would suggest the presence of interactions between GBP1 and the O-antigen barrier, however, the LPS of *E. coli* mutants lacking the O-antigen is still bound by GBP1, just as *Salmonella* mutants lacking the O-antigen or outer core are effectively targeted by GBP1 and caspase-4³⁶⁰. In addition, the structure of GBP1 pipelines, formed by the docking of polymeric GBP1, and the ring structure of polymers await further demonstration in a cellular system. Further, a recently published pre-print from the same group demonstrates that overexpression of either GBP1 or GBP2 triggers cell death in IFN γ -primed GBP1-deficient A549 cells after *S. flexneri* infection, raising the hypothesis that GBP2 may mediate pyroptosis in a GBP1-independent manner⁴⁸⁴.

Interestingly, *in vitro* GBP-binding assays show that GBP2 binding on the bacterial surface depends on mixed polymer formation with GBP1, implying that the GBP2-dependent cell death observed in GBP1-deficient cells does not require GBP2 docking⁴⁸⁴. Therefore, it would be interesting to investigate whether mixed GBP1/GBP2 polymers are organized in ring-like structures, as proposed for GBP1 polymers, or whether the aforementioned model needs to be revised. Furthermore, whereas GBP2-mediated bacterial killing requires IFN γ stimulation, LPS transfection results in GBP1- and GBP2-dependent cell death independent of priming; in fact, like GBP1, GBP2 can bind LPS directly⁴⁸⁴. These results are in sharp contrast with our data showing that biotin-LPS is able to pull down GBP1 and GBP3, but not GBP2 and -4³⁶⁰. Likewise, in lysates of epithelial cells only GBP1 and GBP3 associate with caspase-4 in an LPS-dependent manner³⁶¹. Hence, we excluded the participation of GBP2 in direct recognition of LPS. Surprisingly, they also found that GBP1 binding is dispensable to mediate pyroptosis and bacterial killing. Thus, other IFN-inducible genes upstream of GBP1 and GBP2 might participate in the LPS recognition and trigger caspase-4 activation⁴⁸⁴. In contrast to the notion that the complex formed by GBP binding on bacterial surfaces promotes caspase-4 activation without the requirement of additional IFN γ -inducible factors. Also, our data demonstrate that individual GBP expression is not sufficient to trigger LPS-induced pyroptosis in response to cytosolic LPS^{360,361}. Importantly, this study ascribes a redundant role to GBP1 and GBP2 in A549 lung epithelial cells, which could be in favor of cell- or tissue-specific functions of GBPs. Indeed, GBP2 can directly bind LPS but with a lower affinity than GBP1, so it might be beneficial in some tissues (e.g., gut) to generate a less robust and more specific immune response against harmful invading bacteria⁴⁸⁴. However, its physiological relevance has yet to be proven. Their data also show that a triple arginine motif on the C-terminus of GBP1 is responsible for GBP binding on *Shigella*⁴³⁰. In contrast, mutation of the triple arginine motif does not affect the binding of GBP1 to LPS micelles, although the GBP1 triple arginine mutant fails to target *Salmonella*³⁶⁰. Thus, rather than directly participating in LPS recognition, this C-terminal motif might participate in GBP coat stabilization. Overall, further studies are needed to define a model that provides a detailed mechanistic framework to explain how GBPs recognize and exploit Gram-negative bacteria's cell wall components.

4.2 Research Project II: Guanylate-Binding Protein-Dependent Noncanonical Inflammasome Activation Prevents *Burkholderia thailandensis*-Induced Multinucleated Giant Cell Formation

4.2.1) Why does the GBPs coat not block the polymerization of *Burkholderia* actin tails?

Actin-based motility enables some cytosolic bacteria, such as the Gram-negative *S. flexneri* and *B. thailandensis*, or the Gram-positive *Listeria monocytogenes*, to move within the cells and spread into neighboring cells without exiting the intracellular environment. While *Listeria* does not recruit GBPs, it was shown that the hierarchical recruitment of human GBP1-4 on *Shigella*, reliant on GBP1, inhibits its actin-based motility and, thus, cell-to-cell spread^{430,431}. Interestingly, *Shigella* re-establishes its actin-dependent motility by triggering the proteasomal degradation of GBPs through the bacterial effector IpaH9.8, an E3 ubiquitin ligase released into the cytosol of the host cell⁴³¹. Surprisingly, the hGBP1-4 coat on *Burkholderia* does not impair its ability to polymerize actin tails and spread throughout the cells⁴⁴⁸. To enable actin-based motility, pathogens encode proteins that mimic host actin nucleator factors to promote the polymerization of actin monomers into actin filaments, which have been identified in the trans-outer membrane IcsA and BimA autotransporters of *Shigella* and *Burkholderia*, respectively^{485,486}. When localized to a pole of the bacterium, IcsA and BimA hijack the host actin polymerization machinery by binding the actin regulatory protein N-WASP, which in turn interacts with the actin nucleator complex Arp2/3⁴⁸⁷. It has been shown that GBP1-targeted *Shigella* loses unipolar IcsA localization, resulting in a lack of N-WASP and Arp2/3 recruitment⁴⁴⁹. A comparable experimental setting might therefore be useful to test whether GBP recruitment on *Burkholderia* leads to a similar outcome. However, it is possible to speculate that different functions of the GBP coat are related to intrinsic differences within bacterial nucleating factors. Indeed, polar localization of IcsA is ensured by outer membrane IcsP proteases, which cleave the N-WASP interaction domain of non-polar-localized IcsA⁴⁸⁸. While the localization of BimA is mediated by the unipolar protein BimC, which is localized underneath the actin tail polymerization site, by a poorly defined mechanism⁴⁸⁹. Therefore, it would be interesting to study whether, in the case of *Shigella* infections, the GBP coat could form a barrier that hinders IcsP protease activity while blocking the recruitment of N-WASP and Arp2/3.

Whereas localization of BimC in the inner leaflet of the bacterial outer membrane could overcome such inhibition. Intriguingly, differently from what we observed in human epithelial cells, Gbp recruitment on cytosolic *B. thailandensis* restricts bacterial actin tail polymerization via inhibition of the Arp2/3-dependent actin polymerization machinery and, thus, MNGC formation in murine macrophages⁴³³. It is conceivable that this discrepancy is a result of species-dependent differences; for instance, murine macrophages may express additional IFN-inducible factors which cooperate with the Gbps to restrict *B. thailandensis* spread. In addition, it would be interesting to investigate whether the Gbp coat also impairs *B. thailandensis* actin tail polymerization in murine epithelial cells or whether this mechanism is cell-type specific.

4.2.2) Would *B. pseudomallei* be able to activate caspase-4-mediated pyroptosis?

The *Burkholderia pseudomallei* complex includes the Gram-negative bacteria *B. mallei*, the etiological agent of glanders in equine, *B. pseudomallei*, the causative agent of human melioidosis, and the closely related but less pathogenic species *B. thailandensis*. Although *B. pseudomallei* and *B. thailandensis* share an identical intracellular life cycle, *B. pseudomallei* appears to trigger weaker immune responses than *B. thailandensis*, most likely related to unique features in its LPS structure. Indeed, in vitro stimulation of human and murine macrophages with LPS from *B. pseudomallei* results in reduced production of TNF α , nitric oxide, and inflammatory cytokines (e.g., IL-6; IL-10) compared with those stimulated with LPS from *B. thailandensis*, enabling pathogens to escape macrophage killing⁴⁹⁰. Sepsis is the most common cause of death in patients affected by melioidosis and it has been described to be mediated by the lipophilic portion of LPS, the lipid A moiety. Mass-spectrometry analysis of *B. pseudomallei* lipid A revealed that the bi-phosphorylated disaccharide backbone is modified with 4-amino-4-deoxy-arabinose (Ara4N) residues and penta-acylated with tetradecanoic acid (C_{14:0}), 2-hydroxytetradecanoic (C_{14:0}(2-OH)), 3-hydroxytetradecanoic acid (C_{14:0}(3-OH)), hexadecanoic acid (C_{16:0}), and 3-hydroxyhexadecanoic acid (C_{16:0}(3-OH)). While lipid A of *B. thailandensis* is penta- or tetra-acylated with a similar fatty acid composition, except for C_{14:0}(2-OH) which is found exclusively in *B. pseudomallei*. Moreover, it presents a different

amount of Ara4N substitutions⁴⁹⁰. Alteration in the number or length of acyl chains or capping of phosphate groups is used by many gram-negative bacteria as a strategy to evade antibacterial mechanisms. In fact, the lipid A of *B. thailandensis* and *B. pseudomallei* differs from the more biologically active form found in *E. coli* and *S. Typhimurium*, which consists of hexa-acylated lipid A (with 12 or 14 carbons) and unmodified phosphate groups. Thus, the unique characteristics found in lipid A of *B. pseudomallei* may explain why it succeeds in dampening the immune response of host cells. Further studies might be useful to understand whether the GBP-dependent activation of the non-canonical inflammasome that we observed in human epithelial cells infected with *B. thailandensis* might facilitate *B. pseudomallei* clearance. Or whether its unique lipid A composition escapes GBP recognition. However, in Switzerland *B. pseudomallei* is classified as a biosafety level 3 pathogen, which prevented us from testing its ability to activate or inhibit the inflammasome. In addition, its LPS could be used to further investigate the role that acylation and phosphate groups exert in GBP-mediated LPS sensing.

4.2.3) Can GSDMD directly kill bacteria?

In agreement with the previous studies showing that in mouse macrophages Nlrp4-dependent IL-18 release drive IFN γ -dependent caspase-11 activation in mouse epithelial cells⁴⁶⁹, we found that in human epithelial cells non-canonical inflammasome activation provides protection against *B. thailandensis*⁴⁹¹. Furthermore, in correlation with the aforementioned study, in hMDMs infected with *B. thailandensis*, cell death is driven by IFN γ -dependent and -independent mechanisms, and IFN γ signaling promotes faster clearance of the bacterial replication niche, acting as a second layer of defense⁴⁹¹. Taken together, these results suggest that GSDMD-mediated pyroptosis in response to canonical inflammasome activation is restricted to immune cells. Interestingly, caspase-1-mediated processing of recombinant GsdmD has been shown to directly kill *B. thailandensis*. Indeed, bacteria harvested from wild-type mice were more susceptible to microbicidal effectors (e.g., hydrogen peroxide) than those harvested from *Gsdmd*^{-/-} mice⁴⁹². Hence, the processing of GSDMD by inflammatory caspases may represent an additional microbicidal mechanism driven by pyroptosis. Since both mouse and human caspases process GSDMD in the linker between its amino-terminal and carboxy-terminal domains, it is

conceivable that human GSDMD^{N-term} may also function as a direct microbicidal effector⁴⁵³. To this end, it would be important to determine whether GSDMD^{N-term} co-localize with cytosolic bacteria. In agreement with the proposed function of GSDMD as a microbicidal effector, bacterial viability was found to be severely impaired in wild-type IFN γ -primed HeLa cells compared with GSDMD-deficient cells; however, in this system, it is difficult to pinpoint the exact contribution of GSDMD-directed killing⁴⁹¹. Reconstitution of *CASP4*^{-/-} cells with an inducible GSDMD^{N-term} could be a useful tool to dissect whether GSDMD is recruited onto bacteria and directly participates in their clearance or whether the enhanced bacterial viability detected in GSDMD-deficient cells is purely determined by caspase-4-induced pyroptosis. Although the increased cell death observed in IFN γ -stimulated hMDMs could result in increased processing of GSDMD, which could contribute to displaying its localization on cytosolic bacteria under more physiological conditions, the rapid cell death detected, and the low efficiency of any genetic manipulation would make it difficult to use primary human macrophages to decipher the microbicidal activity of GSDMD.

4.3 Research Project III: Interferon gamma-induced murine guanylate-binding protein 4 (GBP4) orchestrates caspase-11-mediated pyroptosis.

4.3.1) Are the non-canonical mouse and human inflammasomes regulated differently by GBPs?

Gs, a family of large IFN-inducible GTPases, have been described as LPS sensors upstream of the human and murine non-canonical inflammasome. Nevertheless, despite their requirement for caspase-4/-11 activation, they function differently in the two experimental model systems. Indeed, while the hGBP1-4 coating on Gram-negative bacteria forms a signaling platform for caspase-4 recruitment and activation^{360,361}, bacteria decorated by mGbp2 and mGbp5 were proposed to require an additional factor, Irgb10, to trigger caspase-11 activation²⁵⁶. The bacteriolytic activity of Irgb10, which belongs to the family of IFN-inducible IRGs no longer expressed in humans (apart from a truncated form of the IRGM copy and IRGC), is hypothesized to liberate bacterial ligands, such as LPS, to elicit caspase-11-induced cell death²⁵⁶. Likewise, Irgb10-dependent release of bacterial DNA into the host cell cytosol leads to activation of the Aim2 inflammasome in response to infection with *F. novicida*, whose tetra-acylated LPS fails to be recognized by caspase-11 (but it is recognized by caspase-4)^{256,455,483}. Intriguingly, the lack of caspase-11 severely impairs inflammasome activation in response to Gram-negative bacteria, although these are targeted by Irgb10, which could potentially trigger Aim2 inflammasome activation^{185,256}. It is therefore conceivable that Irgb10 exerts several functions beyond its bacteriolytic activity, for example, it could stabilize the Gbp coat by promoting caspase-11 activation. These data may also suggest that caspase-11 has an upstream function in canonical inflammasome activation, as proposed by the studies of Hara et al. on *Listeria*²⁷⁹. In summary, although further studies are needed to better define how human Gbps interact with LPS, the caspase-4 activation pathway clearly relies on the signaling hub formed by hGBPs^{360,361,491}, whereas the exact mechanisms by which LPS activates caspase-11 and mGbps promote caspase-11-induced pyroptosis await to be fully elucidated. Here, it would be important to show if Gbps recruit caspase-11 to the bacterial surface, and if this is affected by the absence of Irgb10.

4.3.2) What are the murine Gbps involved in LPS-driven caspase-11 activation?

A recent pre-print using CRISPR-Cas9 chromosomal ablation of individual *Gbp* on chromosome 3 revealed that mGbp2 and mGbp3 are critical for mediating caspase-11 activation in response to intracellular LPS³⁷⁷, which is corroborated by our. Knock-down studies. Indeed, in agreement with our data, *Gbp2*^{-/-} and *Gbp3*^{-/-} BMDMs show defective release of LDH and IL-1 β in response to LPS transfection, which is rescued by their genomic complementation³⁷⁷. Localization of Gbp3 on LPS is impaired in BMDMs lacking Gbp2, suggesting that mGbp2 is the most upstream IFN-inducible factor involved in noncanonical inflammasome activation, and thus the functional ortholog of human GBP1³⁷⁷. Interestingly, while Gbp2 is designated as the factor driving the interaction of caspase-11 with its ligand, as demonstrated by pull-down assays, the study hypothesizes that Gbp3 does not promote caspase-11 activation but instead supports the pre-assembly of the Gsdmd^{N-term} into pre-pores complexes immediately after cleavage by caspase-11, and the trafficking of these to the plasma membrane. Mechanistically, conformational changes in the Gbp3 structure following GTP hydrolysis aid the integration of Gsdmd^{N-term} into complexes. Yet, no direct interaction between Gbp3 and Gsdmd was detected, suggesting that an additional factor is needed for the formation of Gsdmd macromolecules³⁷⁷. Since this model contradicts a number of studies into inflammasome-mediated GSDMD activation,

further analyses are needed to investigate the role of Gbp3 in driving Gsdmd assembly and trafficking. In particular, it is known that GSDMD-dependent cell death in response to canonical inflammasome stimuli is not affected by the loss of Gbp2 or Gbp3, nor is IFN priming required for GSDMD pore formation.

Furthermore, although Gbp2 and Gbp3 are protective in the murine LPS sepsis shock model, the Gbp-caspase-11 axis might function differently in response to *in vivo* infection with Gram-negative bacteria. For example, albeit the lack of mGbp1 does not affect pyroptosis in response to LPS delivery³⁷⁷, *Gbp1*-deficient mice infected with *S. Typhimurium* and *S. flexneri* succumb earlier, whereas *mGbp2* knockout mice are protected only in the early stage of infection³⁶¹. Moreover, unlike what has been proposed for LPS transfection-dependent pyroptosis, which requires only Gbp2 and Gbp3³⁷⁷, other studies have suggested that mGbp5, together with mGbp2, is involved in the caspase-11-dependent pyroptosis upon *E. coli* infection

²⁵⁶. However, the role of individual mGbps in response to Gram-negative bacteria has been poorly explored; therefore, Gbp-knockout mice may help to understand their specific functions. Moreover, our data show that Gbps are differentially regulated in response to several priming conditions, an important factor to consider in order to achieve a more comprehensive view of their participation in noncanonical inflammasome activation.

4.3.3) What is the role of the Gbp cluster on chromosome 5 in non-canonical inflammasome activation?

Collectively, our data show that murine Gbps encoded by the chromosome 5 cluster are required for caspase-11-mediated pyroptosis in response to cytosolic LPS. Remarkably, the involvement of Gbp^{Chr5} in LPS-driven caspase-11 activation is priming-dependent and only detectable with IFN γ priming, but not in cells primed with LPS or type I IFN. Among the 6 Gbps on chromosome 5, mGbp4 plays a prominent role, revealing a close similarity in the hierarchical organization of murine and human GBPs. However, it is yet to be clarified the contribution of other GbpChr5 in caspase-11-mediated pyroptosis. In human epithelial cells, the GBPs forming the signaling hub that promotes the recruitment and activation of caspase-4 on *Salmonella*, have distinct functional roles, in fact, GBP1 and GBP4 are required for the recruitment of caspase-4, while GBP3 for its activation^{360,361}. It is therefore conceivable that mGbp4 may enhance caspase-11 recruitment or mimic the activator function of hGBP3, albeit hGBP3 and mGbp4 are not tightly related phylogenetically⁴⁹³.

Interestingly, unlike cell death induced by LPS transfection, *Salmonella*-triggered cell death in IFN γ -primed mouse macrophages is only slightly or not dependent on GbpChr5. Further studies are needed to verify whether this is due to a *Salmonella* effector that specifically blocks Gbp4, or intrinsic differences between the transfected LPS (*E. coli*) and *Salmonella* LPS, which might account for the differential requirement for Gbp4.

Another important experiment is to investigate the hierarchical recruitment of mouse Gbps to bacteria, in order to reveal similarities or differences to the human GBP system. Here, the use of immortalized BMDM expressing fluorescently-tagged Gbps may reveal whether Gbps are differentially recruited on cytosolic *Salmonella* and LPS. Finally, the reconstitution of single Gbps in Gbp^{Chr3/Chr5}-deficient mice may help

to dissect individual functions of mGbp2, mGbp3, and mGbp4. To this end, we are currently generating double knockout mice. Eventually, the generation of chimeras, together with point mutations and biochemical analysis, and their evaluation for increased or lost targeting toward LPS and *Salmonella*, could unveil protein regions essential for non-canonical inflammasome activation.

4.4 Discussion and future research

During my PhD, I investigated the role of human GBPs in activating the caspase-4 non-canonical inflammasome in response to *S. Typhimurium* and *B. thailandensis* in human epithelial cells and macrophages.

Our data suggest that GBP1 functions as an LPS sensor in the context of Gram-negative bacterial infections. Mechanistically, we found that the negative charges on the LPS lipid A moiety, as well as the positively charged patch in the globular domain of GBP1, are essential for mediating *Salmonella* targeting and, thus, inducing caspase-4 inflammasome activation³⁶⁰. However, the mechanism by which GBPs promote caspase-4 recruitment and activation has not yet been defined. Indeed, it remains unclear whether GBPs function as LBP-like proteins, catalyzing the transfer of LPS molecules to caspase-4, or whether they disrupt the outer membrane of Gram-negative bacteria by making the LPS lipid A moiety accessible to direct recognition by caspase-4. Therefore, reconstruction of the signaling cascade using recombinant proteins and structural characterization of the interactions of these components by cryo-EM can help establish a model that provides a detailed mechanistic framework to explain how GBPs recognize and exploit the components of Gram-negative bacteria outer membrane. Moreover, it has been suggested that lipid A acylation determines the requirement of different sets of GBPs. Indeed, *S. Typhimurium*, which harbors an hexa-acylated lipid A, is coated by GBP1-4^{360,361,455}, whereas *F. novicida*, whose lipid A is tetra-acylated, is efficiently targeted by GBP1 and 2 but escapes GBP3 and GBP4 recognition⁴⁴². The use of bacterial mutants with different acylation rates could provide a useful tool to understand whether GBP recruitment is affected by lipid A composition and investigate how differences in GBP coating on *Salmonella* (GBP1-4) and *Francisella* (GBP1/GBP2) impact caspase-4 activation. Intriguingly, GBP1 is also recruited on *Toxoplasma* PCVs, where it triggers the apoptosis of the infected cell via AIM2-dependent caspase-8 activation⁴²⁰. Whether the recruitment of GBP1 on *Toxoplasma*-containing vacuoles

promotes the release of parasite ligands for receptor sensing by exerting lytic activity itself or by promoting the recruitment of additional factors with membranolytic activity remains to be determined. Moreover, it is unknown the ligand that triggers GBP1 recruitment on PCVs, which would extend the function of GBP1 beyond LPS recognition.

We also showed that GBPs block *B. thailandensis*-induced MNGC formation by triggering rapid cell death of infected cells. Specifically, GBP1 drives the recruitment and activation of caspase-4, thereby eradicating the intracellular replication niche of *Burkholderia* and its spreading through actin tails. Further studies are needed to understand whether the GBPs have a protective role against *Burkholderia* species more pathogenic for human, such as *B. pseudomallei*, the causative agents of human melioidosis. Indeed, despite *B. thailandensis* and *B. pseudomallei* share a similar intracellular life cycle, their lipid A differs in the number of acyl chains and modification of phosphate groups, a strategy used by many Gram-negative bacteria to evade antibacterial mechanisms. Moreover, unlike other intracellular bacteria whose actin-tail-based motility is inhibited by GBPs, the coat of GBPs on *Burkholderia* does not impair its ability to polymerize actin tails and spread throughout cells. Therefore, it would be interesting to study whether this is due to intrinsic differences within bacterial nucleating factors. Intriguingly, differently from what we observed in human epithelial cells, Gbp recruitment on cytosolic *B. thailandensis* restricts bacterial actin tail polymerization in murine macrophages⁴³³. This discrepancy may be a result of species-dependent differences - for instance, murine macrophages may express additional IFN-inducible factors which cooperate with the Gbps to restrict *B. thailandensis* spread - or whether this mechanism is cell-type specific.

Finally, I sought to define which individual murine Gbps on chromosome 3 and chromosome 5 were necessary for LPS-induced non-canonical inflammasome activation. Although further studies are needed to better define how human GBPs interact with LPS, the caspase-4 activation pathway clearly relies on the signaling hub formed by hGBPs^{360,361,491}, whereas further studies are needed to elucidate how murine Gbps promote caspase-11-induced pyroptosis. It would be important to show if, similar to human GBPs, mGbps recruit caspase-11 to the bacterial surface or to cytosolic LPS. Interestingly, our data show that murine Gbps encoded by the chromosome 5 cluster are required for caspase-11-mediated pyroptosis in response

to cytosolic LPS. Their involvement is priming-dependent and only detectable with IFN γ priming. Investigate the hierarchical recruitment of mouse Gbps to bacteria by using immortalized *Gbp*^{Chr3/Chr5}-deficient BMDMs expressing fluorescently-tagged Gbps may help to get insight into the individual functions of mGbps. Eventually, further studies are needed to better define the role of individual GBPs in activating the human and murine non-canonical inflammasome.

5. Appendix

Related article: Caspase-1 cleaves Bid to release mitochondrial SMAC and drive secondary necrosis in the absence of GSDMD.

Rosalie Heilig¹, Marisa Dilucca¹, Dave Boucher¹, Kaiwen W Chen¹, Dora Hancz¹, Benjamin Demarco¹, Kateryna Shkarina¹, Petr Broz^{1,†}

¹Department of Biochemistry, University of Lausanne, Chemin des Boveresses 155, 1066 Epalinges, Switzerland.

[†]Corresponding author. Email: petr.broz@unil.ch

Statement of contribution:

M. Dilucca: resources, data curation, investigation, and methodology

Specific contributions:

Generation of Bid⁻, Casp9⁻, Casp-8⁻, Casp-8/Casp9⁻, Casp3⁻, and Casp3/7-deficient iBMDMs using the genome-editing system Alt-R-CRISPR/Cas (IDT).

Test of the bulk population by T7 endonuclease assay.

Generation of single clones for the Casp9⁻, Casp-8⁻, Casp-8/Casp9⁻, Casp3⁻ and Casp3/7-deficient bulk population by limiting dilution and verification by immunoblotting that protein expression is absent.

Processing of liver and spleen from *S. Typhimurium*-challenged wild-type, Casp1^{-/-}, and Gsdmd^{-/-} mice (experiments not shown in the publication).



Caspase-1 cleaves Bid to release mitochondrial SMAC and drive secondary necrosis in the absence of GSDMD

Rosalie Heilig, Marisa Dilucca, Dave Boucher , Kaiwen W Chen , Dora Hancz, Benjamin Demarco , Kateryna Shkarina, Petr Broz

Caspase-1 drives a lytic inflammatory cell death named pyroptosis by cleaving the pore-forming cell death executor gasdermin-D (GSDMD). *Gsdmd* deficiency, however, only delays cell lysis, indicating that caspase-1 controls alternative cell death pathways. Here, we show that in the absence of GSDMD, caspase-1 activates apoptotic initiator and executioner caspases and triggers a rapid progression into secondary necrosis. GSDMD-independent cell death required direct caspase-1-driven truncation of Bid and generation of caspase-3 p19/p12 by either caspase-8 or caspase-9. tBid-induced mitochondrial outer membrane permeabilization was also required to drive SMAC release and relieve inhibitor of apoptosis protein inhibition of caspase-3, thereby allowing caspase-3 auto-processing to the fully active p17/p12 form. Our data reveal that cell lysis in inflammasome-activated *Gsdmd*-deficient cells is caused by a synergistic effect of rapid caspase-1-driven activation of initiator caspases-8/-9 and Bid cleavage, resulting in an unusually fast activation of caspase-3 and immediate transition into secondary necrosis. This pathway might be advantageous for the host in counteracting pathogen-induced inhibition of GSDMD but also has implications for the use of GSDMD inhibitors in immune therapies for caspase-1-dependent inflammatory disease.

DOI [10.26508/lsa.202000735](https://doi.org/10.26508/lsa.202000735) | Received 7 April 2020 | Revised 16 April 2020 | Accepted 16 April 2020 | Published online 28 April 2020

Introduction

Inflammasomes are cytosolic signalling platforms assembled after the recognition of host- or pathogen-derived danger signals by cytosolic pattern recognition receptors, such as pyrin, AIM2, and members of the Nod like receptor (NLR) protein family (Broz & Dixit, 2016). These complexes serve as activation platforms for caspase-1, the prototypical inflammatory caspase. Active caspase-1 cleaves the pro-inflammatory cytokines IL-1 β and IL-18 to their mature bioactive form and induces a lytic form of cell death known as pyroptosis, by processing the cell death executor gasdermin-D (GSDMD) (Kayagaki et al, 2015; Shi et al, 2015). Caspase cleavage

at the residue D276 in mouse (D275 in human) removes the inhibitory GSDMD^{CT} and allows GSDMD^{NT} to translocate to cellular membranes and form permeability pores, which disrupt ion homeostasis and the electrochemical gradient (Kayagaki et al, 2015; Shi et al, 2015; Aglietti et al, 2016; Ding et al, 2016; Liu et al, 2016; Sborgi et al, 2016). GSDMD is also cleaved by caspase-11 in mice and by caspase-4 and caspase-5 in humans, which are activated by the so-called noncanonical inflammasome pathway in response to LPS stemming from infections with cytosolic Gram-negative bacteria (Kayagaki et al, 2011, 2013; Hagar et al, 2013; Shi et al, 2014). Uncontrolled inflammasome activation by gain-of-function mutations in inflammasome receptors or in the context of sterile inflammatory disease has been linked to a number of hereditary and acquired inflammatory diseases, such as cryopyrin-associated periodic syndrome (Muckle-Wells syndrome), but also gout, Alzheimer's disease, and atherosclerosis (Masters et al, 2009). It is, thus, of high interest to target and inhibit inflammasome assembly or downstream effector processes such as GSDMD pore formation and IL-1 β release.

Although *Gsdmd* deficiency results in complete abrogation of caspase-11 (-4)-induced lytic cell death, it only delays caspase-1-induced cell lysis (He et al, 2015; Kayagaki et al, 2015). Caspase-1 activation in *Gsdmd*^{-/-} cells correlates with high levels of caspase-3/7 and caspase-8 activity, but whether these apoptotic caspases trigger lysis of *Gsdmd*-deficient cells after caspase-1 activation has not been proven (He et al, 2015), and activation of apoptotic caspases has been observed to occur even in inflammasome-activated WT cells (Lamkanfi et al, 2008; Sagulenko et al, 2018). The lytic death of *Gsdmd*^{-/-} cells is also in contrast to the notion that apoptosis is non-lytic and, thus, immunologically silent. However, it is also known that prolonged apoptotic caspase activity will result in apoptotic cells losing membrane integrity, a process termed "secondary necrosis." Apoptosis is executed by caspase-3/-7, which themselves are activated by either caspase-8 (extrinsic apoptosis pathway) or caspase-9 (intrinsic or mitochondrial apoptosis pathway). Ligation of death receptors at the plasma membrane (FasR, tumor necrosis factor receptor, and Trail) results in the assembly of the death-inducing signalling complex or tumor necrosis factor receptor complex IIa/b, which activates caspase-8, the initiator caspase of the extrinsic pathway. In type-I cells, caspase-8

Department of Biochemistry, University of Lausanne, Epalinges, Switzerland

Correspondence: petr.broz@unil.ch

activity is sufficient to activate the executioner caspases, whereas in type-II cells, caspase-8 requires activation of the intrinsic pathway in addition (Jost et al, 2009). Here, caspase-8 cleaves the Bcl-2 family protein Bid to generate a truncated version (tBid), which triggers Bax/Bak-induced mitochondrial outer membrane permeabilization (MOMP). MOMP results in the release of second mitochondria-derived activator of caspases (SMAC), ATP, and cytochrome c to promote intrinsic apoptosis via formation of the apoptosome. This complex consists of apoptotic protease-activating factor 1 (APAF1), cytochrome c, ATP, and caspase-9 and serves as an activation platform for caspase-9, which in turn cleaves caspase-3. Apoptosis is a tightly regulated process, and disturbance of the equilibrium of cytosolic pool of pro- and anti-apoptotic Bcl-2 family proteins can result in MOMP, apoptosis induction, and cell death (Riley, 2018; Vince et al, 2018). To prevent accidental activation of apoptosis, inhibitor of apoptosis proteins (IAPs), in particular X-linked inhibitor of apoptosis protein (XIAP), suppresses caspase-3/7 and caspase-9 activation by direct binding to the caspases via baculovirus IAP repeat (BIR) domains (Roy et al, 1997; Takahashi et al, 1998; Bratton et al, 2002; Scott et al, 2005). SMAC, which is released during MOMP, antagonizes IAPs, thus removing the brake on caspase auto-processing and allowing full activity of the executioner caspases and apoptotic cell death (Du et al, 2000; Verhagen et al, 2000; Wilkinson et al, 2004).

Here, we investigate the mechanism that induces lytic cell death after caspase-1 activation in *Gsdmd*-deficient cells. We show that cell death in *Gsdmd*^{-/-} macrophages requires caspase-1, Bid-dependent mitochondrial permeabilization, and the executioner caspase-3. Remarkably, *Gsdmd*-deficient cells form apoptotic blebs and bodies only transiently, before shifting rapidly to a necrotic phenotype that is characterized by extensive membrane ballooning. Unexpectedly, we found that Bid cleavage and subsequent MOMP is driven directly by caspase-1 independently of caspase-8, although high levels of cleaved caspase-8 p18 are found in inflammasome-activated *Gsdmd*-deficient cells. Upon investigating the steps downstream of MOMP, we observed that knocking-out *Casp9* in *Gsdmd*^{-/-} cells had only a small effect on cell death, whereas removing both *Casp8* and *Casp9* abrogated GSDMD-independent cell death. The redundancy in caspase-8 and caspase-9 requirement was explained by the observation that either caspase was sufficient to process caspase-3 between the large and small catalytic domains, thereby generating the intermediate caspase-3 p19 and p12 fragments. Caspase-1-dependent Bid cleavage and SMAC release are then required to remove IAP inhibition, thereby allowing auto-cleavage of caspase-3 to the p17/p12 fragments and full caspase activation (Kavanagh et al, 2014). Thus, cell lysis in the absence of GSDMD is driven by the synergistic effect of both rapid caspase-1-driven activation of initiator caspases-8/-9 and Bid cleavage, which results in an unusually fast activation of caspase-3 and immediate transition into secondary necrosis.

Results

Canonical inflammasomes trigger a rapid secondary necrosis in the absence of GSDMD

The canonical and noncanonical inflammasome pathways converge on the caspase-dependent cleavage and activation of the

pyroptosis executor GSDMD (Kayagaki et al, 2015; Shi et al, 2015). However, although GSDMD is essential for lytic cell death (pyroptosis) after LPS-induced noncanonical inflammasome activation (Fig S1A), *Gsdmd* deficiency only delays cell lysis after engagement of canonical inflammasome receptors, such as AIM2 (Figs 1A and S1B–D), NLR4, and NLRP3 (Figs 1A and S1B–D) (Kayagaki et al, 2015). The absence of caspase-1 and caspase-11 in primary BMDMs, by contrast, showed a much stronger reduction in lactate dehydrogenase (LDH) release and propidium iodide (PI) influx, and *Asc* deficiency completely abrogated cell lysis after AIM2 or NLRP3 activation, in line with the reported Apoptosis-associated speck-like protein containing a CARD (ASC)-dependent activation of apoptosis in absence of caspase-1 (Pierini et al, 2012; Man et al, 2013; Sagulenko et al, 2013; Chen et al, 2015; Vajjhala et al, 2015).

We next tested a number of cell death inhibitors for their ability to block cell lysis in *Gsdmd*^{-/-} immortalized BMDMs (iBMDMs) transfected with poly(dA:dT), an activator of the AIM2 inflammasome (Fig S2). Neither 7-Cl-O-Nec1 (RIPK1 kinase inhibitor) nor GSK872 (RIPK3 kinase inhibitor) were able to delay cell death in *Gsdmd*^{-/-} iBMDMs, thereby excluding a role for necroptosis or complex IIb-dependent apoptosis, which require the kinase activity of RIPK3 or RIPK1, respectively (Cho et al, 2009; He et al, 2009; Zhang et al, 2009; Feoktistova et al, 2011; Tenev et al, 2011). Similarly, we ruled out the involvement of calpains, calcium-dependent proteases (PD 150606 and Calpeptin), or cathepsins (pan-cathepsin inhibitor K777), which were previously shown to induce apoptosis through a caspase-3-dependent or caspase-3-independent mechanisms (Stennicke et al, 1998; Chwieralski et al, 2006; Momeni, 2011). Finally, we also tested if caspase inhibitors delayed death in *Gsdmd*^{-/-} or WT iBMDMs. Remarkably, we found that whereas the pan-caspase inhibitor VX765 delayed PI uptake in both WT and *Gsdmd*^{-/-} poly(dA:dT) transfected cells, the specific caspase-3/-7 inhibitor I only blocked cell death in *Gsdmd*^{-/-} but not in WT cells (Figs 1B and S2). VX765 failed to prevent cell death in WT cells at later time points in accordance with previous studies that showed pyroptosis is difficult to block pharmaceutically (Schneider et al, 2017).

Although this suggested that apoptotic executioner caspases were necessary for cell death in *Gsdmd*-deficient cells but dispensable for cell death in WT cells, the speed by which *Gsdmd*-deficient cells underwent apoptosis and subsequently cell lysis was remarkable. *Gsdmd*^{-/-} BMDMs displayed DNA laddering and processing of caspase-3 to the mature p17 fragment within 1 h after poly(dA:dT) transfection, which was faster than even the highest concentrations of either extrinsic or intrinsic apoptosis stimuli tested (Fig 1C and D). It is noteworthy that the highest concentration regularly used to induce apoptosis is yet 20 times lower than the concentration used in our study (Vince et al, 2018). Phenotypically, this rapid activation of caspase-3 resulted in a very fast lytic cell death as measured by PI influx (Fig 1E) and morphological analysis (Fig 1F). Of note, inflammasome-stimulated *Gsdmd*^{-/-} BMDMs initiated membrane blebbing and apoptotic body formation initially, but rapidly lost this morphology and transitioned into a necrotic state, characterized by extensive membrane ballooning (Fig 1F), similarly to the end-stage of GSDMD-induced pyroptosis (Fig S3A–C). We conclude that inflammasome activation in the absence of GSDMD results in rapid cell lysis, which we propose to refer to as “GSDMD-independent secondary necrosis” to reflect both the

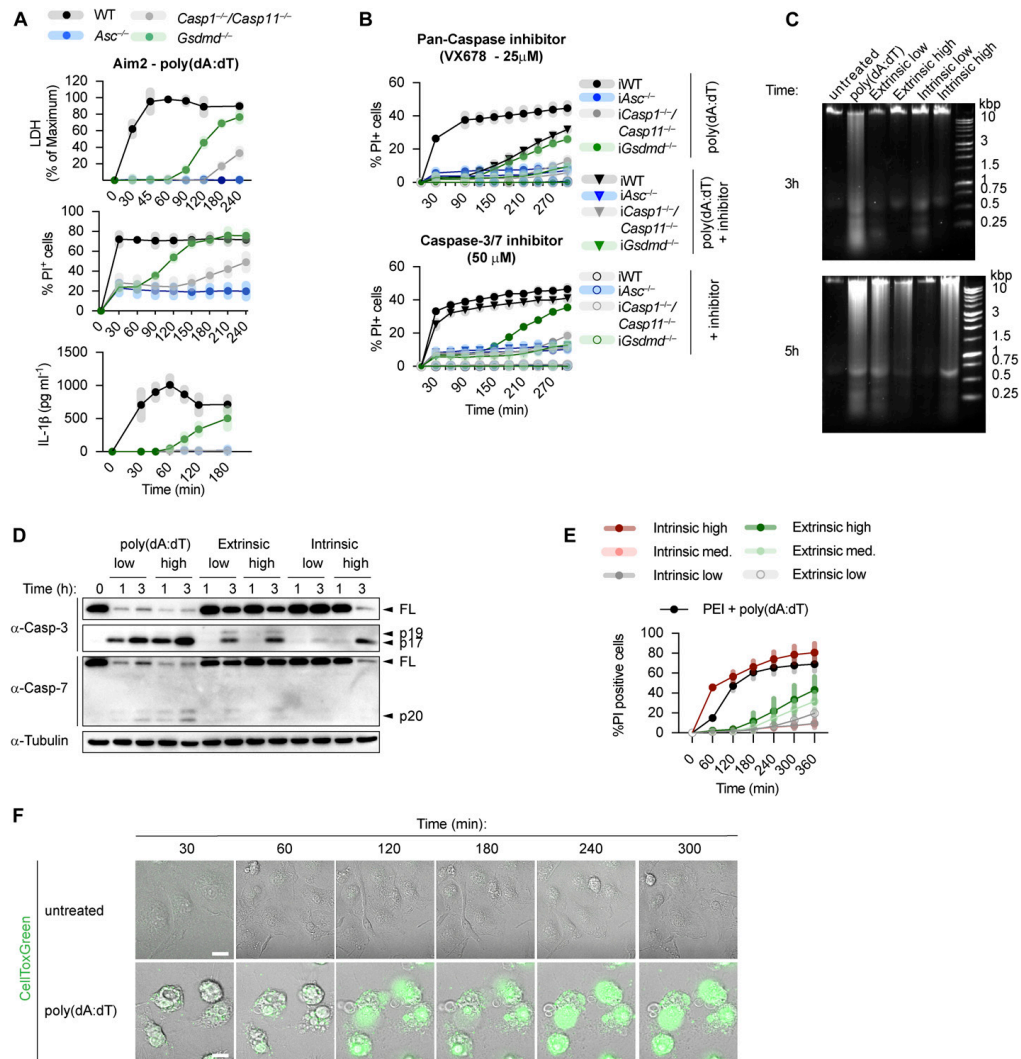


Figure 1. Canonical inflammasome activation *Gsdmd*-deficient macrophages results in rapid secondary necrosis. (A, B) LDH release, PI influx, and IL-1β release from LPS-primed WT, *Asc^{-/-}*, *Casp1^{-/-}/Casp11^{-/-}*, and *Gsdmd^{-/-}* primary or immortalized BMDMs (BMDMs and iBMDMs) after transfection of poly(dA:dT) in the absence or presence of the indicated inhibitors. (C, D, E) DNA cleavage, PI influx, and immunoblots showing caspase-3/-7 processing from LPS-primed *Gsdmd^{-/-}* BMDMs transfected with poly(dA:dT) or treated with 100 ng/ml TNF-α plus 10, 5, or 1 μM AZD5582 (extrinsic apoptosis) or 1 μM ABT-737 plus 10, 1, or 0.5 μM S63845 (intrinsic apoptosis). (F) Confocal images of LPS-primed *Gsdmd^{-/-}* BMDMs transfected with poly(dA:dT) or left untreated and stained with CellTox Green (green). Scale bar = 10 μM. Graphs show mean ± SD. Data and blot are representative of at least three independent experiments.

rapid transition to the necrotic state and the requirement for the activity of the apoptotic executioner caspases-3/-7.

GSDMD-independent secondary necrosis is mainly driven by caspase-3

We next investigated which executioner caspase was required for GSDMD-independent secondary necrosis after caspase-1 activation. High levels of caspase-3/-7 activity was detected in poly(dA:dT)-transfected and *Salmonella*-infected *Gsdmd*^{-/-} and to a lesser degree in *Casp1*^{-/-}/*Casp11*^{-/-} BMDMs, whereas WT or *Asc*^{-/-} BMDMs showed minimal to no activity (Figs 2A and S4A). Because both caspase-3 and caspase-7 cleave the DEVD peptidic substrate, we next determined which executioner caspase was cleaved in *Gsdmd*^{-/-} cells but found that both caspase-3 and caspase-7 were rapidly cleaved (Fig 2B). Although cleaved caspase-7 was detected in both WT and *Gsdmd*-deficient cells, only *Gsdmd*^{-/-} cells display detectable caspase-3/-7 activity and caspase-3 cleavage (Fig 2A). We, therefore, hypothesized that caspase-3 must account for the DEVDase activity in *Gsdmd*^{-/-} BMDMs.

To confirm our hypothesis genetically, we used CRISPR/Cas9 genome engineering to delete either *Casp3* or *Casp7*, or both *Casp3*/*7* in *Gsdmd*^{-/-} BMDMs (Fig S4B) and determined the impact of the deletion on GSDMD-independent secondary necrosis after AIM2 inflammasome activation (Figs 2C and S4C). *Gsdmd*^{-/-}/*Casp3*^{-/-} as well as *Gsdmd*^{-/-}/*Casp3*^{-/-}/*Casp7*^{-/-} iBMDMs were strongly protected against cell death after poly(dA:dT) transfection, whereas *Casp7* single deficiency did not provide protection, despite previous reports that caspase-3 and caspase-7 function in a redundant manner (Figs 2C and S4C) (Walsh et al, 2008; Lamkanfi & Kanneganti, 2010). Caspase-7 appeared to mainly contribute to the cell death observed in *Gsdmd*^{-/-}/*Casp3*^{-/-} iBMDMs, as these had higher LDH levels than *Gsdmd*^{-/-}/*Casp3*^{-/-}/*Casp7*^{-/-} iBMDMs (Fig 2C). These data were further corroborated by knockdown of caspase-3 or caspase-7 in *Gsdmd*^{-/-} iBMDMs (Fig S4D). Finally, we also examined cell morphology after poly(dA:dT) transfection. *Casp7* knockout in *Gsdmd*^{-/-} iBMDMs failed to reduce necrotic features and cell lysis, whereas *Gsdmd*^{-/-}/*Casp3*^{-/-} and *Gsdmd*^{-/-}/*Casp3*^{-/-}/*Casp7*^{-/-} iBMDMs remained alive and intact (Fig 2D) at 3 h posttreatment. In summary, these results demonstrate that although both executioner caspases are cleaved during cell death, it is caspase-3 that drives GSDMD-independent secondary necrosis in inflammasome-activated cells.

Because caspase-3 was shown to cleave gasdermin-E (GSDME), another member of the gasdermin family, and GSDME was proposed to drive secondary necrosis during prolonged apoptosis, we asked whether lack of GSDMD drives an alternative cell death pathway via caspase-3-mediated GSDME cleavage and pore formation. We, thus, measured LDH release and PI influx in WT, *Gsdmd*^{-/-}, *Gsdme*^{-/-}, and *Gsdmd*^{-/-}/*Gsdme*^{-/-} BMDMs upon activation of the AIM2 inflammasome (Figs 2E and S5A). Surprisingly, although GSDME was cleaved in *Gsdmd*^{-/-} at 1 h post-poly(dA:dT) transfection, we did not find a contribution of GSDME to cell death in *Gsdmd*^{-/-} BMDMs because double *Gsdmd*/*Gsdme*-deficiency did not confer any additional protection (Figs 2E and S5A and B). Furthermore, BMDMs lacking only GSDME were comparable with WT

BMDMs, overall suggesting that GSDME does neither contribute to pyroptosis nor GSDMD-independent necrosis.

Caspase-1 is required to cause GSDMD-independent secondary necrosis in inflammasome-activated cells

Because the ASC speck has been reported to control activation of apoptotic caspases independently of caspase-1 (Lee et al, 2018; Mascarenhas et al, 2017; Pierini et al, 2012; Sagulenko et al, 2013; Schneider et al, 2017; Van Opendenbosch et al, 2017), we next generated *Gsdmd*^{-/-}/*Casp1*^{-/-} BMDMs to determine if caspase-1 was required for GSDMD-independent secondary necrosis (Fig 3A). Deletion of caspase-1 in *Gsdmd*-deficient BMDMs strongly reduced LDH release, caspase-3 processing, and caspase-3 activity (Fig 3A–C). LDH levels after 3 and 5 h of poly(dA:dT) transfection were comparable with *Casp1*^{-/-}/*Casp11*^{-/-} BMDMs, but not as low as in *Asc*^{-/-}, confirming that *Casp1* deletion did not affect the cell death that is caused through the ASC-Caspase-8 axis (Fig 3B). It would theoretically be possible that GSDMD-independent secondary necrosis is not driven by the catalytic activity of caspase-1, but by the formation of a caspase-1-containing scaffold and the assembly of an unknown death inducing complex, in analogy to the scaffolding function of caspase-8 (Henry & Martin, 2017). However, we found that poly(dA:dT)-induced PI influx in BMDMs from *Casp1*^{C284A/C284A} mice, which express a catalytically dead caspase-1, was comparable with *Casp1*^{-/-}/*Casp11*^{-/-} or *Casp1*^{-/-} BMDMs, and much lower than PI influx in *Gsdmd*^{-/-}. We formally excluded this possibility (Fig 3D) and thus conclude that caspase-1 enzymatic activity is required to drive GSDMD-independent secondary necrosis.

Bid cleavage is required for mitochondrial damage and GSDMD-independent secondary necrosis

While examining the morphology of inflammasome-activated BMDMs by confocal microscopy, we found that *Gsdmd*^{-/-} cells were characterized by mitochondrial fragmentation and loss of mitochondrial membrane potential (Fig S6A) and a rapid drop of cellular ATP levels (Figs 4A and S6B–D) as early as 30 min after inflammasome activation. Given this rapid loss of mitochondrial integrity, we hypothesized that it was linked to the rapid onset of caspase-3 activation and induction of secondary necrosis in *Gsdmd*-deficient cells.

An imbalance of pro- and anti-apoptotic Bcl2 family members results in the activation of Bax/Bak pore formation and loss of mitochondrial integrity during apoptosis. Often, degradation and/or cleavage of anti-apoptotic Bcl2 proteins as well as activating cleavage of BH3-only protein are responsible for MOMP. To identify which pro-apoptotic Bcl2 proteins are processed in *Gsdmd*^{-/-} BMDMs, we made use of Stable Isotope Labeling with Amino acids in Cell culture (SILAC) mass spectrometry approach (Ong et al, 2002). Differentially isotope-labelled immortalized *Gsdmd*^{-/-} and *Asc*^{-/-} BMDMs were transfected with poly(dA:dT), proteins separated by molecular weight using SDS-PAGE, cut according to MW and each slice analysed by mass spectrometry (Slice-SILAC). The differential analysis of the heavy versus light fraction enabled a comparison between the nonresponsive *Asc*^{-/-} and the responsive *Gsdmd*^{-/-}, wherein appearance of smaller fragments in *Gsdmd*^{-/-} indicated

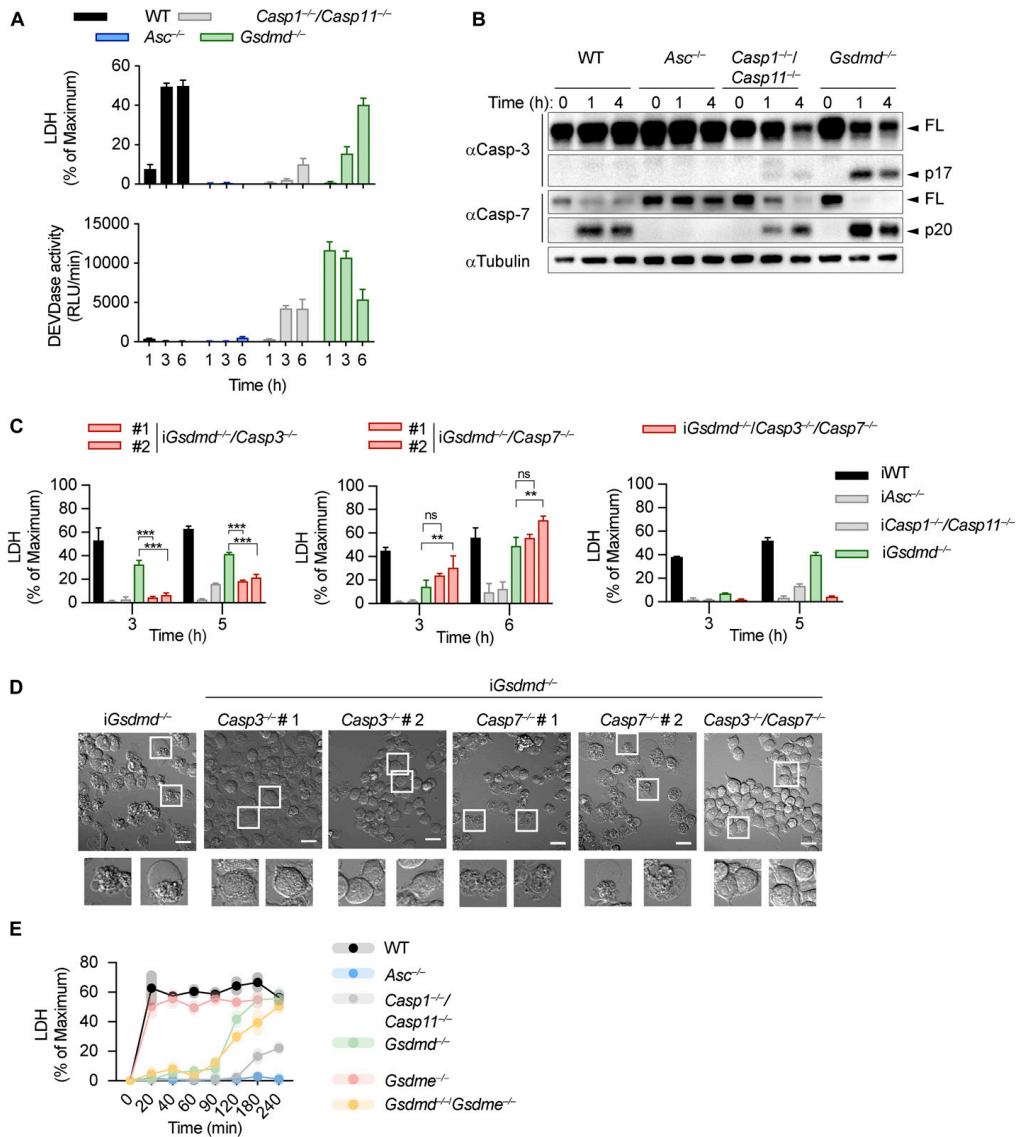


Figure 2. Caspase-3 drives GSDMD-independent secondary necrosis in inflammasome activated cells.

(A, B) LDH release, caspase-3/-7 activity (DEVDase activity) and immunoblots showing caspase-3/-7 processing from LPS-primed WT, $Asc^{-/-}$, $Casp1^{-/-}/Casp11^{-/-}$, and $Gsdmd^{-/-}$ primary BMDMs after transfection of poly(dA:dT). (C) LDH release from LPS-primed WT, $Asc^{-/-}$, $Casp1^{-/-}/Casp11^{-/-}$, $Gsdmd^{-/-}$, $Gsdmd^{-/-}/Casp3^{-/-}$, $Gsdmd^{-/-}/Casp7^{-/-}$, and $Gsdmd^{-/-}/Casp3^{-/-}/Casp7^{-/-}$ iBMDMs after transfection of poly(dA:dT). (C, D) Confocal images of cells from (C). Insets show membrane ballooning in dying cells at 3 h post-transfection. Scale bar = 10 μ m. (E) Quantification of LDH release in LPS primed WT, $Asc^{-/-}$, $Casp1^{-/-}/Casp11^{-/-}$, $Gsdmd^{-/-}$, $Gsdme^{-/-}$, and $Gsdmd^{-/-}/Gsdme^{-/-}$ BMDMs transfected with poly(dA:dT) for 4 h. Graphs show mean \pm SD. ** $P \leq 0.01$, *** $P \leq 0.001$, "ns," no significance (unpaired t test). Data and blot are representative of at least three independent experiments.

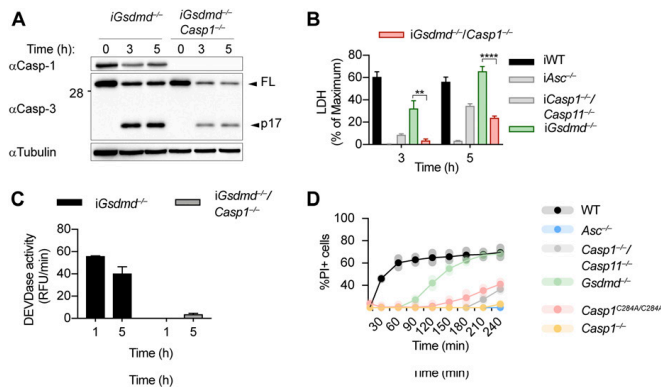


Figure 3. Caspase-1 is required for GSDMD-independent secondary necrosis. (A, B, C) Immunoblot showing Caspase-1 expression and caspase-3 processing, LDH release, and caspase-3/-7 activity (DEVDase activity) from LPS-primed $Gsdmd^{-/-}$ and $Gsdmd^{-/-}/Casp1^{-/-}$ immortalized BMDMs after transfection of poly(dA:dT). (D) PI influx of WT, $Asc^{-/-}$, $Casp1^{+/+}/Casp11^{-/-}$, $Casp1^{+/+}/Casp11^{-/-}, Casp1^{C284A/C284A}$, and $Gsdmd^{-/-}$ primary BMDMs after transfection of poly(dA:dT). Graphs show mean \pm SD. ** $P \leq 0.01$, **** $P \leq 0.0001$ (unpaired t test). Data and blot are representative of at least three independent experiments.

cleavage. We focused on potential cleavage of Bcl-2 family proteins that indicate their inability to inhibit BH3-only proteins or promote BH3-only proteins to induce MOMP (Bock & Tait, 2019). The anti-apoptotic protein Mcl-1 (of Bcl-2, Mcl-1, and Bcl-XL) and the pro-apoptotic proteins Bax, Bak, and Bid (but not Bim) were found to be cleaved in $Gsdmd^{-/-}$, but not in $Asc^{-/-}$ cells (Fig 4B). Because in type-II cells, caspase-8-cleaved tBid translocates to the mitochondria to promote Bax/Bak-dependent pore formation and intrinsic apoptosis, we investigated whether Bid cleavage promoted GSDMD-independent secondary necrosis. Confirming the SILAC data, Bid

was found to be rapidly cleaved in $Gsdmd^{-/-}$ cells but not in $Asc^{-/-}$ after inflammasome activation (Fig 4C). However, because Bid cleavage was also observed in WT and $Casp1^{+/+}/Casp11^{-/-}$ BMDMs, we proceeded to assess its contribution to GSDMD-independent secondary necrosis genetically by generating $Gsdmd^{-/-}/Bid^{-/-}$ iBMDMs (Fig S7A). Knocking out *Bid* in $Gsdmd^{-/-}$ cells significantly reduced the levels of caspase-3 activity (Fig S7B) after poly(dA:dT) transfection and in agreement with that strongly reduced LDH release and PI uptake were observed (Figs 4D and S7C). Strikingly, $Gsdmd^{-/-}/Bid^{-/-}$ cells looked adhered and elongated comparable

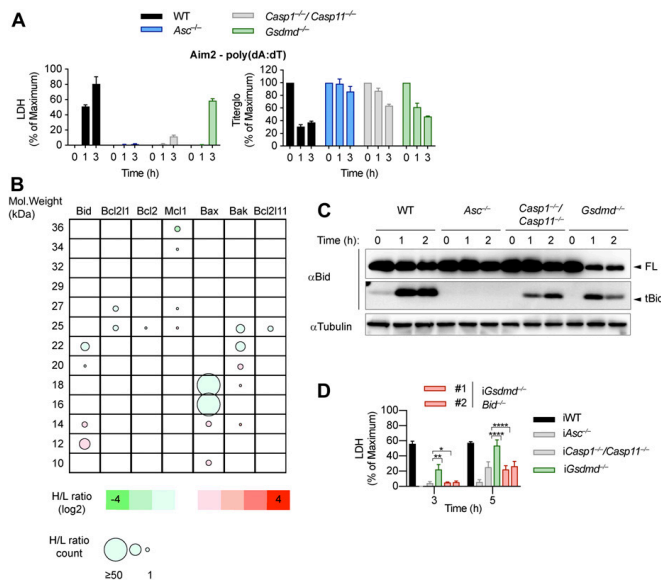


Figure 4. Mitochondrial damage is caused by truncated Bid. (A) LDH release and Titer-Glo measurements from LPS-primed WT, $Asc^{-/-}$, $Casp1^{+/+}/Casp11^{-/-}$, and $Gsdmd^{-/-}$ primary BMDMs after transfection with poly(dA:dT). (B) Schematic cleavage profile of Bcl-2 family members generated from slice SILAC data. Bubble diameters are proportional to the number of quantified peptide matches, whereas the gradient color represents the H/L ratio, as indicated below. The green bubbles (negative log₂H/L) represent protein isoforms reduced in $Gsdmd^{-/-}$ iBMDMs compared with $Asc^{-/-}$ iBMDMs at 3 h post-poly(dA:dT) transfection; red bubbles (positive log₂H/L) represent protein isoforms enriched in $Gsdmd^{-/-}$ iBMDMs compared with $Asc^{-/-}$ iBMDMs. (C) Immunoblots showing Bid processing from LPS-primed WT, $Asc^{-/-}$, $Casp1^{+/+}/Casp11^{-/-}$, and $Gsdmd^{-/-}$ primary BMDMs after transfection with poly(dA:dT). (D) LDH release from WT, $Asc^{-/-}$, $Casp1^{+/+}/Casp11^{-/-}$, $Gsdmd^{-/-}$, and $Gsdmd^{-/-}/Bid^{-/-}$ iBMDMs after transfection with poly(dA:dT). Graphs show mean \pm SD. * $P \leq 0.05$, ** $P \leq 0.01$, **** $P \leq 0.0001$, "ns," no significance (unpaired t test). Data and blots are representative of at least three independent experiments.

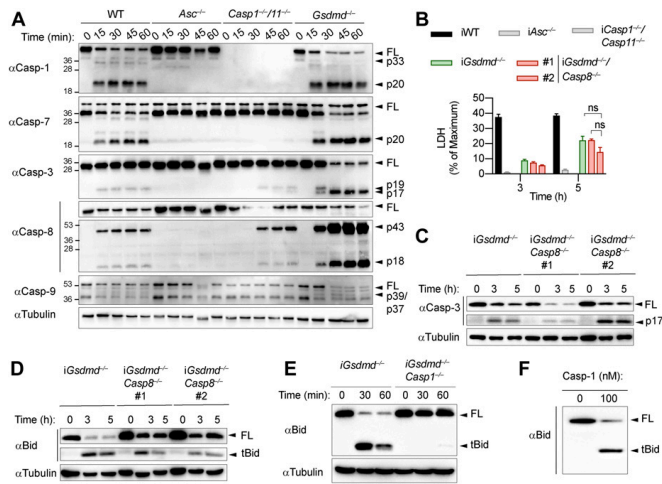


Figure 5. Caspase-1 drives Bid processing during GSDMD-independent secondary necrosis. (A) Immunoblots showing caspase-1, caspase-7, caspase-3, caspase-8, and caspase-9 processing in WT, *Asc*^{-/-}, *Casp1*^{-/-}/*Casp11*^{-/-}, and *Gsdmd*^{-/-} primary BMDMs after transfection with poly(dA:dT). (B) LDH release from WT, *Asc*^{-/-}, *Casp1*^{-/-}/*Casp11*^{-/-}, *Gsdmd*^{-/-}, and *Gsdmd*^{-/-}/*Casp8*^{-/-} iBMDMs after transfection with poly(dA:dT). (C) Immunoblots showing caspase-3 processing in *Gsdmd*^{-/-} and *Gsdmd*^{-/-}/*Casp8*^{-/-} iBMDMs after transfection with poly(dA:dT). (D) Immunoblots showing Bid cleavage in *Gsdmd*^{-/-} and *Gsdmd*^{-/-}/*Casp8*^{-/-} iBMDMs after transfection with poly(dA:dT). (E) Immunoblots showing Bid cleavage in *Gsdmd*^{-/-} and *Gsdmd*^{-/-}/*Casp1*^{-/-} iBMDMs after transfection with poly(dA:dT). (F) In vitro cleavage assay showing processing of recombinant Bid by recombinant caspase-1. Graphs show mean ± SD. * "ns," no significance (unpaired t test). Data and blot are representative of at least three independent experiments.

with untreated iBMDMs upon transfection with poly(dA:dT), which is in contrast to *Gsdmd*^{-/-} iBMDMs which displayed typical necrotic features such as rounding up, permeabilization, shrinkage, and blebbing (Fig 57D). In summary, these results show that Bid is an essential mediator of GSDMD-independent secondary necrosis and suggest that Bid cleavage is required to drive this cell death.

Caspase-1 cleaves Bid to promote caspase-3 activation and cell lysis

Because proteolytic cleavage of Bid precedes MOMP and is required for cell death, we next enquired which upstream caspase is responsible for Bid activation. Immunoblotting for the cleaved p18 fragment of caspase-8 suggested that *Gsdmd*^{-/-} BMDMs contain active caspase-8 at 15–30 min after poly(dA:dT) transfection, whereas very little cleaved caspase-8 p18 was found in WT, *Asc*^{-/-}, or *Casp1*^{-/-}/*Casp11*^{-/-} BMDMs (Figs 5A and 58A). Interestingly, the relatively low levels of caspase-8 cleavage in *Casp1*^{-/-}/*Casp11*^{-/-} compared with *Gsdmd*^{-/-} BMDMs suggested that direct activation of caspase-8 by the ASC speck was negligible and that instead caspase-8 activation in *Gsdmd*^{-/-} cells depended on the presence caspase-1. However, whether caspase-1 would cleave and activate caspase-8 directly or by an indirect pathway could not be deduced.

We next assessed the role of caspase-8 in causing GSDMD-independent secondary necrosis by generating *Gsdmd*^{-/-}/*Casp8*^{-/-} iBMDM lines (Fig 58B). Of note, although *Casp8* deficiency in mice results in embryonic lethality because of the unchecked activation of RIP3-dependent necroptosis (Kaiser et al, 2011; Oberst et al, 2011), *Casp8*-deficient macrophages were reported to be viable unless stimulated with extrinsic apoptotic triggers (Kang et al, 2004; Kaiser et al, 2011; Cuda et al, 2015). Indeed, when testing if *Gsdmd*^{-/-}/*Casp8*^{-/-} BMDMs showed reduced levels of cell death after induction of apoptosis with the extrinsic

apoptosis stimulus TNFα/SMAC, we found that cell death was reduced, but not completely abrogated (Fig 58C). The remaining cell death, however, was block when TNFα/SMAC was combined with the RIPK3 kinase inhibitor GSK'872 (Fig 58C). These results confirmed that the cells were indeed *Casp8* knockouts and that the necroptotic pathway was only initiated when death receptors were engaged. We next compared LDH release in *Gsdmd*^{-/-} and *Gsdmd*^{-/-}/*Casp8*^{-/-} BMDMs after transfection of the AIM2 inflammasome activator poly(dA:dT). Unexpectedly, we found no difference in LDH release nor PI uptake between these two genotypes (Figs 5B and 58D). Furthermore, we were still able to detect Bid cleavage and caspase-3 processing to the active p17 fragment in inflammasome-activated *Gsdmd*^{-/-}/*Casp8*^{-/-} BMDMs (Fig 5C and D). Previous work has implied that Bid can also be a substrate of caspase-1 (Li et al, 1998) because caspase-1 and caspase-8 have partially overlapping substrate spectrum that includes also GSDMD and IL1β (Maelfait et al, 2008; Orning et al, 2018; Sarhan et al, 2018; Chen et al, 2019). In line with caspase-1 controlling Bid cleavage directly and independently of caspase-8, we found that tBid generation after AIM2 activation was completely abrogated in *Gsdmd*^{-/-}/*Casp1*^{-/-} BMDMs at an early time point and strongly reduced after prolonged incubation (Fig 5E) and that caspase-1 was able to efficiently convert Bid to tBid in an in vitro cleavage assay (Fig 5F). In summary, our data thus far suggest that although Bid cleavage is essential for GSDMD-independent secondary necrosis and high levels of active caspase-8 are found in these cells, it is caspase-1 and not caspase-8 that processes Bid and induces mitochondrial permeabilization.

GSDMD-independent secondary necrosis requires both caspase-8 and caspase-9

Having identified caspase-1, Bid and caspase-3 as the essential drivers of GSDMD-independent secondary necrosis, we next asked if activation

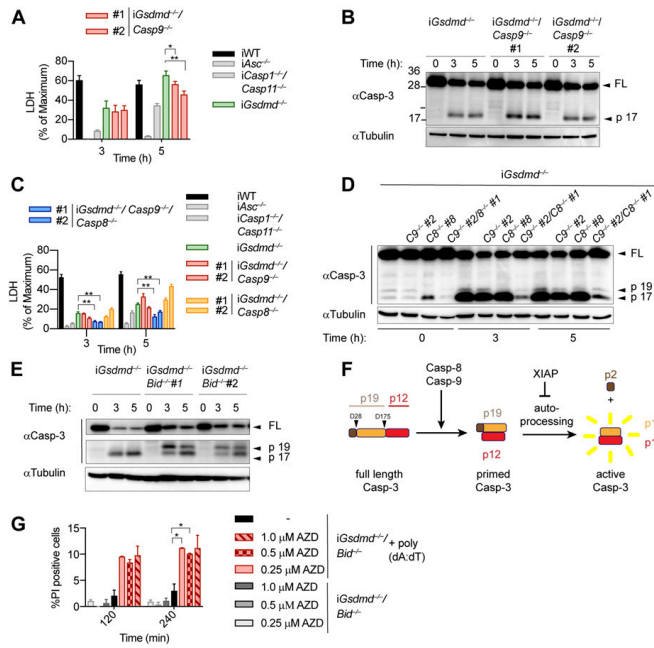


Figure 6. SMAC release and initiator caspases-8/-9 are required for GSDMD-independent secondary necrosis.

(A) LDH release from WT, *Asc*^{-/-}, *Casp11*^{-/-}/*Casp11*^{-/-}, *Gsdmd*^{-/-}, and *Gsdmd*^{-/-}/*Casp9*^{-/-} iBMDMs after transfection with poly(dA:dT). (B) Immunoblots showing caspase-3 cleavage in *Gsdmd*^{-/-} and *Gsdmd*^{-/-}/*Casp9*^{-/-} iBMDMs after transfection with poly(dA:dT). (C) LDH release from WT, *Asc*^{-/-}, *Casp11*^{-/-}/*Casp11*^{-/-}, *Gsdmd*^{-/-}, *Gsdmd*^{-/-}/*Casp8*^{-/-}, *Gsdmd*^{-/-}/*Casp9*^{-/-}, and *Gsdmd*^{-/-}/*Casp8*^{-/-}/*Casp9*^{-/-} iBMDMs after transfection with poly(dA:dT). (D) Immunoblots showing caspase-3 cleavage in *Gsdmd*^{-/-}, *Gsdmd*^{-/-}/*Casp8*^{-/-}, *Gsdmd*^{-/-}/*Casp9*^{-/-}, and *Gsdmd*^{-/-}/*Casp8*^{-/-}/*Casp9*^{-/-} iBMDMs after transfection with poly(dA:dT). (E) Immunoblots showing caspase-3 processing from *Gsdmd*^{-/-} and *Gsdmd*^{-/-}/*Bid*^{-/-} iBMDMs after transfection with poly(dA:dT). (F) Schematic summary of the mechanism of caspase-3 cleavage and activation. (G) PI influx in untreated or poly(dA:dT)-transfected *Gsdmd*^{-/-}/*Bid*^{-/-} iBMDMs in the presence or absence of the SMAC mimetic AZD5582. Graphs show mean ± SD. **P* ≤ 0.05, ***P* ≤ 0.01 (unpaired *t* test). Data and blot are representative of at least three independent experiments.

of caspase-9 downstream of mitochondrial permeabilization and cytochrome *c* release provides the link between Bid and caspase-3 activation. We, thus, generated *Gsdmd*^{-/-}/*Casp9*^{-/-} iBMDM lines by CRISPR/Cas9 genome targeting and verified that they lacked caspase-9 expression and no longer responded to intrinsic apoptosis induction (Fig S9A and B).

However, we found that in analogy to *Casp8*-deficiency, knocking out of *Casp9* in *Gsdmd*^{-/-} had only a small impact on poly(dA:dT)-induced secondary necrosis after 5 h of treatment, whereas no impact was detectable at an earlier time point (Figs 6A and S9C). Furthermore, caspase-3 processing was also found to be unaffected in these cell lines (Fig 6B).

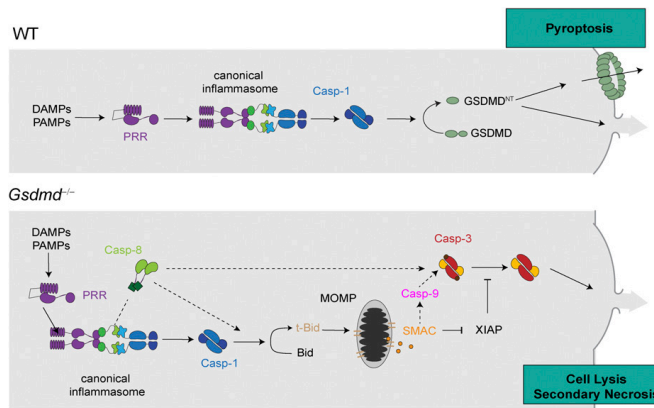


Figure 7. Model of cell death in *Gsdmd*-deficient myeloid cells after activation of caspase-1. Model depicting the mechanism of canonical inflammasome activation in WT cells undergoing caspase-1- and GSDMD-dependent pyroptosis and *Gsdmd*^{-/-} cells undergoing caspase-1-induced GSDMD-independent secondary necrosis.

These results raised the possibility that caspase-8 and caspase-9 activity was redundant or that caspase-1 was driving Bid cleavage and caspase-3 activation somehow independently of both initiator caspases. We addressed these two scenarios by creating *Gsdmd*^{-/-}/*Casp8*^{-/-}/*Casp9*^{-/-} iBMDM lines (Fig S9D) and compared their phenotype after AIM2 inflammasome activation to our other knockout lines. Poly(dA:dT)-transfected *Gsdmd*^{-/-}/*Casp8*^{-/-}/*Casp9*^{-/-} BMDMs displayed significantly reduced levels of LDH release compared with *Gsdmd*^{-/-}, *Gsdmd*^{-/-}/*Casp8*^{-/-}, or *Gsdmd*^{-/-}/*Casp9*^{-/-} cells (Fig 6C). Consistent with the reduced levels of cell lysis, we also found that caspase-3 processing was significantly reduced in *Gsdmd*^{-/-}/*Casp8*^{-/-}/*Casp9*^{-/-} when compared with the other genotypes (Fig 6D), confirming that activity of either initiator caspase was sufficient to drive caspase-3 activation and GSDMD-independent secondary necrosis.

Bid-induced mitochondrial permeabilization is required to release SMAC and promote conversion of caspase-3 p19 to p17

The finding that single deficiency in either caspase-8 or caspase-9 had no impact on caspase-3 activation and GSDMD-independent secondary necrosis, whereas double-deficiency abrogated cell lysis was unexpected and puzzling. Because Bid was essential for GSDMD-independent secondary necrosis, whereas caspase-9 was not, we hypothesized that other factors released from permeabilized mitochondria were required. Besides cytochrome c, which activates Apaf-1 to assemble the apoptosome and promote caspase-9 activity, mitochondria also release ATP and SMAC. SMAC binds IAPs, in particular XIAP, which normally suppresses caspase-3/7 and caspase-9 activity, and thus relieves the block on apoptosis induction (Deveraux et al, 1997; Wu et al, 2000). We, thus, closely examined caspase-3 processing between poly(dA:dT)-transfected *Gsdmd*^{-/-} and *Gsdmd*^{-/-}/*Bid*^{-/-} and found that while only the p17 fragment of caspase-3 was found in *Gsdmd*^{-/-} BMDMs, *Gsdmd*^{-/-}/*Bid*^{-/-} featured two cleaved caspase-3 bands, at 19 and 17 kD (Figs 6E and S9E). Previous studies showed that p19 fragment is generated by apical caspases cleaving in the linker domain between the large and small subunit, whereas the p17 is generated by auto-processing of the pro-peptide by caspase-3 itself (Kavanagh et al, 2014) (Fig 6F). We hypothesize that *Bid* deficiency delayed IAP release and, thus, conversion from the p19 to the p17 fragment and full activity of caspase-3 and that this was a critical factor for GSDMD-independent secondary necrosis. Indeed, treatment with the SMAC mimetic AZD5582 increased generation of caspase-3 p17 (Fig S9F) and partially restored cell death in *Gsdmd*^{-/-}/*Bid*^{-/-} BMDMs (Fig 6G). These results suggest that during GSDMD-independent secondary necrosis, Bid cleavage and mitochondrial permeabilization are mainly required for the release of SMAC and subsequent binding to XIAP but not to drive caspase-9 activation. However, because either caspase-8 or caspase-9 are needed to process caspase-3 (Fig 6D), caspase-1 cannot induce GSDMD-independent secondary necrosis in the absence of both initiator caspases (Fig 7).

Discussion

Here, we show that the cell lysis that occurs in *Gsdmd*-deficient cells upon activation of canonical inflammasomes is a rapid form of

secondary necrosis (referred to as “GSDMD-independent secondary necrosis” in this article) and that it depends on the caspase-1-dependent activation of either caspase-8 or caspase-9, Bid cleavage, SMAC release, and caspase-3 activity. Secondary necrosis describes the loss of membrane integrity of apoptotic cells or apoptotic bodies and is, thus, appropriate because death in *Gsdmd*-deficient cells relies on initiator caspases and the executor caspase-3 and results in a loss of membrane integrity. Yet, it is remarkably different from regular apoptosis in the signalling pathways that underlie its induction, cellular morphology, and the speed by which cells undergo death.

GSDMD-independent cell lysis is characterized by a rapid loss of mitochondrial potential and rapid activation of caspase-3 and an atypical apoptotic morphology. Indeed, cells undergoing this type of cell death show only initially the signs of regular apoptotic blebs or apoptotic body formation and quickly lose membrane integrity and start ballooning, similarly to pyroptotic cells. This morphology has in the past led to the speculation that caspase-1 might directly or indirectly cleave an alternative lytic cell death executor, such as another gasdermin family member. Indeed, recently Tsuchiya et al (2019) proposed that caspase-3 processes GSDME in *Gsdmd*-deficient CL26 cells that harbor dimerizer-activated caspase-1 (Tsuchiya et al, 2019). Our data in primary mouse macrophages, however, show no involvement of GSDME in GSDMD-independent secondary necrosis (Figs 2E and S5A and B), although GSDME is detectable and processed (Fig S5B). This discrepancy is most likely caused by differences in GSDME expression levels between different cell types. Recent results show that a number of cancer cell lines express sufficiently high levels of GSDME to cause pyroptosis upon treatment with apoptosis-inducing chemotherapy drugs (Wang et al, 2017b). It remains to be determined how much GSDME is expressed by CL-26 cells, a murine colorectal carcinoma cell line, compared with macrophages (Tsuchiya et al, 2019), but overwhelming evidence suggest that at least in macrophages, GSDME expression or activity appear to be insufficient to induce GSDME-dependent cell death after caspase-3 activation (Lee et al, 2018; Sarhan et al, 2018; Vince et al, 2018; Chen et al, 2019). Thus, other yet undefined factors drive the lysis of *Gsdmd*-deficient BMDMs.

Another striking difference between regular apoptosis and GSDMD-independent secondary necrosis is the signalling pathway underlying caspase-3 activation. Our data show that the main driver of this cell death is active caspase-1 and that it promotes cell death by cleaving several targets. The most critical of these targets appears to be Bid, which is converted by caspase-1 to tBid (independently of caspase-8) and which induces mitochondrial permeabilization and the release of cytochrome c, ATP, and SMAC. Moreover, caspase-1 acts as a kind of “super-initiator” caspase by activating initiator caspases-8/-9. It is worth noting that caspase-8 activation is mostly driven by caspase-1 with a negligible contribution of direct caspase-8 activation at the ASC speck, as evident from much reduced caspase-8 cleavage in *Casp1*/*Casp11*-deficient compared with *Gsdmd*-deficient cells. This could potentially be driven by direct caspase-1-induced cleavage of caspase-8, or by caspase-1, somehow enhancing ASC-dependent caspase-8 activation. Caspase-9 activation, however, is downstream of Bid cleavage. The requirement for either caspase-8 and caspase-9

appears to stem from the fact that caspase-1 fails to process caspase-3 efficiently, despite previous reports suggesting that caspase-1 cleaved caspase-3 directly (Taabazuuing et al, 2017; Sagulenko et al, 2018). However, caspase-1 is efficient enough to activate Bid to induce SMAC release, to relieve inhibition by IAPs, and allows full conversion to caspase-3 p17/p12.

Our findings are in contradiction to the recent report by the Suda Laboratory, which proposed that cell death in *Gsdmd*-deficient cells is solely caused by the Bid–caspase-9–caspase-3 axis (Tsuchiya et al, 2019). The discrepancy is potentially related to cell line–intrinsic differences or to the method used to activate caspase-1. Tsuchiya et al (2019) performed experiments in CL26 cells, which, for example, lack ASC and, thus, lack the ASC speck-induced activation of caspase-8 (Pierini et al, 2012; Sagulenko et al, 2013; Vajjhala et al, 2015; Fu et al, 2016), whereas we used immortalized macrophages, which recapitulate the behavior of primary BMDMs. Furthermore, they used a dimerizer-based system to activate caspase-1, which most likely induces higher levels of caspase-1 activity compared with physiological inflammasome triggers and, thus, might explain why Tsuchiya et al (2019) did not observe a role for caspase-8, which we find necessary to amplify caspase-1 activity after treatment with canonical inflammasome triggers. However, both studies agree that Bid cleavage is essential for cell death in *Gsdmd*-deficient cells and that Bid is cleaved by caspase-1 independently of caspase-8.

Recent work has revealed a surprisingly high level of redundancy and cross talk between the apoptotic, necroptotic, and pyroptotic cell death pathways. Interestingly, in many cases, these pathways or the cross talk are normally not detectable or only turned on when another pathway is inhibited. For example, deletion of caspase-8 or mutation of its auto-processing sites are known to result in activation of RIP3/MLKL-dependent necroptosis, a pathway that is otherwise not observed, and catalytic-dead caspase-8 results in activation of necroptosis and pyroptosis (Kaiser et al, 2011; Oberst et al, 2011; Kang et al, 2018; Newton, 2019a; 2019b). It is assumed that this redundancy developed as a defense mechanism to guard against pathogen-induced inhibition of apoptosis, and accordingly viral inhibitors of the three major cell death pathways have been identified (Li & Stollar, 2004; Taxman et al, 2010; Nailwal & Chan, 2019), which highlights that necroptosis is not an artifact caused by lack of caspase-8 activity. Similarly, it could be speculated that the ability of caspase-1 to induce rapid secondary necrosis by activating apoptotic caspases might have developed as a safeguard against viruses that inhibit GSDMD. Indeed, recently, the pathogenic enterovirus 71, which is known to trigger the NLRP3 inflammasome (Wang et al, 2017a), was shown to interfere with GSDMD activation. In particular, the viral protease 3C was shown to cleave GSDMD at Q193/194, interfering with N-terminal fragment formation, oligomerization, and GSDMD pore formation (Wang et al, 2015). Furthermore, GSDMD-independent secondary necrosis appears to contribute to the clearance of bacterial infection, as it could be shown that *Gsdmd*^{-/-} mice are less susceptible to infection with *Francisella novicida* compared with *Casp1*^{-/-} or *Aim2*-deficient animals (Schneider et al, 2017; Kanneganti et al, 2018b). Along the same lines, *Gsdmd*-deficient mice infected with *Burkholderia thailandensis* show lower CFUs and lower IL-1 β levels than *Casp1*/*Casp11*-deficient animals (Wang et al, 2019). Similarly, it was reported that peritoneal IL-1 β levels are higher in *Salmonella*

typhimurium-infected *Gsdmd*^{-/-} mice than *Casp1*^{-/-} controls (Monteleone et al, 2018). These studies, thus, allow the conclusion that GSDMD-independent cell death is also engaged in vivo and that it allows partial protection against intracellular bacterial pathogens. Unexpectedly, however, GSDMD-independent secondary necrosis does not appear to be important in models of auto-inflammatory diseases because *Gsdmd* deficiency rescues mice expressing mutant NLRP3 or Pylrin, linked to neonatal-onset multisystem inflammatory disease and familial Mediterranean fever (Xiao et al, 2018; Kanneganti et al, 2018a).

Considering that knockout of GSDMD showed a big improvement in pro-inflammatory symptoms associated with the auto-inflammatory diseases neonatal-onset multisystem inflammatory disease and familial Mediterranean fever and the importance of the canonical inflammasome pathway in sterile inflammatory disease, research has focused on the discovery of GSDMD-specific inhibitors. To date, several inhibitors have been identified, although off-target effects and specificity still need to be evaluated in more detail (Rathkey et al, 2018; Sollberger et al, 2018; Rashidi et al, 2019). Furthermore, it is important to consider that caspase-1 activity is unrestrained by these inhibitors and that, thus, caspase-1 might induce cell death and inflammation through the back-up pathway described in our study.

Materials and Methods

Antibodies, chemicals, and reagents

Drugs

VX-765 (MedChemExpress), Caspase-3/7 inhibitor I (CAS 220509-74-0; Santa Cruz Biotechnology), Q-VD-Oph (Selleck Chemicals), AZD5582 (Selleck Chemicals), 7-Cl-O-Nect1 (Abcam), GSK872 (Selleck Chemicals), K777 (AdipoGen), PD 150606 (Tocris), Calpeptin (Selleck Chemicals), ABT-737 (Selleck Chemicals), S63845 (Selleck Chemicals), and Nigericin (InvivoGen).

Antibodies

GSDMD (Ab209845; Abcam), Casp-1 (Casper1, AG-20B-0042-C100; AdipoGen), Tubulin (Ab40742; Abcam), IL-1 β (AF-401-NA; R&D Systems), Caspase-3 (#9662; Cell Signaling Technology), Caspase-7 (#9492; Cell Signaling Technology), Caspase-8 (#9429 and 4927; Cell Signaling Technology), Caspase-9 (#9508 and #9504; Cell Signaling Technology), and Bid (#2003; Cell Signaling Technology).

Animal experiments

All experiments were performed with approval from the veterinary office of the Canton de Vaud and according to the guidelines from the Swiss animal protection law (license VD3257). C57BL/6J mice were purchased from Janvier Labs and housed at specific pathogen-free facility at the University of Lausanne. Mice lacking Asc, *Casp1*, *Casp1/11*, *Gsdmd*, *Gsdme*, or expressing mutant *Casp1*^{C294A} have been previously described (Mariathasan et al, 2004; Kayagaki et al, 2011; Schneider et al, 2017; Chen et al, 2019). All mice were either generated (*Gsdmd*^{-/-} and *Gsdme*^{-/-}) or backcrossed (other lines) in the C56BL/6J background.

Cell culture and immortalization of macrophages

Primary mouse macrophages (BMDMs) were differentiated for 6 d and cultured for up to 9 d in DMEM (Gibco) supplemented with 10% FCS (Bioconcept), 20% 3T3 supernatant (MCSF), 10% Hepes (Gibco), and 10% nonessential amino acids (Gibco). Immortalization of macrophages was performed as previously described (Blasi et al, 1985; Broz et al, 2010). Immortalized macrophages (iBMDMs) were cultured in DMEM complemented with 10% FCS (Bioconcept), 10% MCSF (3T3 supernatant), 10% Hepes (Amimed), and 10% nonessential amino acids (Life Technologies). To passage the BMDMs and iBMDMs, the cells were washed with PBS and left to detach at 4°C for 15 min and scraped using cell scrapers (Sarstedt), spun down at 300g for 5 min at 4°C, and resuspended in the appropriate amount of medium.

CRISPR genome editing in immortalized macrophages

Bid-, *Casp9*-, *Casp8*-, *Casp8/Casp9*-, *Casp1*-, *Casp3*-, *Casp7*-, and *Casp3/7*-deficient iBMDMs were generated using the genome-editing system Alt-R-CRISPR/Cas (IDT) according to the manufacturer's protocol. Briefly, the gene-specific targeting crRNA (*Bid*: TGGCTGTAATCGCCCAAGAGC TGG *Caspase-9*: CACACGCACGGGCTCCAAC TGG, *Caspase-8*: CTCCTAGACTGCAACCGAG AGG, *Caspase-1*: AATGAAGACTGTACTCTGGC AGG, *Caspase-7*: GATAAG TGGGCACTCGGTCC TGG, and *Caspase-3*: AATGTCATCTCGCTCTGGTA CGG or TGGGCC-TGAAATACCAAGTC AGG) was mixed with the universal RNA oligo tracrRNA to form a gRNA complex (crRNA–tracrRNA). The addition of the recombinant Cas9 nuclease V3 allowed the formation of an RNP complex specific for targeting the desired genes. The tracrRNA only or RNP complexes were subsequently reverse transfected into either WT or *Gsdmd*^{-/-} immortalized iBMDMs using RNAiMax (Invitrogen). The bulk population was tested for successful gene mutation using the T7 endonuclease digestion assay as follows: the cells were lysed by the KAPA Biosystems Kit according to the manufacturer's protocol, and genomic DNA flanking the guide RNA (crRNA)–binding site was amplified by PCR using gene-specific primers (*Bid*: fw: CTGGACATTAGTGGGGCAG, rv: CTCGATAGCCC-CTTGGTGTC; *Caspase-9*: fw: CAAGCTCTCCAGACCTGACC, rv: GAGATCT-GACGGGCACCAT; *Caspase-8*: fw: GGGATGTTGGAGGAAGGCAA, rv: GGCACAGACTTTGAGGGGT; *Caspase-1*: fw: CAGACAAGATCCTGAGGGCA, rv: AGATGAGGATCCAGCGAGTAT; *Caspase-7*: fw: TTGCCTGACCCAAG GTTTGT, rv: CCCAGCAACAGGAAAGCAAC; and *Caspase-3*: fw: GTG GGGGATATCGTGTCTAT, rv: TGTGTAAGGATGCGGACTGC). The amplified genomic DNA was used to perform the heteroduplex analysis according to the manufacturer's protocol (IDT). Single clones were derived from the bulk population by limiting dilution, and the absence of protein expression in single clones was verified by immunoblotting and sequencing of genomic regions, where required.

siRNA knockdown

2.5 × 10⁵ *Gsdmd*-deficient iBMDMs were seeded per well of a six-well plate and incubated overnight. For the siRNA transfection, the medium was changed to OptiMEM, and siRNA transfection was carried out according to the manufacturer's protocol, transfecting 25 pmol siRNA (non-targeting: siGENOME non-targeting siRNA control pools [D-001206-14; Dharmacon], caspase-3: Casp3 SMART

POOL [M-043042-01; Dharmacon], and caspase-7: Casp7 SMART POOL [M-057362-01; Dharmacon]) with 7.5 μl Lipofectamine RNAiMax (Invitrogen) per well. Medium was exchanged for DMEM (10% FCS, 10% MCSF, 1% NeAA, and 1% Hepes) after 6 h. 48 h post-transfection, the cells were collected and reseeded in a 96-well plate at 3 × 10⁴ cells/well. The cells were primed and treated as in cell death assays.

Cell death assays

The cells were seeded in 96-well plates (100 μl/well) or 12-well plates (1 ml/well) at a density of 0.5 × 10⁶ cells/ml overnight and primed the next day with 100 ng/ml ultrapure LPS-B5 (055:B5; InvivoGen) for 4 h. AIM2 inflammasome activation was achieved by transfecting 0.4 μg poly(dA:dT) (InvivoGen) per 10⁵ cells. In separate tubes, poly(dA:dT) and linear polyethylenimine (1 μg per 10⁵ cells; PolyScience) were mixed with OptiMEM by vortexing and left for 3 min at room temperature. Then poly(dA:dT) and polyethylenimine (PEI) were mixed together, vortexed shortly, and left for 15 min before adding a quarter of the total volume on top of the cells. Transfection was facilitated by spinning cells for 5 min at 300g at 37°C. *Salmonella enterica* serovar Typhimurium SL1344 and *Francisella tularensis* subsp. *novicida* U112 (*F. novicida*) infection were performed in OptiMEM. For *S. typhimurium* infection, bacteria were grown overnight and subcultured 1/40 for 3 h and 30 min in Luria low-salt broth (LB low salt) supplemented with appropriate antibiotics, whereas infection with *Francisella* were performed from the overnight culture grown in brain heart infusion broth supplemented with 0.2% L-cysteine (Sigma-Aldrich) and appropriate antibiotics. Bacteria were then added on top of the cells in OptiMEM, spun at 300g for 5 min and incubated at 37°C for the duration of the experiment or extracellular bacterial growth suppressed by addition of gentamycin at 30 and 120 min postinfection for *S. typhimurium*, and *F. novicida*, respectively. For the NLRP3 inflammasome activation, LPS-B5 (055:B5; InvivoGen) priming was carried out in OptiMEM for 4 h before addition of 5 μM nigericin (Sigma-Aldrich) and incubated for indicated time. Similarly, the cells were primed with 100 ng/ml LPS LPS-B5 (055:B5; InvivoGen) for 4 h in OptiMEM. LPS/FuGeneHD complexes were prepared by mixing 100 μl OptiMEM with 2 μg ultrapure LPS O111:B4 (InvivoGen) and 0.5 μl of FuGENE HD (Sigma-Aldrich) per well to be transfected. The transfection mixture was vortexed briefly, incubated for 10 min at room temperature, and added dropwise to the cells. The plates were centrifuged for 5 min at 200g and 37°C. Extrinsic apoptosis was induced by adding 100 ng/ml TNF-α and the SMAC mimetic AZD5582 at the indicated concentration. Intrinsic apoptosis was induced by addition of the BH3 mimetic small molecule inhibitor ABT-737 in combination with the Mcl-1 inhibitor S63845 at the indicated concentrations.

Cell death and cytokine release measurement

Cell lysis was assessed by quantifying the amount of lactate dehydrogenase in the cell supernatant using the LDH cytotoxicity kit (Takara) according to the manufacturer's instructions. To measure cell permeabilization, propidium iodide (Thermo Fisher Scientific) was added to the medium at 12.5 μg/ml and fluorescent

emission measured by Cytation5 (Biotek) over time. LDH and PI uptake were normalized to untreated control and 100% lysis. Cytokine release into the supernatant in particular IL-1 β was measured by Elisa (Thermo Fisher Scientific) according to the manufacturer's instructions.

DNA fragmentation assay

DNA fragmentation during apoptosis and pyroptosis was assessed by agarose gel electrophoresis as described before (Kasibhatla et al, 2006). In brief, *Gsdmd*^{-/-} BMDMs were seeded in a 12-well plate and treated with apoptotic triggers or transfected with poly(dA:dT) as described under Cell Death Assays section.

Cell lysis and immunoblotting

After treatment of cells, cell supernatant was collected and 1 \times sample buffer (Thermo Fisher Scientific) complemented with 66 nM Tris, and 2% SDS was added to the cell lysate. The proteins of the supernatant were precipitated on ice using an end concentration of 4% TCA (wt/vol) for 30 min. Supernatant was then spun down at 20,000g for 20 min at 4°C washed with 100% acetone and centrifuged at 20,000g for 20 min at 4°C. The protein pellet was air-dried and resuspended with the lysate. The samples were boiled for 10 min at 70°C and separated by a 10% or 12% SDS page gel. Transfer to the 0.2 μ M Polyvinylidene fluoride (PVDF) membranes was accomplished by Trans-Blot Turbo System. The membranes were blocked with 5% milk in TBS-T and incubated with the primary antibody for 2 h at RT or overnight. Membranes were washed three times with TBS-T and HRP-coupled antibodies added in 5% milk in TBST-T for 1 h. After washing, the membranes were revealed by FUSION imager (VILBER) using Pierce ECL Western Blotting Substrate (Thermo Fisher Scientific) or Pierce ECL Plus Western Blotting Substrate (Thermo Fisher Scientific).

Live cell imaging

BMDMs or iBMDMs were seeded 5 \times 10⁴/well in eight-well tissue culture-treated μ -Slides (iBidi) or 96-well Cell Culture Microplates, μ Clear (Greiner Bio-One) overnight and primed the next day with 100 ng/ml LPS 055:B5 for 4 h. The AIM2 inflammasome was activated by transfection of poly(dA:dT) (see the Cell Death Assay section). For time-lapse microscopy, cells were incubated with CellTox Green (Promega) 1:10,000 and AnnexinV (BioLegend) at 500 ng/ml or for mitochondrial health assessment MitoTracker Green and MitoTracker CMXRos were added to OptiMEM at a final concentration of 125 nM. Images were taken every 5 min or every 15 min, respectively. Zeiss LSM800 point scanning confocal microscope equipped with 63 \times Plan-Apochromat NA 1.4 oil objective, Zeiss ESID detector module, LabTek heating/CO₂ chamber, and motorized scanning stage.

Slice-SILAC

Gsdmd⁻ and *Asc*-deficient iBMDMs were grown in SILAC DMEM (Thermo Fisher Scientific) medium supplemented with 10% dialyzed FBS, 200 mg/ml proline, 150 mg/ml heavy or light lysine and 50 mg/

ml arginine, respectively. The cells were passaged five to six times until 100% labelling was achieved. For the experiment, the cells were seeded at 5 \times 10⁵/well in 12-well plates overnight and primed the next day with 100 ng/ml LPS 055:B5 for 4 h. Poly(dA:dT) transfection was then carried out as described under Cell Death Assays section and plates incubated for 3 h. The cells were scraped in OptiMEM, and proteins were precipitated by 4% TCA. The obtained protein pellet was then resuspended in FASP buffer (4% SDS, 0.1 M DTT, and 100 mM Tris, pH 7.5), heated for 5 min at 95°C, sonicated, and cleared by 10-min centrifugation at 12,000g. Downstream sample preparation, including SDS gel preparation, mass spectrometry, and data analysis have been described before (Di Micco et al, 2016).

Caspase activity assay

Caspase-3/7 activity was either measured by luminescence using the Caspase-Glo 3/7 (Promega) according to the manufacturer's protocol or by fluorescence. The caspase activity assay was performed as follows using the fluorescent substrate N-acetyl-Asp-Glu-Val-Asp-7-amido-4-trifluoromethylcoumarin (Sigma-Aldrich). The cells were lysed directly in the medium by adding 5 \times lysis buffer (250 mM Hepes, 25 mM CHAPS, and 25 mM DTT) and pipetting up and down. 30 μ l of lysed cells was incubated with 30 μ l of 2 \times assay buffer (40 mM Hepes, 200 mM NaCl, 2 mM EDTA, 0.2% CHAPS, 20% sucrose, and 20 mM DTT), and 50 μ M final concentration of substrate was taken in black opaque OptiPlate-96 (PerkinElmer) and read at 400/505 at 37°C every 2 min for 10 min.

Metabolic activity—ATP content

Metabolic activity was measured by Titer-Glo (Promega) according to the manufacturer's protocol. In brief, cells plus 25 μ l supernatant were incubated with 25 μ l Titer-Glo, shook for 2 min at 600 rpm, and incubated for 10 min at room temperature before reading.

In vitro caspase cleavage assay

Active recombinant caspase-1 was purified as described before (Sborgi et al, 2016). For the in vitro cleavage assay, cell lysate from *iGsdmd*^{-/-}/*Casp-3*^{-/-}/*Casp-7*^{-/-} was prepared as described before (Boucher et al, 2012). Briefly, the cells were lysed in ice-cold buffer (50 mM Hepes, pH 7.4, 150 mM NaCl, and 1% IGEPAL) and incubated on ice for 30 min. Cellular proteins were recovered by centrifugation at 7,000g for 10 min and kept at -80°C in 30- μ l aliquots. Purified active caspase-1 (50, 100 nM) was added to cell lysate and incubated for 2 h at 37°C. The mixture was then analysed by immunoblot.

Supplementary Information

Supplementary Information is available at <https://doi.org/10.26508/lsa.202000735>.

Acknowledgements

This work was supported by grants from the European Research Council (ERC-2017-CoG-770988—InflamCellDeath) and from the Swiss National Science Foundation (310030_175576) to P Broz. KW Chen is supported by a Marie Skłodowska-Curie Actions (MSCA) incoming fellowship (MSCA-IF-2018-838252). We thank Prof Dr Thomas Henry and Prof Dr Olaf Gross for sharing *Asc^{-/-}*, *Casp1^{-/-}* and *Casp^{C284A/C284A}* bone marrow, respectively, and Vanessa Mack for technical assistance. In addition, we would also like to thank the University of Lausanne (UNIL) microscopy and proteomics core facilities for their help with data generation and analysis.

Author Contributions

R Heilig: conceptualization, data curation, formal analysis, validation, investigation, visualization, methodology, and writing—original draft, review, and editing.

M Diluca: resources, data curation, investigation, and methodology.

D Boucher: resources, data curation, formal analysis, investigation, methodology, and writing—original draft.

KW Chen: resources, data curation, formal analysis, investigation, methodology, and writing—original draft.

D Hancz: resources, data curation, formal analysis, investigation, methodology, and writing—original draft.

B Demarco: resources, data curation, formal analysis, investigation, methodology, and writing—original draft.

K Shkarina: resources, data curation, formal analysis, investigation, methodology, and writing—original draft.

P Broz: conceptualization, formal analysis, supervision, funding acquisition, project administration, and writing—original draft, review, and editing.

Conflict of Interest Statement

The authors declare that they have no conflict of interest.

References

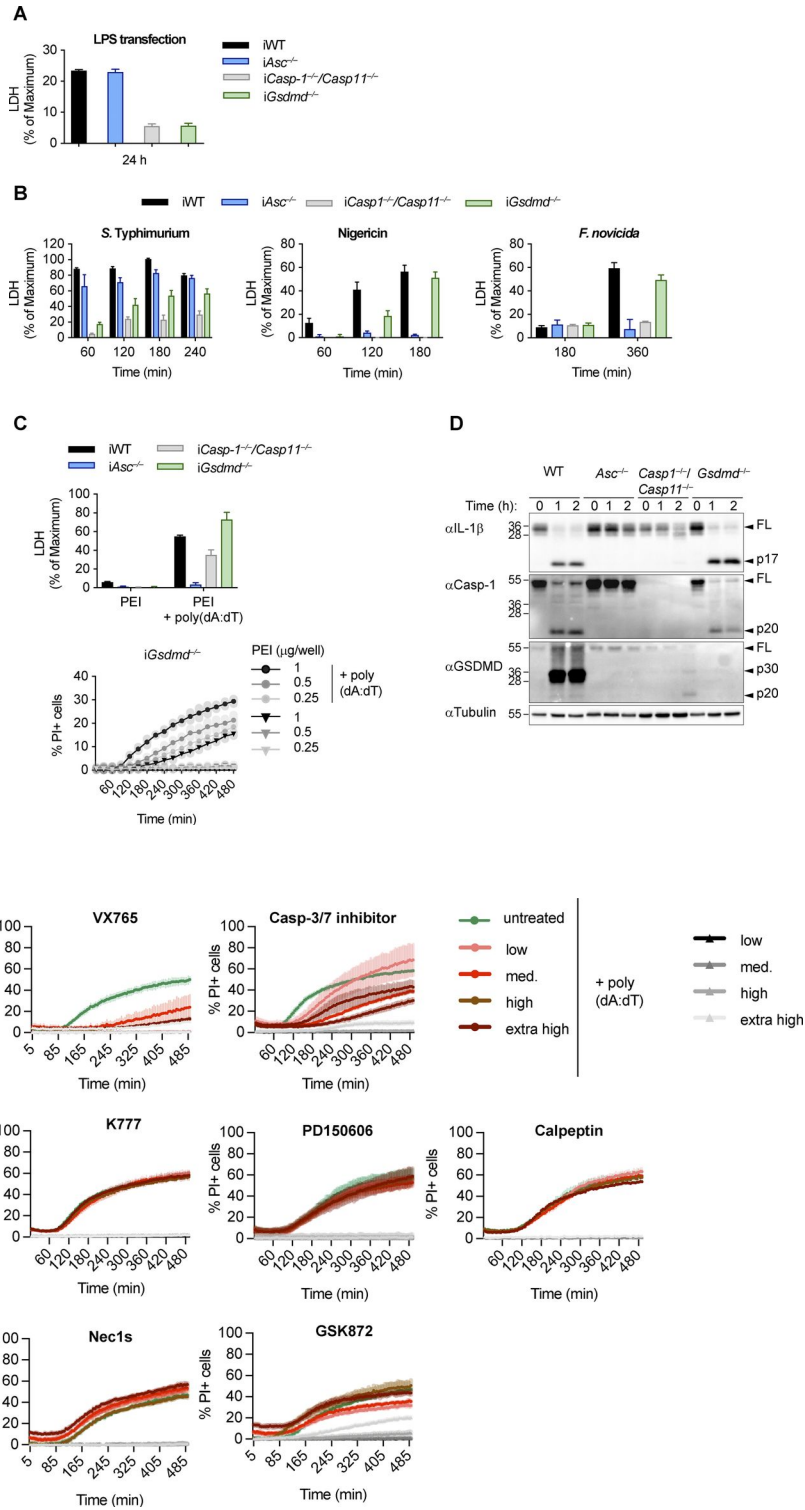
- Aglietti RA, Estevez A, Gupta A, Ramirez MG, Liu PS, Kayagaki N, Ciferri C, Dixit VM, Dueber EC (2016) GsdmD p30 elicited by caspase-11 during pyroptosis forms pores in membranes. *Proc Natl Acad Sci U S A* 113: 7858–7863. doi:10.1073/pnas.1607769113
- Blasi E, Mathieson BJ, Varesio L, Cleveland JL, Borchert PA, Rapp UR (1985) Selective immortalization of murine macrophages from fresh bone marrow by a raf/myc recombinant murine retrovirus. *Nature* 318: 667–670. doi:10.1038/318667a0
- Bock FJ, Tait SWG (2019) Mitochondria as multifaceted regulators of cell death. *Nat Rev Mol Cell Biol* 21: 85–100. doi:10.1038/s41580-019-0173-8
- Boucher D, Blais V, Denault J-B (2012) Caspase-7 uses an exosite to promote poly(ADP ribose) polymerase 1 proteolysis. *Proc Natl Acad Sci U S A* 109: 5669–5674. doi:10.1073/pnas.1200934109
- Bratton SB, Lewis J, Butterworth M, Duckett CS, Cohen GM (2002) XIAP inhibition of caspase-3 preserves its association with the Apaf-1 apoptosome and prevents CD95- and Bax-induced apoptosis. *Cell Death Differ* 9: 881–892. doi:10.1038/sj.cdd.4401069
- Broz P, Dixit VM (2016) Inflammasomes: Mechanism of assembly, regulation and signalling. *Nat Rev Immunol* 16: 407–420. doi:10.1038/nri.2016.58
- Broz P, Von Moltke J, Jones JW, Vance RE, Monack DM (2010) Differential requirement for caspase-1 autoproteolysis in pathogen-induced cell death and cytokine processing. *Cell Host Microbe* 8: 471–483. doi:10.1016/j.chom.2010.11.007
- Chen KW, Demarco B, Heilig R, Shkarina K, Boettcher A, Farady CJ, Pelczar P, Broz P (2019) Extrinsic and intrinsic apoptosis activate pannexin-1 to drive NLRP3 inflammasome assembly. *EMBO J* 38: e101638. doi:10.15252/embj.2019101638
- Chen M, Xing Y, Lu A, Fang W, Sun B, Chen C, Liao W, Meng G (2015) Internalized *Cryptococcus neoformans* activates the canonical caspase-1 and the noncanonical caspase-8 inflammasomes. *J Immunol* 195: 4962–4972. doi:10.4049/jimmunol.1500865
- Cho YS, Challa S, Moquin D, Genga R, Ray TD, Guildford M, Chan FK-M (2009) Phosphorylation-driven assembly of the RIP1-RIP3 complex regulates programmed necrosis and virus-induced inflammation. *Cell* 137: 1112–1123. doi:10.1016/j.cell.2009.05.037
- Chwieralski CE, Welte T, Bühling F (2006) Cathepsin-regulated apoptosis. *Apoptosis* 11: 143–149. doi:10.1007/s10495-006-3486-y
- Cuda CM, Misharin AV, Khare S, Saber R, Tsai FN, Archer AM, Homan PJ, Haines GK, Hutcheson J, Dorfleutner A, et al (2015) Conditional deletion of caspase-8 in macrophages alters macrophage activation in a RIPK-dependent manner. *Arthritis Res Ther* 17: 1–16. doi:10.1186/s13075-015-0794-z
- Deveraux QL, Takahashi R, Salvesen GS, Reed JC (1997) X-linked IAP is a direct inhibitor of cell-death proteases. *Nature* 388: 300–304. doi:10.1038/40901
- Di Micco A, Frera G, Lugrin J, Jamilloux Y, Hsu E-T, Tardivel A, De Gassart A, Zaffalon L, Bujisic B, Siegert S, et al (2016) AIM2 inflammasome is activated by pharmacological disruption of nuclear envelope integrity. *Proc Natl Acad Sci U S A* 113: E4671–E4680. doi:10.1073/pnas.1602419113
- Ding J, Wang K, Liu W, She Y, Sun Q, Shi J, Sun H, Wang D, Shao F (2016) Pore-forming activity and structural autoinhibition of the gasdermin family. *Nature* 535: 111–116. doi:10.1038/nature18590
- Du C, Fang M, Li Y, Li L, Wang X (2000) Smac, a mitochondrial protein that promotes cytochrome c-dependent caspase activation by eliminating IAP inhibition. *Cell* 102: 33–42. doi:10.1016/S0092-8674(00)00008-8
- Feoktistova M, Geserick P, Kellert B, Dimitrova DP, Langlais C, Hupe M, Cain K, MacFarlane M, Häcker G, Leverkus M (2011) CIAPs block ripoptosome formation, a RIP1/caspase-8 containing intracellular cell death complex differentially regulated by cFLIP isoforms. *Mol Cell* 43: 449–463. doi:10.1016/j.molcel.2011.06.011
- Fu TM, Li Y, Lu A, Li Z, Vajjhala PR, Cruz AC, Srivastava DB, DiMaio F, Penczek PA, Siegel RM, et al (2016) Cryo-EM structure of caspase-8 tandem DED filament reveals assembly and regulation mechanisms of the death-inducing signaling complex. *Mol Cell* 64: 236–250. doi:10.1016/j.molcel.2016.09.009
- Hagar JA, Powell DA, Aachoui Y, Ernst RK, Miao EA (2013) Cytoplasmic LPS activates caspase-11: Implications in TLR4-independent endotoxic shock. *Science* 341: 1250–1253. doi:10.1126/science.1240988
- He S, Wang L, Miao L, Wang T, Du F, Zhao L, Wang X (2009) Receptor interacting protein kinase-3 determines cellular necrotic response to TNF- α . *Cell* 137: 1100–1111. doi:10.1016/j.cell.2009.05.021
- He W, Wan H, Hu L, Chen P, Wang X, Huang Z, Yang Z-H, Zhong C-Q, Han J (2015) Gasdermin D is an executor of pyroptosis and required for interleukin-1 β secretion. *Cell Res* 25: 1285–1298. doi:10.1038/cr.2015.139
- Henry CM, Martin SJ (2017) Caspase-8 acts in a non-enzymatic role as a scaffold for assembly of a pro-inflammatory “FADDosome” complex upon TRAIL stimulation. *Mol Cell* 65: 715–729.e5. doi:10.1016/j.molcel.2017.01.022
- Jost PJ, Grabow S, Gray D, McKenzie MD, Nachbur U, Huang DCS, Bouillet P, Thomas HE, Borner C, Silke J, et al (2009) XIAP discriminates between

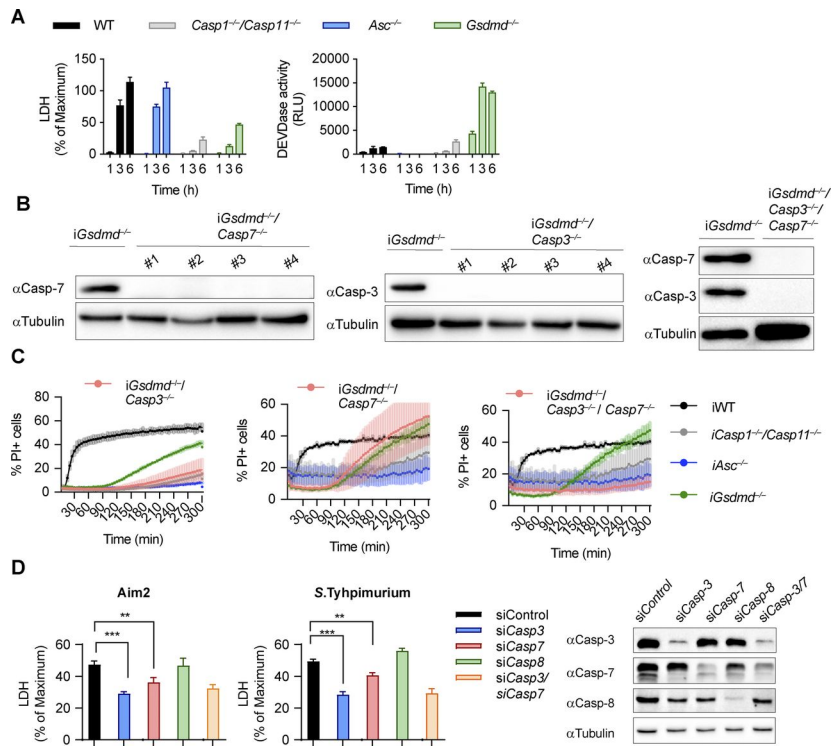
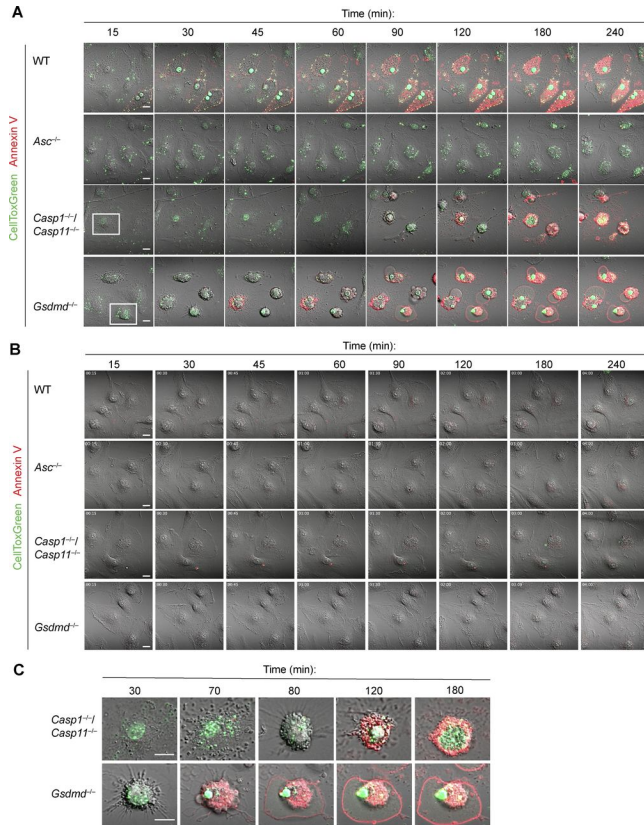
- type i and type II Fas-induced apoptosis. *Nature* 460: 1035–1039. doi:10.1038/nature08229
- Kaiser WJ, Upton JW, Long AB, Livingston-Rosanoff D, Daley-Bauer LP, Hakem R, Caspary T, Mocarski ES (2011) RIP3 mediates the embryonic lethality of caspase-8-deficient mice. *Nature* 471: 368–373. doi:10.1038/nature09857
- Kang T-B, Ben-Moshe T, Varfolomeev EE, Pewzner-Jung Y, Yogev N, Jurewicz A, Waisman A, Brenner O, Haffner R, Gustafsson E, et al (2004) Caspase-8 serves both apoptotic and nonapoptotic roles. *J Immunol* 173: 2976–2984. doi:10.4049/jimmunol.173.5.2976
- Kang TB, Jeong JS, Yang SH, Kovalenko A, Wallach D (2018) Caspase-8 deficiency in mouse embryos triggers chronic RIPK1-dependent activation of inflammatory genes, independently of RIPK3. *Cell Death Differ* 25: 1107–1117. doi:10.1038/s41418-018-0104-9
- Kanneganti A, Malireddi RKS, Saavedra PHV, Vande Walle L, Van Gorp H, Kambara H, Tillman H, Vogel P, Luo HR, Xavier RJ, et al (2018a) GSDMD is critical for autoinflammatory pathology in a mouse model of familial Mediterranean fever. *J Exp Med* 215: 1519–1529. doi:10.1084/jem.20172060
- Kanneganti T-D, Zhu Q, Zheng M, Balakrishnan A, Karki R (2018b) Francisella novicida protection against activation and is required for host gasdermin D promotes AIM2 inflammasome. *J Immunol* 201: 3662–3668. doi:10.4049/jimmunol.1800788
- Kasibhatla S, Amarante-Mendes GP, Finucane D, Brunner T, Bossy-Wetzel E, Green DR (2006) Analysis of DNA fragmentation using agarose gel electrophoresis. *CSH Protoc* 2006: pdb.prot4429. doi:10.1101/pdb.prot4429
- Kavanagh E, Rodhe J, Burguillos MA, Venero JL, Joseph B (2014) Regulation of caspase-3 processing by cIAP2 controls the switch between pro-inflammatory activation and cell death in microglia. *Cell Death Dis* 5: e1565. doi:10.1038/cddis.2014.514
- Kayagaki N, Stowe IB, Lee BL, O'Rourke K, Anderson K, Warming S, Cuellar T, Haley B, Roose-Girma M, Phung QT, et al (2015) Caspase-11 cleaves gasdermin D for non-canonical inflammasome signalling. *Nature* 526: 666–671. doi:10.1038/nature15541
- Kayagaki N, Warming S, Lamkanfi M, Vande Walle L, Louie S, Dong J, Newton K, Qu Y, Liu J, Heldens S, et al (2011) Non-canonical inflammasome activation targets caspase-11. *Nature* 479: 117–121. doi:10.1038/nature10558
- Kayagaki N, Wong MT, Stowe IB, Ramani SR, Gonzalez LC, Akashi-Takamura S, Miyake K, Zhang J, Lee WP, Forsberg LS, et al (2013) Independent of TLR4. *Science* 330: 1246–1249. doi:10.5061/dryad.bt51g
- Lamkanfi M, Kanneganti T-D (2010) Caspase-7: A protease involved in apoptosis and inflammation. *Int J Biochem Cell Biol* 42: 21–24. doi:10.1016/j.biocel.2009.09.013
- Lamkanfi M, Kanneganti T-D, Van Damme P, Vanden Berghe T, Vanoverberghe I, Vandekerckhove J, Vandenabeele P, Gevaert K, Núñez G (2008) Targeted peptide-centric proteomics reveals caspase-7 as a substrate of the caspase-1 inflammasomes. *Mol Cell Proteomics* 7: 2350–2363. doi:10.1074/mcp.M800132-MCP200
- Lee BL, Mirrashidi KM, Stowe IB, Kummerfeld SK, Watanabe C, Haley B, Cuellar TL, Reichelt M, Kayagaki N (2018) ASC- and caspase-8-dependent apoptotic pathway diverges from the NLR4 inflammasome in macrophages. *Sci Rep* 8: 3788. doi:10.1038/s41598-018-21998-3
- Li H, Zhu H, Xu C, Yuan J (1998) Cleavage of BID by caspase 8 mediates the mitochondrial damage in the fas pathway of apoptosis. *Cell* 94: 491–501. doi:10.1016/S0092-8674(00)81590-1
- Li ML, Stollar V (2004) Alphaviruses and apoptosis. *Int Rev Immunol* 23: 7–24. doi:10.1080/08830180490265529
- Liu X, Zhang Z, Ruan J, Pan Y, Magupalli VG, Wu H, Lieberman J (2016) Inflammasome-activated gasdermin D causes pyroptosis by forming membrane pores. *Nature* 535: 153–158. doi:10.1038/nature18629
- Maelfait J, Vercammen E, Janssens S, Schotte P, Haegman M, Magez S, Beyaert R (2008) Stimulation of Toll-like receptor 3 and 4 induces interleukin-1 β maturation by caspase-8. *J Exp Med* 205: 1967–1973. doi:10.1084/jem.20071632
- Man SM, Tourlomis P, Hopkins L, Monie TP, Fitzgerald KA, Bryant CE (2013) Salmonella infection induces recruitment of caspase-8 to the inflammasome to modulate IL-1 β production. *J Immunol* 191: 5239–5246. doi:10.4049/jimmunol.1301581
- Mariathasan S, Hewton K, Monack DM, Vucic D, French DM, Lee WP, Roose-Girma M, Erickson S, Dixit VM (2004) Differential activation of the inflammasome by caspase-1 adaptors ASC and Ipaf. *Nature* 430: 213–218. doi:10.1038/nature02664
- Mascarenhas DPA, Cerqueira DM, Pereira MSF, Castanheira FVS, Fernandes TD, Manin GZ, Cunha LD, Zamboni DS (2017) Inhibition of caspase-1 or gasdermin-D enable caspase-8 activation in the Naip5/NLRC4/ASC inflammasome. *PLoS Pathog* 13: e1006502. doi:10.1371/journal.ppat.1006502
- Masters SL, Simon A, Aksentijevich I, Kastner DL (2009) Horror autoinflammaticus: The molecular pathophysiology of autoinflammatory disease. *Annu Rev Immunol* 27: 621–668. doi:10.1146/annurev.immunol.25.022106.141627
- Momeni HR (2011) Role of calpain in apoptosis. *Cell J* 13: 65–72.
- Monteleone M, Stanley AC, Chen KW, Sweet MJ, Stow JL, Correspondence KS, Brown DL, Bezbradica JS, Von Pein JB, Holley CL, et al (2018) Interleukin-1 β maturation triggers its relocation to the plasma membrane for gasdermin-D-dependent and -independent secretion. *Cell Rep* 24: 1425–1433. doi:10.1016/j.celrep.2018.07.027
- Nailwal H, Chan FKM (2019) Necroptosis in anti-viral inflammation. *Cell Death Differ* 26: 4–13. doi:10.1038/s41418-018-0172-x
- Newton K, et al (2019a) Activity of caspase-8 determines plasticity between cell death pathways. *Nature* 575: 679–682. doi:10.1038/s41586-019-1752-8
- Newton K, et al (2019b) Cleavage of RIPK1 by caspase-8 is crucial for limiting apoptosis and necroptosis. *Nature* 574: 428–431. doi:10.1038/s41586-019-1548-x
- Oberst A, Dillon CP, Weinlich R, McCormick LL, Fitzgerald P, Pop C, Hakem R, Salvesen GS, Green DR (2011) Catalytic activity of the caspase-8-FLIP L complex inhibits RIPK3-dependent necrosis. *Nature* 471: 363–368. doi:10.1038/nature09852
- Ong SE, Blagoev B, Kratchmarova I, Kristensen DB, Steen H, Pandey A, Mann M (2002) Stable isotope labeling by amino acids in cell culture, SILAC, as a simple and accurate approach to expression proteomics. *Mol Cell Proteomics* 1: 376–386. doi:10.1074/mcp.M200025-MCP200
- Orning P, Weng D, Starheim K, Ratner D, Best Z, Lee B, Brooks A, Xia S, Wu H, Kelliher MA, et al (2018) Pathogen blockade of TAK1 triggers caspase-8-dependent cleavage of gasdermin D and cell death. *Science* 2818: eaau2818. doi:10.1126/science.aau2818
- Pierini R, Juruj C, Perret M, Jones CL, Mangeot P, Weiss DS, Henry T (2012) AIM2/ASC triggers caspase-8-dependent apoptosis in Francisella-infected caspase-1-deficient macrophages. *Cell Death Differ* 19: 1709–1721. doi:10.1038/cdd.2012.51
- Rashidi M, Simpson DS, Hempel A, Frank D, Petrie E, Vince A, Feltham R, Murphy J, Chatfield SM, Salvesen GS, et al (2019) The pyroptotic cell death effector gasdermin D is activated by gout-associated uric acid crystals but is dispensable for cell death and IL-1 β release. *J Immunol* 203: 736–748. doi:10.4049/jimmunol.1900228
- Rathkey JK, Zhao J, Liu Z, Chen Y, Yang J, Kondolf HC, Benson BL, Chirieleison SM, Huang AY, Dubyak GR, et al (2018) Chemical disruption of the pyroptotic pore-forming protein gasdermin D inhibits inflammatory cell death and sepsis. *Sci Immunol* 3: eaat2738. doi:10.1126/sciimmunol.aat2738
- Riley JS, et al (2018) Mitochondrial inner membrane permeabilisation enables mtDNA release during apoptosis. *EMBO J* 37: e99238. doi:10.15252/emj.201899238

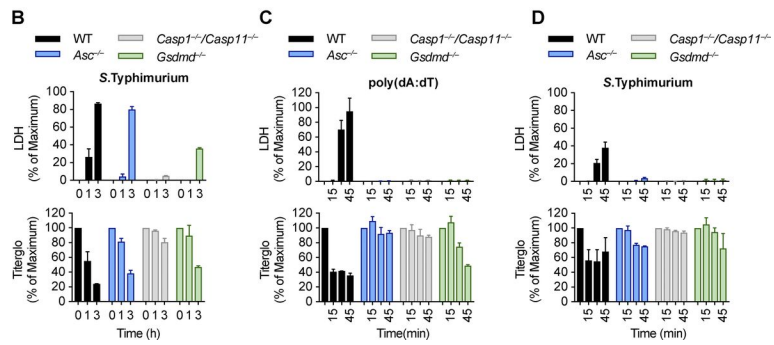
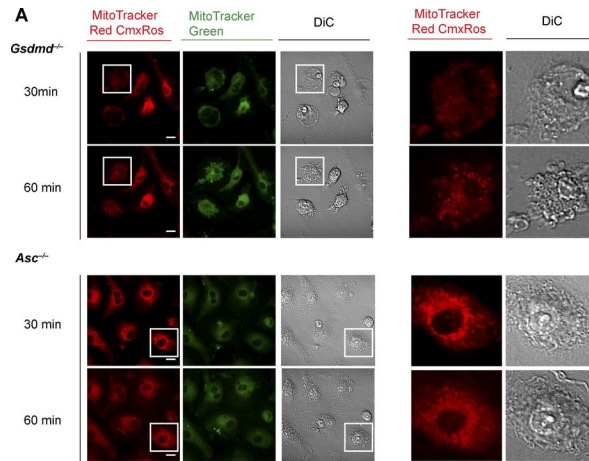
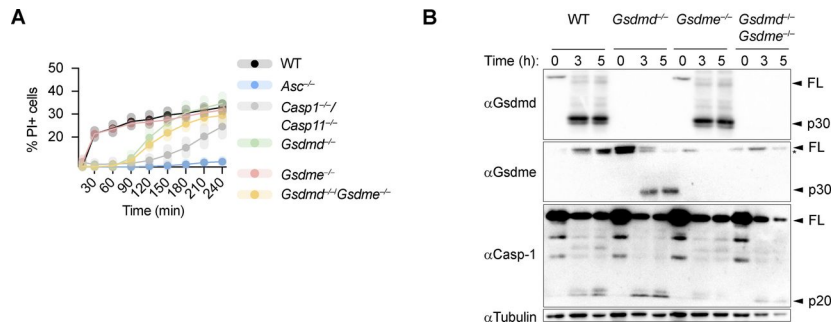
- Roy N, Deveraux QL, Takahashi R, Salvesen GS, Reed JC, Robertson M, Ghayur T, Wong WW, Kamen R, Weichselbaum R (1997) The c-IAP-1 and c-IAP-2 proteins are direct inhibitors of specific caspases. *EMBO J* 16: 6914–6925. doi:10.1093/emboj/16.23.6914
- Sagulenko V, Thygesen SJ, Sester DP, Idris A, Cridland JA, Vajjhala PR, Roberts TL, Schroder K, Vince JE, Hill JM, et al (2013) AIM2 and NLRP3 inflammasomes activate both apoptotic and pyroptotic death pathways via ASC. *Cell Death Differ* 20: 1149–1160. doi:10.1038/cdd.2013.37
- Sagulenko V, Vitak N, Vajjhala PR, Vince JE, Stacey KJ (2018) Caspase-1 is an apical caspase leading to caspase-3 cleavage in the AIM2 inflammasome response, independent of caspase-8. *J Mol Biol* 430: 238–247. doi:10.1016/j.jmb.2017.10.028
- Sarhan J, Liu BC, Muendlein HI, Li P, Nilson R, Tang AY, Rongvaux A, Bunnell SC, Shao F, Green DR, et al (2018) Caspase-8 induces cleavage of gasdermin D to elicit pyroptosis during Yersinia infection [immunology and inflammation]. *Proc Natl Acad Sci U S A* 115: E10888–E10897. doi:10.1073/pnas.1809548115
- Sborgi L, Rühl S, Mulvihill E, Pipercevic J, Heilig R, Stahlberg H, Farady C, Müller D, Broz P, Hiller S (2016) GSDMD membrane pore formation constitutes the mechanism of pyroptotic cell death. *EMBO J* 35: e201694696–13. doi:10.15252/emboj.201694696
- Schneider KS, Groß CJ, Dreier RF, Saller BS, Mishra R, Gorka O, Heilig R, Meunier E, Dick MS, Ciković T, et al (2017) The inflammasome drives GSDMD-independent secondary pyroptosis and IL-1 release in the absence of caspase-1 protease activity. *Cell Rep* 21: 3846–3859. doi:10.1016/j.celrep.2017.12.018
- Scott FL, Denault JB, Riedel SJ, Shin H, Renatus M, Salvesen GS (2005) XIAP inhibits caspase-3 and -7 using two binding sites: Evolutionary conserved mechanism of IAPs. *EMBO J* 24: 645–655. doi:10.1038/sj.emboj.7600544
- Shi J, Zhao Y, Wang K, Shi X, Wang Y, Huang H, Zhuang Y, Cai T, Wang F, Shao F (2015) Cleavage of GSDMD by inflammatory caspases determines pyroptotic cell death. *Nature* 526: 660–665. doi:10.1038/nature15514
- Shi J, Zhao Y, Wang Y, Gao W, Ding J, Li P, Hu L, Shao F (2014) Inflammatory caspases are innate immune receptors for intracellular LPS. *Nature* 514: 187–192. doi:10.1038/nature13683
- Sollberger G, Choidas A, Burn GL, Habenberger P, Di Lucrezia R, Kordes S, Menninger S, Eickhoff J, Nussbaumer P, Klebl B, et al (2018) Gasdermin D plays a vital role in the generation of neutrophil extracellular traps. *Sci Immunol* 3: eaar6689. doi:10.1126/sciimmunol.aar6689
- Stennicke HR, Jürgensmeier JM, Shin H, Deveraux Q, Wolf BB, Yang X, Zhou Q, Ellerby HM, Ellerby LM, Bredesen D, et al (1998) Pro-caspase-3 is a major physiologic target of caspase-8. *J Biol Chem* 273: 27084–27090. doi:10.1074/jbc.273.42.27084
- Taabazuizing CY, Okondo MC, Bachovchin DA (2017) Pyroptosis and apoptosis pathways engage in bidirectional crosstalk in monocytes and macrophages. *Cell Chem Biol* 24: 507–514.e4. doi:10.1016/j.jchembiol.2017.03.009
- Takahashi R, Deveraux Q, Tamm I, Welsh K, Assa-Munt N, Salvesen GS, Reed JC (1998) A single BIR domain of XIAP sufficient for inhibiting caspases. *J Biol Chem* 273: 7787–7790. doi:10.1074/jbc.273.14.7787
- Taxman DJ, Huang MTH, Ting JPY (2010) Inflammasome inhibition as a pathogenic stealth mechanism. *Cell Host Microbe* 8: 7–11. doi:10.1016/j.chom.2010.06.005
- Tenev T, Bianchi K, Darding M, Broemer M, Langlais C, Wallberg F, Zachariou A, Lopez J, MacFarlane M, Cain K, et al (2011) The ripoptosome, a signaling platform that assembles in response to genotoxic stress and loss of IAPs. *Mol Cell* 43: 432–448. doi:10.1016/j.molcel.2011.06.006
- Tsuchiya K, Nakajima S, Hosojima S, Thi Nguyen D, Hattori T, Manh Le T, Hori O, Mahib MR, Yamaguchi Y, Miura M, et al (2019) Caspase-1 initiates apoptosis in the absence of gasdermin D. *Nat Commun* 10: 2091. doi:10.1038/s41467-019-09753-2
- Vajjhala PR, Lu A, Brown DL, Pang SW, Sagulenko V, Sester DP, Cridland SO, Hill JM, Schroder K, Stow JL, et al (2015) The inflammasome adaptor ASC induces procaspase-8 death effector domain filaments. *J Biol Chem* 290: 29217–29230. doi:10.1074/jbc.M115.687731
- Van Opdenbosch N, Van Gorp H, Verdonck M, Saavedra PHV, de Vasconcelos NM, Gonçalves A, Vande Walle L, Demon D, Matusiak M, Van Hauwermeiren F, et al (2017) Caspase-1 engagement and TLR-induced c-FLIP expression suppress ASC/caspase-8-dependent apoptosis by inflammasome sensors NLRP1b and NLR4. *Cell Rep* 21: 3427–3444. doi:10.1016/j.celrep.2017.11.088
- Verhagen AM, Ekert PG, Pakusch M, Silke J, Connolly LM, Reid GE, Moritz RL, Simpson RJ, Vaux DL (2000) Identification of DIABLO, a mammalian protein that promotes apoptosis by binding to and antagonizing IAP proteins. *Cell* 102: 43–53. doi:10.1016/S0092-8674(00)00009-X
- Vince JE, De Nardo D, Gao W, Vince AJ, Hall C, McArthur K, Simpson D, Vijayaraj S, Lindqvist LM, Bouillet P, et al (2018) The mitochondrial apoptotic effectors BAX/BAK activate caspase-3 and -7 to trigger NLRP3 inflammasome and caspase-8 driven IL-1 β activation. *Cell Rep* 25: 2339–2353.e4. doi:10.1016/j.celrep.2018.10.103
- Walsh JG, Cullen SP, Sheridan C, Lüthi AU, Gerner C, Martin SJ (2008) Executioner caspase-3 and caspase-7 are functionally distinct proteases. *Proc Natl Acad Sci U S A* 105: 12815–12819. doi:10.1073/pnas.0707715105
- Wang H, Lei X, Xiao X, Yang C, Lu W, Huang Z, Leng Q, Jin Q, He B, Meng G, et al (2015) Reciprocal regulation between enterovirus 71 and the NLRP3 inflammasome. *Cell Rep* 12: 42–48. doi:10.1016/j.celrep.2015.05.047
- Wang J, Deobald K, Re F (2019) Bacteria through pyroptosis and direct killing of gasdermin D protects from melioidosis. *J Immunol* 202: 3468–3473. doi:10.4049/jimmunol.1900045
- Wang W, Xiao F, Wan P, Pan P, Zhang Y, Liu F, Wu K, Liu Y, Wu J (2017a) EV71 3D protein binds with NLRP3 and enhances the assembly of inflammasome complex. *PLoS Pathog* 6: e1006123. doi:10.1371/journal.ppat.1006123
- Wang Y, Gao W, Shi X, Ding J, Liu W, He H, Wang K, Shao F (2017b) Chemotherapy drugs induce pyroptosis through caspase-3 cleavage of a gasdermin. *Nature* 547: 99–103. doi:10.1038/nature22393
- Wilkinson JC, Wilkinson AS, Scott FL, Csomos RA, Salvesen GS, Duckett CS (2004) Neutralization of Smac/Diablo by inhibitors of apoptosis (IAPs): A caspase-independent mechanism for apoptotic inhibition. *J Biol Chem* 279: 51082–51090. doi:10.1074/jbc.M408655200
- Wu G, Chai J, Suber TL, Wu JW, Du C, Wang X, Shi Y (2000) Structural basis of IAP recognition by Smac/DIABLO. *Nature* 408: 1008–1012. doi:10.1038/35050012
- Xiao J, Wang C, Yao J-C, Alippe Y, Xu C, Kress D, Civitelli R, Abu-Amer Y, Kanneganti T-D, Link DC, et al (2018) Gasdermin D mediates the pathogenesis of neonatal-onset multisystem inflammatory disease in mice. *PLoS Biol* 16: e3000047. doi:10.1371/journal.pbio.3000047
- Zhang D-W, Shao J, Lin J, Zhang N, Lu B-J, Lin S-C, Dong M-Q, Han J (2009) RIP3, an energy metabolism regulator that switches TNF-induced cell death from apoptosis to necrosis. *Science* 325: 332–336. doi:10.1126/science.1172308

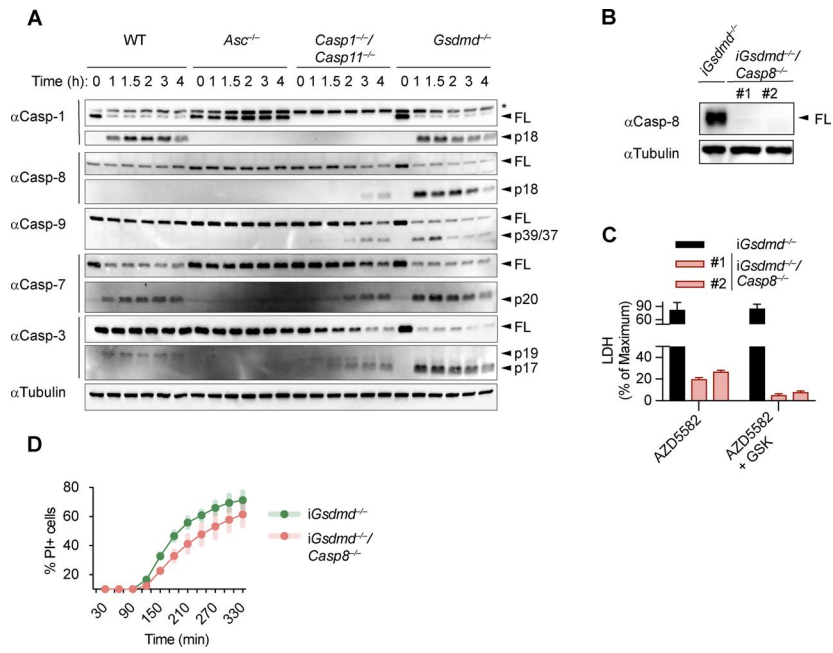
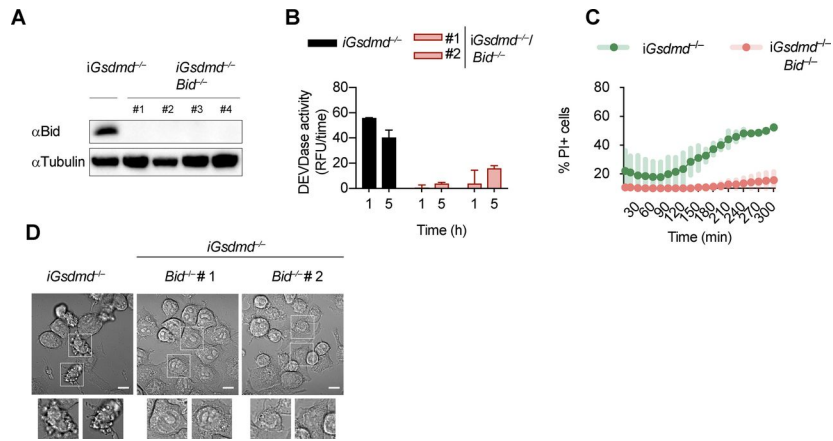


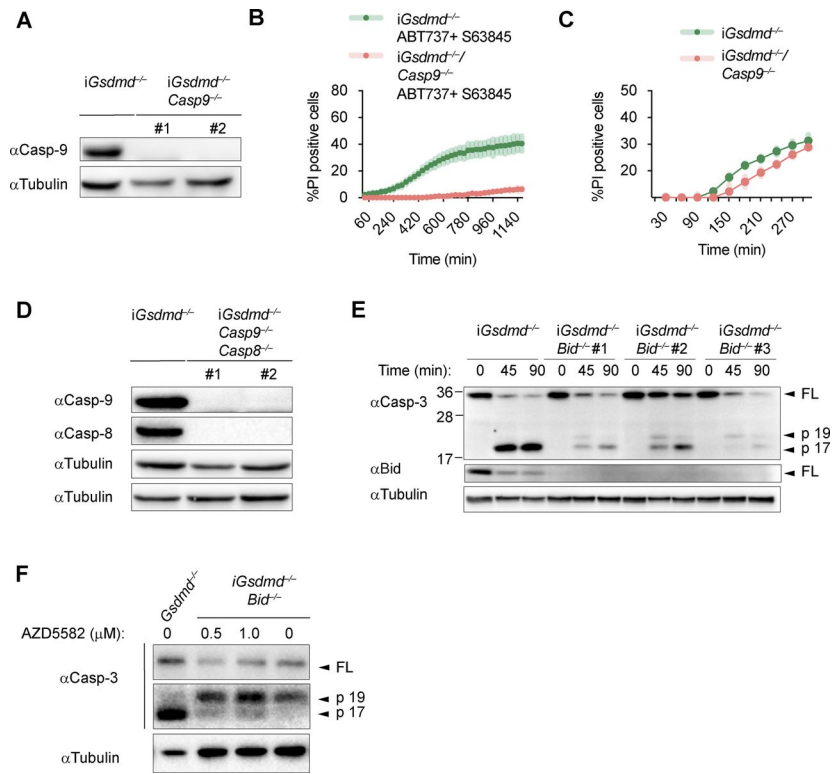
License: This article is available under a Creative Commons License (Attribution 4.0 International, as described at <https://creativecommons.org/licenses/by/4.0/>).











6. References

1. Chaplin, D. D. Overview of the Immune Response. *J. Allergy Clin. Immunol.* **125**, S3 (2010).
2. Netea, M. G. *et al.* Defining trained immunity and its role in health and disease. *Nat. Rev. Immunol.* 2020 206 **20**, 375–388 (2020).
3. Medzhitov, R. Origin and physiological roles of inflammation. *Nature* **454**, 428–435 (2008).
4. Janeway, C. A. Approaching the asymptote? Evolution and revolution in immunology. *Cold Spring Harb. Symp. Quant. Biol.* **54 Pt 1**, 1–13 (1989).
5. Medzhitov, R. & Janeway, C. A. Innate immunity: impact on the adaptive immune response. *Curr. Opin. Immunol.* **9**, 4–9 (1997).
6. Janeway, C. A. The immune system evolved to discriminate infectious nonself from noninfectious self. *Immunol. Today* **13**, 11–16 (1992).
7. Matzinger, P. Tolerance, Danger, and the Extended Family. <https://doi.org/10.1146/annurev.iy.12.040194.005015> **12**, 991–1045 (2003).
8. Liston, A. & Masters, S. L. Homeostasis-altering molecular processes as mechanisms of inflammasome activation. *Nat. Rev. Immunol.* **17**, 208–214 (2017).
9. Gasteiger, G. & Rudensky, A. Y. Interactions between innate and adaptive lymphocytes. *Nat. Rev. Immunol.* 2014 149 **14**, 631–639 (2014).
10. Zinkernagel, R. M. & Doherty, P. C. The discovery of MHC restriction. *Immunol. Today* **18**, 14–17 (1997).
11. Joshi, N. S. & Kaech, S. M. Effector CD8 T cell development: a balancing act between memory cell potential and terminal differentiation. *J. Immunol.* **180**, 1309–1315 (2008).
12. Luckheeram, R. V., Zhou, R., Verma, A. D. & Xia, B. CD4+T Cells: Differentiation and Functions. *Clin. Dev. Immunol.* **2012**, 12 (2012).
13. Sakaguchi, S. Naturally arising CD4+ regulatory t cells for immunologic self-tolerance and negative control of immune responses. *Annu. Rev. Immunol.* **22**, 531–562 (2004).
14. Cyster, J. G. & Allen, C. D. C. B Cell Responses: Cell Interaction Dynamics and Decisions. *Cell* **177**, 524–540 (2019).
15. Schroeder, H. W. & Cavacini, L. Structure and function of immunoglobulins. *J. Allergy Clin. Immunol.* **125**, (2010).
16. A, I. & J, L. Virus interference. I. The interferon. *Proc. R. Soc. London. Ser. B, Biol. Sci.* **147**, 258–267 (1957).
17. Virus interference. II. Some properties of interferon. *Proc. R. Soc. London. Ser. B - Biol. Sci.* **147**, 268–273 (1957).
18. ISAACS, A. & BURKE, D. C. Viral interference and interferon. *Br. Med. Bull.* **15**, 185–8 (1959).
19. Pestka, S., Langer, J. A., Zoon, K. C. & Samuel, C. E. Interferons and their actions. *Annu. Rev. Biochem.* **56**, 727–777 (1987).
20. Pestka, S., Krause, C. D. & Walter, M. R. Interferons, interferon-like cytokines, and their receptors. *Immunol. Rev.* **202**, 8–32 (2004).
21. Havell, E. A. *et al.* Two antigenically distinct species of human interferon. *Proc. Natl. Acad. Sci. U. S. A.* **72**, 2185–2187 (1975).
22. Li, D. & Wu, M. Pattern recognition receptors in health and diseases. *Signal Transduct. Target. Ther.* 2021 61 **6**, 1–24 (2021).

23. Alexopoulou, L., Holt, A. C., Medzhitov, R. & Flavell, R. A. Recognition of double-stranded RNA and activation of NF-kappaB by Toll-like receptor 3. *Nature* **413**, 732–738 (2001).
24. Yamamoto, M. *et al.* Role of adaptor TRIF in the MyD88-independent toll-like receptor signaling pathway. *Science* **301**, 640–643 (2003).
25. Sharma, S. *et al.* Triggering the interferon antiviral response through an IKK-related pathway. *Science* **300**, 1148–1151 (2003).
26. Fitzgerald, K. A. *et al.* IKKepsilon and TBK1 are essential components of the IRF3 signaling pathway. *Nat. Immunol.* **4**, 491–496 (2003).
27. Hemmi, H. *et al.* The roles of two I kappa B kinase-related kinases in lipopolysaccharide and double stranded RNA signaling and viral infection. *J. Exp. Med.* **199**, 1641–1650 (2004).
28. Yamamoto, M. *et al.* Cutting edge: a novel Toll/IL-1 receptor domain-containing adapter that preferentially activates the IFN-beta promoter in the Toll-like receptor signaling. *J. Immunol.* **169**, 6668–6672 (2002).
29. Moynagh, P. N. TLR signalling and activation of IRFs: revisiting old friends from the NF-kappaB pathway. *Trends Immunol.* **26**, 469–476 (2005).
30. Heinz, L. X. *et al.* TASL is the SLC15A4-associated adaptor for IRF5 activation by TLR7–9. *Nature* **581**, 316–322 (2020).
31. Luo, D., Kohlway, A. & Pyle, A. M. Duplex RNA activated ATPases (DRAs): platforms for RNA sensing, signaling and processing. *RNA Biol.* **10**, 111–120 (2013).
32. Kato, H. *et al.* Differential roles of MDA5 and RIG-I helicases in the recognition of RNA viruses. *Nature* **441**, 101–105 (2006).
33. Loo, Y.-M. *et al.* Distinct RIG-I and MDA5 signaling by RNA viruses in innate immunity. *J. Virol.* **82**, 335–345 (2008).
34. Gitlin, L. *et al.* Essential role of mda-5 in type I IFN responses to polyriboinosinic:polyribocytidylic acid and encephalomyocarditis picornavirus. *Proc. Natl. Acad. Sci. U. S. A.* **103**, 8459–8464 (2006).
35. Sun, L., Wu, J., Du, F., Chen, X. & Chen, Z. J. Cyclic GMP-AMP Synthase is a Cytosolic DNA Sensor that Activates the Type-I Interferon Pathway. *Science* **339**, 786–791 (2013).
36. Leber, J. H. *et al.* Distinct TLR- and NLR-Mediated Transcriptional Responses to an Intracellular Pathogen. *PLOS Pathog.* **4**, e6 (2008).
37. Pandey, A. K. *et al.* NOD2, RIP2 and IRF5 play a critical role in the type I interferon response to Mycobacterium tuberculosis. *PLoS Pathog.* **5**, (2009).
38. Watanabe, T. *et al.* NOD1 contributes to mouse host defense against Helicobacter pylori via induction of type I IFN and activation of the ISGF3 signaling pathway. *J. Clin. Invest.* **120**, 1645–1662 (2010).
39. Frederick Wheelock, E. Interferon-like virus-inhibitor induced in human leukocytes by phytohemagglutinin. *Science* **149**, 310–311 (1965).
40. Orange, J. S., Wang, B., Terhorst, C. & Biron, C. A. Requirement for natural killer cell-produced interferon gamma in defense against murine cytomegalovirus infection and enhancement of this defense pathway by interleukin 12 administration. *J. Exp. Med.* **182**, 1045–1056 (1995).
41. Brady, J. *et al.* The Interactions of Multiple Cytokines Control NK Cell Maturation. *J. Immunol.* **185**, 6679–6688 (2010).
42. Bacon, C. M. *et al.* Interleukin 12 (IL-12) induces tyrosine phosphorylation of JAK2 and TYK2: differential use of Janus family tyrosine kinases by IL-2 and IL-12. *J. Exp. Med.* **181**, 399 (1995).

43. Jacobson, N. G. *et al.* Interleukin 12 signaling in T helper type 1 (Th1) cells involves tyrosine phosphorylation of signal transducer and activator of transcription (Stat)3 and Stat4. *J. Exp. Med.* **181**, 1755–1762 (1995).
44. Mavropoulos, A., Sully, G., Cope, A. P. & Clark, A. R. Stabilization of IFN-gamma mRNA by MAPK p38 in IL-12- and IL-18-stimulated human NK cells. *Blood* **105**, 282–288 (2005).
45. Sheppard, P. *et al.* IL-28, IL-29 and their class II cytokine receptor IL-28R. *Nat. Immunol.* **4**, 63–68 (2003).
46. Kotenko, S. V. *et al.* IFN-lambdas mediate antiviral protection through a distinct class II cytokine receptor complex. *Nat. Immunol.* **4**, 69–77 (2003).
47. Prokunina-Olsson, L. *et al.* A variant upstream of IFNL3 (IL28B) creating a new interferon gene IFNL4 is associated with impaired clearance of hepatitis C virus. *Nat. Genet.* **45**, 164–171 (2013).
48. O'Brien, T. R., Prokunina-Olsson, L. & Donnelly, R. P. IFN- λ 4: the paradoxical new member of the interferon lambda family. *J. Interferon Cytokine Res.* **34**, 829–838 (2014).
49. Blazek, K. *et al.* IFN- λ resolves inflammation via suppression of neutrophil infiltration and IL-1 β production. *J. Exp. Med.* **212**, 845–853 (2015).
50. Broggi, A., Tan, Y., Granucci, F. & Zanoni, I. IFN- λ suppresses intestinal inflammation by non-translational regulation of neutrophil function. *Nat. Immunol.* **18**, 1084–1093 (2017).
51. Österlund, P. I., Pietilä, T. E., Veckman, V., Kotenko, S. V. & Julkunen, I. IFN regulatory factor family members differentially regulate the expression of type III IFN (IFN-lambda) genes. *J. Immunol.* **179**, 3434–3442 (2007).
52. Onoguchi, K. *et al.* Viral infections activate types I and III interferon genes through a common mechanism. *J. Biol. Chem.* **282**, 7576–7581 (2007).
53. Thomson, S. J. P. *et al.* The role of transposable elements in the regulation of IFN-lambda1 gene expression. *Proc. Natl. Acad. Sci. U. S. A.* **106**, 11564–11569 (2009).
54. Odendall, C. *et al.* Diverse intracellular pathogens activate type III interferon expression from peroxisomes. *Nat. Immunol.* **15**, 717–726 (2014).
55. Dixit, E. *et al.* Peroxisomes are signaling platforms for antiviral innate immunity. *Cell* **141**, 668–681 (2010).
56. Novick, D., Cohen, B. & Rubinstein, M. The human interferon alpha/beta receptor: characterization and molecular cloning. *Cell* **77**, 391–400 (1994).
57. Wilks, A. F. Two putative protein-tyrosine kinases identified by application of the polymerase chain reaction. *Proc. Natl. Acad. Sci. U. S. A.* **86**, 1603–1607 (1989).
58. Identification and chromosomal mapping of new human tyrosine kinase genes - PubMed. <https://pubmed.ncbi.nlm.nih.gov/2156206/>.
59. Fu, X. Y., Schindler, C., Improtta, T., Aebersold, R. & Darnell, J. E. The proteins of ISGF-3, the interferon alpha-induced transcriptional activator, define a gene family involved in signal transduction. *Proc. Natl. Acad. Sci. U. S. A.* **89**, 7840–7843 (1992).
60. Velazquez, L., Fellous, M., Stark, G. R. & Pellegrini, S. A protein tyrosine kinase in the interferon alpha/beta signaling pathway. *Cell* **70**, 313–322 (1992).
61. Der, S. D., Zhou, A., Williams, B. R. G. & Silverman, R. H. Identification of genes differentially regulated by interferon alpha, beta, or gamma using oligonucleotide arrays. *Proc. Natl. Acad. Sci. U. S. A.* **95**, 15623–15628 (1998).

62. Veer, M. J. de *et al.* Functional classification of interferon-stimulated genes identified using microarrays. *J. Leukoc. Biol.* **69**, 912–920 (2001).
63. Plataniias, L. C. Mechanisms of type-I- and type-II-interferon-mediated signalling. *Nat. Rev. Immunol.* **5**, 375–386 (2005).
64. Aguet, M., Dembić, Z. & Merlin, G. Molecular cloning and expression of the human interferon-gamma receptor. *Cell* **55**, 273–280 (1988).
65. Jung, V. *et al.* Human chromosomes 6 and 21 are required for sensitivity to human interferon gamma. *Proc. Natl. Acad. Sci. U. S. A.* **84**, 4151–4155 (1987).
66. Shuai, K., Schindler, C., Prezioso, V. R. & Darnell, J. E. Activation of transcription by IFN-gamma: tyrosine phosphorylation of a 91-kD DNA binding protein. *Science* **258**, 1808–1812 (1992).
67. Silvennoinen, O., Ihle, J. N., Schlessinger, J. & Levy, D. E. Interferon-induced nuclear signalling by Jak protein tyrosine kinases. *Nature* 1993 3666455 **366**, 583–585 (1993).
68. Igarashi, K. I. *et al.* Interferon-gamma induces tyrosine phosphorylation of interferon-gamma receptor and regulated association of protein tyrosine kinases, Jak1 and Jak2, with its receptor. *J. Biol. Chem.* **269**, 14333–14336 (1994).
69. Greenlund, A. C. *et al.* Stat recruitment by tyrosine-phosphorylated cytokine receptors: an ordered reversible affinity-driven process. *Immunity* **2**, 677–687 (1995).
70. Decker, T., Kovarik, P. & Meinke, A. GAS elements: a few nucleotides with a major impact on cytokine-induced gene expression. *J. Interferon Cytokine Res.* **17**, 121–134 (1997).
71. Gad, H. H. *et al.* Interferon- λ Is Functionally an Interferon but Structurally Related to the Interleukin-10 Family. *J. Biol. Chem.* **284**, 20869–20875 (2009).
72. Wack, A., Terczyńska-Dyla, E. & Hartmann, R. Guarding the frontiers: the biology of type III interferons. *Nat. Immunol.* 2015 168 **16**, 802–809 (2015).
73. Zhou, Z. *et al.* Type III interferon (IFN) induces a type I IFN-like response in a restricted subset of cells through signaling pathways involving both the Jak-STAT pathway and the mitogen-activated protein kinases. *J. Virol.* **81**, 7749–7758 (2007).
74. Mordstein, M. *et al.* Lambda interferon renders epithelial cells of the respiratory and gastrointestinal tracts resistant to viral infections. *J. Virol.* **84**, 5670–5677 (2010).
75. Sommereyns, C., Paul, S., Staeheli, P. & Michiels, T. IFN-lambda (IFN-lambda) is expressed in a tissue-dependent fashion and primarily acts on epithelial cells in vivo. *PLoS Pathog.* **4**, (2008).
76. Pott, J. *et al.* IFN-lambda determines the intestinal epithelial antiviral host defense. *Proc. Natl. Acad. Sci. U. S. A.* **108**, 7944–7949 (2011).
77. Schneider, W. M., Chevillotte, M. D. & Rice, C. M. Interferon-Stimulated Genes: A Complex Web of Host Defenses. *Annu. Rev. Immunol.* **32**, 513 (2014).
78. Meunier, E. & Broz, P. Interferon-inducible GTPases in cell autonomous and innate immunity. *Cell. Microbiol.* **18**, 168–180 (2016).
79. Silverman, R. H. Viral Encounters with 2',5'-Oligoadenylate Synthetase and RNase L during the Interferon Antiviral Response. *J. Virol.* **81**, 12720 (2007).
80. Wreschner, D. H., McCauley, J. W., Skehel, J. J. & Kerr, I. M. Interferon action--sequence specificity of the ppp(A2'p)nA-dependent ribonuclease.

- Nature* **289**, 414–417 (1981).
81. Floyd-Smith, G., Slattery, E. & Lengyel, P. Interferon action: RNA cleavage pattern of a (2'-5')oligoadenylate--dependent endonuclease. *Science* **212**, 1030–1032 (1981).
 82. Zhou, A. *et al.* Interferon action and apoptosis are defective in mice devoid of 2',5'-oligoadenylate-dependent RNase L. *EMBO J.* **16**, 6355–6363 (1997).
 83. Castelli, J. A. C. *et al.* The role of 2'-5' oligoadenylate-activated ribonuclease L in apoptosis. *Cell Death Differ.* **1998 54 5**, 313–320 (1998).
 84. Castelli, J. A. C. *et al.* A study of the interferon antiviral mechanism: apoptosis activation by the 2-5A system. *J. Exp. Med.* **186**, 967–972 (1997).
 85. Malathi, K., Dong, B., Gale, M. & Silverman, R. H. Small self-RNA generated by RNase L amplifies antiviral innate immunity. *Nature* **448**, 816–819 (2007).
 86. Roberts, W. K., Hovanessian, A., Brown, R. E., Clemens, M. J. & Kerr, I. M. Interferon-mediated protein kinase and low-molecular-weight inhibitor of protein synthesis. *Nature* **264**, 477–480 (1976).
 87. Zilberstein, A., Kimchi, A., Schmidt, A. & Revel, M. Isolation of two interferon-induced translational inhibitors: a protein kinase and an oligo-isoadenylate synthetase. *Proc. Natl. Acad. Sci. U. S. A.* **75**, 4734–4738 (1978).
 88. Gale, M. & Katze, M. G. Molecular mechanisms of interferon resistance mediated by viral-directed inhibition of PKR, the interferon-induced protein kinase. *Pharmacol. Ther.* **78**, 29–46 (1998).
 89. Brass, A. L. *et al.* The IFITM proteins mediate cellular resistance to influenza A H1N1 virus, West Nile virus, and dengue virus. *Cell* **139**, 1243–1254 (2009).
 90. Shapira, S. D. *et al.* A physical and regulatory map of host-influenza interactions reveals pathways in H1N1 infection. *Cell* **139**, 1255–1267 (2009).
 91. Haller, O. & Kochs, G. Human MxA protein: an interferon-induced dynamin-like GTPase with broad antiviral activity. *J. Interferon Cytokine Res.* **31**, 79–87 (2011).
 92. Gao, S. *et al.* Structural basis of oligomerization in the stalk region of dynamin-like MxA. *Nature* **465**, 502–506 (2010).
 93. Van Gent, M., Sparrer, K. M. J. & Gack, M. U. TRIM Proteins and Their Roles in Antiviral Host Defenses. *Annu. Rev. Virol.* **5**, 385 (2018).
 94. Stremlau, M. *et al.* The cytoplasmic body component TRIM5 α restricts HIV-1 infection in Old World monkeys. *Nature* **427**, 848–853 (2004).
 95. Wolf, D. & Goff, S. P. Host restriction factors blocking retroviral replication. *Annu. Rev. Genet.* **42**, 143–163 (2008).
 96. Anderson, J. L. *et al.* Proteasome Inhibition Reveals that a Functional Preintegration Complex Intermediate Can Be Generated during Restriction by Diverse TRIM5 Proteins. *J. Virol.* **80**, 9754 (2006).
 97. Pertel, T. *et al.* TRIM5 is an innate immune sensor for the retrovirus capsid lattice. *Nature* **472**, 361–365 (2011).
 98. Sheehy, A. M., Gaddis, N. C., Choi, J. D. & Malim, M. H. Isolation of a human gene that inhibits HIV-1 infection and is suppressed by the viral Vif protein. *Nature* **418**, 646–650 (2002).
 99. Vartanian, J. P., Meyerhans, A., Asjö, B. & Wain-Hobson, S. Selection, recombination, and G---A hypermutation of human immunodeficiency virus type 1 genomes. *J. Virol.* **65**, 1779–1788 (1991).
 100. Pishesha, N., Harmand, T. J. & Ploegh, H. L. A guide to antigen processing and presentation. *Nat. Rev. Immunol.* **2022 1–14** (2022) doi:10.1038/s41577-022-00707-2.

101. Zhao, W., Cha, E. N., Lee, C., Park, C. Y. & Schindler, C. Stat2-dependent regulation of MHC class II expression. *J. Immunol.* **179**, 463–471 (2007).
102. Cresswell, P. Intracellular surveillance: controlling the assembly of MHC class I-peptide complexes. *Traffic* **1**, 301–305 (2000).
103. Mitroulis, I. *et al.* Leukocyte integrins: Role in leukocyte recruitment and as therapeutic targets in inflammatory disease. *Pharmacol. Ther.* **0**, 123 (2015).
104. Nguyen, K. B. *et al.* Coordinated and distinct roles for IFN-alpha beta, IL-12, and IL-15 regulation of NK cell responses to viral infection. *J. Immunol.* **169**, 4279–4287 (2002).
105. Le Bon, A. *et al.* Cutting edge: enhancement of antibody responses through direct stimulation of B and T cells by type I IFN. *J. Immunol.* **176**, 2074–2078 (2006).
106. Le Bon, A. *et al.* Type I interferons potently enhance humoral immunity and can promote isotype switching by stimulating dendritic cells in vivo. *Immunity* **14**, 461–470 (2001).
107. MacMicking, J. D. Interferon-inducible effector mechanisms in cell-autonomous immunity. *Nat. Rev. Immunol.* **2012** *125* **12**, 367–382 (2012).
108. Nathan, C. & Shiloh, M. U. Reactive oxygen and nitrogen intermediates in the relationship between mammalian hosts and microbial pathogens. *Proc. Natl. Acad. Sci. U. S. A.* **97**, 8841–8848 (2000).
109. Nathan, C. & Ding, A. SnapShot: Reactive Oxygen Intermediates (ROI) Intermediates (ROI). *Cell* **140**, (2010).
110. Lambeth, J. D. NOX enzymes and the biology of reactive oxygen. *Nat. Rev. Immunol.* **2004** *43* **4**, 181–189 (2004).
111. Bustamante, J. *et al.* Germline CYBB mutations that selectively affect macrophages in kindreds with X-linked predisposition to tuberculous mycobacterial disease. *Nat. Immunol.* **12**, 213–221 (2011).
112. Moskwa, P. *et al.* A novel host defense system of airways is defective in cystic fibrosis. *Am. J. Respir. Crit. Care Med.* **175**, 174–183 (2007).
113. Botteaux, A., Hoste, C., Dumont, J. E., Van Sande, J. & Allaoui, A. Potential role of Noxes in the protection of mucosae: H₂O₂ as a bacterial repellent. *Microbes Infect.* **11**, 537–544 (2009).
114. Flores, M. V. *et al.* Dual oxidase in the intestinal epithelium of zebrafish larvae has anti-bacterial properties. *Biochem. Biophys. Res. Commun.* **400**, 164–168 (2010).
115. Ng, V. H., Cox, J. S., Sousa, A. O., MacMicking, J. D. & McKinney, J. D. Role of KatG catalase-peroxidase in mycobacterial pathogenesis: countering the phagocyte oxidative burst. *Mol. Microbiol.* **52**, 1291–1302 (2004).
116. Myers, J. T., Tsang, A. W. & Swanson, J. A. Localized reactive oxygen and nitrogen intermediates inhibit escape of *Listeria monocytogenes* from vacuoles in activated macrophages. *J. Immunol.* **171**, 5447–5453 (2003).
117. Nairz, M. *et al.* Interferon-gamma limits the availability of iron for intramacrophage *Salmonella typhimurium*. *Eur. J. Immunol.* **38**, 1923–1936 (2008).
118. Jabado, N. *et al.* Natural resistance to intracellular infections: natural resistance-associated macrophage protein 1 (Nramp1) functions as a pH-dependent manganese transporter at the phagosomal membrane. *J. Exp. Med.* **192**, 1237–1247 (2000).
119. Zaharik, M. L. *et al.* The *Salmonella enterica* serovar typhimurium divalent cation transport systems MntH and SitABCD are essential for virulence in an

- Nramp1G169 murine typhoid model. *Infect. Immun.* **72**, 5522–5525 (2004).
120. Wagner, D. *et al.* Changes of the phagosomal elemental concentrations by Mycobacterium tuberculosis Mramp. *Microbiology* **151**, 323–332 (2005).
 121. White, C., Lee, J., Kambe, T., Fritsche, K. & Petris, M. J. A role for the ATP7A copper-transporting ATPase in macrophage bactericidal activity. *J. Biol. Chem.* **284**, 33949–33956 (2009).
 122. Trost, M. *et al.* The phagosomal proteome in interferon-gamma-activated macrophages. *Immunity* **30**, 143–154 (2009).
 123. Zhang, H., Zoued, A., Liu, X., Sit, B. & Waldora, M. K. Type I interferon remodels lysosome function and modifies intestinal epithelial defense. *Proc. Natl. Acad. Sci. U. S. A.* **117**, 29862–29871 (2020).
 124. Kumar, Y. & Valdivia, R. H. Leading a sheltered life: intracellular pathogens and maintenance of vacuolar compartments. *Cell Host Microbe* **5**, 593–601 (2009).
 125. Walker, D. H. & Ismail, N. Emerging and re-emerging rickettsioses: endothelial cell infection and early disease events. *Nat. Rev. Microbiol.* **2008** **6**, 375–386 (2008).
 126. Wiersinga, W. J. *et al.* Melioidosis. *Nat. Rev. Dis. Prim.* **2018** **4**, 1–22 (2018).
 127. Creasey, E. A. & Isberg, R. R. Maintenance of Vacuole Integrity by Bacterial Pathogens. *Curr. Opin. Microbiol.* **17**, 46 (2014).
 128. Kim, B. H., Shenoy, A. R., Kumar, P., Bradfield, C. J. & MacMicking, J. D. IFN- γ -inducible GTPases in Host Defense. *Cell Host Microbe* **12**, 432 (2012).
 129. Schneider, W. M., Chevillotte, M. D. & Rice, C. M. Interferon-stimulated genes: a complex web of host defenses. *Annu. Rev. Immunol.* **32**, 513–545 (2014).
 130. Shenoy, A. R. *et al.* Emerging themes in IFN- γ -induced macrophage immunity by the p47 and p65 GTPase Families. *Immunobiology* **212**, 771 (2007).
 131. Coers, J. Self and Non-self Discrimination of Intracellular Membranes by the Innate Immune System. *PLoS Pathog.* **9**, (2013).
 132. Singh, S. B. *et al.* Human IRGM Regulates Autophagy and Its Cell-Autonomous Immunity Functions Through Mitochondria. *Nat. Cell Biol.* **12**, 1154 (2010).
 133. Bekpen, C. *et al.* The interferon-inducible p47 (IRG) GTPases in vertebrates: loss of the cell autonomous resistance mechanism in the human lineage. *Genome Biol.* (2005) doi:10.1186/gb-2005-6-11-r92.
 134. Cemma, M., Kim, P. K. & Brumell, J. H. The ubiquitin-binding adaptor proteins p62/SQSTM1 and NDP52 are recruited independently to bacteria-associated microdomains to target Salmonella to the autophagy pathway. *Autophagy* **7**, 341–345 (2011).
 135. TL, T., G, R., S, B., N, von M. & F, R. The TBK1 adaptor and autophagy receptor NDP52 restricts the proliferation of ubiquitin-coated bacteria. *Nat. Immunol.* **10**, 1215–1222 (2009).
 136. Wild, P. *et al.* Phosphorylation of the autophagy receptor optineurin restricts Salmonella growth. *Science* **333**, 228–233 (2011).
 137. Thurston, T. L. M., Wandel, M. P., Von Muhlinen, N., Foeglein, Á. & Randow, F. Galectin 8 targets damaged vesicles for autophagy to defend cells against bacterial invasion. *Nature* **482**, 414–418 (2012).
 138. Deretic, V., Saitoh, T. & Akira, S. Autophagy in infection, inflammation and immunity. *Nat. Rev. Immunol.* **13**, 722–737 (2013).
 139. MacMicking, J. D., Taylor, G. A. & McKinney, J. D. Immune control of

- tuberculosis by IFN-gamma-inducible LRG-47. *Science* **302**, 654–659 (2003).
140. Henry, S. C. *et al.* Impaired macrophage function underscores susceptibility to Salmonella in mice lacking Irgm1 (LRG-47). *J. Immunol.* **179**, 6963–6972 (2007).
 141. Lippmann, J. *et al.* Dissection of a type I interferon pathway in controlling bacterial intracellular infection in mice. *Cell. Microbiol.* **13**, 1668–1682 (2011).
 142. Al-Zeer, M. A., Al-Younes, H. M., Braun, P. R., Zerrahn, J. & Meyer, T. F. IFN-gamma-inducible Irga6 mediates host resistance against Chlamydia trachomatis via autophagy. *PLoS One* **4**, (2009).
 143. Miyairi, I. *et al.* The p47 GTPases Iigp2 and Irgb10 regulate innate immunity and inflammation to murine Chlamydia psittaci infection. *J. Immunol.* **179**, 1814–1824 (2007).
 144. Lapaquette, P., Glasser, A. L., Huett, A., Xavier, R. J. & Darfeuille-Michaud, A. Crohn's disease-associated adherent-invasive E. coli are selectively favoured by impaired autophagy to replicate intracellularly. *Cell. Microbiol.* **12**, 99–113 (2010).
 145. Tiwari, S., Choi, H. P., Matsuzawa, T., Pypaert, M. & MacMicking, J. D. Targeting of the GTPase Irgm1 to the phagosomal membrane via PtdIns(3,4)P(2) and PtdIns(3,4,5)P(3) promotes immunity to mycobacteria. *Nat. Immunol.* **10**, 907–917 (2009).
 146. Cai, Q. & Sheng, Z. H. Uncovering the role of Snapin in regulating autophagy-lysosomal function. *Autophagy* **7**, 445–447 (2011).
 147. Nelson, D. E. *et al.* Chlamydial IFN-gamma immune evasion is linked to host infection tropism. *Proc. Natl. Acad. Sci. U. S. A.* **102**, 10658–10663 (2005).
 148. Bernstein-Hanley, I. *et al.* The p47 GTPases Iigtp and Irgb10 map to the Chlamydia trachomatis susceptibility locus Ctrq-3 and mediate cellular resistance in mice. *Proc. Natl. Acad. Sci. U. S. A.* **103**, 14092–14097 (2006).
 149. Chauhan, S., Mandell, M. A. & Deretic, V. IRGM Governs the Core Autophagy Machinery to Conduct Antimicrobial Defense. *Mol. Cell* **58**, 507–521 (2015).
 150. Hölscher, C. *et al.* Defective nitric oxide effector functions lead to extreme susceptibility of Trypanosoma cruzi-infected mice deficient in gamma interferon receptor or inducible nitric oxide synthase. *Infect. Immun.* **66**, 1208–1215 (1998).
 151. Liew, F. Y., Millott, S., Parkinson, C., Palmer, R. M. & Moncada, S. Macrophage killing of Leishmania parasite in vivo is mediated by nitric oxide from L-arginine. *J. Immunol.* **144**, (1990).
 152. Fleckenstein, M. C. *et al.* A Toxoplasma gondii pseudokinase inhibits host IRG resistance proteins. *PLoS Biol.* **10**, 14 (2012).
 153. Zhao, Y. *et al.* Virulent Toxoplasma gondii evade immunity-related GTPase-mediated parasite vacuole disruption within primed macrophages. *J. Immunol.* **182**, 3775–3781 (2009).
 154. Scharon-Kersten, T. M., Yap, G., Magram, J. & Sher, A. Inducible nitric oxide is essential for host control of persistent but not acute infection with the intracellular pathogen Toxoplasma gondii. *J. Exp. Med.* **185**, 1261–1273 (1997).
 155. Pfefferkorn, E. R. Interferon gamma blocks the growth of Toxoplasma gondii in human fibroblasts by inducing the host cells to degrade tryptophan. *Proc. Natl. Acad. Sci. U. S. A.* **81**, 908–912 (1984).
 156. Knubel, C. P. *et al.* Indoleamine 2,3-dioxygenase (IDO) is critical for host resistance against Trypanosoma cruzi. *FASEB J.* **24**, 2689–2701 (2010).

157. Hunn, J. P. *et al.* Regulatory interactions between IRG resistance GTPases in the cellular response to *Toxoplasma gondii*. *EMBO J.* **27**, 2495–2509 (2008).
158. Khaminets, A. *et al.* Coordinated loading of IRG resistance GTPases on to the *Toxoplasma gondii* parasitophorous vacuole. *Cell. Microbiol.* **12**, 939–961 (2010).
159. Zhao, Y. O., Khaminets, A., Hunn, J. P. & Howard, J. C. Disruption of the *Toxoplasma gondii* parasitophorous vacuole by IFN γ -inducible immunity-related GTPases (IRG proteins) triggers necrotic cell death. *PLoS Pathog.* **5**, (2009).
160. Friedlander, A. M. Macrophages are sensitive to anthrax lethal toxin through an acid-dependent process. *J. Biol. Chem.* **261**, 7123–7126 (1986).
161. Zychlinsky, A., Prevost, M. C. & Sansonetti, P. J. *Shigella flexneri* induces apoptosis in infected macrophages. *Nature* **358**, 167–169 (1992).
162. Chen, L. M., Kaniga, K. & Galán, J. E. *Salmonella* spp. are cytotoxic for cultured macrophages. *Mol. Microbiol.* **21**, 1101–1115 (1996).
163. Monack, D. M., Raupach, B., Hromockyj, A. E. & Falkow, S. *Salmonella typhimurium* invasion induces apoptosis in infected macrophages. *Proc. Natl. Acad. Sci. U. S. A.* **93**, 9833–9838 (1996).
164. Thornberry, N. A. *et al.* A novel heterodimeric cysteine protease is required for interleukin-1 β processing in monocytes. *Nature* 1992 3566372 **356**, 768–774 (1992).
165. Cerretti, D. P. *et al.* Molecular Cloning of the Interleukin-1 β Converting Enzyme. *Science* **256**, 97–100 (1992).
166. Zychlinsky, A., Fitting, C., Cavaillon, J. M. & Sansonetti, P. J. Interleukin 1 is released by murine macrophages during apoptosis induced by *Shigella flexneri*. *J. Clin. Invest.* **94**, 1328–1332 (1994).
167. Hersh, D. *et al.* The *Salmonella* invasin SipB induces macrophage apoptosis by binding to caspase-1. *Proc. Natl. Acad. Sci.* **96**, 2396–2401 (1999).
168. Hilbi, H., Chen, Y., Thirumalai, K. & Zychlinsky, A. The interleukin 1 β -converting enzyme, caspase 1, is activated during *Shigella flexneri*-induced apoptosis in human monocyte-derived macrophages. *Infect. Immun.* **65**, 5165–5170 (1997).
169. Hilbi, H. *et al.* *Shigella*-induced Apoptosis Is Dependent on Caspase-1 Which Binds to IpaB *. *J. Biol. Chem.* **273**, 32895–32900 (1998).
170. Brennan, M. A. & Cookson, B. T. *Salmonella* induces macrophage death by caspase-1-dependent necrosis. *Mol. Microbiol.* **38**, 31–40 (2000).
171. Watson, P. R. *et al.* *Salmonella enterica* serovars Typhimurium and Dublin can lyse macrophages by a mechanism distinct from apoptosis. *Infect. Immun.* **68**, 3744–3747 (2000).
172. Cookson, B. T. & Brennan, M. A. Pro-inflammatory programmed cell death. *Trends Microbiol.* **9**, 113–114 (2001).
173. Martinon, F., Burns, K. & Tschopp, J. The Inflammasome: A Molecular Platform Triggering Activation of Inflammatory Caspases and Processing of proIL- β . *Mol. Cell* **10**, 417–426 (2002).
174. Bertin, J. & DiStefano, P. S. The PYRIN domain: a novel motif found in apoptosis and inflammation proteins. *Cell Death Differ.* 2000 712 **7**, 1273–1274 (2000).
175. Hlaing, T. *et al.* Molecular cloning and characterization of DEFCAP-L and -S, two isoforms of a novel member of the mammalian Ced-4 family of apoptosis proteins. *J. Biol. Chem.* **276**, 9230–9238 (2001).

176. Martinon, F., Hofmann, K. & Tschopp, J. The pyrin domain: a possible member of the death domain-fold family implicated in apoptosis and inflammation. *Curr. Biol.* **11**, R118–R120 (2001).
177. Janeway, C. A. & Medzhitov, R. Innate immune recognition. *Annu. Rev. Immunol.* **20**, 197–216 (2002).
178. Masumoto, J. *et al.* ASC, a novel 22-kDa protein, aggregates during apoptosis of human promyelocytic leukemia HL-60 cells. *J. Biol. Chem.* **274**, 33835–33838 (1999).
179. Srinivasula, S. M. *et al.* The PYRIN-CARD protein ASC is an activating adaptor for caspase-1. *J. Biol. Chem.* **277**, 21119–21122 (2002).
180. Stehlik, C. *et al.* Apoptosis-Associated Speck-Like Protein Containing a Caspase Recruitment Domain Is a Regulator of Procaspase-1 Activation. *J. Immunol.* **171**, 6154–6163 (2003).
181. Tschopp, J., Martinon, F. & Burns, K. NALPs: a novel protein family involved in inflammation. *Nat. Rev. Mol. Cell Biol.* **4**, 95–104 (2003).
182. Aganna, E. *et al.* Association of mutations in the NALP3/CIAS1/PYPAF1 gene with a broad phenotype including recurrent fever, cold sensitivity, sensorineural deafness, and AA amyloidosis. *Arthritis Rheum.* **46**, 2445–2452 (2002).
183. Hoffman, H. M., Mueller, J. L., Broide, D. H., Wanderer, A. A. & Kolodner, R. D. Mutation of a new gene encoding a putative pyrin-like protein causes familial cold autoinflammatory syndrome and Muckle-Wells syndrome. *Nat. Genet.* **29**, 301–305 (2001).
184. Ghayur, T. *et al.* Caspase-1 processes IFN-gamma-inducing factor and regulates LPS-induced IFN-gamma production. *Nature* **386**, 619–623 (1997).
185. Kayagaki, N. *et al.* Non-canonical inflammasome activation targets caspase-11. *Nature* 2011 4797371 **479**, 117–121 (2011).
186. Broz, P. *et al.* Caspase-11 increases susceptibility to Salmonella infection in the absence of caspase-1. *Nature* 2012 4907419 **490**, 288–291 (2012).
187. Broz, P. & Monack, D. M. Newly described pattern recognition receptors team up against intracellular pathogens. *Nat. Rev. Immunol.* **13**, 551–565 (2013).
188. Von Moltke, J., Ayres, J. S., Kofoed, E. M., Chavarría-Smith, J. & Vance, R. E. Recognition of bacteria by inflammasomes. *Annu. Rev. Immunol.* **31**, 73–106 (2013).
189. Yu, P. *et al.* Pyroptosis: mechanisms and diseases. *Signal Transduct. Target. Ther.* 2021 61 **6**, 1–21 (2021).
190. Broz, P. & Dixit, V. M. Inflammasomes: mechanism of assembly, regulation and signalling. *Nat. Rev. Immunol.* 2016 167 **16**, 407–420 (2016).
191. Boyden, E. D. & Dietrich, W. F. Nalp1b controls mouse macrophage susceptibility to anthrax lethal toxin. *Nat. Genet.* **38**, 240–244 (2006).
192. Stephen, J. Anthrax toxin. *Pharmacol. Ther.* **12**, 501–513 (1981).
193. Levinsohn, J. L. *et al.* Anthrax lethal factor cleavage of Nlrp1 is required for activation of the inflammasome. *PLoS Pathog.* **8**, (2012).
194. Hellmich, K. A. *et al.* Anthrax lethal factor cleaves mouse nlrp1b in both toxin-sensitive and toxin-resistant macrophages. *PLoS One* **7**, (2012).
195. Chavarría-Smith, J. & Vance, R. E. Direct proteolytic cleavage of NLRP1B is necessary and sufficient for inflammasome activation by anthrax lethal factor. *PLoS Pathog.* **9**, (2013).
196. Zhong, F. L. *et al.* Germline NLRP1 Mutations Cause Skin Inflammatory and Cancer Susceptibility Syndromes via Inflammasome Activation. *Cell* **167**, 187-

- 202.e17 (2016).
197. Chavarría-Smith, J., Mitchell, P. S., Ho, A. M., Daugherty, M. D. & Vance, R. E. Functional and Evolutionary Analyses Identify Proteolysis as a General Mechanism for NLRP1 Inflammasome Activation. *PLoS Pathog.* **12**, (2016).
 198. Chui, A. J. *et al.* N-terminal degradation activates the NLRP1B inflammasome. *Science* **364**, 82–85 (2019).
 199. Sandstrom, A. *et al.* Functional degradation: A mechanism of NLRP1 inflammasome activation by diverse pathogen enzymes. *Science* **364**, (2019).
 200. Cirelli, K. M. *et al.* Inflammasome sensor NLRP1 controls rat macrophage susceptibility to *Toxoplasma gondii*. *PLoS Pathog.* **10**, (2014).
 201. Ewald, S. E., Chavarría-Smith, J. & Boothroyd, J. C. NLRP1 is an inflammasome sensor for *Toxoplasma gondii*. *Infect. Immun.* **82**, 460–468 (2014).
 202. Gorfu, G. *et al.* Dual role for inflammasome sensors NLRP1 and NLRP3 in murine resistance to *Toxoplasma gondii*. *MBio* **5**, (2014).
 203. Neiman-Zenevich, J., Stuart, S., Abdel-Nour, M., Girardin, S. E. & Mogridge, J. *Listeria monocytogenes* and *Shigella flexneri* Activate the NLRP1B Inflammasome. *Infect. Immun.* **85**, (2017).
 204. Okondo, M. C. *et al.* Inhibition of Dpp8/9 Activates the Nlrp1b Inflammasome. *Cell Chem. Biol.* **25**, 262-267.e5 (2018).
 205. Hollingsworth, L. R. *et al.* DPP9 sequesters the C terminus of NLRP1 to repress inflammasome activation. *Nature* **592**, 778–783 (2021).
 206. Huang, M. *et al.* Structural and biochemical mechanisms of NLRP1 inhibition by DPP9. *Nature* **592**, 773–777 (2021).
 207. Tsu, B. V. *et al.* Diverse viral proteases activate the nlrp1 inflammasome. *Elife* **10**, 1–76 (2021).
 208. Robinson, K. S. *et al.* Enteroviral 3C protease activates the human NLRP1 inflammasome in airway epithelia. *Science* **370**, (2020).
 209. Bauernfried, S. & Hornung, V. Human NLRP1: From the shadows to center stage. *J. Exp. Med.* **219**, (2021).
 210. Yang, X. *et al.* KSHV-encoded ORF45 activates human NLRP1 inflammasome. *Nat. Immunol.* 2022 236 **23**, 916–926 (2022).
 211. Strowig, T., Henao-Mejia, J., Elinav, E. & Flavell, R. Inflammasomes in health and disease. *Nature* **481**, 278–286 (2012).
 212. Menu, P. & Vince, J. E. The NLRP3 inflammasome in health and disease: the good, the bad and the ugly. *Clin. Exp. Immunol.* **166**, 1–15 (2011).
 213. Bauernfeind, F. G. *et al.* Cutting edge: NF-kappaB activating pattern recognition and cytokine receptors license NLRP3 inflammasome activation by regulating NLRP3 expression. *J. Immunol.* **183**, 787–791 (2009).
 214. Franchi, L., Eigenbrod, T. & Núñez, G. Cutting edge: TNF-alpha mediates sensitization to ATP and silica via the NLRP3 inflammasome in the absence of microbial stimulation. *J. Immunol.* **183**, 792–796 (2009).
 215. Xing, Y. *et al.* Cutting Edge: TRAF6 Mediates TLR/IL-1R Signaling-Induced Nontranscriptional Priming of the NLRP3 Inflammasome. *J. Immunol.* **199**, 1561–1566 (2017).
 216. Cai, X. *et al.* Prion-like polymerization underlies signal transduction in antiviral immune defense and inflammasome activation. *Cell* **156**, 1207–1222 (2014).
 217. Lu, A. *et al.* Unified polymerization mechanism for the assembly of ASC-dependent inflammasomes. *Cell* **156**, 1193–1206 (2014).
 218. Boucher, D. *et al.* Caspase-1 self-cleavage is an intrinsic mechanism to

- terminate inflammasome activity. *J. Exp. Med.* **215**, 827–840 (2018).
219. Swanson, K. V., Deng, M. & Ting, J. P. Y. The NLRP3 inflammasome: molecular activation and regulation to therapeutics. *Nat. Rev. Immunol.* **2019** *19*, 477–489 (2019).
 220. Muñoz-Planillo, R. *et al.* K⁺ efflux is the common trigger of NLRP3 inflammasome activation by bacterial toxins and particulate matter. *Immunity* **38**, 1142–1153 (2013).
 221. Schmid-Burgk, J. L. *et al.* A Genome-wide CRISPR (Clustered Regularly Interspaced Short Palindromic Repeats) Screen Identifies NEK7 as an Essential Component of NLRP3 Inflammasome Activation. *J. Biol. Chem.* **291**, 103–109 (2016).
 222. He, Y., Zeng, M. Y., Yang, D., Motro, B. & Núñez, G. NEK7 is an essential mediator of NLRP3 activation downstream of potassium efflux. *Nature* **530**, 354–357 (2016).
 223. Shi, H. *et al.* NLRP3 activation and mitosis are mutually exclusive events coordinated by NEK7, a new inflammasome component. *Nat. Immunol.* **17**, 250–258 (2016).
 224. Gangopadhyay, A. *et al.* NLRP3 licenses NLRP11 for inflammasome activation in human macrophages. *Nat. Immunol.* **2022** *236* **23**, 892–903 (2022).
 225. Aksentijevich, I. *et al.* De novo CIAS1 mutations, cytokine activation, and evidence for genetic heterogeneity in patients with neonatal-onset multisystem inflammatory disease (NOMID): a new member of the expanding family of pyrin-associated autoinflammatory diseases. *Arthritis Rheum.* **46**, 3340–3348 (2002).
 226. Poyet, J. L. *et al.* Identification of Ipaf, a human caspase-1-activating protein related to Apaf-1. *J. Biol. Chem.* **276**, 28309–28313 (2001).
 227. Mariathasan, S. *et al.* Differential activation of the inflammasome by caspase-1 adaptors ASC and Ipaf. *Nature* **430**, 213–218 (2004).
 228. Franchi, L. *et al.* Cytosolic flagellin requires Ipaf for activation of caspase-1 and interleukin 1beta in salmonella-infected macrophages. *Nat. Immunol.* **7**, 576–582 (2006).
 229. Miao, E. A. *et al.* Cytoplasmic flagellin activates caspase-1 and secretion of interleukin 1beta via Ipaf. *Nat. Immunol.* **7**, 569–575 (2006).
 230. Miao, E. A. *et al.* Innate immune detection of the type III secretion apparatus through the NLRC4 inflammasome. *Proc. Natl. Acad. Sci. U. S. A.* **107**, 3076–3080 (2010).
 231. Zhao, Y. *et al.* The NLRC4 inflammasome receptors for bacterial flagellin and type III secretion apparatus. *Nature* **2011** *477* **477**, 596–600 (2011).
 232. Kofoed, E. M. & Vance, R. E. Innate immune recognition of bacterial ligands by NAIPs determines inflammasome specificity. *Nature* **477**, 592–597 (2011).
 233. Kortmann, J., Brubaker, S. W. & Monack, D. M. Cutting Edge: Inflammasome Activation in Primary Human Macrophages Is Dependent on Flagellin. *J. Immunol.* **195**, 815–819 (2015).
 234. Zamboni, D. S. *et al.* The Birc1e cytosolic pattern-recognition receptor contributes to the detection and control of Legionella pneumophila infection. *Nat. Immunol.* **7**, 318–325 (2006).
 235. Li, Y. *et al.* Cryo-EM structures of ASC and NLRC4 CARD filaments reveal a unified mechanism of nucleation and activation of caspase-1. *Proc. Natl. Acad. Sci. U. S. A.* **115**, 10845–10852 (2018).
 236. Matyszewski, M. *et al.* Cryo-EM structure of the NLRC4 CARD filament

- provides insights into how symmetric and asymmetric supramolecular structures drive inflammasome assembly. *J. Biol. Chem.* **293**, 20240–20248 (2018).
237. Broz, P., Von Moltke, J., Jones, J. W., Vance, R. E. & Monack, D. M. Differential Requirement for Caspase-1 Autoproteolysis in Pathogen-Induced Cell Death and Cytokine Processing. *Cell Host Microbe* **8**, 471–483 (2010).
 238. Gutierrez, O., Pipaon, C. & Fernandez-Luna, J. L. Ipaf is upregulated by tumor necrosis factor- α in human leukemia cells. *FEBS Lett.* **568**, 79–82 (2004).
 239. Sadasivam, S. *et al.* Caspase-1 activator Ipaf is a p53-inducible gene involved in apoptosis. *Oncogene* **24**, 627–636 (2005).
 240. Qu, Y. *et al.* Phosphorylation of NLRC4 is critical for inflammasome activation. *Nature* **490**, 539–542 (2012).
 241. Liu, W. *et al.* LRRK2 promotes the activation of NLRC4 inflammasome during *Salmonella Typhimurium* infection. *J. Exp. Med.* **214**, 3051–3066 (2017).
 242. Suzuki, S. *et al.* Shigella type III secretion protein Mxil is recognized by Naip2 to induce Nlrc4 inflammasome activation independently of Pkc δ . *PLoS Pathog.* **10**, (2014).
 243. Mao, K. *et al.* β -arrestin1 is critical for the full activation of NLRP3 and NLRC4 inflammasomes. *J. Immunol.* **194**, 1867–1873 (2015).
 244. Muruve, D. A. *et al.* The inflammasome recognizes cytosolic microbial and host DNA and triggers an innate immune response. *Nature* **452**, 103–107 (2008).
 245. Hornung, V. *et al.* AIM2 recognizes cytosolic dsDNA and forms a caspase-1-activating inflammasome with ASC. *Nature* **458**, 514–518 (2009).
 246. Fernandes-Alnemri, T., Yu, J. W., Datta, P., Wu, J. & Alnemri, E. S. AIM2 activates the inflammasome and cell death in response to cytoplasmic DNA. *Nature* **458**, 509–513 (2009).
 247. Roberts, T. L. *et al.* HIN-200 proteins regulate caspase activation in response to foreign cytoplasmic DNA. *Science* **323**, 1057–1060 (2009).
 248. Cridland, J. A. *et al.* The mammalian PYHIN gene family: phylogeny, evolution and expression. *BMC Evol. Biol.* **12**, (2012).
 249. Jin, T. *et al.* Structures of the HIN domain:DNA complexes reveal ligand binding and activation mechanisms of the AIM2 inflammasome and IFI16 receptor. *Immunity* **36**, 561–571 (2012).
 250. Jin, T., Perry, A., Smith, P., Jiang, J. & Xiao, T. S. Structure of the Absent in Melanoma 2 (AIM2) Pyrin Domain Provides Insights into the Mechanisms of AIM2 Autoinhibition and Inflammasome Assembly. *J. Biol. Chem.* **288**, 13225–13235 (2013).
 251. Morrone, S. R. *et al.* Assembly-driven activation of the AIM2 foreign-dsDNA sensor provides a polymerization template for downstream ASC. *Nat. Commun.* **6**, 1–13 (2015).
 252. Rathinam, V. A. K. *et al.* The AIM2 inflammasome is essential for host defense against cytosolic bacteria and DNA viruses. *Nat. Immunol.* **11**, 395–402 (2010).
 253. Meunier, E. *et al.* Guanylate-binding proteins promote activation of the AIM2 inflammasome during infection with *Francisella novicida*. *Nat. Immunol.* **16**, 476–484 (2015).
 254. Jones, J. W. *et al.* Absent in melanoma 2 is required for innate immune recognition of *Francisella tularensis*. *Proc. Natl. Acad. Sci. U. S. A.* **107**, 9771–9776 (2010).

255. Fernandes-Alnemri, T. *et al.* The AIM2 inflammasome is critical for innate immunity to *Francisella tularensis*. *Nat. Immunol.* **11**, 385–393 (2010).
256. Man, S. M. *et al.* IRGB10 Liberates Bacterial Ligands for Sensing by the AIM2 and Caspase-11-NLRP3 Inflammasomes. *Cell* **167**, 382–396.e17 (2016).
257. Sauer, J. D. *et al.* *Listeria monocytogenes* triggers AIM2-mediated pyroptosis upon infrequent bacteriolysis in the macrophage cytosol. *Cell Host Microbe* **7**, 412–419 (2010).
258. Meunier, E. *et al.* Guanylate-binding proteins promote activation of the AIM2 inflammasome during infection with *Francisella novicida*. *Nat. Immunol.* (2015) doi:10.1038/ni.3119.
259. Dombrowski, Y. *et al.* Cytosolic DNA triggers inflammasome activation in keratinocytes in psoriatic lesions. *Sci. Transl. Med.* **3**, (2011).
260. Javierre, B. M. *et al.* Changes in the pattern of DNA methylation associate with twin discordance in systemic lupus erythematosus. *Genome Res.* **20**, 170–179 (2010).
261. Dihlmann, S. *et al.* Lack of Absent in Melanoma 2 (AIM2) expression in tumor cells is closely associated with poor survival in colorectal cancer patients. *Int. J. cancer* **135**, 2387–2396 (2014).
262. Ponomareva, L. *et al.* AIM2, an IFN-inducible cytosolic DNA sensor, in the development of benign prostate hyperplasia and prostate cancer. *Mol. Cancer Res.* **11**, 1193–1202 (2013).
263. Chae, J. J. *et al.* The B30.2 domain of pyrin, the familial Mediterranean fever protein, interacts directly with caspase-1 to modulate IL-1 β production. *Proc. Natl. Acad. Sci. U. S. A.* **103**, 9982–9987 (2006).
264. Hesker, P. R., Nguyen, M. T., Kovarova, M., Ting, J. P. Y. & Koller, B. H. Genetic loss of murine pyrin, the Familial Mediterranean Fever protein, increases interleukin-1 β levels. *PLoS One* **7**, (2012).
265. Xu, H. *et al.* Innate immune sensing of bacterial modifications of Rho GTPases by the Pyrin inflammasome. *Nature* 2014 5137517 **513**, 237–241 (2014).
266. Waite, A. L. *et al.* Pyrin and ASC co-localize to cellular sites that are rich in polymerizing actin. *Exp. Biol. Med. (Maywood)*. **234**, 40–52 (2009).
267. Kim, M. L. *et al.* Aberrant actin depolymerization triggers the pyrin inflammasome and autoinflammatory disease that is dependent on IL-18, not IL-1 β . *J. Exp. Med.* **212**, 927 (2015).
268. Gao, W., Yang, J., Liu, W., Wang, Y. & Shao, F. Site-specific phosphorylation and microtubule dynamics control Pyrin inflammasome activation. *Proc. Natl. Acad. Sci. U. S. A.* **113**, E4857–E4866 (2016).
269. Park, Y. H., Wood, G., Kastner, D. L. & Chae, J. J. Pyrin inflammasome activation and RhoA signaling in the autoinflammatory diseases FMF and HIDS. *Nat. Immunol.* **17**, 914–921 (2016).
270. Magnotti, F. *et al.* Pyrin dephosphorylation is sufficient to trigger inflammasome activation in familial Mediterranean fever patients. *EMBO Mol. Med.* **11**, (2019).
271. Magnotti, F. *et al.* Steroid hormone catabolites activate the pyrin inflammasome through a non-canonical mechanism. *Cell Rep.* **41**, 111472 (2022).
272. Unterholzner, L. *et al.* IFI16 is an innate immune sensor for intracellular DNA. *Nat. Immunol.* **11**, 997–1004 (2010).
273. Storek, K. M., Gertsvolf, N. A., Ohlson, M. B. & Monack, D. M. cGAS and Ifi204 cooperate to produce type I IFNs in response to *Francisella* infection. *J.*

- Immunol.* **194**, 3236–3245 (2015).
274. Kerur, N. *et al.* IFI16 acts as a nuclear pathogen sensor to induce the inflammasome in response to Kaposi Sarcoma-associated herpesvirus infection. *Cell Host Microbe* **9**, 363–375 (2011).
275. Doitsh, G. *et al.* Cell death by pyroptosis drives CD4 T-cell depletion in HIV-1 infection. *Nature* **505**, 509–514 (2014).
276. Monroe, K. M. *et al.* IFI16 DNA sensor is required for death of lymphoid CD4 T cells abortively infected with HIV. *Science* **343**, 428–432 (2014).
277. Elinav, E. *et al.* NLRP6 inflammasome regulates colonic microbial ecology and risk for colitis. *Cell* **145**, 745–757 (2011).
278. Levy, M. *et al.* Microbiota-Modulated Metabolites Shape the Intestinal Microenvironment by Regulating NLRP6 Inflammasome Signaling. *Cell* **163**, 1428–1443 (2015).
279. Hara, H. *et al.* The NLRP6 Inflammasome Recognizes Lipoteichoic Acid and Regulates Gram-Positive Pathogen Infection. *Cell* **175**, 1651-1664.e14 (2018).
280. Shen, C. *et al.* Phase separation drives RNA virus-induced activation of the NLRP6 inflammasome. *Cell* **184**, 5759-5774.e20 (2021).
281. Chen, H. *et al.* TLR4-MyD88 pathway promotes the imbalanced activation of NLRP3/NLRP6 via caspase-8 stimulation after alkali burn injury. *Exp. Eye Res.* **176**, 59–68 (2018).
282. Anand, P. K. *et al.* NLRP6 negatively regulates innate immunity and host defence against bacterial pathogens. *Nature* **488**, 389–393 (2012).
283. Wang, Y. *et al.* PYNOD, a novel Apaf-1/CED4-like protein is an inhibitor of ASC and caspase-1. *Int. Immunol.* **16**, 777–786 (2004).
284. Kinoshita, T., Wang, Y., Hasegawa, M., Imamura, R. & Suda, T. PYPAF3, a PYRIN-containing APAF-1-like Protein, Is a Feedback Regulator of Caspase-1-dependent Interleukin-1 β Secretion. *J. Biol. Chem.* **280**, 21720–21725 (2005).
285. Próchnicki, T. *et al.* Mitochondrial damage activates the NLRP10 inflammasome. doi:10.21203/rs.3.rs-1295136/v1.
286. Zhu, S. *et al.* Nlrp9b inflammasome restricts rotavirus infection in intestinal epithelial cells. *Nature* 2017 5467660 **546**, 667–670 (2017).
287. Kayagaki, N. *et al.* Noncanonical inflammasome activation by intracellular LPS independent of TLR4. *Science* **341**, 1246–1249 (2013).
288. Hagar, J. A., Powell, D. A., Aachoui, Y., Ernst, R. K. & Miao, E. A. Cytoplasmic LPS activates caspase-11: implications in TLR4-independent endotoxic shock. *Science* **341**, 1250–1253 (2013).
289. Kayagaki, N. *et al.* Caspase-11 cleaves gasdermin D for non-canonical inflammasome signalling. *Nature* 2015 5267575 **526**, 666–671 (2015).
290. Yi, Y. S. Functional crosstalk between non-canonical caspase-11 and canonical NLRP3 inflammasomes during infection-mediated inflammation. *Immunology* **159**, 142–155 (2020).
291. Baker, P. J. *et al.* NLRP3 inflammasome activation downstream of cytoplasmic LPS recognition by both caspase-4 and caspase-5. *Eur. J. Immunol.* **45**, 2918–2926 (2015).
292. Schmid-Burgk, J. L. *et al.* Caspase-4 mediates non-canonical activation of the NLRP3 inflammasome in human myeloid cells. *Eur. J. Immunol.* **45**, 2911–2917 (2015).
293. Rühl, S. & Broz, P. Caspase-11 activates a canonical NLRP3 inflammasome by promoting K(+) efflux. *Eur. J. Immunol.* **45**, 2927–2936 (2015).

294. Zanoni, I. *et al.* An endogenous caspase-11 ligand elicits interleukin-1 release from living dendritic cells. *Science* **352**, 1232–1236 (2016).
295. Chu, L. H. *et al.* The oxidized phospholipid oxPAPC protects from septic shock by targeting the non-canonical inflammasome in macrophages. *Nat. Commun.* **9**, (2018).
296. Poelzl, A. *et al.* TYK2 licenses non-canonical inflammasome activation during endotoxemia. *Cell Death Differ.* 2020 282 **28**, 748–763 (2020).
297. Sakaguchi, N. *et al.* Role of Gate-16 and Gabarap in Prevention of Caspase-11-Dependent Excess Inflammation and Lethal Endotoxic Shock. *Front. Immunol.* **11**, 2261 (2020).
298. Eren, E. *et al.* Irgm2 and Gate-16 cooperatively dampen Gram-negative bacteria-induced caspase-11 response. *EMBO Rep.* **21**, (2020).
299. Finethy, R. *et al.* Dynamin-related Irgm proteins modulate LPS-induced caspase-11 activation and septic shock. *EMBO Rep.* **21**, e50830 (2020).
300. Casson, C. N. *et al.* Human caspase-4 mediates noncanonical inflammasome activation against gram-negative bacterial pathogens. *Proc. Natl. Acad. Sci. U. S. A.* **112**, 6688–6693 (2015).
301. Shi, J. *et al.* Inflammatory caspases are innate immune receptors for intracellular LPS. *Nature* (2014) doi:10.1038/nature13683.
302. Rathinam, V. A. K. *et al.* TRIF licenses caspase-11-dependent NLRP3 inflammasome activation by gram-negative bacteria. *Cell* **150**, 606–619 (2012).
303. Saeki, N., Kuwahara, Y., Sasaki, H., Satoh, H. & Shiroishi, T. Gasdermin (Gsdm) localizing to mouse Chromosome 11 is predominantly expressed in upper gastrointestinal tract but significantly suppressed in human gastric cancer cells. *Mamm. Genome* **11**, 718–724 (2000).
304. Van Laer, L. *et al.* Nonsyndromic hearing impairment is associated with a mutation in DFNA5. *Nat. Genet.* **20**, 194–197 (1998).
305. Van Rossom, S. *et al.* The splicing mutant of the human tumor suppressor protein DFNA5 induces programmed cell death when expressed in the yeast *Saccharomyces cerevisiae*. *Front. Oncol.* **2**, (2012).
306. De Beeck, K. O. *et al.* The DFNA5 gene, responsible for hearing loss and involved in cancer, encodes a novel apoptosis-inducing protein. *Eur. J. Hum. Genet.* 2011 199 **19**, 965–973 (2011).
307. Shi, J. *et al.* Cleavage of GSDMD by inflammatory caspases determines pyroptotic cell death. *Nature* 2015 5267575 **526**, 660–665 (2015).
308. He, W. T. *et al.* Gasdermin D is an executor of pyroptosis and required for interleukin-1 β secretion. *Cell Res.* 2015 2512 **25**, 1285–1298 (2015).
309. Gonzalez Ramirez, M. L. *et al.* Extensive peptide and natural protein substrate screens reveal that mouse caspase-11 has much narrower substrate specificity than caspase-1. *J. Biol. Chem.* **293**, 7058–7067 (2018).
310. Rogers, C. *et al.* Cleavage of DFNA5 by caspase-3 during apoptosis mediates progression to secondary necrotic/pyroptotic cell death. *Nat. Commun.* 2017 81 **8**, 1–14 (2017).
311. Wang, Y. *et al.* Chemotherapy drugs induce pyroptosis through caspase-3 cleavage of a gasdermin. *Nature* 2017 5477661 **547**, 99–103 (2017).
312. Chen, K. W. *et al.* Extrinsic and intrinsic apoptosis activate pannexin-1 to drive NLRP3 inflammasome assembly. *EMBO J.* **38**, (2019).
313. Taabazuing, C. Y., Okondo, M. C. & Bachovchin, D. A. Pyroptosis and Apoptosis Pathways Engage in Bidirectional Crosstalk in Monocytes and

- Macrophages. *Cell Chem. Biol.* **24**, 507-514.e4 (2017).
314. Orning, P. *et al.* Pathogen blockade of TAK1 triggers caspase-8-dependent cleavage of gasdermin D and cell death. *Science* **362**, 1064–1069 (2018).
 315. Sarhan, J. *et al.* Caspase-8 induces cleavage of gasdermin D to elicit pyroptosis during *Yersinia* infection. *Proc. Natl. Acad. Sci. U. S. A.* **115**, E10888–E10897 (2018).
 316. Sollberger, G. *et al.* Gasdermin D plays a vital role in the generation of neutrophil extracellular traps. *Sci. Immunol.* **3**, (2018).
 317. Kambara, H. *et al.* Gasdermin D Exerts Anti-inflammatory Effects by Promoting Neutrophil Death. *Cell Rep.* **22**, 2924–2936 (2018).
 318. Chen, K. W. *et al.* Noncanonical inflammasome signaling elicits gasdermin D-dependent neutrophil extracellular traps. *Sci. Immunol.* **3**, (2018).
 319. Ding, J. *et al.* Pore-forming activity and structural autoinhibition of the gasdermin family. *Nature* **535**, 111–116 (2016).
 320. Liu, X. *et al.* Inflammasome-activated gasdermin D causes pyroptosis by forming membrane pores. *Nature* 2016 5357610 **535**, 153–158 (2016).
 321. Aglietti, R. A. *et al.* GsdmD p30 elicited by caspase-11 during pyroptosis forms pores in membranes. *Proc. Natl. Acad. Sci. U. S. A.* **113**, 7858–7863 (2016).
 322. Sborgi, L. *et al.* GSDMD membrane pore formation constitutes the mechanism of pyroptotic cell death. *EMBO J.* **35**, 1766–1778 (2016).
 323. Chao, K. L., Kulakova, L. & Herzberg, O. Gene polymorphism linked to increased asthma and IBD risk alters gasdermin-B structure, a sulfatide and phosphoinositide binding protein. *Proc. Natl. Acad. Sci. U. S. A.* **114**, E1128–E1137 (2017).
 324. Mulvihill, E. *et al.* Mechanism of membrane pore formation by human gasdermin-D. *EMBO J.* **37**, (2018).
 325. Ruan, J., Xia, S., Liu, X., Lieberman, J. & Wu, H. Cryo-EM structure of the gasdermin A3 membrane pore. *Nature* 2018 5577703 **557**, 62–67 (2018).
 326. Fink, S. L. & Cookson, B. T. Apoptosis, pyroptosis, and necrosis: mechanistic description of dead and dying eukaryotic cells. *Infect. Immun.* **73**, 1907–1916 (2005).
 327. Kayagaki, N. *et al.* NINJ1 mediates plasma membrane rupture during lytic cell death. *Nature* 2021 5917848 **591**, 131–136 (2021).
 328. Viganò, E. *et al.* Human caspase-4 and caspase-5 regulate the one-step non-canonical inflammasome activation in monocytes. *Nat. Commun.* **6**, (2015).
 329. Heilig, R. *et al.* The Gasdermin-D pore acts as a conduit for IL-1 β secretion in mice. *Eur. J. Immunol.* **48**, 584–592 (2018).
 330. Chen, K. W. *et al.* The neutrophil NLRC4 inflammasome selectively promotes IL-1 β maturation without pyroptosis during acute *Salmonella* challenge. *Cell Rep.* **8**, 570–582 (2014).
 331. Xia, S. *et al.* Gasdermin D pore structure reveals preferential release of mature interleukin-1. *Nature* 2021 5937860 **593**, 607–611 (2021).
 332. De Torre-Minguela, C., Barberà-Cremades, M., Gómez, A. I., Martín-Sánchez, F. & Pelegrín, P. Macrophage activation and polarization modify P2X7 receptor secretome influencing the inflammatory process. *Sci. Rep.* **6**, (2016).
 333. Cunha, L. D. *et al.* AIM2 Engages Active but Unprocessed Caspase-1 to Induce Noncanonical Activation of the NLRP3 Inflammasome. *Cell Rep.* **20**, 794–805 (2017).
 334. Banerjee, I. *et al.* Gasdermin D Restrains Type I Interferon Response to Cytosolic DNA by Disrupting Ionic Homeostasis. *Immunity* **49**, 413-426.e5

- (2018).
335. Rühl, S. *et al.* ESCRT-dependent membrane repair negatively regulates pyroptosis downstream of GSDMD activation. *Science* **362**, 956–960 (2018).
 336. Marks, B. *et al.* GTPase activity of dynamin and resulting conformation change are essential for endocytosis. *Nature* 2001 4106825 **410**, 231–235 (2001).
 337. Shpetner, H. S. & Vallee, R. B. Dynamin is a GTPase stimulated to high levels of activity by microtubules. *Nature* 1992 3556362 **355**, 733–735 (1992).
 338. Praefcke, G. J. K. & McMahon, H. T. The dynamin superfamily: universal membrane tubulation and fission molecules? *Nat. Rev. Mol. Cell Biol.* 2004 52 **5**, 133–147 (2004).
 339. Ferguson, S. M. & De Camilli, P. Dynamin, a membrane-remodelling GTPase. *Nat. Rev. Mol. Cell Biol.* 2012 132 **13**, 75–88 (2012).
 340. Osaka, N. *et al.* Divergent Mechanisms Activating RAS and Small GTPases Through Post-translational Modification. *Front. Mol. Biosci.* **8**, 642 (2021).
 341. Martens, S. & Howard, J. The Interferon-Inducible GTPases. <http://dx.doi.org/10.1146/annurev.cellbio.22.010305.104619> **22**, 559–589 (2006).
 342. Li, G., Zhang, J., Sun, Y., Wang, H. & Wang, Y. The evolutionarily dynamic IFN-inducible GTPase proteins play conserved immune functions in vertebrates and cephalochordates. *Mol. Biol. Evol.* **26**, 1619–1630 (2009).
 343. Klamp, T., Boehm, U., Schenk, D., Pfeffer, K. & Howard, J. C. A giant GTPase, very large inducible GTPase-1, is inducible by IFNs. *J. Immunol.* **171**, 1255–1265 (2003).
 344. Prakash, B., Praefcke, G. J. K., Renault, L., Wittinghofer, A. & Herrmann, C. Structure of human guanylate-binding protein 1 representing a unique class of GTP-binding proteins. *Nature* **403**, 567–571 (2000).
 345. Prakash, B., Renault, L., Praefcke, G. J. K., Herrmann, C. & Wittinghofer, A. Triphosphate structure of guanylate-binding protein 1 and implications for nucleotide binding and GTPase mechanism. *EMBO J.* **19**, 4555–4564 (2000).
 346. Praefcke, G. J. K. *et al.* Identification of residues in the human guanylate-binding protein 1 critical for nucleotide binding and cooperative GTP hydrolysis. *J. Mol. Biol.* **344**, 257–269 (2004).
 347. Vetter, I. R. & Wittinghofer, A. The guanine nucleotide-binding switch in three dimensions. *Science* **294**, 1299–1304 (2001).
 348. Vöpel, T. *et al.* Mechanism of GTPase-activity-induced self-assembly of human guanylate binding protein 1. *J. Mol. Biol.* **400**, 63–70 (2010).
 349. Ince, S. *et al.* Catalytic activity of human guanylate-binding protein 1 coupled to the release of structural restraints imposed by the C-terminal domain. *FEBS J.* **288**, 582–599 (2021).
 350. Ince, S., Kutsch, M., Shydlovskiy, S. & Herrmann, C. The human guanylate-binding proteins hGBP-1 and hGBP-5 cycle between monomers and dimers only. *FEBS J.* **284**, 2284–2301 (2017).
 351. Cheng, Y. S., Patterson, C. E. & Staeheli, P. Interferon-induced guanylate-binding proteins lack an N(T)KXD consensus motif and bind GMP in addition to GDP and GTP. *Mol. Cell. Biol.* **11**, 4717–4725 (1991).
 352. Schwemmler, M. & Staeheli, P. The interferon-induced 67-kDa guanylate-binding protein (hGBP1) is a GTPase that converts GTP to GMP. *J. Biol. Chem.* **269**, 11299–11305 (1994).
 353. Ghosh, A., Praefcke, G. J. K., Renault, L., Wittinghofer, A. & Herrmann, C. How guanylate-binding proteins achieve assembly-stimulated processive

- cleavage of GTP to GMP. *Nature* **440**, 101–104 (2006).
354. Abdullah, N., Srinivasan, B., Modiano, N., Cresswell, P. & Sau, A. K. Role of individual domains and identification of internal gap in human guanylate binding protein-1. *J. Mol. Biol.* **386**, 690–703 (2009).
 355. Vöpel, T. *et al.* Triphosphate induced dimerization of human guanylate binding protein 1 involves association of the C-terminal helices: a joint double electron-electron resonance and FRET study. *Biochemistry* **53**, 4590–4600 (2014).
 356. Kravets, E. *et al.* Guanylate binding proteins directly attack *Toxoplasma gondii* via supramolecular complexes. *Elife* **5**, (2016).
 357. Shydlovskiy, S. *et al.* Nucleotide-dependent farnesyl switch orchestrates polymerization and membrane binding of human guanylate-binding protein 1. *Proc. Natl. Acad. Sci. U. S. A.* **114**, E5559–E5568 (2017).
 358. Stickney, J. T. & Buss, J. E. Murine guanylate-binding protein: incomplete geranylgeranyl isoprenoid modification of an interferon-gamma-inducible guanosine triphosphate-binding protein. *Mol. Biol. Cell* **11**, 2191–2200 (2000).
 359. Kravets, E. *et al.* The GTPase activity of murine guanylate-binding protein 2 (mGBP2) controls the intracellular localization and recruitment to the parasitophorous vacuole of *Toxoplasma gondii*. *J. Biol. Chem.* **287**, 27452–27466 (2012).
 360. Santos, J. C. *et al.* Human GBP1 binds LPS to initiate assembly of a caspase-4 activating platform on cytosolic bacteria. *Nat. Commun.* **11**, 1–15 (2020).
 361. Wandel, M. P. *et al.* Guanylate-binding proteins convert cytosolic bacteria into caspase-4 signaling platforms. *Nat. Immunol.* (2020) doi:10.1038/s41590-020-0697-2.
 362. Tretina, K., Park, E. S., Maminska, A. & MacMicking, J. D. Interferon-induced guanylate-binding proteins: Guardians of host defense in health and disease. *J. Exp. Med.* **216**, 482 (2019).
 363. Kutsch, M., Orn Coers, J., Kutsch, C. M. & Coers, J. Human guanylate binding proteins: nanomachines orchestrating host defense. *FEBS J.* **288**, 5826–5849 (2021).
 364. Kim, B. H. *et al.* A family of IFN- γ -inducible 65-kD GTPases protects against bacterial infection. *Science* **332**, 717–721 (2011).
 365. Santos, J. C. & Broz, P. Sensing of invading pathogens by GBPs: At the crossroads between cell-autonomous and innate immunity. *Journal of Leukocyte Biology* (2018) doi:10.1002/JLB.4MR0118-038R.
 366. Kutsch, M. & Coers, J. Human guanylate binding proteins: nanomachines orchestrating host defense. *FEBS Journal* (2020) doi:10.1111/febs.15662.
 367. Shenoy, A. R. *et al.* GBP5 promotes NLRP3 inflammasome assembly and immunity in mammals. *Science* **336**, 481–485 (2012).
 368. Olszewski, M. A., Gray, J. & Vestal, D. J. In silico genomic analysis of the human and murine guanylate-binding protein (GBP) gene clusters. *J. Interferon Cytokine Res.* **26**, 328–352 (2006).
 369. Côte-Real, J. V., Baldauf, H. M., Melo-Ferreira, J., Abrantes, J. & Esteves, P. J. Evolution of Guanylate Binding Protein (GBP) Genes in Muroid Rodents (Muridae and Cricetidae) Reveals an Outstanding Pattern of Gain and Loss. *Front. Immunol.* **13**, (2022).
 370. Nei, M. & Rooney, A. P. Concerted and Birth-and-Death Evolution of Multigene Families. *Annu. Rev. Genet.* **39**, 121 (2005).
 371. Côte-Real, J. V., Baldauf, H. M., Abrantes, J. & Esteves, P. J. Evolution of the guanylate binding protein (GBP) genes: Emergence of GBP7 genes in

- primates and further acquisition of a unique GBP3 gene in simians. *Mol. Immunol.* **132**, 79–81 (2021).
372. Vernet, B. *et al.* Excavating Neandertal and Denisovan DNA from the genomes of Melanesian individuals. *Science* **352**, 235 (2016).
 373. Enard, D. & Petrov, D. A. Evidence that RNA viruses drove of adaptive introgression between Neanderthals and modern humans. *Cell* **175**, 360 (2018).
 374. Palesch, D. *et al.* Sooty mangabey genome sequence provides insight into AIDS resistance in a natural SIV host. *Nature* **553**, 77 (2018).
 375. Krapp, C. *et al.* Guanylate Binding Protein (GBP) 5 Is an Interferon-Inducible Inhibitor of HIV-1 Infectivity. *Cell Host Microbe* **19**, 504–514 (2016).
 376. Yamamoto, M. *et al.* A Cluster of Interferon- γ -Inducible p65 GTPases Plays a Critical Role in Host Defense against *Toxoplasma gondii*. *Immunity* **37**, 302–313 (2012).
 377. Park, E.-S. *et al.* A hierarchical GBP network promotes cytosolic LPS recognition and sepsis. *bioRxiv* 2021.08.25.457662 (2021) doi:10.1101/2021.08.25.457662.
 378. Cao, S. *et al.* Subversion of GBP-mediated host defense by E3 ligases acquired during *Yersinia pestis* evolution. *Nat. Commun.* 2022 **13**, 1–17 (2022).
 379. Meunier, E. & Broz, P. Evolutionary Convergence and Divergence in NLR Function and Structure. *Trends Immunol.* **38**, 744–757 (2017).
 380. Kim, B. H. *et al.* Interferon-induced guanylate-binding proteins in inflammasome activation and host defense. *Nature Immunology* (2016) doi:10.1038/ni.3440.
 381. Ingram, J. P. *et al.* A Nonpyroptotic IFN- γ -Triggered Cell Death Mechanism in Nonphagocytic Cells Promotes *Salmonella* Clearance In Vivo. *J. Immunol.* **200**, 3626–3634 (2018).
 382. Mostafavi, S. *et al.* Parsing the Interferon Transcriptional Network and Its Disease Associations. *Cell* **164**, 564–578 (2016).
 383. Yan, L. *et al.* Single-cell RNA-Seq profiling of human preimplantation embryos and embryonic stem cells. *Nat. Struct. Mol. Biol.* **20**, 1131–1139 (2013).
 384. Wu, X. *et al.* Intrinsic Immunity Shapes Viral Resistance of Stem Cells. *Cell* **172**, 423–438.e25 (2018).
 385. Yamagata, T., Benoist, C. & Mathis, D. A shared gene-expression signature in innate-like lymphocytes. *Immunol. Rev.* **210**, 52–66 (2006).
 386. Britzen-Laurent, N. *et al.* GBP-1 acts as a tumor suppressor in colorectal cancer cells. *Carcinogenesis* **34**, 153–162 (2013).
 387. Nguyen, T. T., Hu, Y., Widney, D. P., Mar, R. A. & Smith, J. B. Murine GBP-5, a new member of the murine guanylate-binding protein family, is coordinately regulated with other GBPs in vivo and in vitro. *J. Interferon Cytokine Res.* **22**, 899–909 (2002).
 388. Darnell, J. E., Kerr, I. M. & Stark, G. R. Jak-STAT pathways and transcriptional activation in response to IFNs and other extracellular signaling proteins. *Science* **264**, 1415–1421 (1994).
 389. Boehm, U. *et al.* Two Families of GTPases Dominate the Complex Cellular Response to IFN- γ . *J. Immunol.* **161**, (1998).
 390. Briken, V. *et al.* Interferon regulatory factor 1 is required for mouse *Gbp* gene activation by gamma interferon. *Mol. Cell. Biol.* **15**, 975–982 (1995).
 391. Decker, T. *et al.* Two distinct alpha-interferon-dependent signal transduction

- pathways may contribute to activation of transcription of the guanylate-binding protein gene. *Mol. Cell. Biol.* **11**, 5147 (1991).
392. Alase, A. A. *et al.* IFN λ Stimulates MxA Production in Human Dermal Fibroblasts via a MAPK-Dependent STAT1-Independent Mechanism. *J. Invest. Dermatol.* **135**, 2935–2943 (2015).
 393. Bolen, C. R., Ding, S., Robek, M. D. & Kleinstein, S. H. Dynamic expression profiling of type I and type III interferon-stimulated hepatocytes reveals a stable hierarchy of gene expression. *Hepatology* **59**, 1262–1272 (2014).
 394. Lin, X. *et al.* miR-433 is aberrantly expressed in myeloproliferative neoplasms and suppresses hematopoietic cell growth and differentiation. *Leukemia* **27**, 344–352 (2013).
 395. Atianand, M. K. *et al.* A Long Noncoding RNA lincRNA-EPS Acts as a Transcriptional Brake to Restrain Inflammation. *Cell* **165**, 1672–1685 (2016).
 396. Anderson, S. L., Carton, J. M., Lou, J., Xing, L. & Rubin, B. Y. Interferon-Induced Guanylate Binding Protein-1 (GBP-1) Mediates an Antiviral Effect against Vesicular Stomatitis Virus and Encephalomyocarditis Virus. *Virology* **256**, 8–14 (1999).
 397. Zou, Z. *et al.* Guanylate-Binding Protein 1 Inhibits Nuclear Delivery of Kaposi's Sarcoma-Associated Herpesvirus Virions by Disrupting Formation of Actin Filament. *J. Virol.* **91**, (2017).
 398. Itsui, Y. *et al.* Expressional screening of interferon-stimulated genes for antiviral activity against hepatitis C virus replication. *J. Viral Hepat.* **13**, 690–700 (2006).
 399. Itsui, Y. *et al.* Antiviral effects of the interferon-induced protein guanylate binding protein 1 and its interaction with the hepatitis C virus NS5B protein. *Hepatology* **50**, 1727–1737 (2009).
 400. Nordmann, A., Wixler, L., Boergeling, Y., Wixler, V. & Ludwig, S. A new splice variant of the human guanylate-binding protein 3 mediates anti-influenza activity through inhibition of viral transcription and replication. *FASEB J.* **26**, 1290–1300 (2012).
 401. Checkley, M. A., Lutge, B. G. & Freed, E. O. HIV-1 Envelope Glycoprotein Biosynthesis, Trafficking, and Incorporation. *J. Mol. Biol.* **410**, 582 (2011).
 402. Braun, E. *et al.* Guanylate-Binding Proteins 2 and 5 Exert Broad Antiviral Activity by Inhibiting Furin-Mediated Processing of Viral Envelope Proteins. *Cell Rep.* **27**, 2092-2104.e10 (2019).
 403. Carter, C. C., Gorbacheva, V. Y. & Vestal, D. J. Inhibition of VSV and EMCV replication by the interferon-induced GTPase, mGBP-2: differential requirement for wild-type GTP binding domain. *Arch. Virol.* **150**, 1213–1220 (2005).
 404. Biering, S. B. *et al.* Viral Replication Complexes Are Targeted by LC3-Guided Interferon-Inducible GTPases. *Cell Host Microbe* **22**, 74-85.e7 (2017).
 405. Hu, Y. *et al.* Guanylate binding protein 4 negatively regulates virus-induced type I IFN and antiviral response by targeting IFN regulatory factor 7. *J. Immunol.* **187**, 6456–6462 (2011).
 406. Feng, M. *et al.* Inducible Guanylate-Binding Protein 7 Facilitates Influenza A Virus Replication by Suppressing Innate Immunity via NF- κ B and JAK-STAT Signaling Pathways. *J. Virol.* **95**, (2021).
 407. Feng, J. *et al.* Inducible GBP5 Mediates the Antiviral Response via Interferon-Related Pathways during Influenza A Virus Infection. *J. Innate Immun.* **9**, 419–435 (2017).

408. Degrandi, D. *et al.* Extensive Characterization of IFN-Induced GTPases mGBP1 to mGBP10 Involved in Host Defense. *J. Immunol.* **179**, 7729–7740 (2007).
409. Yamamoto, M. *et al.* A cluster of interferon- γ -inducible p65 GTPases plays a critical role in host defense against *Toxoplasma gondii*. *Immunity* **37**, 302–313 (2012).
410. Virreira Winter, S. *et al.* Determinants of GBP Recruitment to *Toxoplasma gondii* Vacuoles and the Parasitic Factors That Control It. *PLoS One* **6**, (2011).
411. Degrandi, D. *et al.* Murine guanylate binding protein 2 (mGBP2) controls *Toxoplasma gondii* replication. *Proc. Natl. Acad. Sci. U. S. A.* **110**, 294–299 (2013).
412. Selleck, E. M. *et al.* Guanylate-binding protein 1 (Gbp1) contributes to cell-autonomous immunity against *Toxoplasma gondii*. *PLoS Pathog.* **9**, (2013).
413. Hunter, C. A. & Sibley, L. D. Modulation of innate immunity by *Toxoplasma gondii* virulence effectors. *Nat. Rev. Microbiol.* **10**, 766–778 (2012).
414. Gay, G. *et al.* *Toxoplasma gondii* TgIST co-opts host chromatin repressors dampening STAT1-dependent gene regulation and IFN- γ -mediated host defenses. *J. Exp. Med.* **213**, 1779–1798 (2016).
415. Olias, P., Etheridge, R. D., Zhang, Y., Holtzman, M. J. & Sibley, L. D. *Toxoplasma* Effector Recruits the Mi-2/NuRD Complex to Repress STAT1 Transcription and Block IFN- γ -Dependent Gene Expression. *Cell Host Microbe* **20**, 72–82 (2016).
416. Steffens, N. *et al.* Essential role of mGBP7 for survival of *toxoplasma gondii* infection. *MBio* **11**, (2020).
417. Qin, A. *et al.* Guanylate-binding protein 1 (GBP1) contributes to the immunity of human mesenchymal stromal cells against *Toxoplasma gondii*. *Proc. Natl. Acad. Sci. U. S. A.* **114**, 1365–1370 (2017).
418. Johnston, A. C. *et al.* Human GBP1 does not localize to pathogen vacuoles but restricts *Toxoplasma gondii*. *Cell. Microbiol.* **18**, 1056–1064 (2016).
419. Ohshima, J. *et al.* Role of mouse and human autophagy proteins in IFN- γ -induced cell-autonomous responses against *Toxoplasma gondii*. *J. Immunol.* **192**, 3328–3335 (2014).
420. Fisch, D. *et al.* Human GBP 1 is a microbe-specific gatekeeper of macrophage apoptosis and pyroptosis. *EMBO J.* (2019) doi:10.15252/emj.2018100926.
421. Niedelman, W., Sprokholt, J. K., Clough, B., Frickel, E. M. & Saeij, J. P. J. Cell death of gamma interferon-stimulated human fibroblasts upon *Toxoplasma gondii* infection induces early parasite egress and limits parasite replication. *Infect. Immun.* **81**, 4341–4349 (2013).
422. Berghout, J. *et al.* Irf8-Regulated Genomic Responses Drive Pathological Inflammation during Cerebral Malaria. *PLoS Pathog.* **9**, e1003491 (2013).
423. Liehl, P. *et al.* Host-cell sensors for *Plasmodium* activate innate immunity against liver-stage infection. *Nat. Med.* **20**, 47–53 (2014).
424. Apinjoh, T. O. *et al.* Association of candidate gene polymorphisms and TGF- β /IL-10 levels with malaria in three regions of Cameroon: a case-control study. *Malar. J.* **13**, (2014).
425. Sohrabi, Y. *et al.* Genetic regulation of guanylate-binding proteins 2b and 5 during leishmaniasis in mice. *Front. Immunol.* **9**, (2018).
426. Haldar, A. K., Nigam, U., Yamamoto, M., Coers, J. & Goyal, N. Guanylate Binding Proteins Restrict *Leishmania donovani* Growth in Nonphagocytic Cells

- Independent of Parasitophorous Vacuolar Targeting. *MBio* **11**, 1–19 (2020).
427. Kumar, R. & Kushawaha, P. K. Interferon inducible guanylate binding protein 1 restricts the growth of *Leishmania donovani* by modulating the level of cytokines/chemokines and MAP kinases. *Microb. Pathog.* **168**, 105568 (2022).
428. Haldar, A. K. *et al.* Ubiquitin systems mark pathogen-containing vacuoles as targets for host defense by guanylate binding proteins. *Proc. Natl. Acad. Sci. U. S. A.* **112**, E5628–E5637 (2015).
429. Feeley, E. M. *et al.* Galectin-3 directs antimicrobial guanylate binding proteins to vacuoles furnished with bacterial secretion systems. *Proc. Natl. Acad. Sci. U. S. A.* **114**, E1698–E1706 (2017).
430. Piro, A. S. *et al.* Detection of cytosolic shigella flexneri via a C-terminal triple-arginine motif of GBP1 inhibits actin-based motility. *MBio* (2017) doi:10.1128/mBio.01979-17.
431. Wandel, M. P. *et al.* GBPs Inhibit Motility of *Shigella flexneri* but Are Targeted for Degradation by the Bacterial Ubiquitin Ligase IpaH9.8. *Cell Host Microbe* (2017) doi:10.1016/j.chom.2017.09.007.
432. Lindenbergh, V. *et al.* Broad recruitment of mGBP family members to *Chlamydia trachomatis* inclusions. *PLoS One* **12**, (2017).
433. Place, D. E. *et al.* Interferon inducible GBPs restrict *Burkholderia thailandensis* motility induced cell-cell fusion. *PLoS Pathog.* (2020) doi:10.1371/journal.ppat.1008364.
434. Kim, B. H. *et al.* IFN-induced Guanylate Binding Proteins in Inflammasome Activation and Host Defense. *Nat. Immunol.* **17**, 481 (2016).
435. Broz, P. & Dixit, V. M. Inflammasomes: Mechanism of assembly, regulation and signalling. *Nature Reviews Immunology* (2016) doi:10.1038/nri.2016.58.
436. Meunier, E. *et al.* Caspase-11 activation requires lysis of pathogen-containing vacuoles by IFN-induced GTPases. *Nature* **509**, 366–370 (2014).
437. Man, S. M. *et al.* The transcription factor IRF1 and guanylate-binding proteins target activation of the AIM2 inflammasome by *Francisella* infection. *Nat. Immunol.* (2015) doi:10.1038/ni.3118.
438. Marty-Roix, R. *et al.* Identification of QS-21 as an Inflammasome-activating Molecular Component of Saponin Adjuvants. *J. Biol. Chem.* **291**, 1123–1136 (2016).
439. Hornung, V. *et al.* Silica crystals and aluminum salts activate the NALP3 inflammasome through phagosomal destabilization. *Nat. Immunol.* **9**, 847–856 (2008).
440. Sheedy, F. J. *et al.* CD36 coordinates NLRP3 inflammasome activation by facilitating intracellular nucleation of soluble ligands into particulate ligands in sterile inflammation. *Nat. Immunol.* **14**, 812–820 (2013).
441. Feng, S. *et al.* Pathogen-selective killing by guanylate-binding proteins as a molecular mechanism leading to inflammasome signaling. *Nat. Commun.* **2022** **13**, 1–15 (2022).
442. Valeva, S. V. *et al.* Bacterial factors drive the differential targeting of Guanylate Binding Proteins to *Francisella* and *Shigella*. *bioRxiv* 2021.06.16.448779 (2021) doi:10.1101/2021.06.16.448779.
443. Finethy, R. *et al.* Guanylate binding proteins enable rapid activation of canonical and noncanonical inflammasomes in *Chlamydia*-infected macrophages. *Infect. Immun.* **83**, 4740–4749 (2015).
444. Pilla, D. M. *et al.* Guanylate binding proteins promote caspase-11-dependent

- pyroptosis in response to cytoplasmic LPS. *Proc. Natl. Acad. Sci. U. S. A.* (2014) doi:10.1073/pnas.1321700111.
445. Santos, J. C. *et al.* LPS targets host guanylate-binding proteins to the bacterial outer membrane for non-canonical inflammasome activation. *EMBO J.* (2018) doi:10.15252/embj.201798089.
 446. Lagrange, B. *et al.* Human caspase-4 detects tetra-acylated LPS and cytosolic Francisella and functions differently from murine caspase-11. *Nat. Commun.* 2018 91 **9**, 1–14 (2018).
 447. Thurston, T. L. M. *et al.* Growth inhibition of cytosolic Salmonella by caspase-1 and caspase-11 precedes host cell death. *Nat. Commun.* 2016 71 **7**, 1–15 (2016).
 448. Dilucca, M., Ramos, S., Shkarina, K., Santos, J. C. & Broz, P. Guanylate-binding protein-dependent noncanonical inflammasome activation prevents burkholderia thailandensis-induced multinucleated giant cell formation. *MBio* **12**, (2021).
 449. Kutsch, M. *et al.* Direct binding of polymeric GBP1 to LPS disrupts bacterial cell envelope functions. *EMBO J.* (2020) doi:10.15252/embj.2020104926.
 450. Takeuchi, O. & Akira, S. Pattern Recognition Receptors and Inflammation. *Cell* **140**, 805–820 (2010).
 451. Shi, J. *et al.* Inflammatory caspases are innate immune receptors for intracellular LPS. *Nature* 2014 5147521 **514**, 187–192 (2014).
 452. Kayagaki, N. *et al.* Caspase-11 cleaves gasdermin D for non-canonical inflammasome signalling. *Nature* (2015) doi:10.1038/nature15541.
 453. Shi, J. *et al.* Cleavage of GSDMD by inflammatory caspases determines pyroptotic cell death. *Nature* (2015) doi:10.1038/nature15514.
 454. Pilla, D. M. *et al.* Guanylate binding proteins promote caspase-11-dependent pyroptosis in response to cytoplasmic LPS. *Proc. Natl. Acad. Sci. U. S. A.* (2014) doi:10.1073/pnas.1321700111.
 455. Lagrange, B. *et al.* Human caspase-4 detects tetra-acylated LPS and cytosolic Francisella and functions differently from murine caspase-11. *Nat. Commun.* (2018) doi:10.1038/s41467-017-02682-y.
 456. Wandel, M. P. *et al.* Guanylate-binding proteins convert cytosolic bacteria into caspase-4 signaling platforms. *Nat. Immunol.* **21**, 880–891 (2020).
 457. Wiersinga, W. J., van der Poll, T., White, N. J., Day, N. P. & Peacock, S. J. Melioidosis: Insights into the pathogenicity of Burkholderia pseudomallei. *Nature Reviews Microbiology* (2006) doi:10.1038/nrmicro1385.
 458. Galyov, E. E., Brett, P. J. & Deshazer, D. Molecular insights into Burkholderia pseudomallei and Burkholderia mallei pathogenesis. *Annual Review of Microbiology* (2010) doi:10.1146/annurev.micro.112408.134030.
 459. Cheng, A. C. & Currie, B. J. Melioidosis: Epidemiology, pathophysiology, and management. *Clinical Microbiology Reviews* (2005) doi:10.1128/CMR.18.2.383-416.2005.
 460. Stevens, M. P. *et al.* An Inv/Mxi-Spa-like type III protein secretion system in Burkholderia pseudomallei modulates intracellular behaviour of the pathogen. *Mol. Microbiol.* **46**, 649–659 (2002).
 461. French, C. T. *et al.* Dissection of the Burkholderia intracellular life cycle using a photothermal nanoblade. *Proc. Natl. Acad. Sci. U. S. A.* **108**, 12095–12100 (2011).
 462. Benanti, E. L., Nguyen, C. M. & Welch, M. D. Virulent burkholderia species mimic host actin polymerases to drive actin-based motility. *Cell* (2015)

- doi:10.1016/j.cell.2015.02.044.
463. WONG, K. T., PUTHUCHEARY, S. D. & VADIVELU, J. The histopathology of human melioidosis. *Histopathology* (1995) doi:10.1111/j.1365-2559.1995.tb00620.x.
464. Toesca, I. J., French, C. T. & Miller, J. F. The Type VI secretion system spike protein VgrG5 mediates membrane fusion during intercellular spread by pseudomallei group Burkholderia species. *Infect. Immun.* **82**, 1436–1444 (2014).
465. Lennings, J., West, T. E. & Schwarz, S. The Burkholderia Type VI secretion system 5: Composition, regulation and role in virulence. *Frontiers in Microbiology* (2019) doi:10.3389/fmicb.2018.03339.
466. Aachoui, Y. *et al.* Caspase-11 protects against bacteria that escape the vacuole. *Science* (2013) doi:10.1126/science.1230751.
467. Ceballos-Olvera, I., Sahoo, M., Miller, M. A., del Barrio, L. & Re, F. Inflammasome-dependent pyroptosis and IL-18 protect against Burkholderia pseudomallei lung infection while IL-1 β is deleterious. *PLoS Pathog.* **7**, (2011).
468. Aachoui, Y. *et al.* Canonical Inflammasomes Drive IFN- γ to Prime Caspase-11 in Defense against a Cytosol-Invasive Bacterium. *Cell Host Microbe* **18**, 320–332 (2015).
469. Kovacs, S. B. *et al.* Neutrophil Caspase-11 Is Essential to Defend against a Cytosol-Invasive Bacterium. *Cell Rep.* **32**, (2020).
470. Place, D. E. *et al.* Interferon inducible GBPs restrict Burkholderia thailandensis motility induced cell-cell fusion. *PLoS Pathog.* **16**, (2020).
471. Randow, F., MacMicking, J. D. & James, L. C. Cellular Self-Defense: How Cell-Autonomous Immunity Protects Against Pathogens. *Science* **340**, 701–706 (2013).
472. Krishnaswamy, J. K. *et al.* Coincidental loss of DOCK8 function in NLRP10-deficient and C3H/HeJ mice results in defective dendritic cell migration. *Proc. Natl. Acad. Sci. U. S. A.* **112**, 3056–3061 (2015).
473. Bjanes, E. *et al.* Genetic targeting of Card19 is linked to disrupted NINJ1 expression, impaired cell lysis, and increased susceptibility to Yersinia infection. *PLoS Pathog.* **17**, (2021).
474. Zahid, A., Ismail, H., Li, B. & Jin, T. Molecular and Structural Basis of DNA Sensors in Antiviral Innate Immunity. *Front. Immunol.* **11**, 3094 (2020).
475. Schroder, K. & Tschopp, J. Review The Inflammasomes Supplement. *Cell* (2010) doi:10.1016/j.cell.2010.01.040.
476. Brubaker, S. W., Brewer, S. M., Massis, L. M., Napier, B. A. & Monack, D. M. A Rapid Caspase-11 Response Induced by IFN γ Priming Is Independent of Guanylate Binding Proteins. *iScience* **23**, 101612 (2020).
477. Park, B. S. *et al.* The structural basis of lipopolysaccharide recognition by the TLR4–MD-2 complex. *Nature* 2009 4587242 **458**, 1191–1195 (2009).
478. Gioannini, T. L. *et al.* Isolation of an endotoxin-MD-2 complex that produces Toll-like receptor 4-dependent cell activation at picomolar concentrations. *Proc. Natl. Acad. Sci. U. S. A.* **101**, 4186–4191 (2004).
479. Kravets, E. *et al.* Guanylate binding proteins directly attack toxoplasma gondii via supramolecular complexes. *Elife* **5**, (2016).
480. Frickel, E. M. & Hunter, C. A. Lessons from toxoplasma: Host responses that mediate parasite control and the microbial effectors that subvert them. *J. Exp. Med.* **218**, (2021).
481. Bertani, B. & Ruiz, N. Function and biogenesis of lipopolysaccharides. *EcoSal*

- Plus* **8**, (2018).
482. Harberts, E. M. *et al.* Position-Specific Secondary Acylation Determines Detection of Lipid A by Murine TLR4 and Caspase-11. *Infect. Immun.* **90**, (2022).
 483. Alexander-Floyd, J. *et al.* Lipid A Variants Activate Human TLR4 and the Noncanonical Inflammasome Differently and Require the Core Oligosaccharide for Inflammasome Activation. *Infect. Immun.* **90**, (2022).
 484. Dickinson, M. S. *et al.* GBP2 aggregates LPS and activates the caspase-4 inflammasome independent of the bacterial encapsulation factor GBP1. *bioRxiv* 2022.10.05.511023 (2022) doi:10.1101/2022.10.05.511023.
 485. Goldberg, M. B. & Theriot, J. A. Shigella flexneri surface protein IcsA is sufficient to direct actin-based motility. *Proc. Natl. Acad. Sci. U. S. A.* **92**, 6572–6576 (1995).
 486. Sitthidet, C. *et al.* Actin-based motility of Burkholderia thailandensis requires a central acidic domain of BimA that recruits and activates the cellular Arp2/3 complex. *J. Bacteriol.* **192**, 5249–5252 (2010).
 487. Lamason, R. L. & Welch, M. D. Actin-based motility and cell-to-cell spread of bacterial pathogens. *Curr. Opin. Microbiol.* **35**, 48 (2017).
 488. Egile, C., D’Hauteville, H., Parsot, C. & Sansonetti, P. J. SopA, the outer membrane protease responsible for polar localization of IcsA in Shigella flexneri. *Mol. Microbiol.* **23**, 1063–1073 (1997).
 489. Lu, Q., Xu, Y., Yao, Q., Niu, M. & Shao, F. A polar-localized iron-binding protein determines the polar targeting of Burkholderia BimA autotransporter and actin tail formation. *Cell. Microbiol.* **17**, 408–424 (2015).
 490. Sengyee, S., Yoon, S. H., Eoin West, T., Ernst, R. K. & Chantratita, N. Lipopolysaccharides from different Burkholderia species with different lipid a structures induce toll-like receptor 4 activation and react with melioidosis patient sera. *Infect. Immun.* **87**, (2019).
 491. Dilucca, M., Ramos, S., Shkarina, K., Santos, J. C. & Broz, P. Guanylate-Binding Protein-Dependent Noncanonical Inflammasome Activation Prevents Burkholderia thailandensis-Induced Multinucleated Giant Cell Formation. *MBio* **12**, (2021).
 492. Wang, J., Deobald, K. & Re, F. Gasdermin D Protects from Melioidosis through Pyroptosis and Direct Killing of Bacteria. *J. Immunol.* **202**, 3468–3473 (2019).
 493. Ngo, C. C. & Man, S. M. Mechanisms and functions of guanylate-binding proteins and related interferon-inducible GTPases: Roles in intracellular lysis of pathogens. *Cellular Microbiology* (2017) doi:10.1111/cmi.12791.

